Buildings, Energy and Environment Research Group

Department of Architecture and Built Environment

Faculty of Engineering

Investigation into Sustainable Technologies for Mitigating Urban Heat Island Effects in Subtropical Monsoon Climate

Thesis by

Tianhong Zheng, BEng

Thesis submitted to the University of Nottingham

For the Degree of Doctor of Philosophy

March 2023

ABSTRACT

The urban heat island (UHI) is a concerning environmental phenomenon, and mitigation strategies have been proposed to reduce its adverse effects. This study conducted a literature review of UHI and UHI mitigation strategies, finding that urban cooling technologies such as green roofs, cool roofs, and urban vegetation can comprehensively affect meteorological parameters (temperature, sky view factor, radiation, etc.), urban building energy use, carbon emissions and improve human comfort. Additionally, thermal energy storage technologies were also reviewed, with a focus on mitigating UHI. The study assessed the effectiveness of conventional and thermal energy storage-based UHI mitigation strategies through meteorological simulations using the software ENVI-met and a novel model called UHIMS-ECHE. The simulation results showed that conventional UHI mitigation scenarios can reduce UHI intensity, building cooling energy use, carbon emissions, and improve human thermal comfort. Moreover, the integration of phase change materials (PCMs) and photovoltaic (PV) systems was analysed by the UHIMS-ECHE model, which demonstrated that the integration of PCM and PV technologies can significantly reduce UHI, improve energy efficiency, and enhance human thermal comfort in urban environments. A case study has been conducted in Osaka, Japan, which is a typical city under subtropical monsoon weather condition. Consequently, the PCM-Roof -A36H -10cm model reduced outdoor air temperatures by up to 7.09°C and total urban building cooling energy use cooling loads by up to 23.68% compared to the baseline case. These findings provide insights for policymakers, urban planners, and building designers to create sustainable urban environments. Further

research is recommended to investigate the feasibility and cost-effectiveness of these technologies in different urban contexts and climatic conditions.

List of publications

International Journal Papers

[1] Zheng T, Qu K, Darkwa J, Calautit JK. Evaluating urban heat island mitigation strategies for a subtropical city centre (a case study in Osaka, Japan). Energy. 2022;250:123721.

[2] Zheng T, Qu K, Wang Y, Darkwa J, Calautit JK. A Novel Urban Heat Island Mitigation Strategies-Engaged City-Scale Building Energy Consumption Prediction Workflow: Case Study and Validation. SSRN. 2022.

International conference papers

[1] Zheng T, Qu K, Wang Y, Darkwa J, Calautit JK. A novel urban heat island calculation workflow: case study and validation. 19th International Conference on Sustainable Energy Technologies (SET 2022), Istanbul, Tukey.

[2] Zheng T, Qu K, Wang Y, Darkwa J, Calautit JK. . Evaluating urban heat island mitigation strategies for a subtropical city centre (a case study in Osaka, Japan). Proceedings of Ecos 2021 - The 34th International Conference On Efficiency, Cost, Optimization, Simulation and Environmental Impact of Energy Systems June 27-July 2, 2021, Taormina, Italy.

[3] Qu K, Zheng T, Cimini V, Riffat S. An inclusive decision-making approach for selection of comprehensive energy-retrofit combinations in a typical Italian 1960s' multi-family house. Proceedings of Ecos 2021 - The 34th International Conference On Efficiency, Cost, Optimization, Simulation and Environmental Impact of Energy Systems June 27-July 2, 2021, Taormina, Italy

Acknowledgement

Completing a PhD thesis is a long and challenging journey, and I would like to express my deepest gratitude to all those who supported me along the way.

First and foremost, I am grateful for the unwavering support of my family, who have always encouraged me to pursue my dreams and have been there for me through the highs and lows of this journey. I would especially like to thank my parents for their constant love and financial support, and for instilling in me the value of education.

I am deeply grateful for the mentorship and guidance of my supervisors, Professor Jo Darkwa and Doctor John Kaiser Calautit. Their expertise, patience, and encouragement have been instrumental in helping me navigate the challenges of my research and thesis writing. Their feedback and insights have been critical in shaping the direction and focus of my work, and I am grateful for their mentorship.

My friends have been a constant source of inspiration and support, and I am grateful for their encouragement and motivation throughout this journey. I would like to thank Ke Qu, Yanan Zhang and Yixin Wang, among others, for their unwavering support and encouragement, and for being there to celebrate the milestones along the way.

I would also like to thank the participants of my study, whose contributions have been crucial in helping me gather the data for my research. Their willingness to share their experiences and insights has been instrumental in helping me gain a deeper understanding of my research questions.

Lastly, I am grateful for the resources and support provided by the University of Nottingham. The access to research facilities, library resources, and technical support has been invaluable in helping me carry out my research.

Completing this thesis has been one of the most challenging and rewarding experiences of my life, and I could not have done it without the love, encouragement, and support of all those who have stood by me. You have given me the strength and courage to persevere, even when the road ahead seemed insurmountable, and for that, I will be forever grateful.

TABLE OF CONTENTS

List of Figures

List of Table

1 CHAPTER I: INTRODUCTION

1.1 Research background

The emergence of the urban heat island (UHI) effect can be attributed to the Industrial Revolution, which led to its initial observation in London during the 19th century [1]. This phenomenon is characterised by the occurrence of elevated temperatures in urban areas when compared to the surrounding rural areas [2]. Fig.1-1 shows a visual representation of the UHI effect in urban environments, based on World meteorological organization [3].

Figure 1-1 Visual representation of the UHI phenomenon [3]

In recent years, global warming and extreme climate events have emerged as pressing issues, presenting complex challenges for both scientists and policymakers. According to the Sixth Assessment Report by the Intergovernmental Panel on Climate Change (IPCC) [4], limiting global warming to 1.5°C (2.7°F) before 2025 requires reducing global greenhouse gas (GHG) emissions by 43% by 2030. However, despite this urgent need, total net anthropogenic GHG emissions have continued to rise between 2010 and 2019, including cumulative net CO_2 emissions since 1850.

Moreover, UHI effects have been identified as a contributing factor to global warming, and it is prevalent in numerous cities worldwide. Recent research [5]

assessed summer temperature data from more than 30,000 cities globally. Consequently, the issues associated with UHI have become a significant concern globally. Researchers face the challenge of analysing UHI trends and developing strategies to adapt to and mitigate the serious challenges posed by urban heat islands, including energy poverty, carbon emissions, and human comfort, among others.

1.2 Statement of problems

Urban heat island mitigation strategies such as green roofs, cool roofs and cool pavement have long been recognised as effective approaches to improve building energy efficiency, reduce associated carbon emissions, and continuously improve occupant living standards in terms of improved indoor comfort level, and air quality.

However, the obstacles to UHI mitigation are also multi-dimensional and vary primarily according to the local climatic conditions, city characters, building typologies and energy usage by occupants. Thus, determining the most effective UHI mitigation strategies to achieve a sustainable future in cities is a pressing issue and will have an immediate impact on the city in terms of microclimate, micro-environment, economics and human life quality. However, it is apparent that several limitations exist in UHI mitigation strategies.

Most research [6] [7] only uses ambient temperature change to evaluate the efficiency of UHI mitigation strategies and did not analyse the change of radiation or other meteorological parameters. For example, a study [7]was conducted to evaluate the effectiveness of several UHI mitigation strategies in three locations in Toronto. The study found that using the cool pavement, cool roofs, and adding urban vegetation can significantly reduce surface temperatures

and contribute to UHI mitigation. The combination of these techniques can lead to a "cool city" model that can reduce outdoor air temperature by 3.3-4.6 °C. However, the other meteorological parameters have not been considered when assessing the effectiveness of UHI mitigation strategies such as the sky view factor which can affect the intensity of UHI. Therefore, there is a lack of a coupled meteorological assessment system to analyse UHI mitigation.

Besides, some studies [11] [12] [13] [15] [16] only analysed the effectiveness of UHI mitigation strategies without assessing the urban building energy consumption change, human comfort or carbon emissions. Additionally, some research [16] [18] only focused on the single reference building to predict UHI mitigation strategies on building energy consumption, ignoring the dynamic interaction of outdoor air among buildings in a neighbourhood. Moreover, various studies [12] [18] [19] [21] adopted field measurement experiments and observation meteorological data to analyse the UHI mitigation strategies the building energy consumption. However, the experiments are usually conducted from 24 hours to a few days and did not account for the long-term influence of UHI and energy consumption. Furthermore, several research [15] [17] [20] only analysed the effects of UHI mitigation strategies on individual building energy performance by adopting existing meteorological data, such as the EPW files, which are usually collected and managed by the rural weather station and do not accurately reflect the urban microclimate situation in the city centre [22]. Therefore, there is a lack of a comprehensive understanding of the relationship between UHI, energy use, carbon emissions and human comfort.

Furthermore, the current body of research falls short in providing insight into effective methods of utilising and preserving excess heat in urban centres to

mitigate the intensity of UHI. Thermal energy storage (TES) technologies have been developed to store thermal energy for later use. These technologies have gained significant attention in recent years due to their potential to reduce peak loads and conserve energy [26] [27] [28] [29]. Despite the potential of TES technologies to mitigate UHI effects by absorbing and storing thermal energy, there is a lack of analysis on their effectiveness on various aspects of UHI phenomena, such as energy consumption, carbon emissions, economics, and human comfort.

1.3 Aim and objectives

Based on research background and current challenges, this PhD research aims to investigate the most effective urban heat island mitigation strategies in subtropical cities, seeking to improve human thermal comfort, reduce energy consumption and carbon emissions, and promote sustainable urban development in subtropical regions.

To achieve the aim, the following specific objectives have been established:

1. A comprehensive literature review of the development of UHI in subtropical cities and the mechanisms affecting the microclimate were carried out.

2. An impact assessment modelling of different UHI mitigation strategies for the selected subtropical city was undertaken based on different green coverage ratios and urban fabric albedo.

3. A comprehensive model for mitigating subtropical UHI in the research area was developed by considering urban building energy use, human thermal comfort, and carbon emissions.

4. An advanced model for analysing the feasibility, building energy and city micro-environmental prediction of thermal energy storage technologies as urban

heat island mitigation strategies were produced.

5. A case study to evaluate the effectiveness of the developed UHI mitigation strategies in a selected subtropical city was carried out by assessing their impact on human thermal comfort, energy use, carbon emissions, and sustainable urban development.

1.4 Novelty of the research

1.4.1 Performance determination of UHI mitigation strategies by comprehensive meteorological assessment

While previous methods and models have utilized meteorological parameters as assessment criteria, a comprehensive meteorological assessment has yet to be established for accurate UHI intensity estimation. In this study, the effectiveness of UHI mitigation technologies is evaluated using comprehensive meteorological criteria, which include ambient temperature, radiation, and sky view factor. A more thorough analysis is required to review these aspects, identifying the reasons why specific UHI mitigation strategy models were selected and the respective advantages and disadvantages of each.

1.4.2 Rapid and accurate prediction of the relationship between UHI mitigation strategies with energy use, carbon emissions, and human comfort in the subtropical city centre

This doctoral thesis introduces the UHIMS-ECHE model (urban heat island mitigation strategies-energy consumption, carbon emissions, human thermal comfort and economic analysis), which predicts and evaluates the effectiveness of urban heat island (UHI) mitigation strategies at the city level. Unlike previous studies that focused on individual buildings or neighbourhoods, the UHIMS-ECHE model considers the broader urban context and quantifies the effects of

mitigation strategies on a city-wide scale. The model integrates a range of data sets and advanced algorithms to accurately predict the impacts of UHI mitigation strategies on building energy consumption, carbon emissions reduction, thermal comfort enhancement, and economic benefits. The UHIMS-ECHE model represents a significant advancement in urban sustainability research and provides a comprehensive approach for policymakers and urban planners to adopt effective and efficient UHI mitigation strategies.

1.4.3 Thermal energy storage technologies as urban heat island mitigation strategies

UHI is characterised by the storage of massive amounts of thermal energy in urban objects and materials with impervious surfaces that have a higher capacity for heat absorption. This PhD research analyses the effectiveness of thermal energy storage technologies as strategies to mitigate UHI in urban areas.

1.5 Scope of the research

In this study, the effect and performance of different urban heat island mitigation strategies are investigated, focusing on the following points:

(1) The impact of different building materials and design features on urban heat island mitigation. For example, exploring the use of green roofs, reflective surfaces, and ventilation systems in buildings to reduce the urban heat island effect.

(2) The impact of UHI mitigation strategies on air quality. This could involve exploring how UHI mitigation strategies may impact air quality by reducing the formation of ground-level ozone and other pollutants, as well as examining potential trade-offs between UHI mitigation and air quality goals.

(3) The relationship between urban heat island mitigation strategies and public health. For example, examining the impact of extreme heat on vulnerable populations, such as the elderly and those with pre-existing medical conditions, and how mitigation strategies can be tailored to address their needs.

(4) The potential for thermal energy storage technologies in UHI mitigation efforts. This could involve exploring how thermal energy storage technologies can be involved in monitoring the urban heat island effect and implementing mitigation strategies, as well as examining the potential of thermal energy storage technologies on the success of UHI mitigation.

1.6 Research methodology

In this thesis, the methodology is mainly based on the following stages:

1.6.1 Background investigation and literature review

The challenges of mitigating urban heat islands in tropical city centres have been studied and compared. A literature review was conducted to understand the causes and effects of UHI, as well as the main approaches for studying it. The development of UHI intensity and assessment criteria were also reviewed. The literature review analysed previous research on UHI mitigation strategies that focus on urban building energy use, carbon emissions, and human thermal comfort, to identify the advantages and drawbacks of existing modelling concepts. The review of thermal energy storage technologies aimed to assess their performance and limitations, and to analyse the relationship between thermal energy storage and UHI mitigation.

1.6.2 Modelling analysis

To conduct a comprehensive assessment of urban heat island (UHI) mitigation strategies, it is imperative to employ robust and reliable tools that can provide

accurate predictions and evaluations. In this regard, the software ENVI-met has been selected to assess the effects of various mitigation strategies on subtropical UHI. The research area will be subjected to different scenarios with varying green coverage ratios and urban fabric albedo to investigate the effects of these strategies on UHI. The main criteria of assessment will include temperature and radiation, among others.

Furthermore, an hourly parametric model known as UHIMS-ECHE has been developed using the software rhinos and grasshopper. This model will consider various factors such as urban building energy use, carbon emissions, human comfort, and economics to investigate the effectiveness of UHI mitigation strategies comprehensively. By using the UHIMS-ECHE model, it will be possible to identify the most effective strategies for mitigating UHI while considering their economic viability and environmental impact.

Additionally, an advanced UHIMS-ECHE model will be developed to explore the relationship between thermal energy storage and UHI. This model will provide valuable insights into how thermal energy storage can be effectively used to mitigate UHI in subtropical regions. By employing these sophisticated models and tools, it will be possible to conduct a comprehensive assessment of UHI mitigation strategies and identify the most effective approaches for mitigating UHI in subtropical regions.

In conclusion, this study will employ advanced modelling tools and techniques to evaluate the effectiveness of various UHI mitigation strategies comprehensively. The findings of this study will provide important insights into how UHI can be mitigated in subtropical regions while considering economic and environmental factors. This study will contribute to the development of

sustainable urban environments and enhance our understanding of the complex interplay between urbanization, energy use, and climate change.

1.6.3 Modelling operation, validation, and uncertainty analysis

To ensure the operability and universality of the novel model, the use of case studies was implemented. The incorporation of case studies allowed for the evaluation of the model performance in various conditions. Additionally, a field measurement was conducted within the research area to validate the accuracy of the model.

This approach serves to provide robustness to the model, ensuring that it can be applied to a range of scenarios. The inclusion of case studies allows for the exploration of the model's applicability and performance across a variety of contexts. Moreover, the field measurement provides a practical validation of the model's accuracy, giving confidence in its potential use.

The use of case studies offers a valuable methodological approach for testing and refining the model. It provides an opportunity to examine the model's efficacy in real-world scenarios, which can provide critical insights into its performance. The field measurement further contributes to the validation process, ensuring that the model's accuracy is verified within a relevant context. Overall, the adoption of case studies and field measurements strengthens the novel model, increasing its practical applicability and theoretical soundness. Through this approach, the model capabilities can be confidently assessed and applied in various settings.

1.7 Thesis structure

The thesis consists of five main chapters to ensure a systematic investigation of the urban heat island and its mitigation strategies. This thesis follows rigorous

logic, starting with a deep understanding of the urban heat island and its mitigation strategies, followed by an assessment of the efficiency of these strategies. Finally, the negative impacts of UHI are thoroughly analysed to provide a comprehensive understanding of the issues, ultimately leading to the solution of the problem through advanced and novel technologies. The thesis structure is illustrated in Fig. 1-2.

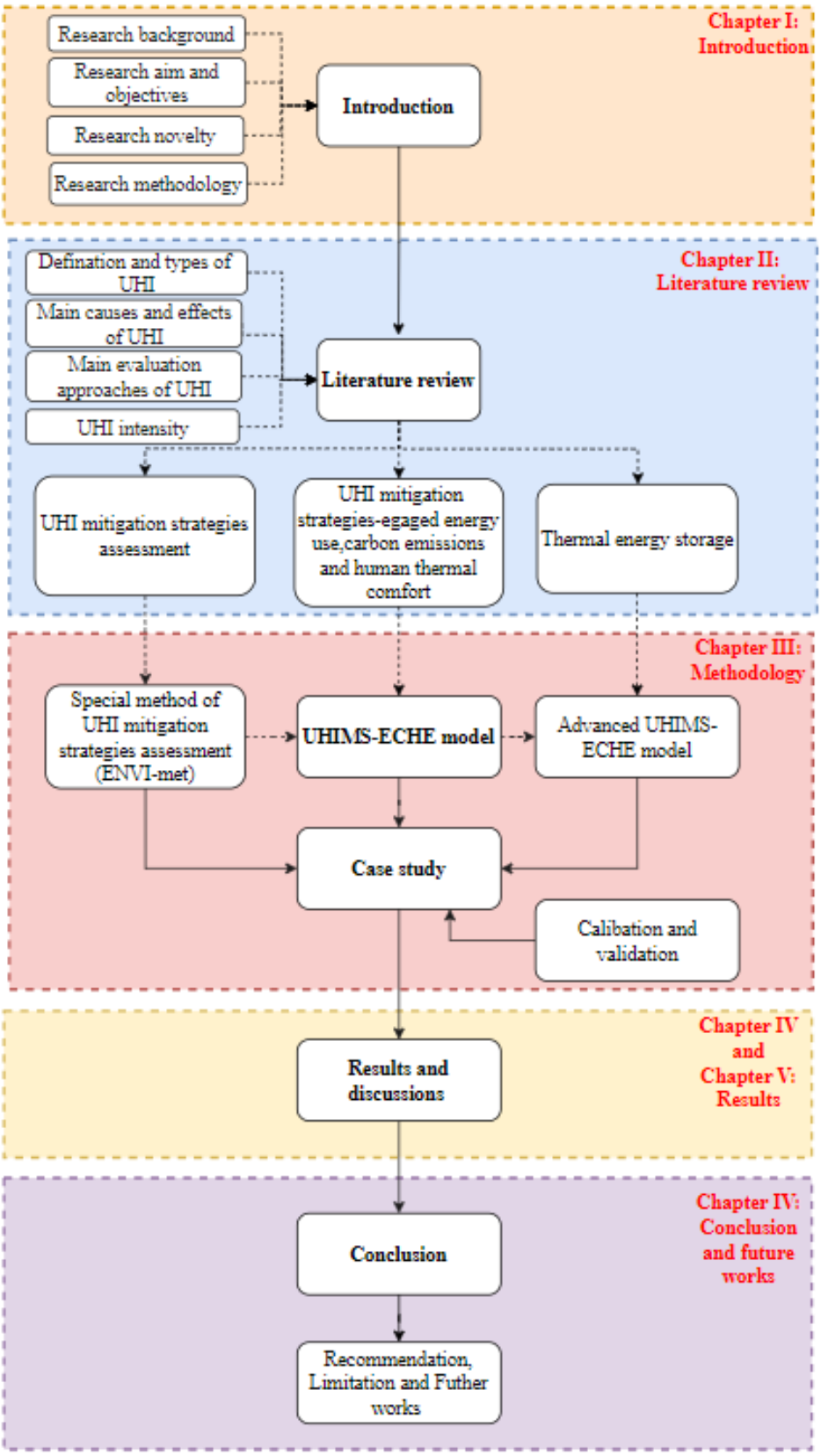

Figure 1-2 Structure of the thesis

The research structure details are summarised below:

CHAPTER I: Introduction: This chapter provides an introduction to the research, including a statement of the background, motivation, aims and objectives, novelty, scope, and main methods of the thesis.

CHAPTER II: literature review: This literature review covers various aspects of UHI, including its definition, causes, and effects. The main conventional mitigation strategies for UHI are also reviewed. The review examines the relationship between UHI mitigation strategies and urban building energy use, carbon emissions, and human comfort. Finally, the review discusses the current development of TES technologies for urban cooling as a potential solution to mitigate UHI, due to the limitations of conventional strategies.

CHAPTER III: Methodology: ENVI-met software is used to simulate these conventional mitigation strategies to comprehensively determine the effects in meteorological parameters. Additionally, an innovative and comprehensive model is proposed to analyse the relationship between UHI mitigation strategies with urban building energy use, carbon emissions, human comfort and economic analysis (UHIMS-ECHE). The UHIMS-ECHE is a more accurate and universally feasible model workflow based on a taxonomic literature review that can model the integration effect between urban building energy consumption, carbon emissions and human comfort and conventional or novel UHI mitigation strategies.

CHAPTER IV: Research results: findings of a study that analysed simulation results to evaluate the effectiveness of UHI mitigation strategies are presented. The study simulated the effects of conventional UHI mitigation strategies on energy use, environment, and human comfort and presented the results. The

study also examined the potential of TES technologies to mitigate UHI and analysed the association between TES technologies and UHI mitigation strategies through modelling, calibration, and validation.

CHAPTER V: Conclusion, recommendation and future work: the main conclusions and discussions of this thesis, along with suggestions for further research and future directions are presented.

2 CHAPTER II: LITERATURE REVIEW

2.1 Introduction

Several factors such as urbanisation, migration of population into cities, etc., have led to the creation of urban heat islands, thus resulting in significantly higher temperatures in urban areas than in surrounding rural areas. UHI can have detrimental effects on human thermal comfort levels, energy consumption in buildings, and carbon emissions. This chapter was therefore aimed at providing a comprehensive literature review of existing mitigation strategies and technologies to establish their limitations and towards achieving effective strategies for sustainable building designs. The review examined the impact of the existing strategies on meteorological parameter variations, building energy use, carbon emissions, and human thermal comfort. The review also covered energy storage technologies, low-carbon cooling systems, and their integration into the processes of sustainable building designs.

2.2 The types of urban heat island

UHI is a complex phenomenon that exhibits a variety of types, and through extensive research, it has been classified primarily into two categories based on the location and source of the temperature increase, namely Atmospheric Urban Heat Island (AUHI) and Surface Urban Heat Island (SUHI). [8]. AUHI is classified into urban canyon layer UHI and urban boundary layer AUHI. Table 1 shows the comparison between AUHI with SUHI.

SUHI: This type of UHI refers to the increased temperature at the surface of urban areas, including roads, buildings, and other man-made structures. The elevated temperatures of the urban surface result from the high density of heat-absorbing materials, such as concrete and asphalt, as well as the absence of

natural features such as vegetation and water bodies, which provide shade and evaporative cooling [9].

AUHI: This type of UHI is characterized by elevated temperatures in the lower atmosphere above urban areas, due to the emission of heat from human activities and the concentration of air pollutants. The increased heat emission from buildings, vehicles, and industrial processes leads to a reduction in the vertical mixing of the atmosphere and an increase in atmospheric stability, leading to a localized increase in temperature [10]. The combination of the urban canyon layer and the urban boundary layer contributes to the AUHI effect. The urban canyon layer traps heat and limits cooling, while the altered airflow patterns and reduced mixing in the urban boundary layer contribute to the retention of heat and pollutants near the surface [11].

Table 2-1 The comparison of AUHI and SUHI [12]

	Urban canyon layer AUHI	Urban boundary layer AUHI	SUHI
Concept	The surface energy balance that influences the air volume inside the canyon through sensible heat transfer from the surface	The extension of urban heat into the UBL by the entrainment of warmer air from above the UBL.	Higher air temperature in an urban area during hot summer days due to intense solar radiation on heat-absorbing materials.
Temporal development	Occurs during the night, pronounced diurnal variations.	Occurs during both day and night and decreases linearly with the height of UBL	Occurs during both day and night, highest intensity during the daytime
Spatial coverage	Local-scale with limited coverage (1-10km)	Meso-scale with high coverage	Micro-scale with limited coverage (1-100m)
Measuring techniques	Stationary weather station	Temperature sensor	Remote sensor and GIS application
Presentation methods	Temperature graphs and isotherm maps	Temperature graphs	Thermal images
Impacts	Energy and water use, thermal comfort and air quality.	Local air circulation and quality, Precipitation and thunder storm activity	Human thermal comfort, air quality, energy consumption, even local ecosystems.

AUHI occurs due to the accumulation of hotter air in urban areas compared to the cooler air in rural surroundings [8]. The AUHI is categorised into the urban canopy layer (UCL) UHI and the urban boundary layer (UBL) UHI (Fig.2-1).

UCL is extended closest to surfaces of cities, whilst the UBL is above UCL level in a few kilometres. The UCL contributes microscale climate conditions and the UBL contributes mesoscale climate conditions [13]. UCL-AUHI mainly occurs in the urban layer below the tops of trees and roofs, while the UBL-AUHI occurs from the rooftop or treetop level up to the level where urban buildings or trees no longer influence the atmosphere [14].

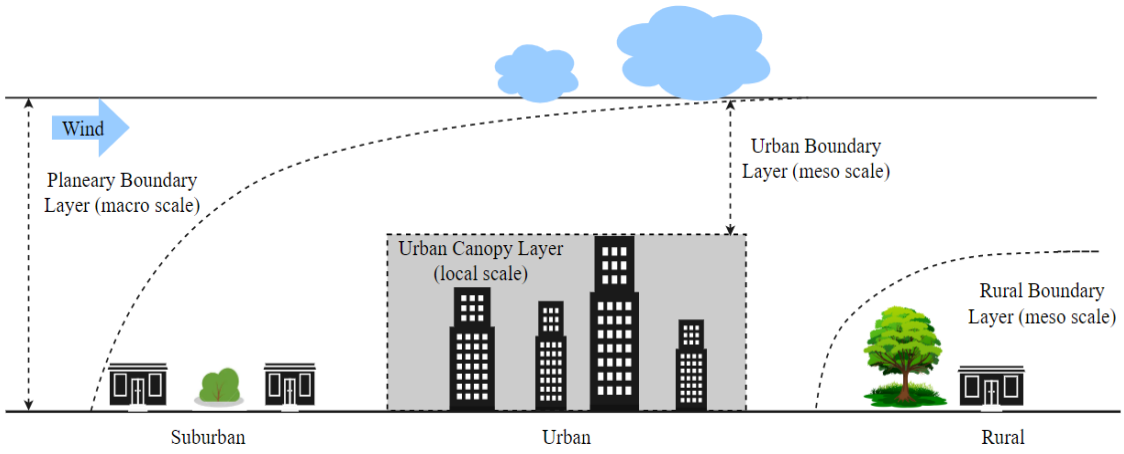

Figure 2-1 The different layers of the urban atmosphere [15]

2.3 Main causes of urban heat island

Several causes can be attributed to the occurrence of UHI in urban areas. The UHI effect is intensified by altered urban microclimates with reduced vegetation and evapotranspiration, increased solar absorption, low albedo, impermeable surfaces, and anthropogenic heat [16]. Fig.2-2. illustrates the relationship between atmospheric heat, increased use of manufactured materials, and various other factors that contribute to the UHI.

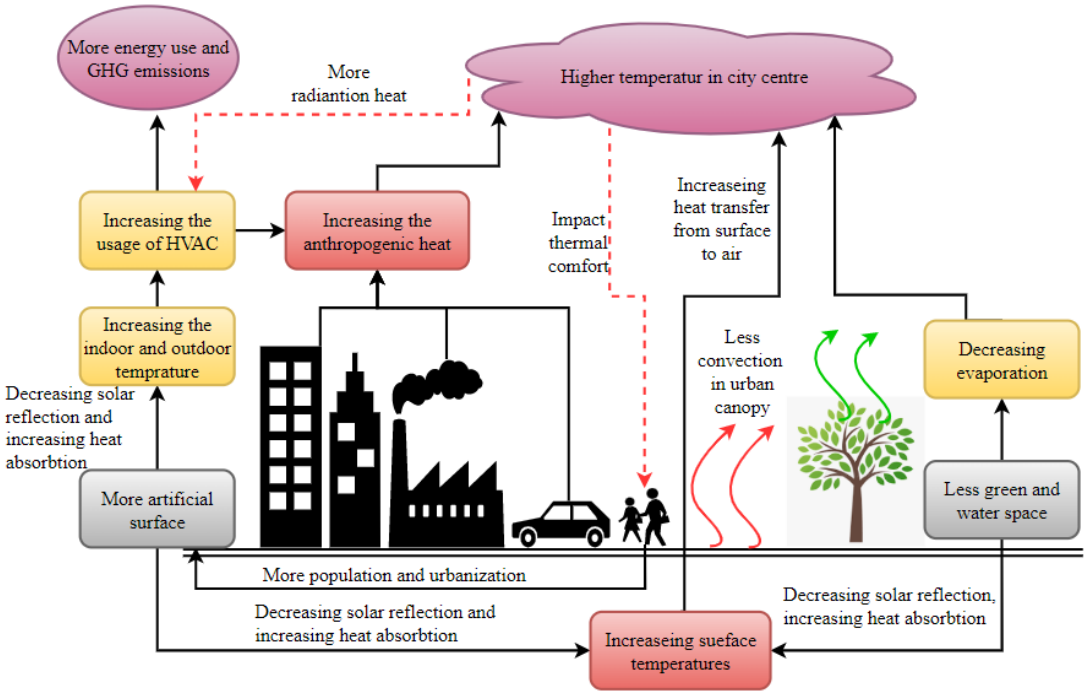

Figure 2-2 Main occurs and effects of UHI [16]

2.3.1 Artificial material

Firstly, the widespread use of construction materials with greater heat storage capacity and low albedo contributes to UHI. These manufactured materials in the building and pavement, characterised by low albedo and higher thermal admittance, can capture, absorb and store the shortwave radiations during the day time and release the absorbed and stored energy by longwave radiations during the night time [17]. Asphalt is widely used as the surface of the pavement, covering 95% of roads in the UK [18] and 94% in the USA [19]. Asphalt pavement can absorb approximately 95% radiation with a thermal conductivity of around 1- 2 W/mK, resulting in a relatively low albedo and high affinity for thermal absorption and conductivity [16], the surface temperature can reach up to 60°C in summer [20] [21] [22].

2.3.2 Less green space

Increased manufactured materials are associated reduction of vegetation and

green space in urban areas is also another important factor influencing the UHI. It can result in a lack of evapotranspiration as well as increased ozone concentrations [6]. There is a significant temperature difference between the most and the least green spaces, such as 2℃ in New York City[23], 2-3℃ in Mexico city [24] 4.01℃ in Singapore [25], 5.26-7.32℃ in Suzhou China [26].

2.3.3 Narrow urban street canyon

The deep urban canyon and intricate street geometry that have a higher height-to-width ratio of the street (Fig.2-3.) can have a substantial impact on UHI by the impeded release of sensible and latent heat, enhancing the penetration of short-wave radiation into the canyons, and result in the increase in energy absorption [27].

Besides, the narrow street canyon can block the natural airflow, leading to stagnant air and reduced ventilation. This can trap heat and pollutants, exacerbating the UHI effect. Moreover, the vertical walls of the buildings in a street canyon create a larger surface area for solar radiation to be absorbed, leading to increased surface temperatures [28]

During the diurnal cycle, urban environments tend to exhibit higher heat retention compared to rural areas. This is due to the reduced sky view factor and constricted street canyons, which impede the cooling rate in urban areas. Conversely, rural objects are characterised by rapid heat loss during the night time, attributed to the greater sky view factor and open exposure [29].

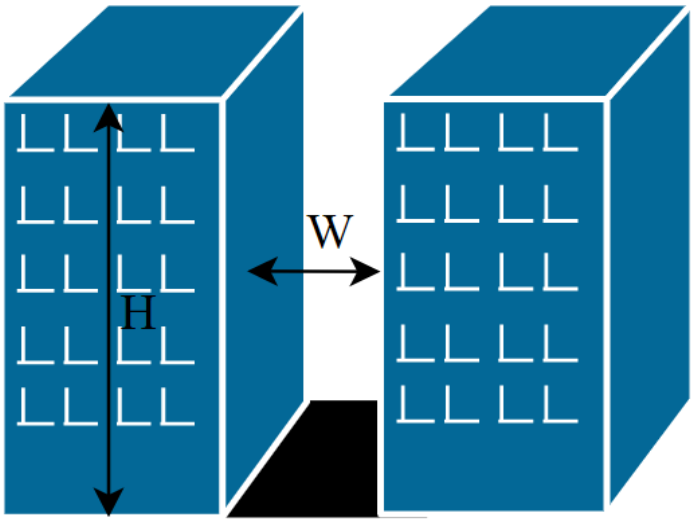

Figure 2-3 Streets with narrower widths (W) and taller buildings height (H)

2.3.4 Increased population and urbanisation

Anthropogenic heat release has been identified as a significant contributor to the intensification of the urban heat island (UHI) phenomenon, Previous research [30] [31] [32] demonstrates a positive correlation between population density in urban centres and the severity of the UHI. Besides, over the last decade, the world has added approximately one billion population and increased population, implying that the world's population numbered is over 8 billion. Based on the medium-variant scenario, indicate a further increase to 11.2 billion by the end of the century [33]. Table 2-2 shows the population trends for the world and various regions.

Table 2-2 Globally population trends [33]

Region	Population in 2030	Population in 2050	Population in 2100
World	8551	9772	11184
Asia	4947	5257	4780
Africa	1704	2528	4468
Europe	739	716	653
Latin America and	718	780	712

the Caribbean			
Northern America	395	435	499
Oceania	48	57	72

The 2018 Revision of World Urbanization Prospects highlights the rapid growth of the urban population, which increased from 751 million in 1950 to 4.2 billion in 2018 [33]. This remarkable increase in the global population has led to the emergence of new megacities, while existing ones have experienced a significant rise in population density. Conversely, the rural population has grown at a much slower pace. As presented in Table 2-2, Africa and Asia are the regions experiencing the most concentrated population growth.

Currently, Tokyo (35.6895°N, 193.6917°E) is the largest city in the world, with an estimated population of 37 million. It is followed by New Delhi (28.6139° N, 77.2090° E), which has 29 million inhabitants, Shanghai (31.2304° N, 121.4737° E) with 26 million, and Mexico City (19.4326° N, 99.1332° W) and São Paulo (23.5505° S, 46.6333° W), both with approximately 22 million inhabitants [33]. All of these cities are located in the tropical (23.5 °N and 23.5° S) or subtropical (up to 30° N and 30°S) climate zone. Therefore, investigating the subtropical UHI is crucial for a comprehensive understanding of the global UHI phenomenon.

Fig. 2-4. presents the world map of climate classification, based on the Köppen-Geiger climate classification system, revealing four sub-climate types in tropical climate as defined by this map Tropical Rainforest or Equatorial (Af), Tropical Monsoon (Am), Tropical Dry summer (As) and Tropical Dry summer winter (Aw) [34].

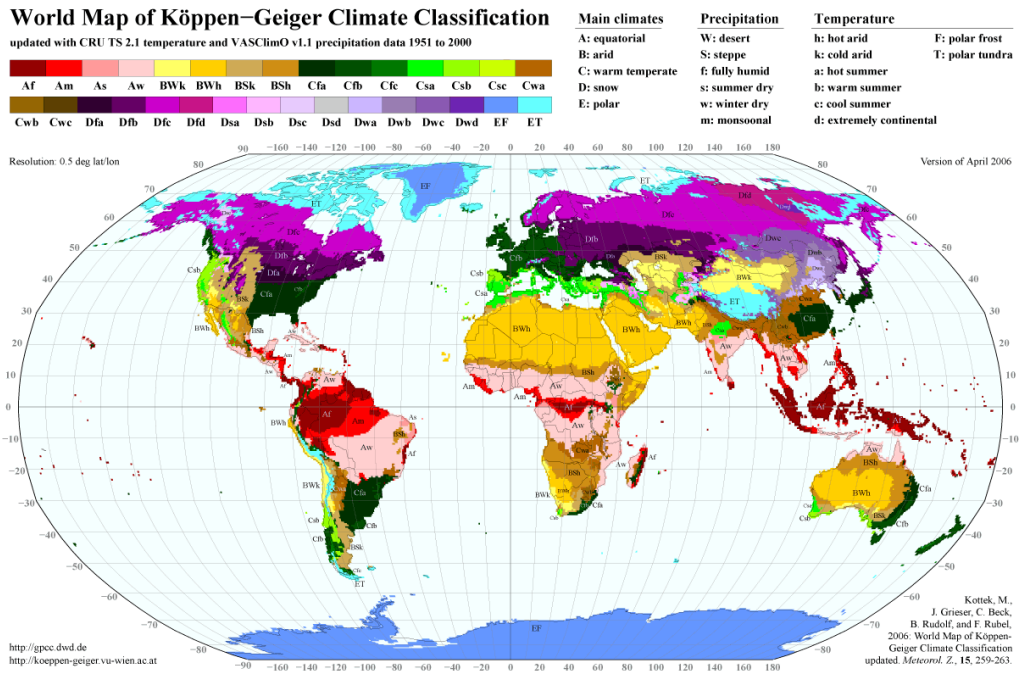

Figure 2-4 The world map of climate classification [34]

2.4 Main urban heat island effects

The development of the UHI is a result of urban construction and human activities. The UHI increase lands to increase land surface temperature, affecting the influence of material flow and energy flow, also exerts a series of ecological and environmental effects on urban climates, urban hydrologic situations, soil properties, atmospheric environment, biological habits, material cycles, energy metabolism and human health [35].

2.4.1 Urban heat island impacts energy consumption

Building energy consumption is influenced by multiple factors such as ambient temperature, building characteristics, performance and occupancy behaviour [36, 37] [38] [39]. Among those factors, the ambient temperature is one of the most important factors that directly drives the operation of the cooling and heating system, which influences the corresponding building cooling and heating energy consumption [39]. Previous studies show that UHI can significantly increase

energy use, especially can increase cooling energy consumption [40] and increase peak energy demand [41] by increased using air conditioning [36]. Existing study studies report the response function for the peak energy demand and the hourly, daily, monthly or annual energy consumption, and also show that The intensity of UHI increase can rise peak energy demand and increase energy consumption [42]. Table 2-3 summarises the existing literature concerning the impact of ambient temperature on peak energy demand or energy consumption.

Table 2-3 Impact of ambient temperature on the peak energy demand or consumption

Research area	Increased peak load per ℃	Percentage increase of base electricity load per degree of temperature increase	Threshold inflexion temperature	Ref.
Thailand	Additional Peak demand of 810 MW/℃	4.6%	N/a	[43]
Athens, Greece	Increase the daily energy consumption of 1300 MW h/℃	4.1%	22	[44]
New Orleans, USA	Increase the daily average electrical load by 15 MW h/℃	3%	22	[45]
Hong Kong, China	Increase the monthly consumption by 111 GW h/℃	4%	18	[46]
Louisiana	Increase the monthly consumption by 40 kW h/person/℃	8.5%	20	[47]
Maryland, USA	Increase the monthly electricity consumption by 22 kW h/p/℃ for the residential sector	8.5%	15.6 °C for residential and 11.7 °C for commercial	[48]
Singapore	Hourly electricity	1. 2%	N/A	[49]

	demand crease			
California, USA	Increase of the monthly consumption by 27 kW h/°C	7. 7%	17	[47]

2.4.2 Urban heat island impacts on outdoor air quality

UHI has been shown to significantly impact outdoor air quality in cities [50]. The high temperatures in the city centre facilitate photochemical reactions in ambient air, which result from chemical interactions between nitrogen oxides and hydrocarbons, resulting in the formation of tropospheric ozone [51]. Numerous studies [52] [53] [54] have demonstrated a substantial association between the formation of tropospheric ozone and high ambient temperature. In addition, the formation of ground ozone is influenced by several factors, including ambient temperature, solar radiation intensity, concentrations of nitrogen oxides and volatile organic compounds, and the ratio of volatile organic compounds to nitrogen oxides [53]. High-ground ozone concentrations are strongly associated with the UHII [55] [56] [57]. Research has indicated that a 1°F increase in temperature corresponds with the days exceeding the ozone thresholds increase by 10% [58] and 18% [53]. Furthermore, a linear correlation between the ozone concentration and the ambient temperature in the city centre. Some research [59] [60] [52] has shown that while the ozone concentration is low in rural areas, it is twice as in the city centre.

In addition to impacting air quality, UHI affects the air flow and turbulent exchange leading to increased concentration of air pollutants [61]. Studies [62] [63] [64] have shown the effect of UHIs on the concentration of atmospheric particulate matter (PM). Increased PM concentration results from increased aerosol-radiation interaction, with increased temperature [65].

Moreover, building energy consumption primarily depends on domestic electricity load for air conditioning and other cooling systems generated from fossil fuel combustion [66]. This increased energy use rises carbon emissions of energy in coal-fired power plants, and thus, UHI directly impacts the carbon emissions. A study conducted in London predicted the CO2 increase by 13-15 % due to UHIs [67]. Besides, high energy use and carbon emissions cause high energy bills. 12-year research [68] analysed the cost that UHI imposes on the $120B residential market with CO2 emissions that exceed 550 M tons in 48 US states. The results indicated that, on average, a 1°C increase in UHI intensity leads to a 40% increase in UHI energy costs, while a 1°C reduction results in a 46% decrease in UHI energy costs. Another 5- year study [69] was carried out in the urban and rural in Baltimore city, and the results showed that atmospheric CO_2 was consistently and significantly increased, on average, by 66 ppm from the rural to the urban site.

2.4.3 Urban heat island impact on human health

Research has exposed that both high and low temperatures can be associated with illness [70] [71]. UHIs represent a noteworthy form of anthropogenic environmental modification, constituting a threat to human health of considerable magnitude. When exposed to temperatures beyond a certain threshold, the human thermoregulation system is unable to counteract the impact of extreme heat, leading to increased indoor and outdoor discomfort [72], and even morbidity and mortality [73]. The human body gains heat by absorption from radiation from the sun and sky and losses heat through respiration and evaporation from the skin. The negative impacts of UHI are able to effect respiration and evaporation of the human body [6], leading to heat syncope,

cardiovascular stress, thermal exhaustion, heart stroke and cardiorespiratory diseases [67]. An investigation was conducted to examine the association between mortality and UHIs, revealing that UHIs had a discernible impact on heat-related fatalities, with an estimated rise of 1.1 deaths per million population [74].

The analysis of the intra-urban variability in heat-related health problems is important as cities are characterised by spatial variabilities in the exposure and spatial variabilities related to the distribution of vulnerable populations [75]. UHI can result in higher ambient temperatures affecting socioeconomic, demographic and health problems and leading to differences in urban vulnerability between the neighbourhoods in a city [76].

There is a well-established association between the local thermal environment and demographic and socioeconomic risk factors. Results indicate that individuals belonging to lower socioeconomic groups are more susceptible to the impacts of heat stress, as they are more likely to reside in urban areas characterized by elevated levels of UHII, reduced vegetation cover, and high population density [77]. Thus, the examination of heat-related health outcomes in cities necessitates a holistic consideration of the interplay between thermal, social, economic, and demographic factors. Table 2-4 summaries the main characteristics and results of intra-cities heat-related mortality with UHI.

Table 2-4 Intra-cities heat-related mortality with UHI

Location	Population concerned	Research period	Outcome	Considered factors	Remark	Ref.
Lisbon, Portugal	All population	1998 to 2008	All-cause mortality	N/a	For universal thermal climate index (UTCI) > 24.8°C, mortality is 14.7, 5.4, 5.1%, and 3.0%/deg.	[78]
Michigan, USA	All population	May to Sept 1990 to 2007	Cardiovascular Mortality	Socioeconomic factors	Cardiovascular mortality during extreme heat events was higher by 39% in the city without green spaces.	[79]
Berlin, Germany	All population	Heat wave 1990 to 2006	All mortality	Socioeconomic factors	Significant correlation between the number of deaths and the proportion of land covered by impervious surfaces during heat waves	[80]

London, UK	All population	May 26th–July 19th, 2006	All mortality	N/a	The strong relationship between UHI and heat-related mortality	[81]
Shanghai, China	All population	Heat waves 1998 to 2004	All mortality	N/a	The maximum additional heat mortality, (27 deaths/million), was reported in Shanghai during the 1998 heat wave and for a heat island intensity close to 3 ℃	[82]
Western Europe	All population	May to August 2003	All mortality	N/a	More than 70,000 additional deaths occurred in Europe during the summer 2003.	[83]

Overall, Studies have shown that urban areas, owing to their positive thermal balance and the presence of the UHI, exhibit a higher incidence of heat-related morbidity when compared to rural or suburban regions [74]. The UHI is responsible and has been identified as a contributor to elevated levels of heat-related mortality, with a range of an additional death between 1.0 to 27 per million of the population [84]. Research has also indicated a significant the UHII increased, and heat-related mortality increases considerably [70].

2.4.4 Impact of urban heat island on vulnerable and low-income population

It is widely accepted that UHI exhibits a strong correlation with biophysical and socioeconomic vulnerability [85] [86] [87]. Several studies [88] [81] [89] have investigated the association between high ambient temperatures in cities and socioeconomic factors such as income, education, racial characteristics, quality of housing, etc. The results have consistently indicated that low-income populations are disproportionately affected by UHI, residing in areas with elevated levels of heat stress and poor thermal quality buildings [89].

Furthermore, low-income and vulnerable populations live in low thermal-quality buildings [90], and the cooling energy bill induced by UHI is higher than that of the rest of the population [91]. Given that the cost of air conditioning is a serious additional burden for the low-income population, most of them cannot afford space cooling [92]. Table 2-5 presents in a tabulated form the main impact of UHI on low-income and vulnerable populations.

Table 2-5 Main impacts of UHI on low-income and vulnerable population

Location	Research Population	Research period	Weather data	Outcome	Considered factors	Remark	Ref.
London, UK	All population	26.05.2006-19.06.2006	Weather station	All cause mortality	House quality	Estimated UHI attributable deaths between 6.1 to 8.14 deaths per million of population. Dwelling characteristics cause a larger variation in temperature exposure and risk, than UHI	[81]
Hong Kong, China	All population	June to September 2001-2009	Weather stations	All cause mortality	Meteorological parameters and PM10 concentration	A 1 ℃ rise above 29 ℃ caused a 4.1% and 0.7% increase in mortality in high and low UHI zones correspondingly.	[93]

St Louis Missouri, USA	Older than 65 years old	Heat wave days 1980, 1983,1988 and 1995	One weather station	All-cause mortality	Age, Socioeconomic deprivation score	When UHII is 1℃, the risk of heat death by 1.004 and 1.070 when acclimatisation or no acclimatisation	[94]
Sydney, Australia	Older than 65 years old	Warm months 1993-2004	Field measurement	All-cause Mortality	Socioeconomic factors	10℃ temperature increased, 0.8-10%higher mortality risk.	[95]
Sao Paolo, Brazil	All population	1993 to1994	Three weather stations	Cardiovascular and Respiratory	N/a	Old people usually live in small old apartments with windows closed, that presented upper temperatures that were on average 2 to 4C higher than those at the other stations.	[96]

Paris, France	Older than 65 years	8-13 August 2003	LANDSAT surface T data	Mean Daily Surface Temp	Social factors and house	The odds ratio concerning the surface temperature around the dwelling was high, 1.82℃	[75]

2.5 Summary of urban heat island causes and effects

UHI phenomenon is the warming of urban areas relative to their rural surroundings. UHIs occur due to the interaction of various factors, including land use changes, urban morphology, anthropogenic heat emissions, and weather patterns. The main causes of UHIs are changes in land use, such as the replacement of vegetation with impervious surfaces like asphalt and concrete, and the construction of buildings, which reduce the ability of the urban landscape to regulate temperature through natural processes like evapotranspiration. Additionally, human activities such as transportation and industrial processes also contribute to UHIs by releasing heat into the environment.

The effects of UHIs include increased energy consumption for cooling, worsened air quality, and negative impacts on human health. UHIs also have ecological impacts, such as altering plant and animal species composition and behaviour and disrupting ecosystem services such as pollination and nutrient cycling. The UHI effect can also exacerbate climate change by increasing the demand for energy and contributing to greenhouse gas emissions.

2.6 Main evaluation approaches of UHI

Previous studies have employed a range of evaluation approaches, such as multi-scale phenomena, observational and simulation methods, to explore the existence of the UHI and potential mitigation strategies[17]. Table 2-5 presented an overview of the diverse approaches used to study UHI along with their respective limitations [97].

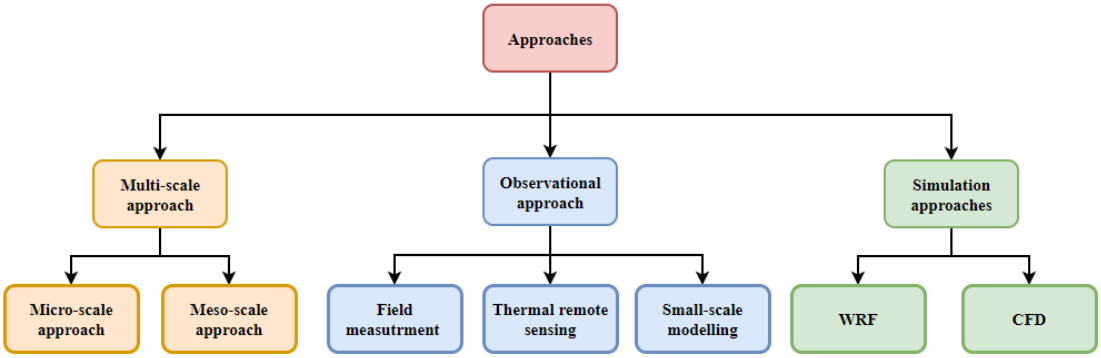

Figure 2-5 Approaches for studying subtropical UHI [97]

2.6.1 Multi-scale approach

The multi-scale approach is a commonly used method for investigating the UHI phenomenon. It involves examining the UHI effect across different spatial and temporal scales, from local to regional and from diurnal to seasonal. This approach has several advantages, including the ability to capture the complexity of the urban environment and provide a comprehensive understanding of the UHI phenomenon. The multi-scale approach includes small-scale processes (human metabolism) and mesoscale processes (atmospheric forces) to evaluate the overall urban thermal pattern [97]. However, there are some limitations to this technique. Firstly, the complexities of the multi-scale approach are to collect an inclusive and comprehensive database for the whole city. Secondly, there is an incompatible phenomenon that happened in the existing theories for analysing the UHI in each scale [98].

2.6.2 Observational approach

The observational approach is a commonly used method for investigating the UHI phenomenon. It involves collecting temperature data at different locations within an urban area to identify areas where the UHI effect is most pronounced. Observational studies can be conducted at different spatial scales and provide

accurate measurements of temperature at specific locations. However, this approach may have limitations related to the identification of the cause of temperature changes and the spatial and temporal resolution of the measurements. Despite these limitations, the observational approach remains an important tool for investigating UHI and has been used in numerous studies to provide valuable insights into the phenomenon. The observational approach includes field measurement, thermal remote sensing and small-scale modelling [97].

2.6.2.1 Field measurement approach

The field measurement approach involves a comparative analysis of near-surface temperature patterns between urban and rural areas, utilizing meteorological statistics obtained from weather stations to assess the urban heat island (UHI) effect in a city. The main variables considered in this approach are the near-surface temperature in urban areas, wind velocity, the concentration of pollutants in the air, and turbulence flow. The results obtained through this approach are primarily used to determine the spatial distribution and intensity of the UHI. Many studies have applied the field measurement approach to investigate the UHI and to determine the effect of building elements on reducing the UHI.

However, the field measurement approach as an independent approach also possesses certain limitations. Firstly, to achieve reliable results, comprehensive data must be collected, which is often costly and time-consuming, given the high cost of purchasing and installing measurement devices across a city. Secondly, due to the usage of a limited stationary network and relatively fewer measured parameters, the field measurement approach cannot identify the three-

dimensional spatial distribution of the quantities in the urban area comprehensively. Lastly, the results obtained through field measurement may not accurately reflect the UHI effect due to the influence of other parameters, making it difficult to correlate the data with the UHI effect, even with sufficient data collection [97].

2.6.2.2 Thermal remote sensing approach

The thermal remote sensing approach involves the use of satellite, airborne, and aircraft platforms to analyse the UHI effect and assess variables such as surface temperature, surface albedo, turbulent transfer from the surface, and surface emissivity. The remote sensing data provides an excellent opportunity to monitor and analyse the UHI effect in a city at a large scale. The thermal remote sensing approach provides an effective way to quantify the magnitude and spatial distribution of the UHI effect.

Researchers can compare the UHI effect in different cities using satellite data, which is readily available for most parts of the world. Satellite data has a high temporal resolution, which enables researchers to analyse the UHI effect over a long period, and thus study the seasonal and temporal variations of the UHI effect. The thermal remote sensing approach can provide valuable information on the UHI effect for city planners and policymakers.

However, the thermal remote sensing approach is costly, and collecting steady and complete images of urban surfaces can be challenging. The accuracy of the thermal remote sensing data is dependent on the spatial resolution of the data. The thermal remote sensing approach can provide useful information at a larger scale, but the spatial resolution of the data may not be sufficient to capture the

fine-scale variations in the UHI effect.

Additionally, the three-dimensional structures of urban environments can limit the vertical extent of the research area that can be fully captured. As a result, the UHI distribution must be extracted from thermal data obtained from a bird-eye point of view by using sensor-view models. Sensor-view models are used to simulate the view of a sensor from a particular location, which can help to extract the UHI distribution from thermal data [99].

2.6.2.3 Small-scale modelling approach

The small-scale modelling approach involves substituting the urban area with a small area model, which is then evaluated in a wind tunnel or outdoor setting to investigate the effect. This method can be used to verify, calibrate, and enhance mathematical models. However, ensuring the similarity between the small-scale model and the real outdoor environment is challenging [97]. Additionally, this approach enables the analysis of the influence of building environment parameters (such as pollution dispersion and dimensions) on a small urban area. Nevertheless, its utilization is limited due to its high cost, time-consuming nature, and complexity in experimentally creating thermal stratification [100].

2.6.3 Simulation approach

In addition to observational methods, a simulation approach has been developed to analyse the UHI phenomenon at a large-scale model. These simulation models simulate the physical processes that occur in the urban environment and can predict the temperature and other meteorological variables at different spatial and temporal scales. There are two types of simulation models commonly used to study UHI: meso-scale models and micro-scale models.

The Weather Research and Forecasting (WRF) model [101] [102] [103], a mesoscale model and the computational fluid dynamics (CFD) model [104], a micro-scale model, are both widely used models to simulate UHII.

2.6.3.1 Weather Research and Forecasting

The Weather Research and Forecasting (WRF) model is a state-of-the-art mesoscale numerical weather prediction system that has been designed for both atmospheric research and operational forecasting applications. The model is built upon a robust software architecture that supports parallel computation and system extensibility, enabling it to provide accurate and reliable predictions for a wide range of meteorological applications at the mesoscale [105].

The WRF model is composed of two dynamical solvers, namely, the Advanced Research WRF (WRF-ARW) [106] and the Non-Hydrostatic Mesoscale Model (WRF-NMM) [107]. These solvers are specifically designed to compute the atmospheric governing equations and provide accurate and reliable predictions for weather phenomena at the mesoscale.

In addition to its dynamical solvers, the WRF model also features a data assimilation system, which enables the model to incorporate real-time observational data and improve the accuracy of its forecasts. The data assimilation system is based on the ensemble Kalman filter method and is capable of assimilating a variety of observation types, including radar, satellite, and conventional observations [108].

The WRF model has been extensively tested and validated, and its performance has been shown to be superior to that of other mesoscale numerical weather prediction systems. The model has been used in a variety of meteorological

applications, including severe weather forecasting, air quality forecasting, and wind energy forecasting, among others [109]. The WRF model has a broad range of users, including atmospheric researchers, operational forecasters, and decision-makers in various sectors, such as agriculture, energy, transportation, and emergency management. Its versatility and accuracy have made it an essential tool for weather prediction and research in both academic and operational settings [106].

2.6.3.2 Computational fluid dynamics

Computational fluid dynamics (CFD) has proven to be a valuable tool for simulating UHI intensity at the microscale, as it provides more precise data on the distribution of UHI within and above building canopies compared to Urban Canopy Models (UCM). Unlike UCM, CFD does not segregate velocity and temperature fields and can solve all fluid governing equations simultaneously across the urban area [110]. However, CFD simulations are limited by the number of control volumes or nodes required to simulate the research area and are typically divided into different scales, namely meso-scale and micro-scale, depending on the specific application and the resolution required. Meso-scale models have horizontal resolutions ranging from one to several hundred kilometres, and the vertical resolution changes with the depth of the Planetary Boundary Layer (PBL), ranging from two hundred meters to two kilometres. Furthermore, the accuracy of meso-scale model predictions depends on data from the Land-Use Land-Cover (LULC). Conversely, micro-scale models resolve conservation equations within the surface layer, but due to high computational costs, are not applicable to an entire city. Consequently, micro-

scale models are horizontally limited to small areas, typically a few hundred meters. Unlike meso-scale models, micro-scale models do not have a comprehensive treatment of the PBL and lack atmospheric interactions. Table 2-6 provides a comparison of each simulation approach for UHI [98].

Table 2-6 Comparison of simulation approaches for UHI [111].

	UCM	Meso-scale	Micro-scale
Approach	Energy balance equation	WRF	CFD
Governing equation	1. Energy balance equation 2. An input assumption for the velocity equation of the canopy layer 3. Heat condition equation for surface	Navier–stokes equations (Including Coriolis term with hydrostatic or non-hydrostatic assumption) Monin–Obukhov for ground surface Heat conduction equation for soil	Navier–stokes equations Monin--Obukhov for surfaces of the urban structures (e.g. wall, ground) Heat conduction equation for surface
Limitations	1. Decoupled velocity field from temperature and moisture 2. Assumption of a city with a similar homogeneous array of buildings 3. Limited resolution of urban geometry 4. Only good for a steady-	1. Assumption of the urban canopy layer as roughness 2. Difficult to provide Land-Use Land-Cover database 3. Accuracy dependent on field measurement 4. Modelling of the turbulence	1. Not including the atmospheric phenomena 2. Difficult to create the database for canopy details 3. Providing boundary conditions 4. Modelling of the turbulence

	state solution 5. Neglecting the atmospheric effect 6. Empirical assumption for convective latent and sensible heat		
Maximum Domain Size	City	City	Building block
Spatial Resolution	1-10m	1-10km	1-10m
Temporal Resolution	Hour	Minute	Second

In summary, it can be elucidated that the Weather Research and Forecasting WRF and CFD models are numerical simulation tools that are employed to investigate atmospheric and fluid flow phenomena. Nevertheless, they are distinct in terms of their designated spatial and temporal scales, as well as the particular equations and numerical techniques utilized.

2.7 Urban heat island intensity

The measurement of urban heat island intensity (UHII) is based on the difference in temperature between an urban site and a rural site and is considered an indicator of the UHI effect [112]. However, the nature of subtropical UHI is complex and is influenced by climate change. The UHII varies in magnitude among different cities and is generally smaller in subtropical regions compared to temperate regions. Additionally, the urban-rural temperature differences in

subtropical UHI are often of the same magnitude as the intra-urban temperature differences, mainly due to the role of vegetation [113]. Roth (2007) [114] reviewed the findings of recent 10-year studies on subtropical urban climate and reported that the ratio of sensible heat to net radiation in rural areas was approximately 28%, while the corresponding ratio increased to around 40% in urban areas.

Moreover, the differences in incoming and outgoing longwave radiative flux between urban and rural areas result in a unique subtropical UHI. The intensity of air temperature-based UHI is strongest during pre-monsoon and monsoon nights, whereas the intensity of surface temperature-based UHI is only strongest during the daytime and pre-monsoon [115]. There are two ways to conduct UHII [116]: measuring the air temperature difference between an urban area and its surrounding rural area, or measuring the land surface temperature difference between an urban area and its surrounding rural area (LST) [117].

2.7.1 Air-temperature based UHII

Air-temperature based UHII encompasses differences in the pattern of air temperature between urban and rural settings. The air-temperature based UHII is an important indicator for evaluating urban heating. In general, UHII is determined by comparing the air temperature between an urban (Tu) and rural area (Tr) by Eq. (1).

$$UHII = \Delta T_{u-r} = T_u - T_r \quad (1)$$

AUHI further falls into one of two categories: The canopy layer and the boundary layer. Canopy layer UHI influences the atmosphere extending from the surface to mean building height or tree canopy, while boundary layer UHI accounts for air beyond the canopy layer. In most studies, air-temperature based

UHII studies are conducted using statistical analysis of weather station data, site survey data, or computer simulation.

2.7.1.1 Data from field measurement

The data on air temperature in urban and rural areas can be collected by field measurement. The field measurement consisted of two types of measurements: fixed station measurements and mobile transverse measurements. Fixed stations can be used for long-term measurements, while mobile transverse measurements can give a full picture of the detailed, spatial distribution of temperature. Some previous research has been collected and summarised in Table 2-7.

Table 2-7 UHII data from filed measurement

Research area	UHII	Method	Research period	Special issues	Ref.
Rotterdam agglomeration, Netherlands	The maximum UHII were found in summer, with 95% values ranging from 4.3 K to more than 8 K,	14 automatic weather stations	Three years (2010-2012)	The intra-urban variability in UHImax is significantly related to the building, impervious and green surface fractions, respectively, as well as to the mean building height.	[118]
Harrisburg, Pennsylvania, USA	The average yearly UHI was 2.25 °C.	20 weather stations (sensors)	June 1st 2014 to May 31st 2015	Relationships between mean UHII and distance to the river indicate that the river provides a warming effect during the UHI hours. For every 1000 m increase in distance from the river, the UHI will decrease by 0.6 °C in summer, 0.5 °C in fall and spring, and 0.3 °C in winter.	[119]
Chongqing, China	The maximum UHII in Chongqing was 2.5℃ at midnight.	Fixed weather stations and mobile transverse	June 2012 to January 2013	An urban cool island exists during the day time. local greenery space can mitigate UHI	[120]

		measurement.			
Rome, Italy	UHII up to 8℃	Five monitor	Summers of 2015 and 2016	he urban heat island increases the building cooling energy needs by 12% in the peripheral neighbourhood and by up to 46% in the city centre,	[121]
Hong Kong, China	UHII is 0.1 °C during the daytime 2.39 °C during the nighttime	12 HOBO weather station	3 days	Floor area ratio, building density and tree cover ratio have negative effects on daytime UHI.	[122]
Shenzhen, China	UHII varied between -1°C and 1.5 °C	9 data logger (HOBO U23- 002) and a GPS	From 9 am to 17 pm, during both the hottest and the coldest month	Spatial factors influencing UHI	[123]
Ulsan, Korea	UHII is 2.5 °C in summer 3.5°C in winter	44 data loggers (DS1922T)	12 months of 2016	The sky view factor (SVF) was positively related to daytime air temperature.	[124]
Tainan, Taiwan	UHII can be at least 3 °C every month and can reach up to 5 °C in the hot season daytime.	100 LOGPRO TR-32	N/A	The impermeable surface and urban development pattern affect UHI	

2.7.1.2 Data from weather station

The collection and organization of hourly data on ambient air temperature, relative humidity, wind speed and direction, radiation, and other relevant meteorological variables is an essential step in quantifying the urban heat island intensity (UHII) in a given area. Local weather stations are key resources for gathering this data, as they possess the necessary instruments and expertise to accurately measure and record these parameters over extended periods of time. To accurately calculate the UHII, it is necessary to compare the air temperature data collected from urban and rural areas, ideally over the same time period and under similar weather conditions. The temperature difference between the two areas can then be used as a proxy for the UHII, which is defined as the difference in temperature between an urban and rural area [125].

In addition to air temperature, other meteorological variables such as relative humidity, wind speed and direction, and radiation can also impact the UHII. For example, wind speed and direction can influence the transport of heat and pollutants within and between urban and rural areas, while radiation can affect the heating and cooling rates of different surfaces. Therefore, it is important to collect and consider data on these variables when quantifying the UHII [126]. Some previous research is summarised, as shown in Table 2-8.

Table 2-8 UHII data from the local weather station

Research area	UHII	Method	Research period	Special issues	Ref.
Bangkok, Thailand	The maximum UHII is	Four weather stations	During 2008-2012	Seasonal UHII is analysed	[118]

	around 6-7 °C during the dry season.				
Delhi, India	Diurnal UHII was from 2.8°C to 3°C.	Two local weather stations	January 2010 to December 2013	LULC influences UHII. UHI increases greenhouse gas emissions	[127]

2.7.1.3 Data from simulation

Previous studies have utilized software tools to model air temperature based on the urban heat island effect (UHII). One commonly-used software tool is the Weather Research and Forecasting Model (WRF), which is able to model actual atmospheric conditions and provides a flexible and computationally-efficient platform for operational forecasting. Furthermore, the use of simulation tools such as WRF has enabled researchers to explore the potential impacts of urban planning and development strategies on UHII and to evaluate the effectiveness of mitigation measures such as green infrastructure and cool roofs. By conducting simulations under different scenarios, researchers have been able to quantify the potential benefits of such measures in terms of reducing UHII and improving the thermal comfort of urban residents. Table 2-9 overviews the UHII data from simulations, including the research area and period, method and key findings.

Overall, UHII simulations have emerged as a powerful tool for studying the impacts of urbanization on air temperature, and for evaluating potential mitigation measures. The continued development of simulation tools and modelling approaches will undoubtedly further enhance our understanding of

this important phenomenon, and develop more effective strategies for managing the impacts of urbanization on the environment and human health.

Table 2-9 UHII data from the simulation

Research area	UHII	Method	Research period	Special issues	Ref.
Singapore	The maximum UHI is 2.2℃ during late night and early morning.	weather research and forecasting (WRF) model	April to May 2007 and 2008	Cool roofs and vegetation both can reduce air temperature, but at different times. Green vegetation is preferable in reducing the nocturnal UHI in a tropical city.	[128]
Kuala Lumpur (GKL), Malaysia	The highest nocturnal UHII was 1.75°C and lowest nocturnal UHII was 1.11°C, and the diurnal UHII was 0.9 °C.	WRF-ARW/Noah LSM	N/A	The correct identification of urban fractions improves the model performance	[129]
Chengdu–Chongqing,	near-surface air temperature increases ranged from 1–1.5	WRF model	July of 2009–2011	Cool roof has a better cooling capability than a green roof when roof albedo	[130]

China	K from 2010 to2030			exceeds 0.68.	
Strasbourg–Kehl, France–Germany	UHII was lower than in other studies, the value <1 °C	WRF-SLEUTH*	2010	The dominant land cover approach cannot represent scattered urban patterns. Realistic planning scenarios have little impact on building energy demands.	[131]
Brussels, Belgium	mean nighttime UHI of Brussels ups to 3.15 ℃	Urban boundary layer climate model (UrbClim)	2000 to 2009	UHII is found to be strongly correlated to inversion strength. Heat wave days in the city increase twice as fast as in the rural surroundings.	[132]
Nantes, Angers and La Roche-sur-Yon, France	UHII is 2.5 °C	Empirical models	13th June 2013	UHI spatial variations are related to one or several heat fluxes	[133]
Abu Dhabi	The average annual UHII was between 1.5℃ and 2℃.	Average grey-box dynamic model	2010	Inverse grey-box dynamic model inferred from load and weather data.	[134]
Abu Dhabi	The highest UHII occurred in	EnergyPlus-	2008-2010	A straightforward methodology to	[135]

	the early morning ranging from 5.6°C and an average value of UHI was 3°C.	Rhino- Matlab		calibrate a large number of buildings, considering the urban microclimate condition.	
Montreal, Canada	UHII was 5.0℃ at 12h in summer and fall. The maximum surface UHII occurred around 14h, and the diurnal variation of surface UHI ranged from 0.5 – 11 °C in summer	CLASS and CLASS +TEB	1981 to 2010	Surface UHI is very small compared to temperature changes. Surface fluxes are very small for urban regions compared to nonurban regions.	[136]
Continental United States	Maximum UHII is 5 °C in summer	LM3- GFDL-UCM- CMIP5	1949 – 2000	Precipitation affects UHII mainly by altering the Bowen ratio in summer and winter, and also the albedo in winter.	[137]

2.7.2 Surface-temperature based UHII

Surface temperature-based urban heat island intensity refers to the difference in land surface temperature between an urban area and its surrounding rural area. This type of UHII is mainly influenced by the physical properties of the surface materials, such as albedo, emissivity, and thermal conductivity. Urban areas typically have a higher fraction of impervious surfaces, such as concrete, asphalt, and buildings, compared to rural areas, which are typically covered with vegetation and soil. These impervious surfaces absorb and store more heat during the day and release it slowly at night, leading to a higher surface temperature in urban areas compared to rural areas [138].

Surface temperature-based UHII studies are typically conducted using remote sensing techniques, such as thermal infrared imaging or satellite imagery, to measure land surface temperature [139]. These methods enable researchers to obtain spatially explicit data on UHII, which can be used to map and analyse the spatial patterns and temporal dynamics of UHII [140]. However, satellite imagery requires the presence of the satellite over the study area and clear skies. Several papers deal with the LST retrieval from space for SUHI analysis [141]. Table 2-10 shows the surface-temperature based UHII in some typical cities with UHII diurnal variations, research area, period and methods.

Table 2-10 Surface-temperature based UHII in some typical cities

Study area	UHII (°C)				
	Daytime	Night-time	Research period	Methods	Ref.
Budapest, Hungary	+3.4(June)	+2.3(March)	2001 to2003	Sensor MODIS on satellite Terra	[142]
Nyiregyhaza,	+4.5(July)	+2.3(August)	2001 to2003	Sensor MODIS on satellite	[142]

Hungary				Terra	
Szombathely, Hungary	+3.9(May)	+2.1(May)	2001 to2003	Sensor MODIS on satellite Terra	[142]
Pécs, Hungary	+4.1(June)	+1.9(July)	2001 to2003	Sensor MODIS on satellite Terra	[142]
Phoenix, USA	+1.5(June)	+1.2(June)	7th June 2004	ASTER imaging	[116]
Athens, Greece	+3.3(May)		08：57 20th May 2000	Landsat Enhanced Thematic Mapper (ETM+) sensor on board Landsat 7 satellite	[143]
Thessaloniki, Greece	+2.7(May)		09:00 30th May 2001	Landsat Enhanced Thematic Mapper (ETM+) sensor on board Landsat 7 satellite	[143]
Petra, Greece	+3.0(May)		09:02 28th June 2000	Landsat Enhanced Thematic Mapper (ETM+) sensor on board Landsat 7 satellite	[143]
Volos, Greece	+0.4(May)		08:56 24th Aguste 2000	Landsat Enhanced Thematic Mapper (ETM+) sensor on board Landsat 7 satellite	[143]
Heraklion, Greece	+1.9(May)		08:45 09th July 2000	Landsat Enhanced Thematic	[143]

				Mapper (ETM+) sensor on board Landsat 7 satellite	
Munich, Germany	+5.3(June)	+2.8(June)	2002	Satellite Terra	[144]
Milan, Italy	+5.8(July)	+4.0(January)	2002	Satellite Terra	[144]
Warsaw, Poland	+3.5(June)	+3.1(May)	2002	Satellite Terra	[144]
Budapest, Hungary	+4.0(June)	+2.9(June)	2002	Satellite Terra	[144]
Shanghai, China	+6.4(April)		1997 to 2008	Landsat TM/ETM+ images	[145]
Rotterdam, Netherlands	+12.0	9.0	2006	NOAA-AVHHR satellite images	[146]
Houston, USA	+1.29k	+0.36k	2000 to 2010	MODIS LST	[147]
Milan, Italy	+10k	+7k	15th July 2007	Terra and Aqua satellites	[148]
Chandigarh, India	+4.7k (monsoon season)	+3.47k(Winter)	2009 to 2013	MODIS Re-projection Tools (MRT)	[149]
Budapest, Hungary	+3.17	+3.24	1992 to 1993	MODIS-Weather Research and Forecasting (WRF) model	[150]
Beijing, China	+4.2k(Summer)	+0.6K(winter)	2002 to 2014	LANDSAT-8 data	[151]
Berlin, Germany	+5.38K(Summer)	+2.84k(Summer)	2010 to 2015	MODIS observed AOD product	[10]
Romania (country scale)	2.4 (summer) 1.1(winter)	1.4(summer) 0.8(winter)	2013 to 2018	MODIS-LST	[152]

2.8 Meteorological parameters for assessing UHI mitigation strategies in the subtropical climate

Meteorological parameters are important to analyse when assessing UHI mitigation strategies because the urban heat island effect is a phenomenon that is driven by changes in the atmospheric and surface energy balance. To mitigate UHI, it is necessary to understand how these factors interact with the local meteorological conditions.

Meteorological indicators, such as the sky view factor, net radiation, thermal radiative power, and physiological equivalent temperature, provide a quantitative assessment of how different mitigation strategies impact the energy balance of the urban environment. By analysing these indicators, it is possible to determine how effective different strategies are at reducing the intensity of UHI and to identify the most promising approaches for future mitigation efforts.

These meteorological indicators have been widely used in studies related to urban heat island mitigation and provide insight into the effectiveness of various strategies in reducing the intensity of UHI.

By analysing the mitigation strategies through these parameters, a deeper understanding can be gained of the most effective solutions for mitigating the negative impacts of UHI in subtropical regions. In turn, this information can be used to inform decision-making processes and guide the implementation of mitigation strategies in a way that optimizes their impact on the environment and human health.

2.8.1 Sky View Factor

The Sky View Factor (SVF) is a widely used index of urban morphology for comparing thermal conditions in different building environments, as it reflects

the fraction of sky visible from a given location [153]. Despite its distinction as a geometric factor rather than a meteorological parameter, the SVF significantly contributes to comprehending the impact of urban configuration on local climate conditions. Beyond its geometric essence, the SVF emerges as a pivotal component in the broader context of urban climatology, as it profoundly influences the distribution of solar radiation [154], thermal patterns [155], and microclimate dynamics [156]within urban environments.

The SVF is essential in describing microclimate at scales below 100m, and serves as a proxy for net radiation, which depends on the height of obstacles in the surrounding area. The SVF was calculated from a rasterized point cloud height dataset (with $6-10$ points per m^2) and depends on grid resolution, search radius and the number of directions [157]. Previous research [158] [159] related the diurnal maximum UHI of the canopy layer to various factors, including the diurnal temperature range, solar irradiance, wind speed, vegetation fraction and SVF.

The SVF can be calculated by fish-eye photos [160] [158], which is an algorithm to divide the photograph into non-overlapping areas classifying sky or non-sky areas. The Sobel edge detection algorithm is used to identify the boundaries between sky and non-sky areas by evaluating the contrast between pixel colours in the surrounding neighbourhood. [161], which is a filter that assigns a value between zero and one to each pixel by evaluating the contrast between pixel colours in its 8-neighbourhood (adjacent pixels that share an edge or node). To make the edge detection more robust, the Sobel filter is modified to emphasize the edges between definite sky and non-sky pixel colours, i.e., if both colour classes are detected within the 8-neighbourhood, then the edge value for that

pixel is set to one. Thus, all edges with a value below a predefined threshold are removed, and the average colour and colour variance is calculated for each area. The remaining edges are subsequently used to flood-fill the obstructed areas (e.g., walls, roof, and trees) to separate the image into sky and non-sky regions [158]. Fig. 2-6 shows the SVF in GSV fisheye photos. The SVF plays a crucial role in urban morphology and is an important factor in describing microclimate conditions in urban environments.

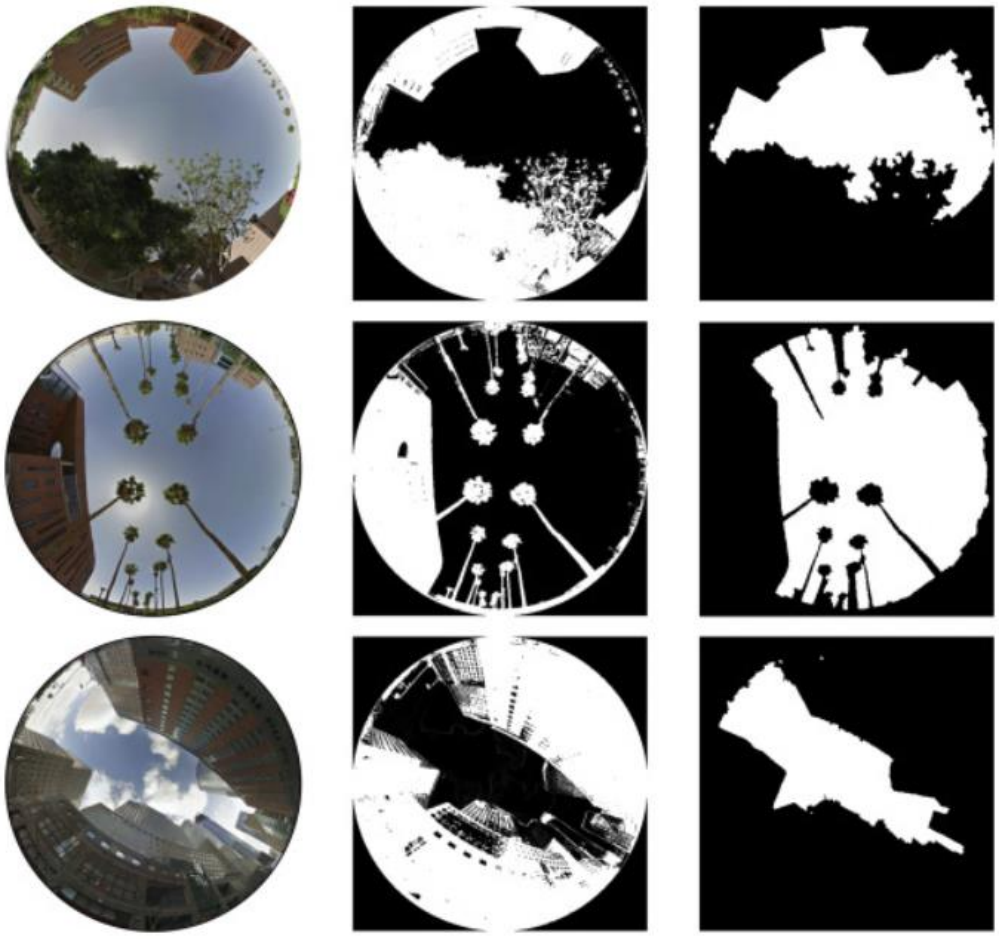

(a) (b) (c)

Figure 2-6 Examples of SVF in GSV fisheye photos, (a) Fisheye photos, (b) Sobel filters, (c) flood-fill algorithms [158]

A modified Steyn method is used to compute the SVF in a fisheye photograph. Each fisheye is partitioned into n annular rings (default n = 36) to calculate the

SVF by summing up the contribution of each ring [162]. The SVF (ψ_s) is calculated by the following Eq. (2).

$$\psi_s = \frac{\pi}{2n} \sum_{i-1}^{n} sin\left[\frac{\pi(2i-1)}{2n}\right] \left(\frac{p_i}{t_i}\right) \quad (2)$$

where s can be sky, tree, or building; n is the total number of rings (here we use 100); i (from 1 to 100) is the index of the ring; p_i and t_i is the ratio between the number of sky pixels to the total number of pixels in ring *i*. The value of SVF from 0 to 1 to measure points in urban space. An SVF of 1 is an entirely open area without any buildings or large objects obstructing the view. On the contrary, an SVF of 0 is the completely closed indoor environment.

2.8.2 Net radiation

Net radiation (Rn) plays a crucial role in determining the temperature and energy balance of urban environments. A lower net radiation value corresponds to a lower heat generation in the urban area, as demonstrated in several studies. The below equation provides a means of evaluating the effect of net radiation on the urban environment by accounting for factors such as the albedo of the ground surface, incoming solar radiation, air temperature, and heat gain from the surrounding environment. The calculation of net radiation is essential in understanding the thermal conditions of urban environments and in developing effective strategies for mitigating urban heat [163]. Some studies [164] [165] showed that the lower the net radiation, the lower heat in the city area.

Rn is calculated by the following Eq. (2) to evaluate its effect on the urban environment [164].

$$Rn = A + H + LE \quad (2)$$

$$A = -\lambda \frac{\partial T}{\partial Z} | Z = 0,$$

$$H = \alpha(T_s - T_a),$$

$$LE = \iota\beta\alpha_W(X_s - X_a) = \iota\beta\alpha/C_p(X_x - X_a)$$

Where A is the soil heat flux (W/m^2), H is the sensible heat flux (W/m^2), and LE is the latent heat flux (W/m^2). λ is the heat conductivity (W/mK), α is the convective heat transfer coefficient (W/m^{2}K), Ts is the surface temperature (°C), Ta is the air temperature (°C),ι is the von Karman constant, is approximately 0.41, β is the evaporative efficiency (-), Cp the Specific heat of air constant pressure (J/kg K), Xs is the Saturated humidity (kg/kg) and Xa is the Air absolute humidity (kg/kg), Xx is the saturation vapour pressure at the air temperature.

2.8.3 Thermal Radiative Power

Thermal radiative power (TRP) is the electromagnetic radiation emitted by a body with a temperature above absolute zero. The amount of energy emitted depends on the temperature of the surface and its ability to emit energy [166]. TRP is used to assess the impact of the solar reflectance of a surface on the UHI effect [167]. The calculation of TRP provides valuable insights into the heat emission properties of different urban surfaces and the contribution of these surfaces to the UHI effect. By considering factors such as emissivity, surface area, and temperature, the TRP helps to identify the sources of heat emission and their impact on the ambient environment. This information can then be used to inform urban planning and design decisions aimed at mitigating the UHI effect, such as selecting materials with higher reflectance and lower emissivity for building surfaces. In summary, the TRP is an important tool for understanding the energy balance and thermal conditions of urban environments and for developing effective strategies for mitigating the UHI effect. The calculation Eq. (3). can be used to calculate TRP by the Stefan-Boltzmann law:

$$TRP = \varepsilon \cdot \sigma \cdot A \cdot T^4 \quad (3)$$

Where ε is emissivity in this research (0.92-0.96 for soil, 0.94 for concrete, and 0.90-0.98 for asphalt); σ is the Stefan–Boltzmann constant (5.67×10^{-8} $Wm^{-2}K^{-4}$), A is the radiating area (m^2), and T is the absolute temperature (K).

2.8.4 Human Thermal Perception

Human thermal comfort is an essential factor to assess the perceived quality of the urban microclimate [168] and UHI mitigation [169], which is defined as the condition of mind which expresses satisfaction with the thermal environment [170]. Human comfort and thermal stress can be subdivided into applicable indoor and outdoor human comfort. The indoor environment is based on the relative stability of the indoor environment in terms of air temperature, humidity radiation and human activity. On the contrary, outdoor thermal comfort is significantly influenced by the rapid variability of the outdoor environment, especially by solar exposure and wind speed [171].

The assessment of human thermal comfort relies on the mean radiant temperature [172], which refers to the uniform temperature of the surroundings in which the radiant heat exchange from the human body is equal to the radiant heat exchange in the actual environment [173]. The Tmrt is influenced by two main components: solar shortwave radiation (direct, diffuse, and reflected) and terrestrial longwave radiation (atmospheric and environmental) [174].

To assess human thermal comfort, several indices have been developed such as the Physiological Equivalent Temperature (PET) [175], Universal Thermal Climate Index (UTCI) [176], and Predicted Mean Vote (PMV) [177]. These indices take into account various environmental factors based on the mean radiant temperature such as air temperature, relative humidity, wind speed, and radiation to calculate an index that represents human thermal comfort. By using

these indices, researchers and urban planners can assess the thermal environment in different urban areas and develop strategies for improving human comfort and reducing thermal stress. In conclusion, human thermal comfort is an important aspect of the urban environment, and a comprehensive understanding of the factors that affect it is crucial for mitigating the UHI effect and improving the quality of life in cities.

2.9 Urban heat island and building energy consumption

The majority of the world energy is consumed by cities, resulting in a more than 70% increase in global carbon emissions in urban areas [178]. According to the United Nations, the global urban population is expected to reach 5.2 billion by 2030 [179]. The overwhelming populations in urban areas are responsible for higher energy consumption and carbon emissions. Energy requirements in urban areas are rising rapidly with the increase in the urban population [180]. Therefore, As a result, the combination of urbanization problems, microclimate, and energy use has become one of the significant challenges worldwide.

In anticipation of emerging global urbanisation and notable reduce urban building energy consumption and GHG emissions for both new and existing neighbourhoods or cities, a better understanding and quantification of climate effects on urban building energy consumption is required. This includes identifying the current sources of high energy consumption and carbon emissions, as well as assessing the potential impact of comprehensive energy retrofitting programs and changes in energy supply infrastructure.

One factor affecting building energy consumption in urban areas is the urban heat island phenomenon [181]. This occurs when temperatures in metropolitan areas are higher than in surrounding rural areas. The UHII refers to the extent to

which heat sources raise temperatures in an urban area compared to rural areas [29]. Studies indicated that increased UHII significantly impacts building energy demand due to land use land cover (LULC) modification and changes in global and regional climatic conditions inevitably increase energy demand [182] [183], such as increased cooling energy consumption [40] and increased peak energy demand [41]. Existing studies showed that each degree of UHII increase can rise peak electricity demand from 0.45% to 4.6%, and increase overall energy consumption between 0.5%-8.5% [42]. Therefore, UHI significantly increases the energy bill as well due to varying heating and cooling costs [68]. In addition, previous studies presented that UHI has positive effects on carbon emissions and has been associated with heat stress and the health of citizens, such as heat rash and cramps, heat exhaustion, and heat stroke [184]. As the consequence of UHII increases, heat-related health risks are raised further [73].

An increase in the ambient temperature affects adversely both the supply and the demand of energy use for cooling purposes. The increased cooling energy consumption of buildings can rises the peak electricity demand during the summer season and in general puts the power generation systems under higher strain [185] [186]. Table 2-11 presents the implications of UHI on the demand and supply side components of electricity [185].

Table 2-11 Implications of UHI and energy [185]

Side	System Component	UHI effect	Implications
Demand	Cooling Load of Buildings	Higher ambient temperature	Increase in the cooling demand for buildings
Demand	Peak Energy Demand	Higher ambient temperature	Increase in the peak electricity demand

Demand	Load Duration curves	Higher ambient temperature	Higher demand curve peaks and load variability increase changing of breaching the market price cap
Demand	Non-Temperature Sensitive Demand	Increased cooling water temperatures	Generation curtailments and potential interruption of power to avoid blackouts
Supply	Thermal Electricity Generation Plants and Components	Increased Ambient Temperatures Increased Water Temperatures	Decreased efficiency of electricity generating equipment like gas turbines, coal power plants, etc.
Supply	Transmission Network	Higher ambient temperatures and longer spells of dry weather	Power disruptions, and increased cost of adaptation designs. Reduced equipment lifetime. Reduced power-carrying capacity
Supply	Substations and Transformers	High Ambient Temperatures	Increased losses within substations and transformers
Supply	Fuel Stock	High Ambient Temperatures	Coal stocks may spontaneously combust or self-ignite

Supply	Power Plants	Increased Ambient temperature and Extreme events	Extra power plants to cover the peaks. The increased cost of electricity production during the peak hours

Six main types of studies are available to investigate and analyse the actual and future impact of UHI on the energy demand of buildings and the energy supply systems. The majority of these studies concentrate on the potential escalation of cooling energy demand and utilisation. Certain studies [187] [188] [189] evaluate the energy impact of UHI on reference buildings (Table 2-12.). In most of these studies, climatic data from reference rural or suburban weather stations are used to perform comparative energy simulations

Table 2-12 energy impact by UHI on reference buildings

Research area	UHII	Research building	Research method	Setpoint	COP	Energy impacts	Ref.
Western Athens, Greece	6	a four-apartment building (320m^2)	Simulation: DOE2.1.E	26	2.25	66% (in 1997) and 33% (in 1998, a hotter year) increase in cooling energy. 99% (in 1997) and 30% (in 1998) increase in peak cooling power	[190]
London, UK	7	A 5-storey typical office (60 m^2)	Calculation: BRE'3TC	24	3.0	Cooling energy increased by 19%	[40]
Tokyo, Japan,	2.5	Commercial sector and Residential sector	Calculation:	N/a	N/a	Cooling energy increased by 27.5%.	[191]

			STM (based on data from multiple years)				
15 cities, USA	2 (Houston)	A typical office (size not reported)	Simulation: EnergyPlus	N/a	N/a	Cooling energy increased by 13-35%.	[192]
Singapore	2	An office building (24000–180000 m^2)	Simulation: IES	N/a	N/a	Cooling energy increased by 4.6-12.18%.	[193]
Pacific Ocean's coast	Around 2	Four types of residential buildings (size not reported)	Simulation: TRNSYS	N/a	N/a	Cooling energy increased by 15-200%.	[194]
Rome, Italy	8	A residential building (270 m2)	Simulation: TRNSYS	26	N/a	Cooling energy increased by 12-46%.	[121]

Overall, the magnitude of the energy consumption for cooling space in reference buildings depends highly on the levels of the ambient temperature and UHI impact. Higher temperatures correspond to increased use of air conditioning and also to a considerable rise in the urban energy demand. The induced by the UHI additional electricity penalty depends on the climatic characteristics of the research area, the quality of the building stock, the efficiency of the air conditioning, the indoor set point temperatures, and the characteristics of the electricity network.

Moreover, some studies aim to investigate the impact of the ambient temperature increase on the total energy consumption of a city, country or global (Table 2-13)

Table 2-13 Impact of the ambient temperature increase on the total energy consumption of a city, country or global

Research area	UHII	Research period	Domain size	Research method	Energy impacts	Ref.
Global	N/a	1970–2010	N/a	Data collection	The average increase in the cooling demand is 23%	[183]
Tokyo, Japan	Maximum 2.5℃ by CSU-MM model	Annual	2×2km	Estimation	Annual energy use for space cooling increased by 27.5%,	[191]
USA	Annual average of 2 ± 1 °C by TEB–	Annual	Subdivide urban into tall-building districts, and high-, medium-, and low-density cities Based on	EnergyPlus	The UHI effect averages 17.25% and −17.04% over the 15 climate locations on cooling and heating, respectively.	[195]

	ISBA model		the urban canyon aspect ration			
Bangkok, Thailand	N/a	2002 to 2006	All Bangkok Metropolis	RECB model	if the average ambient temperature increases by 1 °C, it will cause a 7.49% rise in the monthly electricity consumption	[196]
Hong Kong, China	N/a	1990-2004	All Hong Kong city	Linear regression	1 °C ambient temperature rise, the electricity consumption would increase by 9.2%, 3.0%, and 2.4% in domestic, commercial and industrial sectors, respectively.	[46]

The levels of the additional energy consumption depend highly on the massive collected data of the selected building characteristics and climate conditions, which may not be fully compatible and representative of the energy impact at the city, country even global scale due to the data limitation and shortage.

2.9.1 Urban building energy modelling

Urban building energy modelling (UBEM) is the computational simulation of the energy performance of a group of buildings in the urban context to determine the inter-building effects and urban microclimate [197]. Besides, UBEM is not scaling up energy modelling from a single building to a group of buildings in a linear fashion. It captures the dynamic and complex interconnection and interdependencies between buildings and urban microclimate. Fig.2-7. shows the heat exchange between the envelope of buildings, the interaction of buildings with ambient air and the main mechanisms of heat loss from buildings to ambient air.

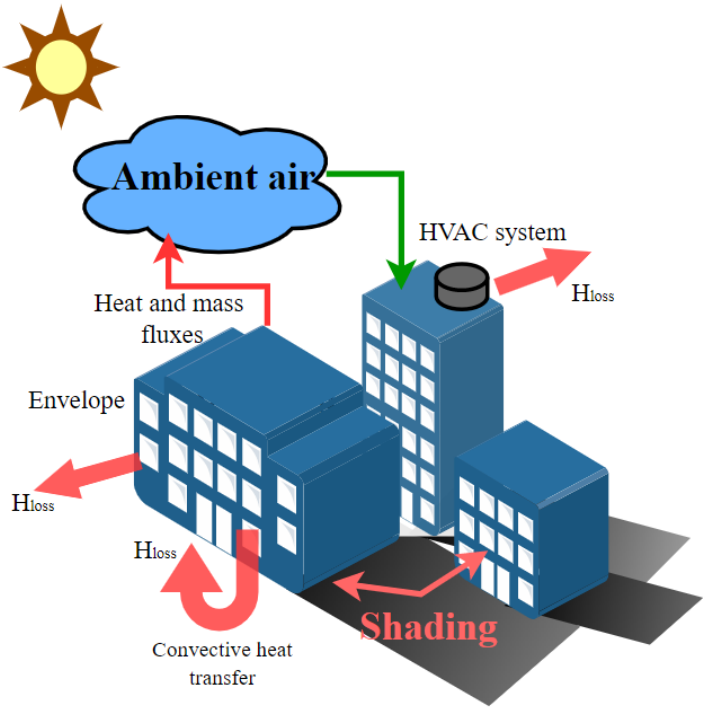

Figure 2-7 Interconnections between buildings and urban microclimate [197]

The existing methods for estimating urban building energy use have been categorised into two fundamental methods [198]: the top-down methods and bottom-up methods. Fig.2-8. shows the basic structure of urban building energy modelling approaches [199].

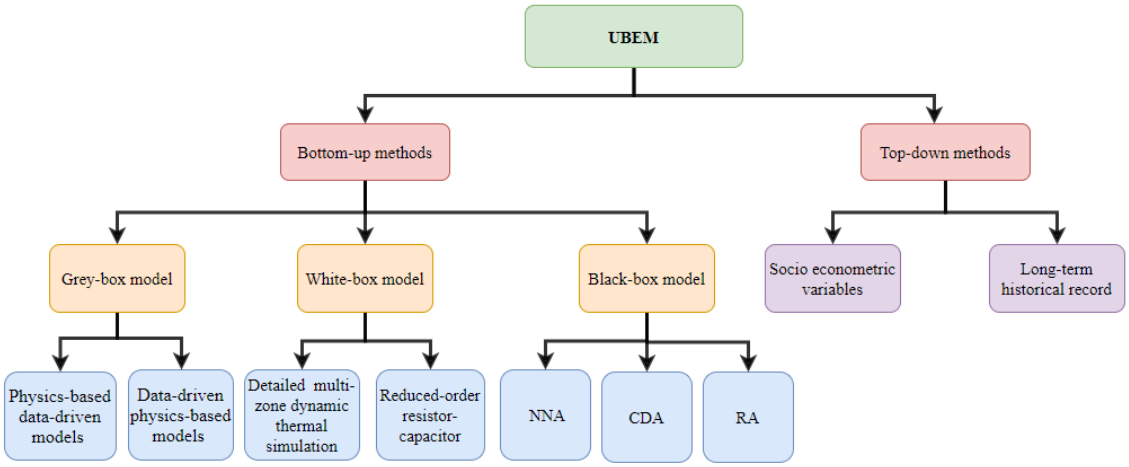

Figure 2-8 The structure of urban building energy modelling approaches

2.9.1.1 The top-down methods

Top-down methods to simulate urban building energy use are a promising approach for estimating energy consumption at a macro-level in urban areas. Such methods are often used in large-scale studies that aim to understand the energy performance of buildings in an entire city or region [200].

Top-down methods for typically predicting urban building energy consumption are based on analysing a long-term historical relationship between the energy use and the significantly associated variables of city building blocks, such as gross domestic product (GDP) fluctuation, the energy unit price floating, occupancy schedules, household sizes and weather condition, etc. One common approach to top-down modelling involves the use of statistical models, such as regression analysis or machine learning [201].

The primary advantage of the top-down methods is that the interactions of energy and economy are utilised to explore energy use under different socio-economic variables [198]. Moreover, the top-down methods can provide benchmarking and guidelines for building energy retrofit policies [202]. Additionally, top-down methods generally require fewer data as input, such as aggregated socio-economic data, without the need for detailed information on the building energy consumption technologies and data [203].

However, top-down methods require a significant amount of historical data to make accurate predictions. They may also suffer from uncertainty and inaccuracies when predicting future energy consumption, due to the changing socio-economic and physical conditions in urban areas, such as rehabilitation and climate change [198].

2.9.1.2 The bottom-up methods

The bottom-up approach to estimating building energy consumption utilizes physical models that simulate heat and mass flow within and around buildings. These models are based on the principles of thermal physics and synthesis characteristics for groups of buildings, and provide a more accurate prediction of energy consumption compared to other methods [204].

One of the key advantages of bottom-up methods is the level of detail in the input data required. This data includes building properties such as orientation, envelope fabric, equipment, climate conditions, indoor temperatures, and occupancy schedules [198]. This information is crucial for the bottom-up approach as it allows the selection of appropriate technological options and

retrofit areas, as well as the ability to perform dynamic energy simulations under different climate conditions [203].

There are three main types of bottom-up energy consumption methods: data-driven models (black-box models), physics-based models (white-box models), and integrated models (grey-box models). Data-driven models use statistical and machine learning techniques to predict building energy consumption based on past data. Physics-based models, on the other hand, use equations based on the laws of physics to simulate energy consumption. Integrated models, also known as grey-box models, combine elements of both data-driven and physics-based models to provide a more comprehensive prediction of building energy consumption.

Overall, the bottom-up approach offers a detailed and comprehensive method for predicting building energy consumption, which is crucial for reducing energy consumption and achieving more sustainable buildings. By considering the various inputs and factors involved in building energy consumption, bottom-up methods provide a valuable tool for decision-makers and building professionals in the design and retrofitting of buildings.

2.9.1.2.1 Data-driven models

Data-driven models (Black-box models) evaluate building energy consumption by data mining and machine learning techniques with three approaches: regression analysis (R.A.), conditional demand analysis (CDA), and neural network analysis (NNA) [199]. The main requirements for a successful data-driven model are a sufficient amount of clean data and appropriate algorithms.

It has multiple advantages, such as lower engineering costs due to the data-in-data-out process. Additionally, less professional knowledge is required as they

are based on is mapping of input and output data. They also have good adaptability as new data can be used to generate updated models [205].

However, Black-box models also have some limitations, including a high requirement for historical consumption data, the need for large sample sizes, and the importance of data quality. In addition, these models lack interpretability and may have high computational costs, especially when deep learning-based algorithms are used. The process of the data-driven model is shown in Fig. 2-9.

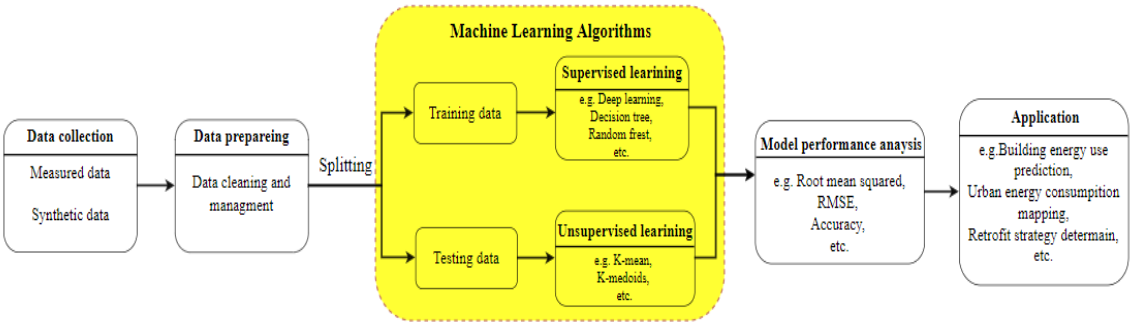

Figure 2-9 The process of the data-driven model

2.9.1.2.2 Physics-based models

Physics-based models also known as engineering models or white-box models are used to assess building energy consumption. These models are based on building characteristics and detailed thermal properties, which offer higher temporal resolution than the data-driven model [206]. Unlike the data-driven models, the physics-based models do not require socio-economic factors and historical energy consumption data.

However, the implementation of physics-based models requires a more significant number of physical parameters, such as building shape, orientation, thermal properties of buildings envelope, types and performance characteristics of heating, ventilation, and air conditioning systems (HVAC), building

ventilation rates, thermostat set points, occupancy schedules, and internal loads [203].

While physics-based models are known for their thoroughness, there are some limitations to consider. One of the main drawbacks is that the process of developing a physics-based model is often time-consuming due to the large number of detailed input parameters required. Additionally, there is a risk of oversimplification, which can compromise the accuracy of the results.

In conclusion, physics-based models provide a comprehensive approach to evaluating building energy consumption. The input of a large number of physical parameters ensures that the results are accurate, but the time-consuming nature of the development process and the risk of oversimplification should be considered. Fig. 2-10 shows the steps to develop a physics-based model for calculating energy consumption.

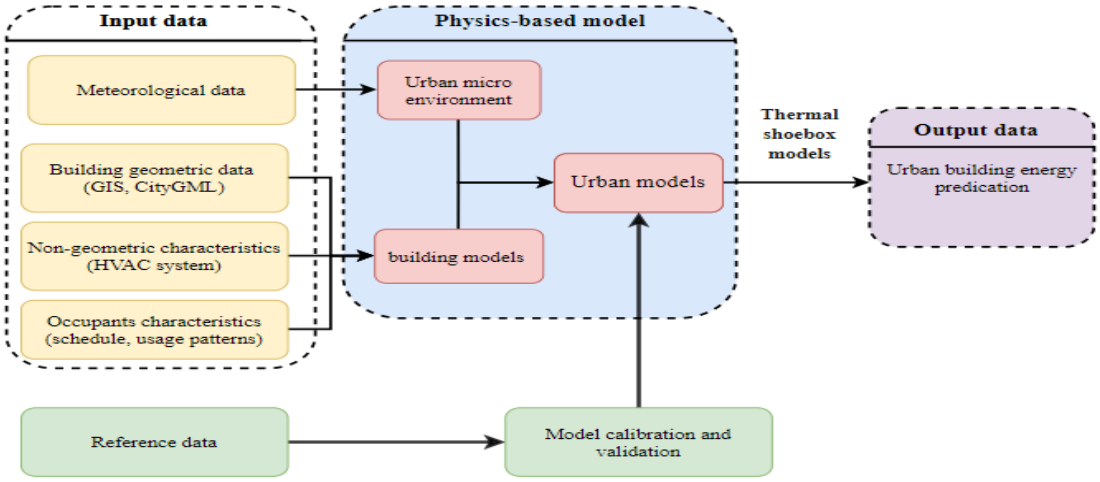

Figure 2-10 The processes of the physics-based models

2.9.1.2.3 Integrated models

Integrated models also known as grey-box models represent a unique approach to evaluating building energy consumption. By combining the advantages of both data-driven and physics-based methods, these models offer a more

comprehensive and accurate representation of energy consumption compared to either approach alone [207].

The most common grey-box model is the resistance-capacitance (R.C.) model [208], which is based on the principle of thermal resistance and thermal capacitance. Thermal resistance represents the ability of a building to resist heat flow, while thermal capacitance refers to the ability of a building to store heat. The R.C. model is divided into two subcategories: the physics-based data-driven model (Forward approach) and the data-driven physical-based (Inverse approach) model [209]. The forward approach calculates the values of R and C using physical parameters, such as building shape, orientation, thermal properties of the envelope, and performance characteristics of heating, ventilation, and air conditioning (HVAC) systems, among others. The inverse approach, on the other hand, uses data-driven methods to obtain the values of R and C by analysing historical energy consumption data [209].

The R.C. model is beneficial because it combines the detailed physical parameters of physics-based models with the ease of data-driven models. This allows for a more comprehensive evaluation of building energy consumption, as it takes into account a wider range of factors and variables. In addition, the use of both physical and data-driven methods helps to reduce the limitations of each approach, such as the time-consuming nature of physics-based models or the oversimplification issue of data-driven models [210]. Fig. 2-11. shows the processes of the grey-box model.

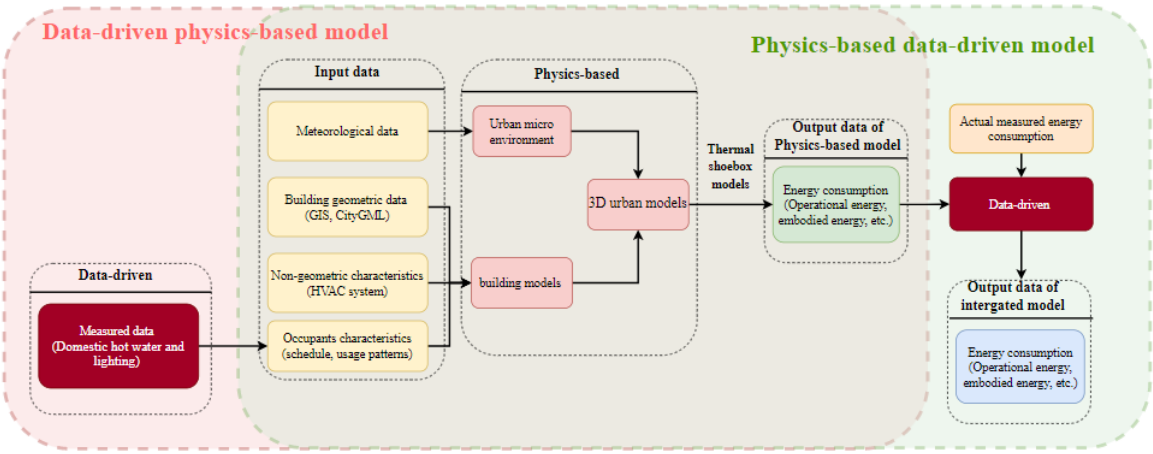

Figure 2-11 The processes of the grey-box model [211]

The forward approach is based on data-driven models that generate datasets through physical models while adopting the output datasets of the physics models as input data, and the urban energy consumption is predicted by the data-driven models [212]. The great advantage is that the detailed occupant behaviour is unnecessary in the models, and the models can estimate energy use in a simple way that can increase the certainty and accuracy of the physics-based model part. The inverse model is based on the physics models that adopt measured data (e.g. Domestic hot water and lighting, etc.) into the data-driven model for training the data of occupancy appliances and use the results as input data into physical models [213].

Overall, the integrated models (grey-box models) have an excellent ability to solve the limitations of data-driven (black-box models) and physics-based (white-box models) models with improved accuracy of prediction. However, due to the grey-box models integrating two modelling techniques, a limitation of the grey-box models is that the grey-box models require high skills from researchers.

2.9.2 Urban building energy use modelling tools

The available UBEM tools have diverse characterises and usually require computational resources and input parameters. Some tools are web-based (e.g. CityBES and Urban Footprint), and some are individual applications (e.g. UMI, CitySim and TASER). Some tools are CityCML-based and use EPW (e.g. CityBES) or Meteonorm (e.g. SimStadt) weather data. Table 2-14 summarises the main UBEM tools for review.

Table 2-14 UBEM modelling tools

Tool	Approach	Marks	Developer	Calculation core	Weather file	Target Users	Ref.
Urban Footprint	Black-box method	Planning tool for access to land use, policy, and resource across a range of sectors	Calthorpe Analytics	Regression	Historic weather data	Policymakers, Urban planners	https://urbanfootprint.com/
CoBAM	Black-box method	The behaviours, interactions, and decision logic of building owners considering adopting energy-efficient technologies.	ANL	Regression	Historic weather data	Policymakers	https://www.anl.gov/esia/commercial-building-agent-based-model [214]

SimStadt	Grey-box method	The application scenarios range from high-resolution simulations of building heating requirements and potential studies for photovoltaics to the simulation of building refurbishment and renewable energy supply scenarios.	HFT Stuttgart	CityGML, Energy ADE, Java	WFS, Meteonorm	Policymakers, Urban planners	https://www.hft-stuttgart.com/research/projects/current/simstadt-20 [215]
Energy Atlas Berlin	Grey-box method	Mapping and estimating the energy consumption and efficiency of buildings, power suppliers and network conditions	Technische Universität München	CityGML, Energy ADE, Generic City Objects and	Real weather data, degree-day	Policymakers, Urban planners	https://www.asg.ed.tum.de/gis/projekte/abgeschlossene-projekte/energieatlas-berlin/ [216]

				Generic Attributes			
TEASER	White-box method (Reduced order model)	An open framework for urban energy modelling of building stocks	RWTH AACHEN university	Modelica model, Python		Policymakers, Building energy managers	https://ebc-tools.eonerc.rwth-aachen.de/en/teaser [217]
City Energy Analyst	White-box method (Reduced order model)	An integrated simulation platform, which allows studying of the effects, trade-offs, and synergies of urban design options and energy infrastructure plans	ETH Zürich	ArcGIS, Python,	Meteonorm	Policymakers, Urban planners	https://www.cityenergyanalyst.com/ [218]

OpenIDEAS	Grey-box method	An open framework developed for integrated district energy simulations rising in the multidisciplinary building energy domain	K.U. Leuven	Modelica	IDEAS. climate	Building energy managers and consultants	https://github.com/open-ideas/IDEAS [219]
CityBES	White-box method	An open web-based data and computing platform are focusing on city energy modelling support district or city-scale efficiency programs.	Lawrence Berkeley National Laboratory	CityGML, Open Studio, EnergyPlus	EPW	Policymakers, Urban planners	https://CityBES.lbl.gov [220]
CitySim	White-box method	A software minimises the net use of non-renewable energy	EPFL	a command-line Integrated Solver	Meteonorm	Policymakers, Urban planners	https://www.epfl.ch/labs/leso/transfer/software/citysim/ [221]

		sources and the GHG emissions					
UHES	White-box method	An open-source ecology of computational resources to support distributed energy system design and management	Empa and ETH Zürich	Energy plus, Aimms	EPW	Policymakers, Urban planners	https://hues.empa.ch. [222]
Boston Citywide Energy Model	White-box method	A citywide UBEM based on official GIS datasets and a custom building archetype library	MIT	Rhinoceros, Energy plus	EPW	Policymakers, Urban planners	https://web.mit.edu/sustainabledesignlab/projects/BostonEnergyModel/index.html [223]

Urban modelling interface (UMI)	White-box method	An urban modelling platform to evaluate the environmental performance of neighbourhoods and cities with respect to operational and embodied energy use, neighbourhood walkability, access to daylighting, urban food production and district-level energy supply analysis.	MIT	Rhinoceros, Energy plus	EPW	Policymakers, Urban planners	https://web.mit.edu/sustainabledesignlab/projects/umi/index.html [224]

2.9.3 Calibration and validation for building energy modelling

It is essential to generate precise and dependable estimates of the energy-saving potential in urban areas to support stakeholders in making informed policy decisions. The accuracy of these estimates is often compromised by discrepancies between simulated and measured results, which are largely a result of assumptions regarding input parameters such as occupant behaviour, when simulating the aggregated group of buildings, inaccuracies in energy estimates have been observed to average out over time [225]. Previous studies have revealed that the total energy use intensity difference can range from 1% to 19% [204]. As such, it is imperative to conduct calibration and validation processes within the UBEM.

Calibration is a crucial process that involves adjusting input parameters to obtain acceptable output parameters that are in line with measured data. Validation is a process of comparing the results obtained from simulation with actual measured data [226]. There are three main methods of calibration: Bayesian calibration [227] [228], bespoke calibration [229] and statistical training. There are three main validation methods: empirical validation [230], comparative studies [231] and analytical verification [232].

Despite the importance of calibration and validation in ensuring the accuracy of energy savings estimates, a significant number of studies in the field have been found to omit these processes. This is particularly true for UBEM studies that use physics-based methods and those that adopt dynamic thermal simulation, where less than 50% of the models that have been examined provide evidence of calibration [226]. The lack of calibration and validation in these studies raises

serious concerns regarding the dependability of their results and the validity of their conclusions.

2.10 Human thermal comfort modelling under urban heat island effects

To achieve effective building use and the sustainability and resilience of cities, understanding the occupancy requirements is imperative, particularly, indoor and outdoor thermal comfort. The UHI mitigation strategies play a crucial role in human thermal comfort by reducing temperature reduction, providing shading or promoting the evapotranspiration process of plants [233].

Assessing human thermal comfort involves the use of indices that reflect the energy balance between metabolic activities, clothing, and environmental parameters (air temperature, mean radiant temperature, wind speed, solar irradiation and relative humidity) on the pedestrian thermal perception. The models that were developed for this purpose are Predicted Mean Vote (PMV) and Standard Effective Temperature (SET*). Both were originally designed for indoor and then adapted to the outdoor environment [168].

It is important to note that individual thermal sensation can vary [234], PMV is an empirical index introduced to indicate indoor thermal comfort, and it is physiologically based on a steady-state model of heat exchanges between the human body and the ambient air [235]. Besides, SET is an outdoor comfort index based on a dynamic two-node model of human temperature regulation [235]. In addition to these indices, personal factors such as clothing and activity are also widely employed as variables to assess thermal comfort [236]. The use of these models and indices allows for a comprehensive understanding of thermal comfort and how it can be improved through UHI mitigation strategies. This

understanding is crucial for ensuring effective building utilization and promoting the sustainability and resilience of cities. Additionally, it is essential for creating an environment that is comfortable and conducive to human activity.

2.11 Carbon emissions modelling under urban heat island effects

The Intergovernmental Panel on Climate Change (IPCC) has highlighted the significant role that buildings play in energy-related carbon emissions, accounting for approximately one-third of such emissions globally [237], Furthermore, the UHI effect has been shown to exacerbate carbon emissions in cities, contributing to the urgent need to reduce these emissions[68].

To address this issue, various mitigation strategies have been proposed and tested, such as incorporating green roofs with high evapotranspiration rates [238], which can help to reduce the amount of energy needed for air conditioning, and highly reflective surfaces [239], which can reduce the amount of heat absorbed by buildings and the surrounding urban environment.

To assess and quantify the carbon emissions associated with building energy use, researchers often adopt a life cycle assessment (LCA) approach [240] [241], which has been identified into four stages: the construction stage (production, transport and construction), the operation stage (use and maintenance), the disposal stage (Dissolution, transportation and landfill) [242]. By taking a comprehensive, life cycle perspective, the LCA approach provides a more accurate picture of the total carbon emissions generated by a building.

In addition to the LCA approach, trend analysis, a form of technical analysis that uses past data to predict future carbon emissions, has been employed to determine urban building carbon emissions. The advantage of this method is its simplicity, as it provides a straightforward approach to analysing carbon

emissions trends over time. However, it is important to note that trend analysis only provides a prediction based on past data and may not fully account for future changes in energy use patterns, building designs, and other factors that could impact carbon emissions [243].

In conclusion, reducing the carbon emissions of buildings is an urgent and critical challenge, and a range of strategies and analytical approaches have been proposed and tested to address this issue. Gaining a better understanding of the carbon emissions associated with building energy use and working to develop more effective and sustainable solutions.

2.12 Economic analysis modelling under urban heat island effects

In the context of investment decisions, it is imperative to consider the financial and environmental impacts of potential investments in UHI mitigation strategies. Carbon emissions and human thermal comfort are essential criteria that must be evaluated in this regard. Given the growing concerns over the adverse effects of UHI on the environment and human health, reducing UHI intensity, building energy usage, and carbon emissions has become increasingly crucial. Hence, investors need to carefully assess the UHI mitigation strategies of potential investments to make informed decisions that align with their values and goals.

Another criterion in making investment decisions is economic analysis. Extensive studies [244] [245] analyse the economics of UHI mitigation strategies, focusing on quantifying the benefits. This research employs various financial metrics, such as net present value (NPV) and discounted Payback Period (DPP). NPV provides a comprehensive picture of the financial return on investment, taking into account the time value of money and the expected cash flows. On the other hand, DPP calculates the amount of time required to achieve

a breakeven point, providing insight into the short-term financial viability of an investment. [246].

The findings of these studies indicate that UHI mitigation strategies often result in high potential profits with relatively low financial risk, making it an attractive investment opportunity for individual investors [245]. For example, by investing in energy-efficient building materials, green infrastructure, and other UHI mitigation strategies, investors can help reduce carbon emissions while also realizing a positive financial return on their investment. Given the dual benefits of UHI mitigation strategies, it is important for investors to consider them as a viable option in their investment portfolios.

In conclusion, investment decisions require a careful evaluation of both financial and environmental factors, with a focus on reducing carbon emissions. The study of the economics of UHI mitigation strategies highlights the potential for high returns with low financial risk, making them a desirable investment opportunity for investors who are looking to align their investments with their values and goals.

2.13 Urban heat island mitigation strategies

In general, it is widely acknowledged that UHI may significantly as the quality and liveability of urban environment. Therefore, techniques for mitigating and controlling the variables regulating the urban environment are more and more impotent for academics, local authorities and policy makers[84].

During the past decades, numerous studies have proposed the UHI mitigation strategies, such as reflective materials (cool materials) [247], high thermal performance materials [248], green roofs [249] [250], urban green spaces (street tree, park, etc.) [249] [251] and some novel technologies (PCM roof [252], PCM

pavement [253], etc.).

2.13.1 UHI mitigation strategies criteria

A series of criteria to evaluate UHI mitigation strategies are discussed. Not all measures should be weighed equally across all mitigation strategies. However, these criteria must be judiciously prioritized under diverse conditions and constraints present in different urban regions.

2.13.1.1 Environmental temperature

Environmental temperatures, including air and surface temperatures, are the most important indicators for UHI. Moreover, the extreme vertical variability in air temperature should be considered in designing and implementing UHI mitigation strategies. The temperature in street canyons has a much steeper vertical gradient near the ground than that at a higher elevation (＞2 m). Though 2-m air temperature is widely used as a measure of UHI intensity, there is a lack of the standard of air temperature to be used for mitigation strategies across all scales and regions, leading to a non-consensus on the measure of UHI mitigation for different strategies [97].

2.13.1.2 Energy Saving

The reduction of environmental temperature, the result of using UHI mitigation strategies, can effectively decrease the cooling loads of buildings, or lead to substantial energy savings during hot seasons [254] [255]. Nevertheless, energy-saving benefit needs to be evaluated in conjunction with other environmental impacts of these strategies, such as human thermal comfort.

2.13.1.3 **Outdoor air quality**

The importance of outdoor air quality (OAQ) has been well-perceived in the literature in terms of its close association with health concerns (World Health Organization (WHO), 2018). UHI tends to decrease the OAQ as the heat increased the chemical reactions in the atmosphere. The UHI mitigation strategies, through the reduction of urban environmental temperatures, can directly affect urban OAQ [256].

2.13.2 Main conventional urban heat island mitigation strategies

Mitigation techniques aim to balance the thermal budget of urban areas by increasing thermal losses and decreasing the corresponding gains [257]. For dissipating the excess heat, among the most important mitigation techniques are those targeting to increase the albedo of the urban environment and to expand the green spaces in cities, such as urban morphology design, green infrastructure developments, and expansion of highly reflective pavements or roofs. All mitigation strategies constitute common relationships between energy and water cycles, environmental and socioeconomic measures, human activities and natural systems. The primary assessment methods have criteria for UHI mitigation [258].

2.13.2.1 **Green infrastructure developments**

Green infrastructure (GI) refers to natural structures that are environmentally friendly and often associated with the colour green. Examples of urban green infrastructure include permeable vegetated surfaces, green roofs, public parks, green walls, urban forests, green alleys and streets, community gardens, and urban wetlands [259]. The GI can reduce surface temperature through increased

evapotranspiration and shading. However, in developed areas, all the natural areas had been converted to artificial material surfaces [260], and roofs take areas for about 40-50% of the total impermeable surface in city centres [261], therefore, green roof offer a solution to change the surface with green spaces. Typically, green roofs are the conventional roof planted with vegetation on the top, as shown in Fig.2-12.

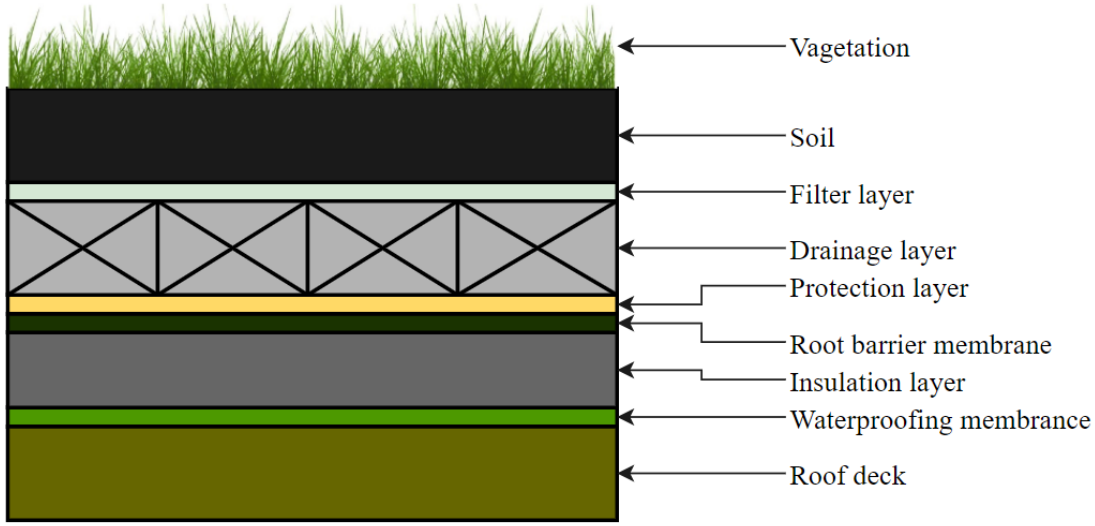

Figure 2-12 Typical components of a green roof [260]

Table 2-15 shows some previous research for analysing the relationship between UHI and green infrastructure. The table provides a detailed overview of the methodology, study area, research period and key findings of each study, enabling a comprehensive understanding of the different approaches employed to analyse the relationship between UHI and green infrastructure.

Table 2-15 Some previous research for analysing the relationship between UHI and green infrastructure

	Location	Methods	Research period	Scale	UHI change	Remark	Ref.
green infrastructure	Roma, Italy	LST derived from Landsat-8 data	Yearly	Meso-scale 129,000 ha		The air temperatures of green areas were significantly lower than urban areas in both the overall summer and winter seasons	[262]
Trees on curbsides, green roofs and green walls	Sri Lankan	ENVI-met microclimatic software (V4)	Daily	Microscale 4.58 ha	Trees on the curbsides reduce by 1.87 °C. 100% green roofing reduced by 1.76 °C.	ENVI-met numerical model by ground monitoring. The cooling effect of green areas was positively correlated with the green area, the average leaf area index (LAI), and the average	[263]

					50% green roofing reduced by 1.79 °C, 50% green walls (T5) reduces by 1.86 °C and a combination (T6) reduces by 1.90 °C.	canopy density.	
Tree and grass	Cairo, Egypt	Field measurements by mobile devices	Motherly	Micro- scale 250 m*250 m	daytime and night-time ranging from 3-4K	The 50% Trees scenario has the most significant effect on PET as it reduces PET by 4 K during the daytime.	[264]

						Trees can reduce energy consumption in indoor spaces from air conditioning by 25.056 Egyptian Pounds (1.252 Euro/day).	
vegetation coverage	Columbus, Ohio, USA	Remotely sensed imagery	Yearly	Meso-scale 46.5 km^2 area	The average temperature was reduced by 0.55°C in August and increases by 0.01 to 0.02 °C in winter.	Increased greenery reduced temperatures in summer and increased temperatures in winter.	[265]
roof vegetation,	Houston, USA	Urban Weather Generator	Daily	Micro- scale 1360 m × 1948 m	UHII is from 1.25°C to 4.35°C.	Sensitivity analyses for different mitigation.	[266]

trees, and grass coverage						The estimations of UHI effects and the performance of UHI mitigation strategies should consider climate conditions.	
Green roof	Adelaide, South Australia	Experiment and ENVI-met	hourly	Micro- scale	UHI reduced by 0.06 °C to 0.25 °C	30% green roof would reduce the electricity consumption by 2.57 (W/m^2/day)	[267]

Hence, there are some limitations to the implementation of green infrastructure. For instance, green roofs, while capable of reducing surface temperature, have high initial and maintenance costs [268] and must be properly placed to avoid the chances of leakage and structural failure of the buildings [269]. Additionally, while trees can mitigate UHI and positive impact on the microclimate in the city centre, they also act as barriers and decrease wind speed in the street canyon [270]. As the wind speed is decreasing, the elevated air temperature will increase, especially at a pedestrian level [271] [272]. Wind speeds of 1m/s to 1.5 m/s can reduce air temperature by around 2°C [273].

2.13.2.2 **Increased albedo in roof**

The cool roofs (Fig.2-13) utilise white or high-reflective materials to maximise the reflection of incoming solar radiation and decrease the net radiation entering the buildings [274] [275]. By reflecting more solar irradiation during the day and emitting stored heat in the opaque material to the outdoors on clear nights [276]. Cool roofs with white coating, high solar reflectance ($\rho > 0.65$) and high thermal emittance ($\varepsilon > 0.75$) can provide passive cooling [277].

Besides, some research [278] [279] [280] has improved the thermal performance of roofs by incorporating phase change materials (PCM) to increase the thermal storage capacity, serving as a passive cooling control strategy for UHI.

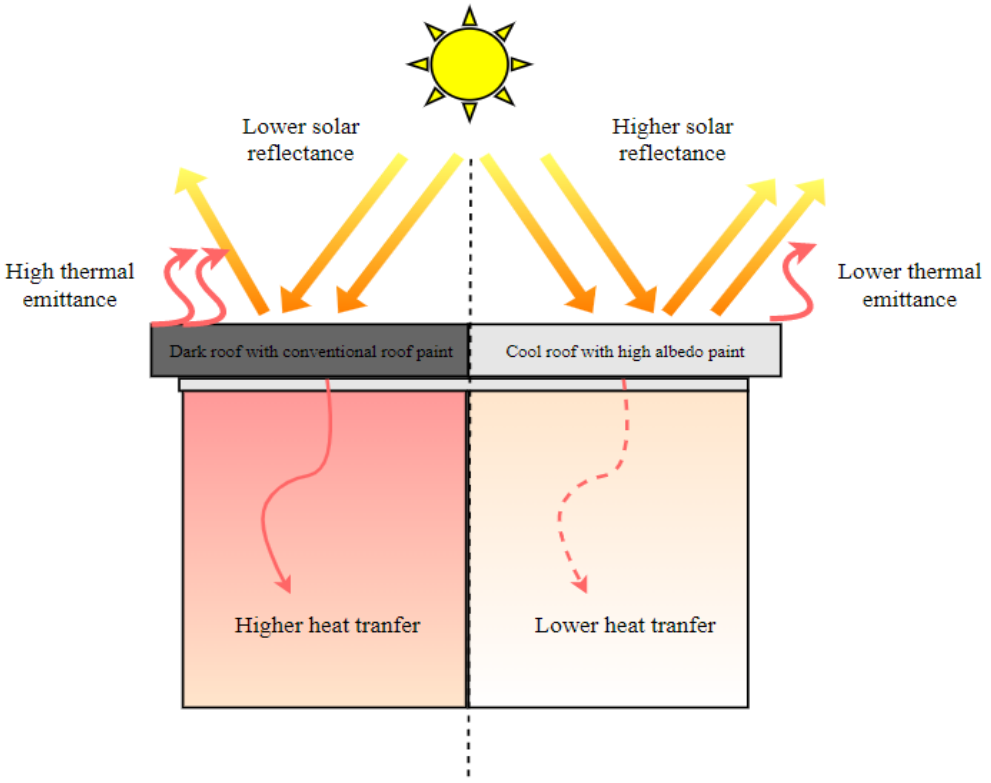

Figure 2-13 A comparison of cool roof and conventional roof [274]

Table 2-16 shows a summary of some previous research for analysing the relationship between UHI and cool roofs. The table provides a detailed overview of the methodology, study area and scale, and key findings of each study, allowing for a thorough understanding of the various approaches employed to explore the relationship between UHI and cool roofs.

By analysing the information presented in Table 2-16, the findings provide valuable insights into the role of cool roofs in reducing urban temperatures and curbing the adverse effects of UHI, which include increased energy consumption and decreased air quality.

Table 2-16 Previous research for analysing the relationship between UHI and cooling roof

	Methods	Research period	Scale	UHI change	Remark	Ref.
Cool roof	WRF simulation	Hourly	Five domains are 24.3 (76×76), 8.1 (79×91), 2.7 (112×112), 0.9 (112×112), and 0.3 km (211×130).	A cool roof can reduce surface temperature by 5℃.	Cool roofs can reduce the near-surface air temperature and surface temperature during the daytime but have little effect during nighttime.	[128]
Cooling roof (0.9, 0.8, 0.7 and	Energy Plus v8.5 and Open Studio 2.3	Hourly	A 3-storey research office building	N/a	Cool roof reduces heat gain by about 0.14 KWh/m^2 (8%), and cool roof reduces heat gain by 15.53 (37%) in the whole summer.	[281]

0.6)						
PCM tiles roof (melting temperature was 28 °C)	Experiment	Hourly	600 mm × 600 mm × 600 mm	PCM decreased surface temperature by 10-20℃	PCM roof can keep the indoor temperature higher than a cool paint roof in winter.	[282]
PCM slab roof	EnergyPlus	Hourly	A reference building	PCM decreased surface temperature by 20℃	Insulation layer variation and PCM slab location inside the roof have a small UHI effect.	[283]
PCM roof	CFD	Hourly	24.5 km^2	The air temperature was decreased by 6.8℃	The urban canopy layer air temperature in the commercial zone was reduced by 7.8 °C in summer and 11.3 °C in winter,	[284]

					and that in the residential zone was decreased by 6.4 °C in summer and 10.5 °C in winter,	
High reflective -PCM roof	Experiment	Daily	2 m×1.5 m×2.7 m	High reflectivity-PCM roof can reduce the inner surface temperature average reduce by 2.2 °C (the maximum is 5.6 °C).	The high reflectivity-PCM roof had better thermal protection performance than the individual cool roof and individual PCM cool roof	[285]

In summary, conventional cool roofs utilise white paint to reduce surface temperature and mitigate urban heat island effects. Innovative cool roofs incorporate phase change materials to absorb and store heat for significant UHI mitigation. However, conventional cool roofs are plagued by issues such as dust accumulation and fading of high-reflective paint, while PCM cool roofs face challenges such as high initial and maintenance costs and potential leakage problems. It is noteworthy that, in the context of PCM cool roofs, the issue of dust accumulation, while a concern for aesthetics, does not significantly compromise the heat transfer capabilities of the PCM material. This resilience to dust accumulation underscores one of the advantages of PCM-based cooling systems. Despite surface contamination, the underlying PCM material continues to effectively manage heat, making PCM cool roofs a robust choice in environments prone to dust and particulate matter.

2.13.2.3 Increased albedo in pavement

In a conventional grid design city, pavement covers approximately 29–45% of the urban ground surface [286]. Typically, pavements have dark surfaces and large thermal inertia, which tend to absorb and store solar radiation, negating evaporative cooling and contributing to the development of urban heat islands. The energy balance of a pavement surface can aid in identifying the outbound flows that cool pavements attempt to promote, as well as the fundamental physical principles that govern them. Therefore, cool pavements can be classified into several types, including reflective pavements, green and evaporative pavements, high-inertia pavements, and heat-conductive pavements

[286]. Additionally, when designing pavements, three major factors should be considered: (a) the horizontal surface exposed to solar radiation; (b) the absorption coefficient; and (c) the thermal capacity of the pavement materials. Materials with rough and dark-coloured surfaces tend to absorb more solar radiation than those with flat and light-coloured surfaces [287].

Cool pavements can be classified into three typical categories (Fig.2-14): reflective pavements (Reflective asphalt pavements and Reflective concrete pavements), evaporative pavements (Porous pavers, Permeable pavers and Pervious paver) and storage pavements (heat-harvesting pavement, phase change material-impregnated pavement and high-conductive pavement) [288].

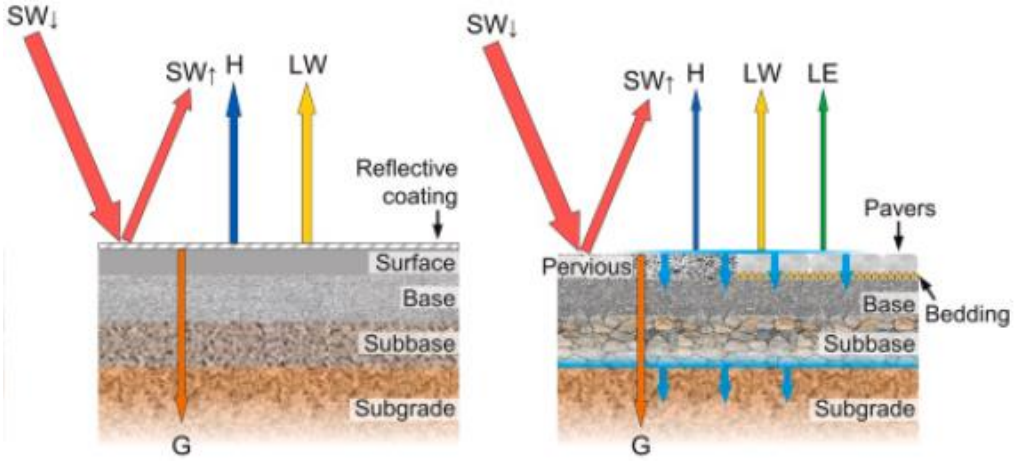

(a) Reflective pavement (b) permeable pavement.

Figure 2-14 Structures of reflective and permeable pavement [289]

Arrows with letters in each subplot show the simplified energy balance for each pavement type: $SW_{\downarrow} - SW_{\uparrow} + LW = G + H + LE$, where $SW_{\downarrow}$, $SW_{\uparrow}$, LW, G, H, and LE denote downward shortwave radiation (solar radiation), upward shortwave radiation (reflected), net longwave radiation, heat conduction, sensible heat flux, and latent heat flux [289].

Reflective pavements are typically made with a high-reflective surface material and a light colour. The high-reflective surface material can help to reduce the

absorption of solar radiation and thus lower the surface temperature. Reflective asphalt pavements and reflective concrete pavements are two types of reflective pavements. Reflective asphalt pavements are made by adding a reflective pigment to the asphalt mix. Reflective concrete pavements are made with white cement, which has high reflectivity, and a light-coloured aggregate. Both types of reflective pavements can significantly reduce the surface temperature compared to traditional dark-coloured pavements.[290].

Evaporative pavements, such as porous pavers, permeable pavers, and pervious pavers, use small voids or pores in the pavement surface to allow water to penetrate the pavement and evaporate. This can help to reduce the surface temperature through evaporative cooling. The water can also recharge the groundwater, reducing the need for irrigation and providing other environmental benefits [291].

Storage pavements, such as heat-harvesting pavements, phase change material-impregnated pavements, and high-conductive pavements, are designed to store heat during the day and release it at night. This can help to reduce the temperature swings in the urban environment and mitigate the UHI effect. Heat-harvesting pavements use thermoelectric generators to convert the heat stored in the pavement into electricity. Phase change material-impregnated pavements are made by adding phase change materials, such as paraffin wax, to the pavement mix. These materials absorb and store heat during the day and release it at night. High-conductive pavements are made with materials that have high thermal conductivity, allowing them to absorb and store heat efficiently [291].

In conclusion, cool pavements can play an important role in mitigating the UHI effect in cities. The design and selection of cool pavements should consider the

surface exposed to solar radiation, the absorption coefficient, and the thermal capacity of the pavement materials. Reflective pavements, evaporative pavements, and storage pavements are three typical categories of cooling pavements, each with its unique benefits and drawbacks. Table 2-17 summarised some previous research on cool pavement affected by UHI. The table provides a comprehensive overview of the study area and scale, methodology, and key findings of each research study, enabling a deeper understanding of the different approaches employed to analyse the relationship between cool pavement and UHI. The findings of these studies underscore the importance of using sustainable urban infrastructure and design to address the challenges posed by UHI, including increased energy consumption, reduced air quality, and negative impacts on human health.

Table 2-17 Summary of different cool pavement effects by UHI

	Methods	Research period	Scale	UHII	Remark	Ref.
Reflective pavement	CFD and monitoring	Hourly	4500 m^2	the peak daily ambient temperature was reduced by 1.9 K during a typical summer day, and the surface temperatures of research areas were reduced by 12 k.	The thermal comfort conditions in the research area were improved at the same time.	[292]
Reflective pavement	CFD and monitoring	Hourly	1km^2	Air temperature reduced by 0.2–0.4 ℃.	Replacing all pavements with surfaces of progressively higher albedo: New asphalt concrete, typical concrete, reflective concrete, making only roofs and walls reflective, and finally replacing all	[293]

					artificial surfaces with a reflective coating.	
Reflective pavement	ENVI-met (albedo 0.1 to 0.5)	Hourly	N/A	Air temperature reduced by 0.66℃.	T_{mrt} and PET were increased to 10.53 and 4.7 °C, by increasing the albedo.	[294]
Permeable pavement	Experiment	Daily	Six 4 m × 4 m	Cooling effects of 15–35 °C over permeable surfaces with watering in the early afternoon in summer	The technical feasibility of combined reflective and permeable pavements for addressing the built environment issues related to both heat island mitigation and storm water runoff management.	[295]
High-conductivity	Experiment	Hourly	100 × 100 × 100 mm	The peak surface temperature of high-conductivity permeable concrete was 1–3 °C lower than that	The increase in thermal conductivity of permeable pavement can further reduce the heat output by 2.5–5.2%.	[296]

permeable pavement				of conventional permeable concrete		
Evaporation-enhancing permeable pavement	Experiment	Hourly	200 × 100 × 50 mm	The new pavement is a maximum cooler 9.4 °C than conventional pavement.	The new pavement provides a longer cooling duration.	[297]
PCM-asphalt concrete pavement	Numerical model	Hourly	N/a	The maximum surface temperature was higher than pavement without PCM.	A critical PCM volume fraction (60%) occurred, and PCM pavement has higher surface temperature values than pavement without PCM.	[298]
PCM-asphalt	Numerical model	minutely	N/a	Reduce the air temperature by 2.5°C.	PCM-pavement slows down the heating (cooling) rate, delays the emergence of	[299]

concrete pavement					extreme high (low) temperatures, short the duration of the extreme high (low) temperature.	

2.13.2.4 **Integrated strategy**

In an urban area, the layout of buildings and structures affects the urban heat island by determining the absorption of solar radiation and the formation of wind streams [300]. Therefore, the integrated strategies have been assessed combined the green and cool strategies for assessing the cooling effects. Previous research has employed integrated mitigation strategies to address UHI (Table 2-18)., such as the combination of Green Infrastructure (GI) and increased albedo strategies. These strategies aim to leverage the advantages of both methods to mitigate UHI by enhancing the reflective properties of urban surfaces and increasing vegetation cover in cities.

Table 2-18 Summary of the integrated strategies

	Methods	Research period	Scale	Mitigation strategies	UHI change	Remark	Ref.
Tehran, Iran	ENVI-met (version 4.3.0)	Hourly	350 m × 350 m	Increased green space. Increased Albedo in roof and pavement. Change rotation.	Changing the orientation of buildings achieved the most significant reduction in air temperature by 1.69 °C.	Proper design of urban forms would largely mitigate UHII.	[301]
Toronto, Canada	ENVI-met	Hourly	300 m × 300 m	Increased green space. Increased Albedo in roof and pavement. Combination model	The cool roof with increasing the roof albedo from 0.3 to 0.7, roof surface temperature could be reduced by up to 11.3 °C.	The duration of direct sun and the mean radiant temperature, which are strongly influenced by the urban form, it is a significant role in thermal comfort.	[7]

While these integrated strategies have shown promising results in reducing UHI, recent studies suggest that they may not be the most effective means of mitigating UHI. For instance, a study found that while the combination of GI and increased albedo reduced surface temperature by 1.2 °C, the individual application of either strategy alone resulted in a more significant reduction of 2.2 °C for increased albedo and 1.8 °C for GI [189]. Therefore, it is important to consider alternative strategies to mitigate UHI that are more effective and tailored to the specific characteristics of a particular city.

2.13.2.5 Summary of the main mitigation strategies in subtropical cities

Existing studies have concluded that many variables can affect the performance of mitigation strategies in subtropical UHI, such as the height and species of vegetation; leaf canopy cover of vegetation; green coverage ratio of vegetation; the colour and density of surface; and the permeability materials.

It is important to consider the climate and weather conditions in a specific area when implementing mitigation strategies. For example, in subtropical regions, there is a high frequency of rainfall and high relative humidity, which can affect the cooling efficiency of some mitigation strategies, such as green roofs and cool pavements. Hence, proper maintenance and selection of materials that can withstand weather conditions are crucial to ensure the sustainability and effectiveness of the mitigation strategies.

Moreover, the scale and design of the mitigation strategies also play a crucial role in their effectiveness. For example, a green roof on a small building may not have a significant impact on mitigating UHI compared to a large green roof covering a large commercial complex. Additionally, the arrangement and

distribution of green spaces, such as parks and gardens, can affect the overall cooling effect on a neighbourhood.

It is also important to consider the social and cultural aspects when implementing mitigation strategies. For instance, the willingness of the community to adopt and maintain green spaces can affect the long-term success of the strategy. Furthermore, the accessibility and equity of green spaces should also be taken into account, as they should be available and accessible for all members of the community, regardless of their socio-economic status.

In conclusion, the effectiveness of mitigation strategies in subtropical UHI requires careful consideration of multiple variables, including climate and weather conditions, scale and design, and social and cultural aspects. A comprehensive and integrated approach that takes these factors into account is essential to ensure the success of the mitigation strategies.

2.14 Thermal energy storage technologies

The challenge of mitigating the impacts of climate change is, in essence, an energy challenge, an energy challenge. Recently, the focus has shifted towards reducing carbon emissions from the energy sector by promoting the use of decarbonized and renewable sources of energy [302]. In line with the goal, IEA released the Net Zero by 2050 for limiting the global temperature increase to 1.5℃. To achieve this, the power sector will need to undergo two parallel transformations for decarbonising: an increasing reliance on variable renewable energy sources for low-carbon power generation, and the electrification of various sectors to drive decarbonisation.

However, the recent COVID-19 pandemic has had a significant impact on energy demand, [303], and carbon emissions in 2021 increased by 14.3–14.9%,

compared with pre-pandemic (2019) [304]. The continued reliance on fossil fuels has resulted in increased prices and environmental concerns. Increasing the use of variable renewable energy sources will help to make power systems more flexible and reduce dependence on fossil fuels.

One of the main challenges associated with the use of renewable energy sources is their fluctuating production patterns (supply and demand). Thermal energy storage (TES) technologies have been proposed as a solution to address this issue by improving the efficiency, possibility and applicability of renewable energy production [305]. Theoretically, TES have the potential to store heat over long time and distances [306] and can replace the fossil fuel-based heat supply with alternative renewable heat sources, such as solar thermal energy, geothermal energy, and waste heat generated from industries. Meanwhile, TES will reduce carbon emissions, primary energy saving and cost saving through the reduction of peak demand [302].

UHI phenomenon occurs when urban areas experience higher temperatures than the rural area surrounding them [181]. This phenomenon contributed to the storage of massive thermal energy in urban objects and materials that have an impervious surface with a higher capacity of heat absorption [307] [308], which is a significant factor in the urban surface energy balance and contributes to the intensity of UHI [181, 309]. Specifically, higher outdoor temperatures lead to increased heat storage on the urban surface via convective and conductive heat transfer [310]. Therefore, there is an interaction and connection between UHI and thermal energy storage.

The conventional UHI mitigation strategies are cool or reflective technologies, which aim to increase the surface albedo and green space. Typically, reflective

technologies have done by [311] applying a liquid material (white paint [164], elastomeric [312], acrylic coatings [313] [314]), or by adopting a single-ply product (Ethylene-Propylene diene-Tetrolymer Membrane (EPDM) [315], Polyvinyl Chloride (PVC) [316], Chlorinated Polyethylene (CPE) [317], Chlorosulfonated Polyethylene (CSPE) [318], Thermoplastic Polyolefin (TPO) [319]. However, the reflective technology has evolved over the years as more and more highly reflective materials are discovered. For example, advances in nanotechnology has led to the conception of highly reflective thermos-chromic paint, which is designed to be thermally reversible. During the hot summer seasons, the cool roof will have a high reflectivity and a high absorption rate during the winter seasons. Although currently more expensive, this technology does present a significant advantage [137].

However, the high and ongoing maintenance costs can be substantial in cool UHI mitigation strategies, and the weight of vegetables for green roofs can be a limiting factor, especially in older buildings with weaker structures. Furthermore, dust and other particulate matter can settle on reflective surfaces, reducing their reflectivity and effectiveness in reducing heat. In addition, the accumulation of dust can also be aesthetically unpleasing and lead to a need for frequent cleaning and maintenance. This can increase the cost and effort required to maintain the effectiveness of these UHI mitigation strategies [98].

Another mitigation technique (i.e. PCM roof, PCM pavement), while not nearly as long-standing as the “cool or reflective” technology, provides an alternative solution. For instance, PCM possesses high latent heat capacity that makes it feasible to use as an energy storage medium in building envelopes. If PCM is widely used in city centre, the extra heat in city centre can be stored and applied,

and the UHII can be affected. Besides, the utilization of TES systems results in two significant environmental benefits: the conservation of fossil fuels through efficiency increases and/or fuel substitution, and reductions in emissions of pollutants such as CO_2, SO_2, and NOx. For example, TES systems have been shown to reduce CO_2 emissions in the United Kingdom by 14 to 46% by shifting electric load to off-peak periods, whereas an Electric Power Research Institute (EPRI)-cosponsored analysis found that TES could reduce CO_2 emissions by 7% compared to conventional electric cooling technologies [347].

Despite the growing interest in TES technology, there has been a shortage of studies that focus specifically on its potential to mitigate UHI effects. This chapter bridges this gap by conducting a comprehensive review of the principles, materials, applications, and optimisations of TES technology.

2.14.1 Classification of thermal energy storage

Numerous studies have reviewed the TES technologies based on their characteristic, including sensible TES (SHTES) [320] [321], latent heat TES (LHTES) [322] [323] [324] [325] and thermochemical TES (TCTES) [326] [327] [328] [329] [330] [331]. These studies have emphasized the distinctive features and benefits of each technology, such as their energy storage density, configuration, and ease of implementation.

SHTES, for example, allows storing energy via changing the temperature of the storage materials (e.g. water, rock bed and ground), which has been implemented and analysed by many studies and also has been applied in a large number of buildings [320]. It has a simple and cheap configuration [306], however, it has low energy storage density (ESD) and is prone to heat loss [332]. For building applications, the ESD of SHTES is around 100MJ/m^3. Water is a common

storage material, the ESD is 290MJ/m^3 [333], which usually occurred a large heat loss.

LHTES adopts the phase-changing process (solid-solid, solid-liquid, liquid-gas, solid-gas and vice versa) of the storage materials (e.g. PCM, hydrate salts and organics) [324] by liquefaction, vaporization and solidification without a significant temperature change. The technology has medium ESD[334], which is around 300-500 MJ/m^3 [333], and also faces challenges such as low thermal stability, corrosion and flammability [335].

TCTES used a heat source based on two reversible reactions (sorption and chemical reaction processes), which include two steps: energy storage and energy release [326, 330]. This technology is applicable in a wide range of temperatures (50℃ to over 1000℃), decreasing the heat loss that would be wasted in the SHTES and LHTES in the form of radiation [336].

Although a larger number of studies have classified the TES simply as SHTES, LHTES and TCTES, a comprehensive classification framework that takes into account the energy reservoirs and building retrofit requirements of TES systems is still lacking. Such a classification framework could provide a better understanding of the suitability and effectiveness of different TES systems in meeting the diverse thermal energy storage needs of different buildings (Fig.2-15). One important aspect that could be considered in such a classification framework is the type of energy reservoir used in TES systems. Energy reservoirs can be categorized as electricity, heat and chemistry. Another aspect that could be considered is the retrofit requirements of TES systems. Retrofitting existing buildings with TES systems can be challenging, as it often requires significant modifications to the building's infrastructure. Therefore, the

classification of TES systems could take into account the retrofit requirements of different TES systems, such as whether they can be integrated into existing building structures without significant modifications or if they require extensive retrofitting.

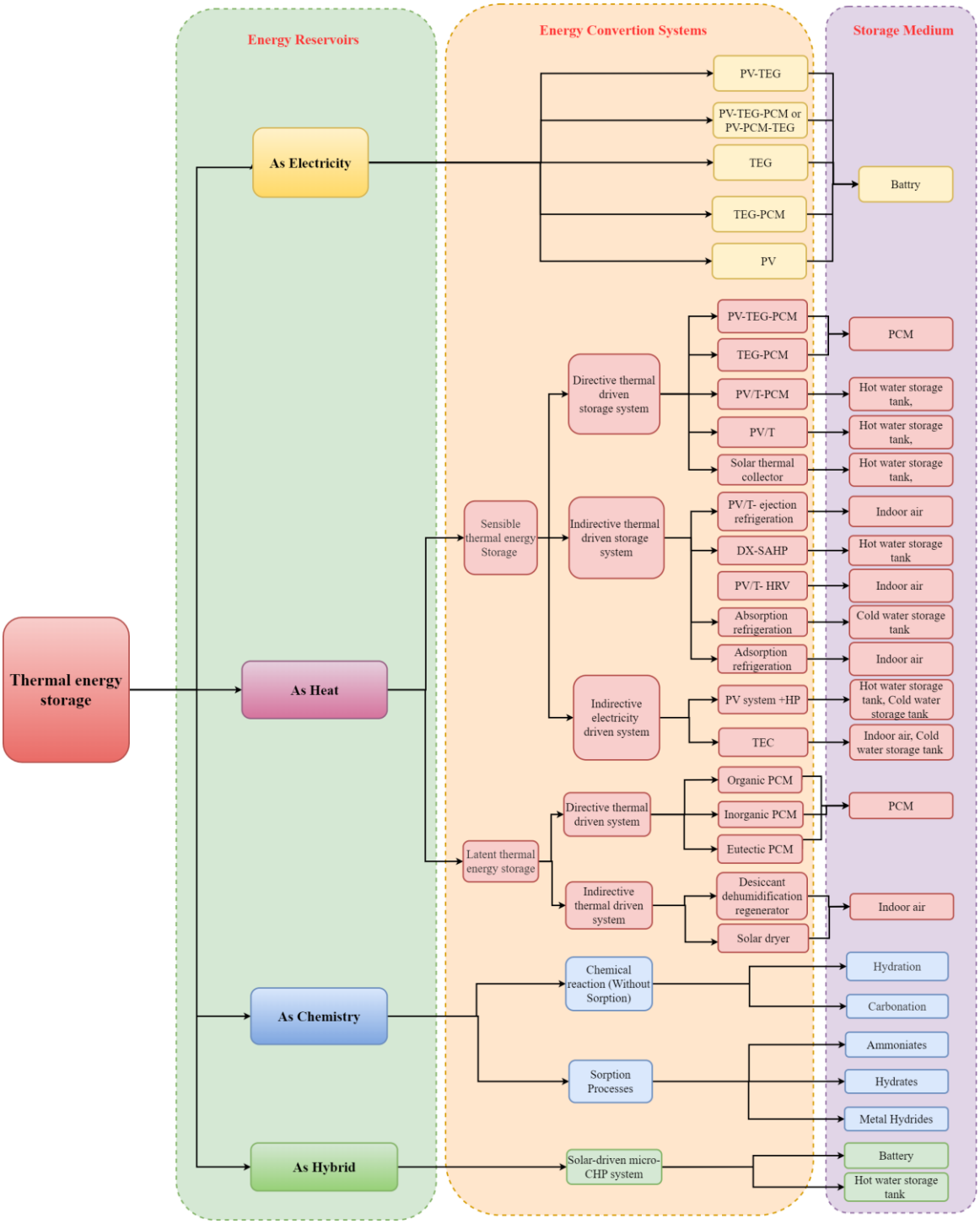

Figure 2-15 The novel classification of thermal energy storage

2.14.2 Sensible-heat storage

The sensible-heat thermal energy storage (SHTES) system utilizes sensible heat to store thermal energy, which is based on the temperature change of the storage materials [320]. This system is characterised by its simple configuration, low cost energy storage materials [306] and low energy storage density (ESD) [332]. Common storage media used in SHTES include water, air, oil, rock bed, brick, and concrete, among others [382]. Sensible-heat thermal energy storage systems are generally simpler and less expensive than latent-heat thermal energy storage systems.

The amount of energy stored is calculated following Eq. (5).

$$Q = \mathrm{m} \cdot C_P \cdot \Delta T \qquad \text{Eq. (5)}$$

where Q is the heat capacity in the material (J), m is the mass of storage material (kg), C_p is the specific heat of the storage material (J/kg · K), and ΔT is the temperature change (K).

SHTES can be further classified into three subcategories based on the drive mode: Directive thermal driving storage system, Indirective thermal driving storage system and indicative electricity driving system.

2.14.2.1 Photovoltaic- thermal system

Photovoltaic- thermal (PVT) system is a combination system that produces both electricity and low-grade thermal energy simultaneously [383]. This technology enables the recovery of part of the waste heat produced by photovoltaic (PV) cells and its utilization for practical applications, while also keeping the temperature of the PV module at a satisfactory level through simultaneous

cooling. Thus, the PVT system is an efficient way to harness solar energy with higher solar conversion and efficiency rates [384]. Additionally, the PVT system typically requires less space than standalone PV and solar thermal systems [385]. Fig.2-21 shows a diagram of the PVT system.

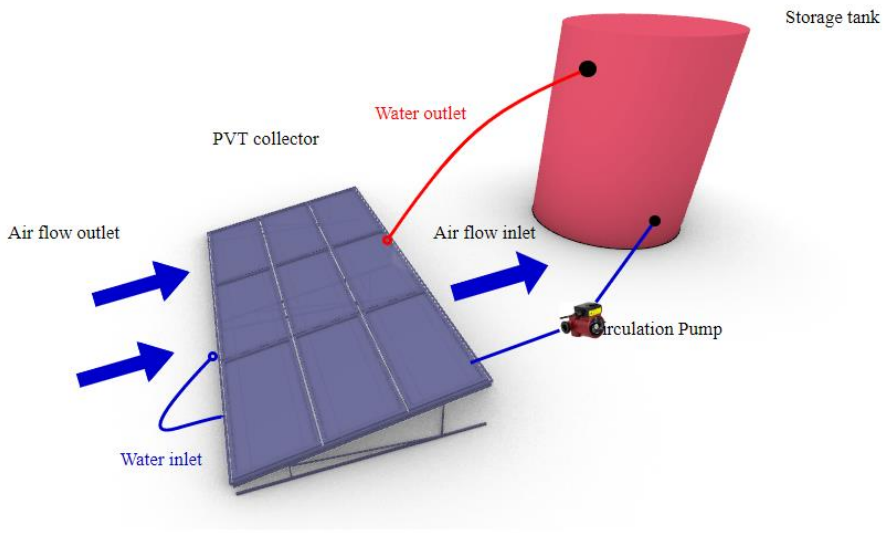

Figure 2-16 Diagram of PVT system [386]

The PVT system can be classified based on the various system parameters (e.g. absorber plate design) and fluid flow systems (natural and forced circulation, single or double pass, channels, etc.). Usually, conventional PVT system has two types based on concentration and non-concentration arrangements of solar radiations [383]. Fg.2-22. shows the classification of PVT systems.

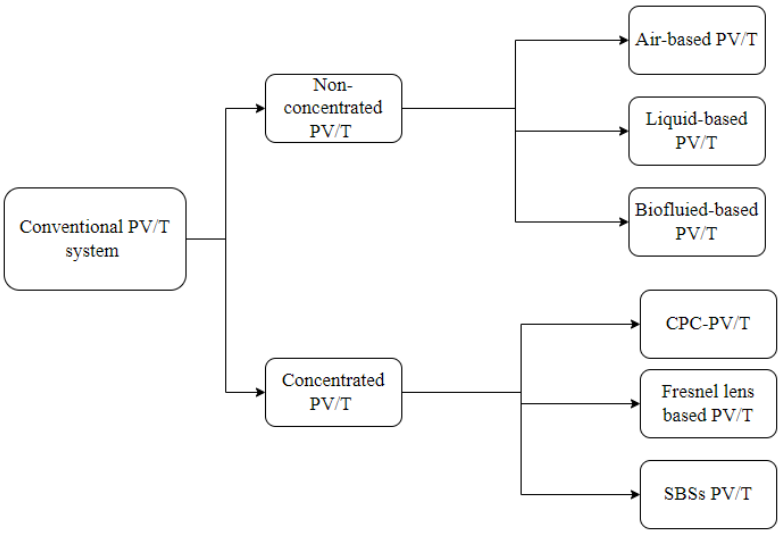

Figure 2-17 The classification of PVT systems

The non-concentrated PVT system represents the simplest form of PVT technology, which does not concentrate solar radiation. Non-concentrated PVTs can be classified into two subcategories based on the storage medium used for heat extraction: air-based and liquid-based PVTs. In air-based PVT systems, air can pass through the PV surface in active or passive mode, using the single or double pass and through different absorbers [385]. However, due to the low density and heat capacity of air, air-based PVT systems are only efficient at low temperatures [387]. Additionally, air-based PVT systems can integrate with space heating in building applications (BIPVT) [388], such as facades [389] [390] [391] [392], roofs [393] [394] [395], windows [396] [397] [398] [399] and shading devices [400] [401] [402] which can help reduce building energy use [403] and carbon emissions [404]. However, Nevertheless, BIPVT systems have technological limitations (e.g. power losses [405], power quality [406] [407], cabling and connection issues [408], etc.), institutional barriers [409] [410],

public acceptance problems [411] [412] [413], financial issues [414] [415] [416] and islanding hazard [408] [417] [418].

Liquid-based PVT systems use a liquid as a medium to extract heat from PV modules, which have a higher heat capacity compared to air [384]. Water, with good heat capacity, is usually used as the prevailing liquid in PVT systems. Water-based PVT systems can generate electricity while heating water [419], which can be used for domestic needs [420] [421] feeding the solar still of the PVT system [422].

For PVT analysis, a 1D steady-state model is suggested [423]. The annual yield of nine different PVT systems has been calculated using this 1-D model, with the results showing that the sheet and tube with zero cover PVT system had the highest electrical efficiency of 9.8%, while the channel above PV design typically had a thermal efficiency of 65% [424]. Additionally, an active solar still integrated PVT system was designed, which had a maximum thermal efficiency of 75%, thermal exergy efficiency of 20.74%, electrical exergy efficiency of 28.53%, overall exergy efficiency of 25%, and overall thermal efficiency of 69.06% [425]. Recently, a glass-covered PVT-integrated solar thermal collector was proposed. The authors also developed a 2D transient mathematical model to analyse the performance of energy and exergy. The results showed that the overall energy efficiency of the PVT system with the solar thermal collector was 41.51%, and the exergy efficiency was 17.63% [426].

Researchers pay special attention to nanofluids, which are advanced coolants made by adding high thermal conductivity nanoparticles to base fluids (conventional coolants) [427]. Due to their excellent thermal properties, nanofluids have been applied to PVT systems [428]. Nanofluids have two main

uses in PVT systems: as a coolant [429] [430] and as a spectral splitter [431] [432] [433]. Besides, many nanoparticles have been adopted into PVT systems, such as CuO [434], SiO_2 [435] [436], Al_2O_3 [437] [438], Fe_3O_4 [439] [440], Ag [441] [442], TiO_2 [443], etc. The present study evaluates the performance of a semi-transparent PVT system utilizing CuO nanofluid as a coolant. The obtained results reveal that the utilization of CuO nanofluid increases the electrical efficiency of the PVT system to 12.55%, as compared to 11.95% when water is used as a coolant. Furthermore, the thermal efficiency of the PVT system is also enhanced from 50.5% to 72% with CuO nanofluid, indicating that the use of nanofluids in PVT systems can improve both exergy and energy efficiency [434]. Recent studies have explored the synthesis, thermo-physical properties, and cooling performance of binary (e.g. Al_2O_3-ZnO [444])and ternary nanofluid (e.g. Al_2O_3-ZnO-Fe_3O_4 [445]) highlighting their potential for enhancing the performance of PVT systems. An analysis of PVT systems utilizing Al_2O_3-ZnO nanofluid reveals that the maximum exergy efficiency of 15.13% can be achieved at a mixture ratio of 0.47 [444]. In addition, the performance of the PVT system employing Al_2O_3-ZnO-Fe_3O_4 nanofluid indicates that the PV cell temperature is reduced by 8.81℃, and the optimum electrical and thermal efficiencies are 13.75% and 59.38%, respectively, when the mixture ratio is 0.33. The overall maximum exergy efficiency of the PVT system is found to be 14.77% [445].

In liquid-based PVT systems, increasing the mass flow rate [446] [447], inlet velocity, and inlet temperature [448] can increase the exergy and energy efficiency. However, challenges exist, such as the high cost of nanofluids [449] [450], and potential issues with nanoparticle aggregation, viscosity, and

sedimentation, which affect the performance of PVT systems [451]. Moreover, the use of liquid coolant may cause erosion and corrosion of thermal devices over time [452] [450].

Furthermore, in concentrated PVT (CPVT) systems, solar concentrators (such as Compound Parabolic collectors (CPC) [453] [454] [455], plan reflecting mirrors [456] [457], Fresnel lenses [458] [459] [460] [461] [462], parabolic dish [463] [464] [465], parabolic troughs [466] [458] [467] [464], etc.) are used to harness the same amount of solar radiation with fewer PV panels [468]. Studies have shown that low-concentrated PVT systems (1< Concentration ratio (CR) <10) and medium-concentrated PVT systems (10< CR <100) exhibit improved performance. The total efficiencies of a PVT system using a linear Fresnel lens are reported to be 53%, where the electrical efficiency decreased from 10.9% to 7.63% due to solar concentration. However, the output power of the PV modules increased by 28% [462]. Another study utilized an integrated PVT-CPC system with double slope solar coupled with a helically coiled heat exchanger. Two nanofluids, namely single-wall carbon nanotubes and multi-wall carbon nanotubes, were utilized as coolants. The results show that the heat transfer coefficients of PV/T-CPC, helically coiled heat exchanger, and double slope solar still increase around 46.4%, 46.7%, and 76.7%, respectively, when single-wall carbon nanotubes nanofluid is utilized [469]. A parabolic trough CPVT was manufactured and analysed. Three variations of PV-module and heat-sink designs were evaluated, demonstrating that the prototype CPVT system attains an overall efficiency of approximately 50%, with thermal and electrical efficiencies of 44% and 6%, respectively [467]. Additionally, a theoretical model of a parabolic dish CPVT system with a hot mirror was developed. The

hot mirror reflects the infrared (IR) and ultraviolet (UV) components of the concentrated solar energy spectrum to the vacuum tube. The modelling results showed that the energy efficiencies of the concentrator, vacuum tube, and overall CPVT system are 15.35%, 49.86%, and 7.3%, respectively. The corresponding exergy efficiencies are 12.06%, 2.0%, and 1.16%, respectively [463].

Despite their potential, CPVT systems have some limitations. The parabolic trough CPVT system requires a larger field of view and incurs higher costs due to its low optical efficiency [470]. The Fresnel lens-based PVT system may suffer from transmittance losses owing to the incidence on the draft face [471]. Furthermore, further research and development are required to address challenges related to high-precision tracking, illumination uniformity, and heat transfer fluid optimization in high-concentration CPVT systems [472].

2.14.2.2 Photovoltaic- thermal system with phase change material

PCM as auxiliary cooling media and heat storage media integrated with PVT can reduce the PV panel temperature [473], and improve the overall energy conversion performances [474]. Various PCMs have high latent heat absorption capacity with slight temperature variation during the phase transition process [475]. Usually, there are three types of PCMs, organic PCM (e.g. paraffin, acids and eutectic mixtures), inorganic PCM (e.g. $CaCl_2H_{12}O_6$, NaOH-KOH and metals) and eutectic PCM (Organic-Organic, organic-inorganic and inorganic and inorganic). Figure 2-23 shows the typical configuration for PVT-PCM.

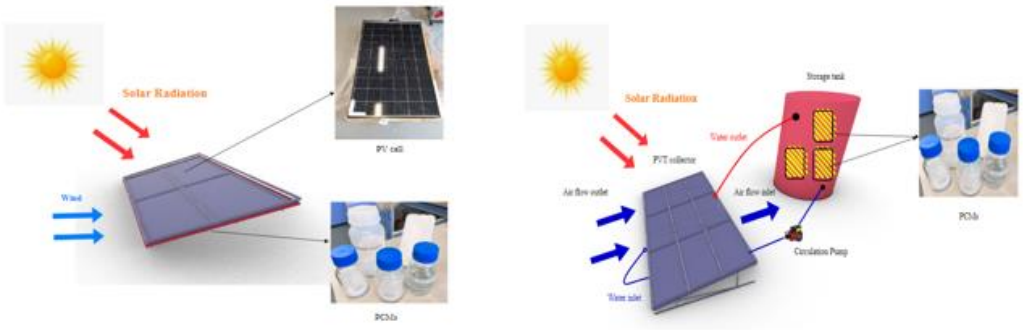

Figure 2-18 Schematic diagram of direct contact PVT-PCM and indirect PCM-water-based PVT system [476]

The thermophysical properties of PCMs used in PVT systems from the literature are summarised in Table 2-19. This table contains critical information on the melting temperature, thermal conductivity and latent heat capacity of the PCM. The inclusion of these properties is essential for the optimal design and performance of PVT systems, as they directly impact the overall energy efficiency and effectiveness of the system.

Table 2-19 Summary of thermophysical properties of PCMs used in PVT systems

PCM (Ref.)	PCM Type	Melting temperature (℃)	Latent heat capacity (KJ/Kg)	Thermal conductivity (W/m·K)	PV/T type	Special technology	Findings
Paraffin [477]	Macro-encapsulation	15	182	0.2	Conventional solar PV/T	Micro-channel heat pipes	The daily average electrical efficiency reaches 36.71%, 35.53% and 31.78% for the PCM, MCHP and regular PV/T systems.
C18, C22, Palmitic /Capric acid,	Paraffin, Paraffin, Acid,	28.85, 43.85, 17.55-22.65,	244, 226, 190,		FPPV/T	Metal foam (copper foam)	Electrical efficiency of the PV/T with metal foam increases by 2.3%.

Sodium phosphate salt, C15 [478]	Salt, paraffin	36.85, 13.85	280, 205				
$CaCl_2 \cdot 6H_2O$ Eutectic of capric-palmitic acid RT20	Inorganic Calcium chloride hexahydrate acid Paraffin wax	22.5 29.8 25.73 26.6	173 191 140.3 232	Solid 0.14 Liquid 0.14 Solid 1.08 Liquid 0.56 Solid 0.2 Liquid 0.2	FPPV/T	Nano PCM	The PV/T/nano PCM (10 wt %) has higher electrical efficiency than PV by 22% in mid-July.

RT25 RT35 +Graphene Nanoplatelets [479]	Paraffin wax Paraffin wax	29-36	130	Solid 0.19 Liquid 0.18 Solid 0.2 Liquid 0.2			
RT 28 RT 35 RT 44 RT 50 [480]	Paraffin Paraffin Paraffin Paraffin	28 35 41-44 50	245 157 255 168	0.2 0.2 0.2 0.2	Mono-crystalline semi-transparent FPPV/T		The maximum diurnal energy efficiency is 35.04% for PV/T and RT35 PCM during the summer. The maximum daily exergy efficiency is 15.17% for PV and RT28 PCM type in the winter.

RT-52 1-tetradecanol, Lauric acid, Decanoic acid synthesis, Decanoic acid natural [481]	Paraffin tetradecanol Acid Acid Acid	52-54 36-40 44-46 27-32 29-33	167.27 259.44 228.90 179.13 178.98	N/A	Two side serpentine flow based PV/T		Maximum energy and exergy efficiency is 87.72% and 12.19% respectively.
PT-30 [482]	Paraffin-wax	57	200-220	0.24	Water-based PV/T		The overall efficiency of PVT-PCM/water system is 26.87% and 40.59% respectively. Electrical efficiency is increased by

							17.33% compared with conventional PV panel.
N/A [483]	Paraffin wax	49	196	0.21	FPPV/T	SiC Nanofluid and nano-PCM	Electrical efficiency increased from 7.1% to 13.7% and thermal efficiency is high to 72%.
N/A NaOH (24%)-KOH (76%) [367]	Paraffin Inorganic	47 62 72 102 147 152 157	168 152 182 200 205 205 205	0.2 0.2 0.2 0.2 0.6 0.6 0.6	Concentrated PV/T	Fresnel lens, Thermoelectric system	The daily overall efficiency of the PV–PCM–TE system is 26.57%.

$CaC_{l2}H_{12}O_6$ [484]	Inorganic, Calcium chloride hexahydrate	31	191	Solid: 1.08 Liquid:0.56	FPPV/T	Al_2O_3 nanoparticles loading in the PCM on PV cell	Al_2O_3 (φ = 1%)/PCM mixture (λ_{PCM} = 25%) + 75% water (5.31 kg/s.m^2) achieved the highest PV performance.
$Na_2HPO_4 \cdot 12H_2O$ [485]	Inorganic	37	265	0.514	FPPV/T	Parallel air source heat pump module	The overall efficiency of this solar PV/T heat pump system can reach above 75%.
$NaSO_4 10H_2O$ $N_2O_6Zn \cdot 6H_2O$	Inorganic	32.4 36	251 146.9	Solid:0.54 Liquid:1.011	BISTPV		The BISTPV module increased power generation from 34,287 to 37,024 W h/year by using PCM.

Inorganic PCMs generally possess higher latent heat than organic PCMs, making them an attractive option for thermal energy storage applications. PCMs can be integrated with photovoltaic thermal (PVT) systems, building integrated PVT (BIPVT) systems, and PVT systems coupled with other energy conversion technologies. BIPVT-PCM systems can be applied on the roofs [486] [487] or façades [488] [489] [490] have demonstrated the ability to manage building energy demand [486], peak load [491] [492] and indoor thermal comfort [493]. However, there is still a lack of comprehensive guidelines for the optimal design and configuration of PVT-PCM systems, and further research is required to assess and compare the performance of different PV-PCM systems. Additionally, more effective phase change processes for PCMs are needed to develop BIPVT-PCM systems.

2.14.3 Latent-heat storage

Latent heat thermal energy storage (LHTES) is a type of thermal energy storage that utilizes the latent heat of a material to store thermal energy. During charging, thermal energy is added to the storage material, causing it to change phase from a solid to a liquid or from a liquid to a gas, and storing the energy as latent heat. During discharge, the material is allowed to solidify or condense, releasing the stored heat energy [552].

The amount of thermal energy stored in an LHTES system is proportional to the mass and latent heat of the storage material. Therefore, materials with the high latent heat of fusion or vaporization are typically used as storage media, such as phase change materials (PCMs) and heat of vaporization materials (HOVMs). PCMs are materials that change the phase between solid and liquid, while HOVMs change the phase between liquid and gas. These materials have the

advantage of storing a large amount of energy in a small volume, compared to sensible heat storage materials [553]

2.14.3.1 Phase change material

As mentioned above, phase change materials (PCM) have high energy storage density and can store thermal energy in a constant temperature phase transition process [554]. The phase change process could be changing the state between liquid and gas by condensation and vaporisation, a change of state between solid and liquid by liquefaction or solidification, or changing the phase between two solid states. Owing to certain technical limitations of the solid-solid and liquid-gas processes, only solid-liquid PCMs are suitable for building heating and cooling applications [555]. The melting point of PCMs is researched by the increase in ambient air temperature, which causes the breaking of chemical bonds, allowing the material to absorb energy as it transitions from solid to liquid. When the ambient air temperature decreases and reaches the freezing point of the PCM, chemical bonds reform and the material releases heat as it reverts to its solid state. An illustration of the change processes is shown in Fig. 2-33.

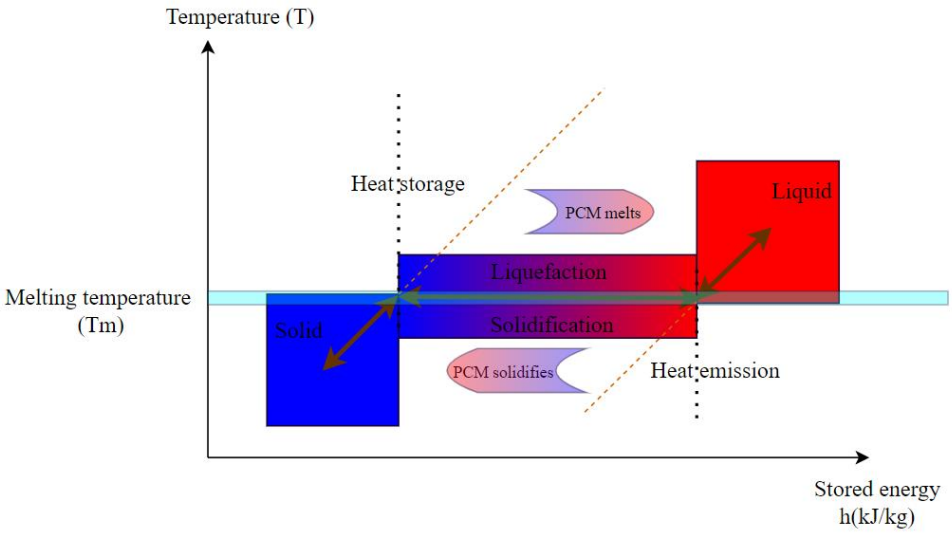

Figure 2-19 Illustration of PCM change processed [556]

PCMs are classified into three types, organic (e.g. Paraffin [557] [558], Polyethylene glycol [559] [560], Fatty acid [561] [562], etc.), inorganic (e.g. salt-hydrates [563] [564], molten salts [565] [566], metals [567] [568], etc.) and eutectic (organic-organic [561], organic-inorganic [569] and inorganic-inorganic [570]).

Besides, the melting temperature of different PCMs varies, and each PCM has its own specific latent heat capacity [556]. In building applications, PCM can be used in roofs [278] [283], façades [571] [572], floors [573] [574] and windows [575] [576] for cooling or heating purposes in both new buildings or retrofitting of existed buildings [577].

Numerous studies have investigated the performance of PCMs in building applications. A numerical analysis of the performance of the PCM roof was conducted. The influence factors of the thermal behaviour of PCM roofs have been investigated, such as solar radiation intensity, transition temperature and latent heat of PCM, roof slope, PCM layer thickness, and absorption coefficients of external roof surface. The results revealed that the PCM roofs significantly

affect the temperature delay in the indoor space, which can delay three hours for peak temperature in the base layer of PCM roofs when compared with the common roof [278]. The relationship between PCM roof and UHI in temperate climatic conditions was experimentally analysed. A mixed hydrophilic paint with microencapsulated PCM was used as a roof-finishing material to create PCM-doped tiles. The results presented that the system can significantly reduce building surface temperatures and chamber temperatures in summer weather conditions, and demonstrated the lowest diurnal variation by 7.2℃. Furthermore, in winter conditions, the PCM-doped tiles keep the surface temperature low while keeping the chamber air temperature high. Therefore, PCM-doped tiles have the potential to mitigate UHI intensity [282].

Besides, a macro-encapsulated PCM (SP22) was used to fill into the air cavity of a ventilated façade to analyse the potential in decreasing the cooling demand in the summer season. This façade can be used as a cold storage unit, which can avoid overheating in the daytime and release cool in the nighttime. The thermal performance of this façade has been experimentally tested. The results showed that the PCM integrated with ventilated façade can reduce the cooling loads of a building through nighttime cooling [578]. Moreover, a PCM (55% decanoic acid and 45% lauric acid) integrated Trombe wall was tested in laboratory conditions. The test results presented that the air temperature inside the laboratory can be increased by 1.88 °C for low heat input mode and 3.27 °C for high heat input mode, respectively. However, the irregular-shape liquid/solid interface, caused by the 2D heat transfer along the height and thickness of the PCM walls, led to large temperature differences in both directions and highlights the need for

PCMs with suitable melting temperatures, longer phase change periods, and higher latent heat capacities [579].

In addition, the thermal performance of a triple-pane window filled with PCM (Paraffin MG29) in the outer cavity was analysed, and have been measured on sunny and rainy summer days. The results showed that the system the peak temperature on the interior surface by 5.5℃, while also reducing the heat that entered the building through the window by 28% on a sunny summer day. Besides, the performance of a window shutter incorporated with a PCM (paraffin RT28HC) was analysed. The numerical models based on 2D analysis are created to model the indoor temperature comparison between the experimental and the simulated model. The results showed that this system decreased the maximum indoor temperature by up to 8.7% in the warming period, also increased 16.7% the minimum indoor temperature at night time and delayed the maximum temperature peak for one hour and 30 minutes for the minimum temperature peak [580].

Overall, PCMs are substances that have the ability to store and release large amounts of thermal energy during phase change processes. In building applications, PCMs are increasingly being used as thermal energy storage materials to regulate indoor temperatures and improve energy efficiency. PCMs offer several advantages, including improved indoor thermal comfort, reduced energy consumption, and lower heating and cooling costs. This is due to the ability of PCMs to store and release heat in response to temperature fluctuations, thereby reducing the load on heating and cooling systems.

However, despite these benefits, the use of PCMs in building construction also presents certain limitations and challenges. The major disadvantage is the high

cost of materials and equipment required for the implementation, which can be prohibitive for some construction projects. Additionally, the integration of PCMs into building components can be a complex and specialized process, requiring technical expertise and specialized knowledge. Besides, some limitations need to be optimised, such as poor thermal conductivity [581], liquid leakage [582], overcooling problems [583] and corrosion issues [584]. Besides, despite those disadvantages of using PCMs, the environmental friend is the key factor restricting their popularisation and use. Therefore, researching the green preparation and cost-effective technology of PCMs is required for developing the energy-saving application.

2.15 Summary

A comprehensive review of the literature on the subtropical UHI and its main mitigation strategies has been undertaken in this chapter to gain a better understanding of this phenomenon.

Urban heat island is a well-known and researched phenomenon that refers to the higher temperatures observed in urban areas compared to surrounding rural areas. The causes of UHI are complex and interrelated and include anthropogenic heat, urban form, surface materials, and land use changes. These factors influence the energy balance and microclimate of urban areas, leading to increased temperatures.

Evaluation approaches for UHI include remote sensing, simulation modelling, and field measurements. Several metrological parameters are used to evaluate UHI, including air temperature, sky view factor, net radiation, thermal radiative power, and mean radiant temperature. However, still lacking a compressive

metrological assessment to analyse the effectiveness of UHI mitigation strategies including radiation variation.

Additionally, UHI has numerous effects, including increased energy consumption and carbon emissions, decreased human thermal comfort, and negative impacts on urban ecosystems. Higher temperatures in urban areas increase the demand for air conditioning and transportation, leading to increased energy consumption and carbon emissions. The negative impacts on human health and well-being due to heat stress and related health effects are also a concern.

Besides, conventional mitigation strategies for UHI include green infrastructure, cool materials, and urban planning measures. These strategies can reduce the urban heat island intensity, improve urban ecosystems, reduce energy consumption and carbon emissions, and enhance human thermal comfort. A comprehensive understanding of those conventional mitigation strategies of UHI and its impacts is essential for effective mitigation and adaptation strategies in urban areas, particularly in light of climate change and urbanization. However, there is still a lake of a comprehensive analysis between UHI mitigation strategies and energy use, carbon emissions and human thermal.

Furthermore, Thermal energy storage is an essential technology for the development of sustainable energy systems, as it enables the storage of heat or cold energy generated from renewable sources for use during periods when energy is not being produced. This technology helps to reduce the reliance on fossil fuels and supports the transition to a low-carbon energy mix. To better understand the relationship between TES and UHI and to analyse the potential ability of UHI mitigation, the main TES systems have been reviewed and

classified into three types, based on user choices: TES stored as electricity, TES stored as heat, and TES stored as chemistry.

TES systems offer several advantages. Firstly, they can improve the energy efficiency of buildings and industrial processes by allowing for the storage of excess energy during periods of low demand and releasing it during periods of high demand. This can help reduce overall energy consumption and costs. Secondly, TES systems can enhance the reliability of energy supply by providing a backup energy source during power outages or periods of high demand. This can help reduce the risk of blackouts and ensure a steady supply of energy. Thirdly, TES systems can help integrate renewable energy sources, such as solar and wind power, into the energy grid by storing excess energy and releasing it when needed. This can increase the reliability and sustainability of the energy system. Fourthly, TES systems can manage peak energy loads by storing energy during periods of low demand and releasing it during periods of high demand, thus reducing the need for additional power generation capacity and improving grid stability. However, some limitations impact the efficiency and effectiveness of TES systems. Firstly, TES systems can be expensive to install and require specialized materials and equipment, making them cost-prohibitive for some applications. Nonetheless, the cost of TES systems is decreasing as the technology becomes more widespread. Secondly, some TES systems have limited operating temperatures, which can limit their usefulness in certain applications. For instance, latent heat storage systems may have limited operating temperatures due to the melting or solidification point of the storage material. Thirdly, TES systems may experience energy loss due to heat leakage, which can reduce their efficiency and effectiveness. This can be mitigated by

using high-quality insulation materials and designing the system to minimize heat loss. Fourthly, certain TES systems, such as chemical TES systems, may require careful handling of materials and pose potential safety risks.

Additionally, TES systems have shown the ability to effectively mitigate the UHI effect. These systems have the capacity to store thermal energy during the day and release it during cooler nighttime temperatures. This results in a reduction of peak temperatures during the day and a more comfortable living environment at night. Specifically, when phase change materials are integrated into a building's roof, they absorb heat during the day and release it at night, ultimately lowering the temperature of the roof and the surrounding area.

In summary, the implementation of TES systems, such as PCM roofs, can significantly alleviate the effects of UHI in urban areas and improve the quality of life for urban residents. However, further research is required to investigate the long-term performance and economic feasibility of TES systems.

3 CHAPTER III: RESEARCH METHODOLOGY

3.1 Introduction

To explore the characteristics and mitigation strategies of the UHI phenomenon in subtropical cities, a simulation method has been selected as the primary means of investigating the most effective mitigation strategies. In addition, an attempt was made to integrate two or more methods to explore the most effective mitigation strategies for the correlation between surface and ambient temperatures and to investigate the formation of UHIs in complex cities. The main mechanism of this simulation method involves the following steps:

Collect data: Collect detailed data on the physical characteristics of the urban

area, such as land use patterns, building morphology, surface materials, and vegetation coverage. This data can be collected through remote sensing, government documents, field surveys, or other sources.

Define scenarios: Define different UHI mitigation scenarios that are appropriate for the local context and that can be realistically implemented. These scenarios can include conventional mitigation strategies, increasing green spaces, installing green roofs, ore using cool pavements, and implementing thermal energy storage as UHI mitigation strategies such as PCM and PV technologies.

Select modelling tools: Select appropriate modelling tools that can simulate the interactions between the urban environment and the atmosphere, such as energy balance models, urban canopy models, and computational fluid dynamics models.

Input data: Input the collected data and the defined scenarios into the selected models, taking into account factors such as diurnal, seasonal and annual weather conditions.

Run simulations: Run the simulations to generate predictions of the effects of each UHI mitigation scenario on meteorological parameters, micro-environment, energy consumption and human comfort.

Collaborate and validation simulations: Implement the most effective and feasible UHI mitigation strategies, and monitor the performance over time to evaluate their long-term impacts on urban temperatures and environmental conditions. This involves collaborating and validating with simulations.

Analyse results: Analyse the simulation results to determine which UHI mitigation scenarios are most effective at reducing energy consumption and improving urban environmental conditions.

To achieve the aim of the research, ENVI-met software was selected as the simulation tool for meteorological parameters to examine the effects of urban UHI mitigation strategies. Moreover, a novel model, UHIMS-ECHE, was developed by integrating Rhinoceros, a 3D computer-aided design and modelling tool, and Grasshopper, a computer visual programming language, with its two plugins, Ladybug and Dragonfly.

The UHIMS-ECHE model was developed and utilised to simulate urban building energy use, carbon emissions, and human thermal comfort, providing a comprehensive analysis of UHI mitigation strategies.

3.2 Meteorological assessment

3.2.1 ENVI-met model set-up and testing

ENVI-met (version 5.0.1) is a software tool used to simulate and analyse microclimates in urban environments. It utilises advanced computational fluid dynamics and radiation transfer algorithms to simulate the interactions between the built environment and the surrounding atmosphere, taking into account physical parameters such as surface geometry, material properties, solar radiation, atmospheric conditions, and vegetation cover. Envi-met is particularly useful for designing and optimizing urban spaces for maximum comfort, energy efficiency, and sustainability, and has been extensively validated against experimental data. Its ability to simulate a wide range of environmental variables at high spatial and temporal resolutions, along with its user-friendly interface, make it an essential tool for sustainable urban development. Fig.3-1 illustrates the flow diagram of ENVI-met.

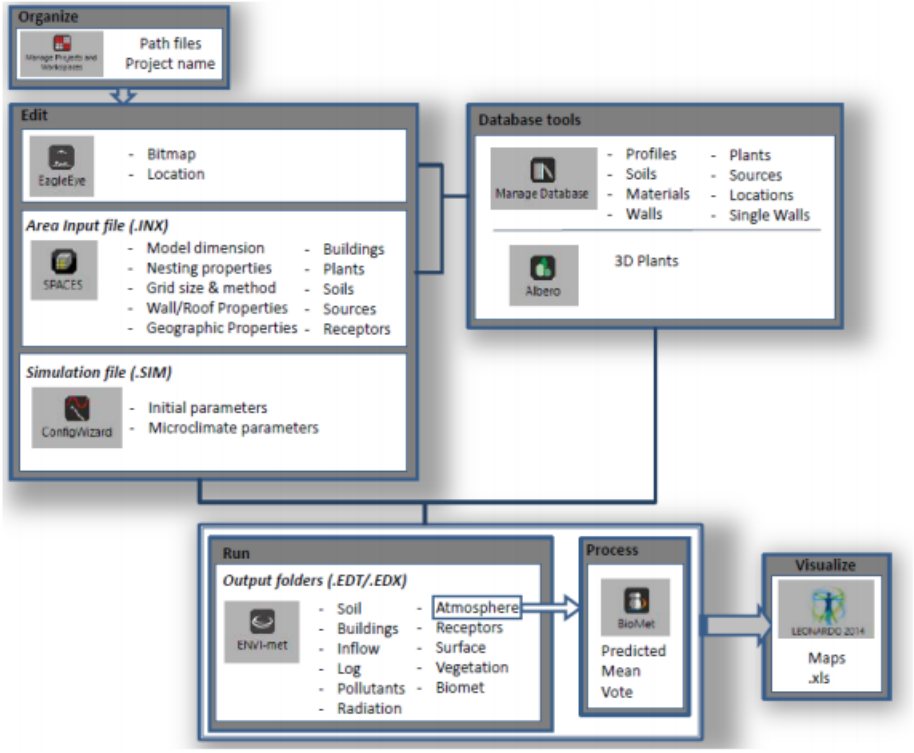

Figure 3-1. The flow diagram of ENVI-met

This study employs a simulation approach utilizing the ENVI-met tool to analyse the efficacy of various UHI mitigation strategies in subtropical cities. The methodology consists of three main steps: inputting the digital geographic maps of the research area, inputting and configuring the required databases for soil types, humidity, air temperature, and other relevant variables, and conducting the simulation of the area.

The ENVI-met tool employs an orthogonal Arakawa C-grid to represent the environment and adopts the finite difference method to solve partial differential equations, making it suitable for the simulation of thermal interactions between building areas, soil, vegetation, and atmospheric conditions. However, the tool only permits linear and rectangular structures, hence, the building structures in the study have been simplified to straight and rectangular shapes for easy simulation. This research uses the simulation approach to analyse the UHI

mitigation strategies in subtropical climate zones by ENVI-met to simulate thermal interactions between building areas, soil, vegetation and atmosphere condition [18,19].

In particular, ENVI-met simulation is suitable for subtropical city centres. A study is conducted in Hong Kong China [20] that demonstrated that proper tree planning is able to mitigate UHI effectively during daytime by using ENVI-met simulation. Besides, ENVI-met can calibrate the subtropical city, São Paulo, Brazil [6] by combining land use data and field campaigns and microclimate measurements. Moreover, Shanghai China as a case study is validated ENVI-met software is still a helpful tool for modelling microclimate in the subtropical city centre [21].

3.2.2 Set up meteorological data in ENVI-met

ENVI-met requires meteorological data to run simulations, which can be obtained from the weather station, climate databases or movement documents. This includes specifying the air temperature, humidity, wind speed, and direction, precipitation, solar radiation, cloud cover, and, etc. Besides, ENVI-met requires boundary conditions to be defined for the meteorological data. This includes setting the boundary height, roughness length, and drag coefficient for each boundary type, such as urban, rural, or water.

3.2.3 Set up simulation parameters in ENVI-met

ENVI-met requires defining the simulation parameters. This includes specifying the start and end times of the simulation, the time step size, and the output settings. Besides, land cover and land use should be set in ENVI-met, the boundary of buildings, pavement, and green spaces, as well as the type and density of vegetation. This step is crucial in ensuring that the simulation is

accurate and appropriate for answering the research question.

3.2.4 Set up output parameter in ENVI-met

The output parameters in ENVI-met are generally divided into two categories: physical parameters (temperature, wind speed, humidity, and radiation) and calculated parameters (comfort, air quality, and energy consumption).

Hourly annual UHII is a crucial parameter that provides insight into the UHI effect's intensity throughout the year. The parameter measures the temperature difference between urban and rural areas, with higher values indicating more substantial UHI effects. The sky view factor represents the fraction of the visible sky from the ground level and is a critical factor in influencing solar radiation and thermal energy exchanges. Higher values of SVF correspond to less obstruction of the sky and can lead to lower temperatures. Net radiation (Rn) is a significant component of the urban energy balance and measures the difference between the incoming and outgoing radiation energy. On the other hand, thermal radiative power (TRP) is a measure of the thermal energy emitted by urban surfaces, which is influenced by surface temperature and emissivity. Mean radiation temperature (MRT) represents the average temperature of all surfaces emitting thermal radiation in an area, including the sky. The combination of these parameters enables the evaluation of the different heat transfer processes in the urban environment, such as the contribution of the urban surface emissivity and absorption to the energy balance.

3.3 Urban heat island mitigation strategies – energy, carbon emission, human thermal comfort economic analysis model

ENVI-met is not specifically tailored for predicting annual energy use and is not typically within its scope. To analyse annual energy consumption, carbon

emissions and human thermal comfort, this paper proposed a comprehensive hourly parametric model (UHIMS-ECHE), which can comprehensively investigate the effectiveness of UHI mitigation strategies by coupling with urban building energy use, carbon emission, human comfort and economic analysis.

The UHIMS-ECHE model considered the primary heat sources generated from buildings, pavement (asphalt and dark concrete), original surface (sand and bare soil) and green infrastructures (parks, trees and grass). Based on the systematic literature review above, the UHIMS-ECHE model adopts Resistance–Capacitance inverse approach of the grey-box model for urban building energy modelling as the main theory and processes, comprised of five steps: Urban weather generation, urban archetype, input data training, urban building energy simulation and calibration and validation, the process steps are shown in Fig.3-2.

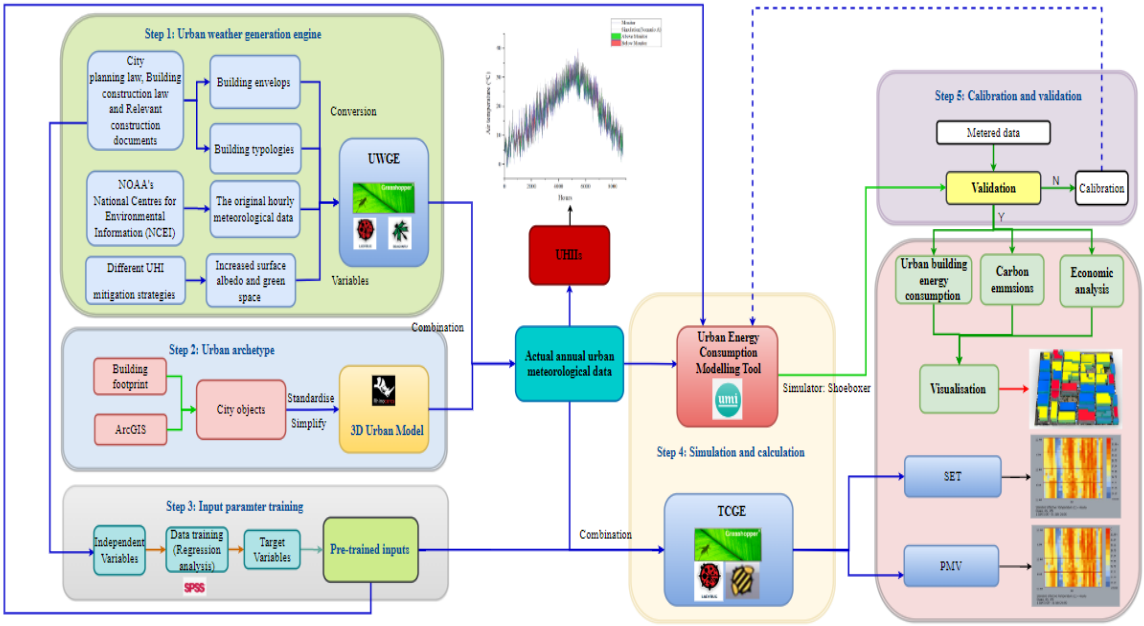

Figure 3-2 Diagram of the UHIMS-ECHE model

3.3.1 Step 1: Urban weather generation engine

The use of Rhinoceros, a powerful 3D computer-aided design and modelling tool, in conjunction with the computer visual programming language Grasshopper and its two plugins, Ladybug and Dragonfly, has resulted in the development of a novel urban weather generation engine (UWGE).

Ladybug is a suite of environmental analysis tools to visualise and analyse climate data, solar radiation, daylighting, and more. Ladybug can be used to perform simulations to evaluate the impact of climate on the performance of a building or urban area. Additionally, Dragonfly is a plugin based on ENVI-met that expands upon the functionality of Ladybug by adding tools for energy and daylight analysis. Dragonfly can be used to perform energy simulations to assess urban building energy consumption.

The UWGE can calculate UHI intensity and produce the urban microclimate condition (e.g. dry bulb temperature, dew point temperature, relative humidity, wind speed and direction, etc.) on the city scale by converting the meteorological information from available weather data.

The UWGE combines the meteorological data from a rural weather station with city-specific characteristics, which are obtained from various sources such as city planning law, building construction law and some relevant construction documents (Fig.3-3.). These data include building typologies (e.g. building ages, building program, floor-to-floor height, etc.) and building envelopes (e.g. glazing ratio, roof albedo, wall albedo, etc.). Related to UHI mitigation strategies in building typologies and envelopes, the UWGE provides a comprehensive and customizable solution for predicting urban weather conditions.

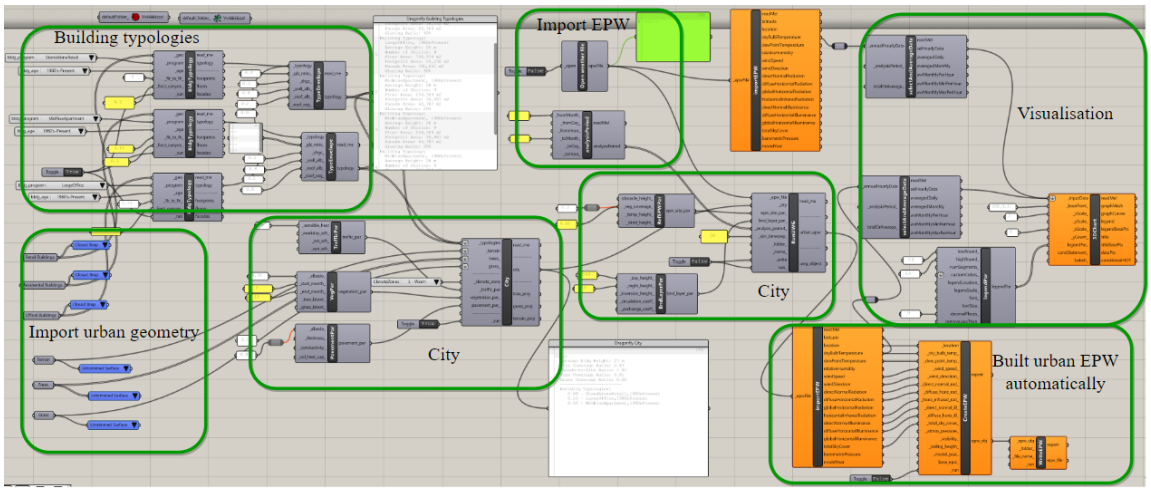

Figure 3-3 UWGE processes in Grasshopper

This innovative tool combines the latest advances in computer-aided design, programming, and meteorology to provide an accurate and reliable solution for predicting and mitigating the effects of the UHI phenomenon. The combination of meteorological data and city-specific characteristics enables the UWGE to generate highly realistic and informative microclimate conditions on a city scale. However, the UWGE requires importing urban geometry. Thus, the data for urban archetypes should be collected in step 2.

3.3.2 Step 2: Urban archetype

The development of a 3D urban model for the research city centre requires comprehensive data pertaining to the various components of the city and individual buildings. The data of city objects (e.g. climate zone, traffic parameters, vegetation space and pavement area, etc.) are collected from ArcGIS and building footprints, which are simplified and standardised by Rhinoceros and converted to the 3D model with the simplified building envelope, urban green space and pavement area.

Each building has a unique building I.D., along with ground surface coordinates, and height coordinates. The simplification standards for the urban archetype are

based on the research conducted by Abolhassani [636]. The ground surface is dissolved to create an outer boundary with the Boolean-union method in Rhinoceros. Afterwards, the ground surface of each building is extruded to the average building height. Each extruded building is considered a large thermal zone for calculating energy demand and consumption. Although this type of geometry and thermal zone may cause calculation inaccuracy, it is time and computer efficient making it suitable for the city scale.

Thus, the 3D urban model is merged with the UWGE, resulting in a dataset that can be converted into EnergyPlus weather files that accurately reflect the urban microclimate conditions.

3.3.3 Step 3: Input data training

The input parameters which can impact the building energy demand are collected from the local building and city plan law or related construction documents and corresponding specifications with detailed specifications parameters for the research area. To identify patterns in these criteria, the input data must undergo training. The target variables include construction materials data, HVAC system and occupancy schedule, lighting, etc.

The occupancy schedule archetypes are categorised based on the type and age of the building. As it is challenging to measure the HVAC system and occupancy schedule with precision, the only choice is to use the occupancy behaviour archetype. However, since different building usages host various occupants with diverse behaviours, the occupancy behaviours are merely an average of several samples. To address this issue, a powerful statistical software Statistical Package for the Social Sciences (SPSS), is introduced to train independent variables to generate the fixed occupancy behaviour.

The results of this training process can then be used as inputs in subsequent simulation and calculation steps. The prediction of the target variable value, based on independent data variables, is carried out using simple linear regression. The R^2 value ranging from 0.95 to 0.98 indicates the reliability of dependent variables, resulting from the independent variable training process. Those trained data are severed as inputs for the next simulation and calculation step.

3.3.4 Step 4: Simulation and calculation

The simulation and calculation step constitutes a pivotal component of the UHIMS-ECHE. The comprehensive thermo-economic simulation and calculation model has been proposed, which includes energy saving, thermal comfort, carbon emissions and economic analysis.

3.3.4.1 Urban heat island intensity

Urban heat island intensity (UHII) is a crucial indicator of the size of UHIs in urbanized areas and explains the intensity of UHI. UHII is determined by comparing the air temperature between an urban (T_u) and a rural area (T_r). In this study, the air temperature in the city centre is generated air temperature (T_g), the rural air temperature is collected by the weather station (T_w), and the UHII can be calculated by Eq. (6).

$$UHII = \Delta T_{g-w} = T_g - T_w \quad (6)$$

3.3.4.2 Urban building energy use

An integrated urban energy modelling platform Urban Modelling Interface (UMI), is selected as the energy consumption modelling tool. The UMI is A plugin based on the Rhinoceros tool and is developed by the Massachusetts

Institute of Technology for capturing operational energy, transportation energy, embodied energy, and on-site renewable energy [637].

UMI requires a variety of input data to simulate urban building energy consumption. These input data include:

Building information: UMI requires detailed information about the building envelope, HVAC systems, lighting, and other energy-related equipment.

District energy system information: UMI requires detailed information about the energy production, storage, and distribution systems in a district.

Weather Data: UMI requires historical weather data to model the impact of environmental factors on energy consumption, this is usually an EPW file.

3.3.4.3 Human thermal comfort

UMI also employs Radiance/Daysim simulation engines, which can combine with Grasshopper and Python programming languages. These features allow UMI to analyse the mutual interactions among buildings, including shadowing and reflections, providing a more accurate analysis of urban energy use. To select representative conditioned zones from buildings, UMI uses a sampling technique called Shoeboxer [638], which is a simplified approach used in urban building energy modelling to estimate the energy consumption of buildings within a city or urban area. Some of the key features of the shoebox model include: geometrical representation, homogeneous zones, single building types, energy consumption parameters (e.g. heating, cooling lighting, etc.) and input data (weather condition, building footprint, building height, occupancy, etc.) [639]. This technique allows for a more detailed and accurate analysis of energy consumption in buildings [224]. A thermal comfort generation engine (TCGE)

has been developed by Grasshopper (Fig.3-4.). The TCGE is capable of identifying various weather conditions, zone masses, and HVAC systems in great detail. Given the variation in individual thermal sensation [234], and the closely related perceived values of the comfort zone for Physiological Equivalent Temperature (PET) and Universal Thermal Climate Index (UTCI), the Predicted Mean Vote (PMV) has been introduced as an empirical index to indicate thermal comfort. This index is physiologically based on a steady-state model of heat exchanges between the human body and the ambient air [235]. The TCGE is capable of generating PMV, which can be utilised to analyse indoor thermal comfort [640]. Additionally, the Standard Effective Temperature (SET) is an outdoor comfort index that is based on a dynamic two-node model of human temperature regulation [235]. The TCGE can generate SET as well, which can be employed to assess outdoor thermal comfort [641].

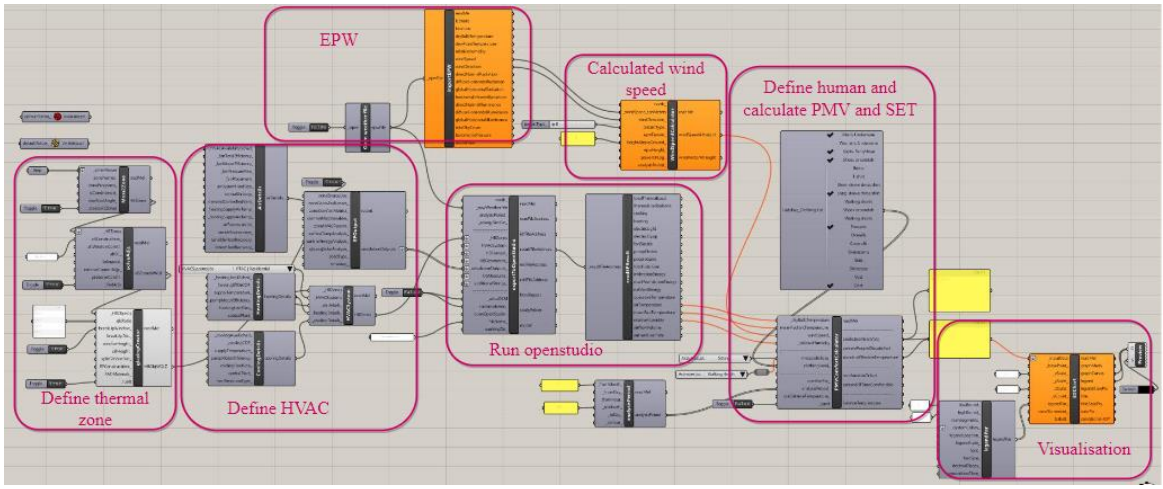

Figure 3-4 The PMV and SET calculation model in grasshopper

3.3.4.4 Carbon emissions

To quantify carbon emissions associated with energy use, trend analysis is an aspect of technical analysis, which is adopted to determine the carbon emissions

of urban buildings. One of the advantages of trend analysis is its simplicity and can predict future carbon emissions based on past data [243]. The value of carbon emissions can be determined by the following Eq. (7):

$$y = \sum_{i=0}^{n} a_n \, \mathrm{Eng}_n \quad (7)$$

where y is the carbon emission in year n, a_n is the carbon emission coefficient. Eng_n is total energy use in year n.

The future a_n is calculated by Eq. (8):

$$a_n = a_{n-1} - \frac{1}{n-1}(a_1 - a_{n-1}) \quad (8)$$

Where a_n is the start year the a_{n-1} is the carbon emission coefficient in year n-1.

In the realm of environmental analysis, the selection of an appropriate baseline year holds paramount significance. This doctoral thesis adopted the advantages associated with initiating environmental assessments from the year 2022 (a_n). In the context of carbon emissions, the rationale for this choice is rooted in the accessibility of contemporary and accurate data, the faithful representation of present environmental and economic conditions, the potential influence of recent policy and technological developments, the increased comparability with existing research, and the improved precision in forecasting future environmental trends.

3.3.4.5 Economic analysis

Moreover, the potential carbon emissions as the criterion are used in making investment decisions. Another criterion in making investment decisions is discounted payback period (DPP), which is used to determine the length of time it takes to reach a breakeven point [246].

The initial investment for a UHI mitigation strategy is calculated by the sum of capital cost and labour cost, which is shown in Eq. (9):

$$INV_{mitigation} = Cost_{capital} + Cost_{labour} \quad (9)$$

The DPP is used to determine the investment benefits, and the cumulative net present value (CNPV) is introduced to identify the DPP, which is calculated by Eq. (10) [642].

$$\text{CNPV} = \sum_{i=1}^{n} \frac{R_i}{(1+r)^i} - INV_{mitigation} \quad (10)$$

Where $INV_{mitigation}$ is a capital cost of new investments for the UHI mitigation strategies, R_i is the estimated net cash flow in the year *i*, *r is* the real discount rate.

The DPP is determined by Eq. (11)

$$\text{DPP (i)} = n, \text{ when CNPV}=0 \quad (11)$$

In this step, a comprehensive simulation and calculation have been provided to analyse the relationship between UHI mitigation strategies with urban building energy use, carbon emissions and citizen thermal comfort. The method of economic analysis also has been presented for making investment decisions on UHI mitigation strategies.

3.3.5 Step 5: Calibration and validation

This step aims to calibrate and validate the energy performance using statistical indexes and disaggregated data of urban buildings for improving modelling accuracy and energy demand quantification. In this step, a proposed data-derived validation method involves comparing a dependent energy metric between reference buildings and the UBEM data for the cluster. The reference building energy use is valid if the performance is close to the median of the cluster. The energy metrics used are the metered data of energy use intensity (EUI).

According to the ASHRAE Guidelines, a correspondence between simulations and measurements has been proposed in this study. The Mean Bias Error (MBE) can indicate the prediction accuracy, which captures the average bias in the prediction and is calculated as Eq. (12).

$$\mathrm{MBE} = \frac{\sum_{i=1}^{n} Simulated\ EUI_i - Metered\ EUI_i}{\sum_{i=1}^{n} Simulated\ EUI_i} \quad (12)$$

In addition, the root mean square error (RMSE) is a good indicator to represent the ability of the model that describes the actual performance of the system. The CV (RMSE) values adopt Eq. (13).

$$\mathrm{CV(RMSE)} = \frac{\sqrt{\sum_{i=1}^{n} (Simulated\ EUI_i - Metered\ EUI_i)^2}}{\frac{1}{n}\sum_{i=1}^{n} Simulated\ EUI_i} \quad (13)$$

According to ASHARE Guide 14-2002, for a building model calibration, the hourly MBE values should be consistent within ±10%, and hourly CV (RMSE) values should be below 30% [643]. CV (RMSE) index is a measure of accumulated error normalised to the mean of the metered values. Thus, the CV(RMSE) more significantly reflects the accumulated magnitude of the error, and it is a better indicator of the overall prediction accuracy of the model [644].

3.4 Advanced Urban heat island mitigation strategies – energy, carbon emission, human thermal comfort economic analysis model

The UHIMS-ECHE model, which is discussed in chapter 3.3, is a tool that can be utilised to compute UHII and to simulate the urban microclimate conditions on a city scale. This can be achieved by integrating meteorological data with information about the characteristics of the urban area.

The city characteristics also have to be coupled with TES technologies to assess the potential of UHI mitigation. In particular, the UHIMS-ECHE model can be

advanced by modifying step 1 (chapter 3.31) of the original model, using TES as a UHI mitigation strategy (Fig.3-5). This modification is made possible by integrating TES technology into the model. The incorporation of TES technology into the model can analyse the feasibility, building energy performance and city micro environmental prediction by the advanced UHIMS-ECHE model.

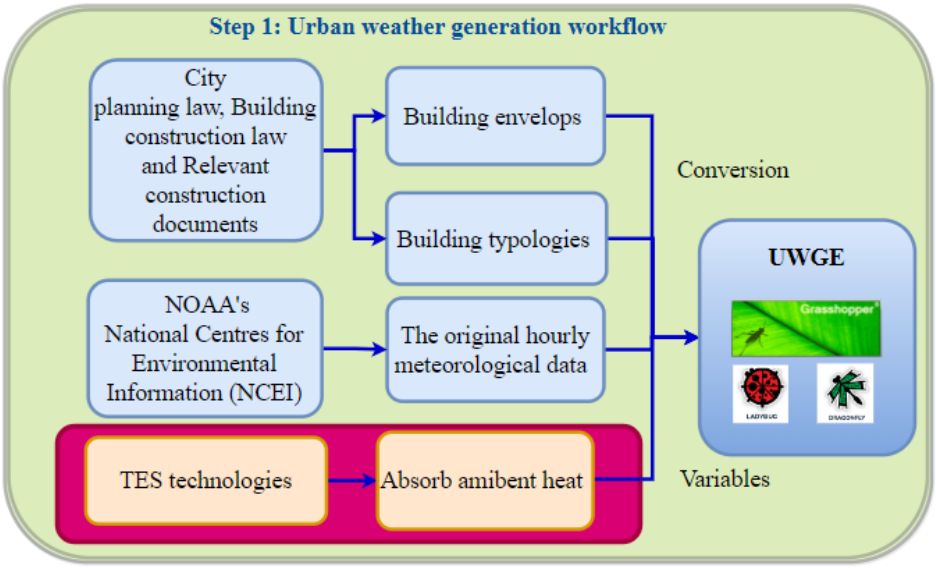

Figure 3-5 Step 1 in advanced UHIMS-ECHE model

Simulating TES technologies entails the computation of the free cooling mechanism, which operates akin to an air conditioner, albeit dispensing cool air to the ambient surroundings. This approach's theoretical foundation is the principle of energy storage, which involves capturing and absorbing solar energy by the TES layer and storing it in a latent heat state. This process reduces environmental heat gains resulting from the emission of minimal heat from the building envelope. In contrast, the TES layer functions as a passive cooling source that provides free air conditioning without any moving components [645].

The thermal energy storage capacity of TES materials/systems is equivalent to the free cooling capacity accessible to the environment [646].

For example, in the case of a building roof with PCM, the system absorbs energy from solar radiation and stores it in the PCM layer as latent heat. The PCM system emits only a minor amount of thermal energy as the heat is transferred to the indoor environment and ambient air. The heat capacity of PCM is simulated as the free cooling capacity. The heat transfer model encompasses all the energy transfer mechanisms involved in the system and ensures that the energy balance is maintained continually Fig 3-6 shows the advanced UHIMS-ECHE model for selected TES technologies in Grasshopper based on the numerical equations.

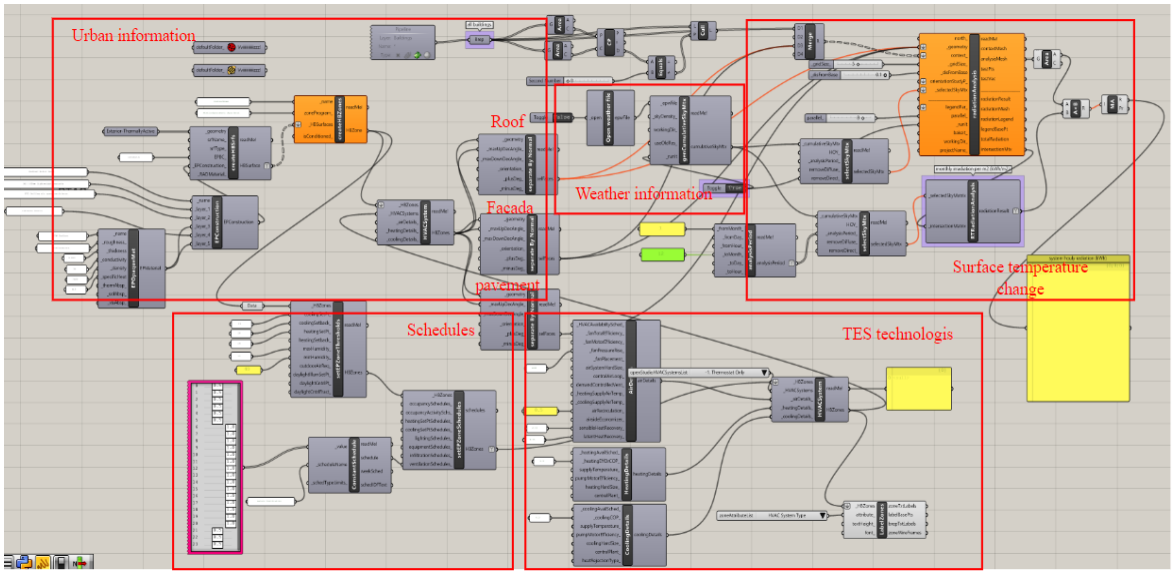

Figure 3-6 Advanced UHIMS-ECHE model for selected TES technologies in Grasshopper based on the numerical equations

In the context of this thesis, it is essential to acknowledge and address several inherent limitations and simplifications of thermal energy storage technology. These considerations are paramount for ensuring the accuracy and applicability of the Advanced UHIMS-ECHE model. Firstly, the PCM serves as a heat absorber during the daytime, transitioning from a solid to a liquid state (melting)

in the process. This phase change effectively prevents the outdoor temperature from escalating too rapidly, thus offering a passive cooling effect. However, during the night, as the PCM solidifies, it releases the heat it absorbed, this research consider that it necessitating the use of certain active systems to facilitate heat transfer through the solidification of the PCM to prevent the stored heat released into ambient environment. Therefore, this modelling schedules (Fig.3-6) only consider the daytime in this research. Besides, the neglect of thermal resistance between the PCM and its surrounding container or heat exchanger, although simplifying calculations, may not fully reflect the real-world scenarios where such resistance can significantly affect heat transfer rates and temperature distribution.

Secondly, to streamline computations and reduce complexity, one-dimensional heat transfer assumptions have been employed, which may not fully capture the multidimensional nature of heat transfer in real-world PCM systems. This limitation can be particularly relevant when dealing with systems that exhibit radial or spatial temperature variations.

Additionally, while assuming constant material properties, such as thermal conductivity, specific heat, and latent heat, simplifies the modelling process, it may not fully account for the dynamic nature of these properties with respect to temperature, pressure, and phase changes. Hence, a more comprehensive approach involving temperature-dependent material properties is essential for improved accuracy, especially during phase change transitions.

Moreover, the isothermal assumption during PCM phase change, where it is assumed to occur at a constant temperature, simplifies calculations but may overlook the intricate temperature gradients that can manifest within the PCM

material during these transitions. To address this limitation, future research should aim to incorporate phase-change-related temperature gradients into the modelling framework.

The omission of natural convection effects, a common simplification in PCM models, can lead to discrepancies in predicting temperature profiles, particularly when dealing with situations involving substantial temperature differentials or larger PCM volumes. Future research should consider more advanced modeling techniques that incorporate natural convection, as it is a significant factor in practical applications.

Lastly, the consideration of the impact of thermal cycling, a common phenomenon in practical applications, has been simplified in the PCM models. Accounting for thermal cycling effects, including potential material degradation and its influence on long-term PCM system performance, is vital for a more comprehensive understanding of PCM behaviour in real-world scenarios.

4 CHAPTER IV: CONVENTIONAL URBAN HEAT ISLAND MITIGATION STRATEGIES

A case study is conducted in the ENVI software and UHIMS-ECHE model. According to the Köppen-Geiger climate classification [647], Osaka, Japan is in the subtropical climate (See Fig.4-1). The latitude is 34.6937° N, and the longitude is 135.5023° E. Besides, in Osaka, the annual mean maximum air temperature is 20.08℃, the annual mean air temperature is 15.9℃, and the annual mean minimum is 11.75℃. The annual relative humidity of Osaka is 65.3%. The annual average wind speed in Osaka is 4.5m/s. Wind velocity in the winter and spring is high, and the wind direction is often from the north

[648]. The fraction of urban green coverage (UGC) in Osaka is under 9%, about 2% in the city centre [181].

According to the 2019 annual report from Osaka Gas Company [649], the consumption of non-renewable energy is 92,492,775GJ, which increased by 3.40% in 2018, 20.14% in 2017, and 26.86% in 2016. Besides, the electricity and fuel consumption was 456,424(1000kWh) in 2019, which increased by 9.34% for 2018, 8.20% for 2017, and 2.21%for 2016. Furthermore, the greenhouse gas (t-CO_2e) emissions were 5,349,768 in 2019, which increased by 3.71% in 2018, 22.62% in 2017, and 28.47% in 2016. To promote activities of reducing climate impact and carbon emissions, Due to the low UGC, increased energy consumption and higher carbon emissions, Osaka is a typical city to analyse the relationship between UHI mitigation and energy consumption, GHG emissions and human comfort. The findings can identify a tremendously efficient approach for local authorities and policymakers in Osaka to manage the environment and energy demand.

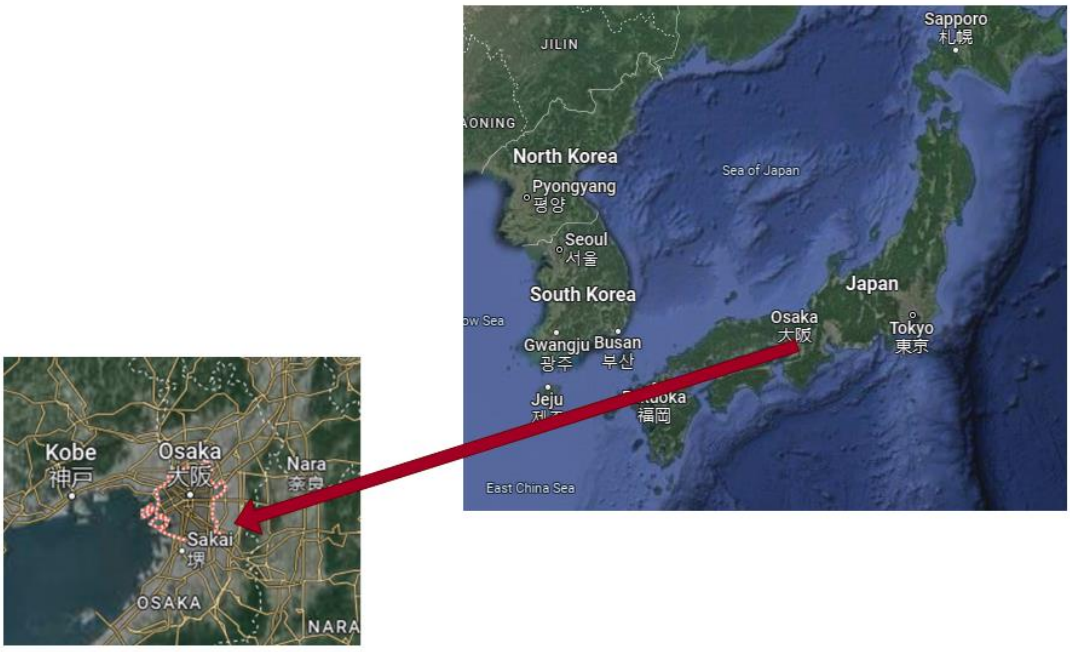

Figure 4-1 Location of research city (Osaka, Japan)

4.1 Introduction

This study comprehensively evaluates the effects of urban heat island mitigation strategies in meteorological variations. The simulation results of each mitigation scenario have been compared with the base model (Scenario A) to determine the discrepancy, as shown in Eq. (31)

$$\text{Discrepancy} = \frac{UHI\ mitigation\ scenarios - Base\ model\ (Scenario\ A)}{Base\ model\ (Scenario\ A)} \quad (31)$$

In this study, an assessment was conducted on the diurnal and annual variations of the urban heat island intensity (UHII), respectively. Furthermore, it was demonstrated that UHI leads to an increase in the consumption of cooling energy and carbon emissions.

Additionally, UHI was found to extend the duration of warm outdoor hours, resulting in prolonged exposure to high temperatures for residents, regardless of whether they are indoors or outdoors.

Furthermore, an analysis has been conducted to evaluate the efficacy of conventional UHI mitigation strategies. The base model, referred to as scenario A, represents the existing conditions and serves as the benchmark for comparison. The disparity between scenario A and the other scenarios has been thoroughly scrutinised. Notably, all conventional and novel UHI mitigation measures have resulted in a reduction of UHI intensity, cooling energy consumption, and carbon emissions, while also enhancing both indoor and outdoor thermal comfort. Moreover, the costs and payback periods (DPP) associated with each UHI mitigation strategy have been computed. The payback periods range from one to six years.

Moreover, this study includes a simulation of the effectiveness of thermal energy storage technologies as mitigation strategies for UHI. The analysis focused on

the discrepancy between scenario A and the remaining TES mitigation scenarios. It was found that all selected TES technologies led to a reduction in UHII, cooling energy consumption, and carbon emissions, while simultaneously improving indoor and outdoor thermal comfort.

4.2 Validation, uncertainty and sensitive analysis

Nowadays, numerical modelling is a capable way to help researchers advance UHI mitigation strategies. ENVI-met has been widely used to support microclimate-sensitive planning. Besides, this research should describe the meaningful characteristics of natural objects. In the Osaka city scale, the modelling process aims to simplify representing the city by computational methods. To ensure the certainty of simulation results, the simulation results of outdoor temperature (Ta*)* have been chosen to compare with the actual outdoor temperature organised by the local weather station and Japan Meteorological Agency (JMA). The average Ta of the local weather station is 30.19 °C and the average simulation Ta is 30.91°Cduring the research period. The percentage difference is 2.35%, which is at a deficient level. Therefore, the simulation results can be considered relatively close and comparable to the real values.

Besides, according to the tutorials of ENVI-met (ENVI-met.com), the typical spatial resolution range is from 0.5 to 10 m. Sdeghat and Sharif (2022) studied that the modelled area is 280 × 510m, and the resolution is 5 m for simulating the urban heat island in Tehran, Iran. [650] However, the research area in this study is 500 × 500, which is bigger and more complex. Therefore, this study has considered saving the computing cost and time and combining the previous studies, limiting the resolution and grid cells to 10 m.

Additionally, it is essential for the UHIMS-ECHE model to accurately describe the significant attributes of authentic urban entities in subtropical city centres. At the urban scale, the modelling process strives to simplify the representation of the city through computational methods. Thus, to corroborate the efficacy of the UHIMS-ECHE model in this research, comparative fieldwork was conducted between January and December 2021. Four i-Button DS1925 data loggers, equipped with radiation shields, were strategically placed on each side of a prototypical residential building (No. 19) to measure the localised microclimate patterns (refer to Figure 4-2). It is noteworthy that the operating temperature range of the DS1925 data logger is -40°C to +85°C, and it has a temperature measurement accuracy of ±0.5°C [651]. Besides, the maximum amplitude of iButton data loggers is 46.5 dB SPL at 1.0 cm-a level, which is generally consider to be relatively quiet. In addition, those four sensors synchronised by master clock by radio transmissions.

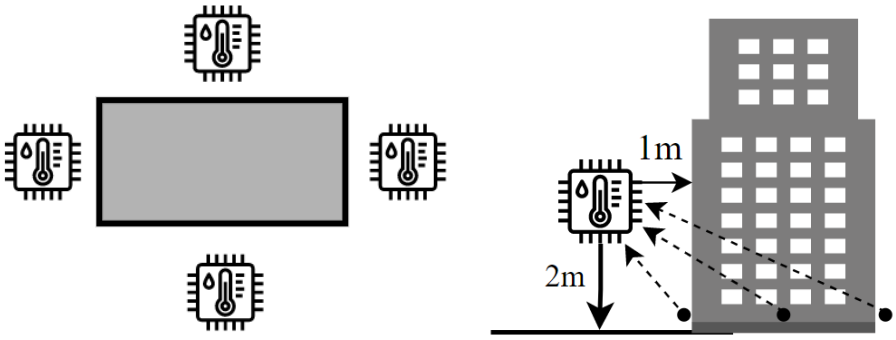

Figure 4-2 Location of data loggers for UHIMS-ECHE validation

The average monitoring air temperature has been compared with Scenario A to determine the accuracy of data loggers, which is shown in Fig.4-3.

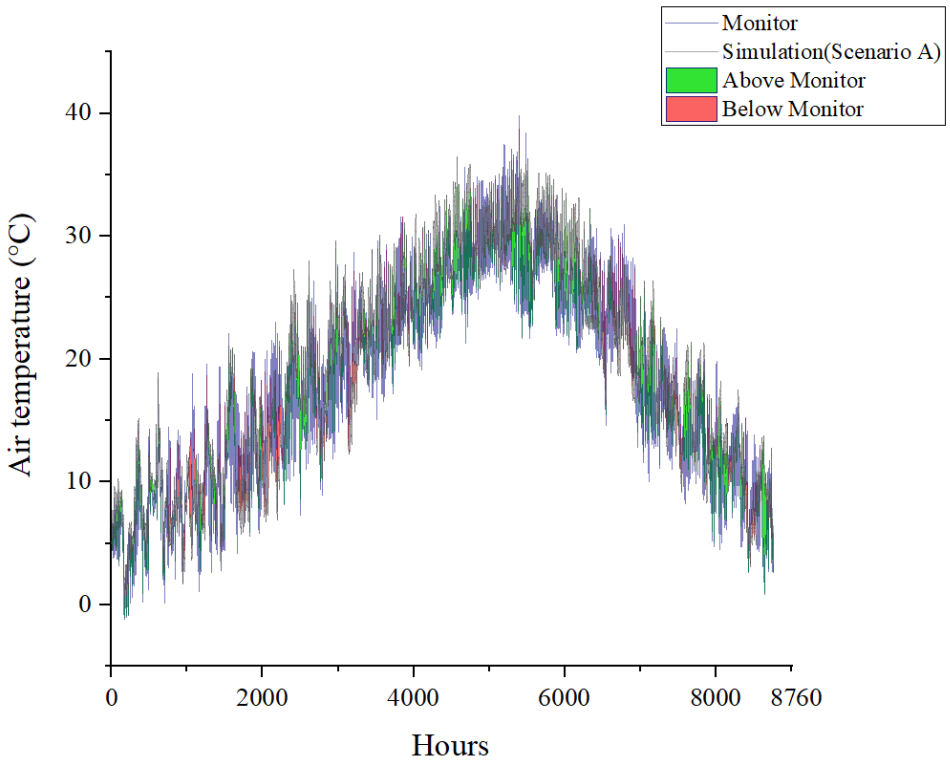

Figure 4-3 Accuracy of data loggers

To obtain the cooling energy use for each building, the microclimate data from monitoring was converted into a monitoring EnergyPlus Weather (EPW) file, which was then input into UHIMS-ECHE for simulation. Building No.19 was selected for analysing the accuracy of UHIMS-ECHE. The cooling energy use and bills were simulated and calculated based on the monitoring EPW file and are presented in Table 4-1. Actual cooling energy use and bills were also collected and are shown in the same table.

Table 4-1 Discrepancies between actual and monitoring

	Actual value for No.19 building	Monitoring value for No.19 building	Discrepancies
Cooling energy use (kWh)	159202.54	153767.82	3.53%
Cooling energy bill ($)	36811.63	35674.12	3.19%

The UHIMS-ECHE model demonstrates a high level of accuracy and reliability in representing actual urban energy use, as evidenced by the observed discrepancies in cooling energy use and billing in a subtropical reference building, which was 3.53% and 3.19%, respectively. These findings support the validity of the outputs of the model and highlight its potential as a valuable tool for assessing and optimising urban energy performance in subtropical areas.

4.3 Urban weather generation parameters in Osaka

To calculate the UHII for the research city centre, UWGE based on Grasshopper is used to generate urban microclimate files using meteorological data measured at the rural weather station.

This study chooses a typical meteorological year (TMY 2007-2021) to analyse the energy impact of the subtropical UHI. The original hourly meteorological data were collected from NOAA's National Centres for Environmental Information (NCEI) and Japan Meteorological Agency (JMA).

The research period is from 00:00 January to 23:00 31 December (8760 hours). A typical hottest summer day (02. August) was selected in ENVI-met for analysing the diurnal variation. The detailed input parameters are shown in Table 4-2.

Table 4-2 The initialization detailed input parameters of Osaka, adopted by the Japan Meteorological Agency.

category	User input
Modelling area (L, W, H) (m)	500×500×600
Configuration file	
Simulation start date	00:00/01. January

Simulation end date	23:00/31. December
Simulation period	8760 hours
Typical hot summer day	02. August
Typical cold winter day	11. December
Simulation output interval for receptors (min)	30
Meteorological inputs	
Wind direction (0=N; 90=E; 180=S; 270=W)	50° Northeast (summer); 10°North (winter)
Wind speed measured in 10m height	6.7 m/s (summer); 8.5m/s (winter)
Mean roughness length (m)	0.5
Initial atmospheric temperature (°C)	21.85
Specific humidity in 2500m (water/kg dry air)	9.0
Relative humidity in 2m (%)	55-85 % (summer); 48–65% (winter)
Global horizontal radiation	171.77 W/m^2
Diffuse horizontal radiation	63.63 W/m^2 (winter)
Direct normal radiation	16854.58 W/m^2
Soil inputs	
In initial soil temperature at upper layer (1-20cm) (k)	313
In initial soil temperature at middle layer (20-50cm) (k)	315
In initial soil temperature at lower layer (below 50cm) (k)	317
Moisture content upper layer (%)	40
Moisture content middle layer (%)	45
Moisture content lower layer (%)	50
Building inputs	
Building interior temperature (°C)	26.0
Mean heat transmission of walls (W/m^2K)	2.0

Mean heat transmission of roofs (W/m^2K)	5.0
Mean wall albedo	0.1
Mean roof albedo	0.2

4.3.1 Conventional urban heat island mitigation scenarios

For dissipating the excess heat, the mitigation strategies of UHI are usually divided into two categories, increasing urban surface albedo and evapotranspiration [181]. Increasing albedo is generally accomplished by increasing the albedo of the roof and pavement. An increase in evapotranspiration is completed by a combination of decreasing the distribution of impervious surfaces and expanding the space of vegetation in urban areas (shade trees, vegetated walls, and rooftop gardens) [181]. In this research, a base model (Scenario A) and four different UHI mitigation strategies (Scenario B to E) are designed to evaluate the impact of urban building energy use. The UHI mitigation strategies are designed [181]. All the parameters and variables of the buildings and city objects in scenarios A to E were simulated by UWGE to ultimately obtain the different urban weather data, which can reflect the urban microclimate changing for each scenario by adopting input variables. The results of UWGE calculation in the adjustment of the reference weather file used in subsequent simulations (in umi).

This study possesses the capability to provide valuable support to local authorities, policy makers, and urban designers in their efforts to combat the urban heat island (UHI) phenomenon. To comprehensively understand various conventional UHI mitigation strategies, the study has also proposed combination scenarios (Scenario BC, BD, and CD). These combination scenarios aim to explore and analyse the implications of integrated mitigation approaches,

considering diverse contextual factors and complexities associated with UHI mitigation. Table 4-3 shows the detailed variables for each UHI mitigation strategies scenario. To increasing the albedo of pavements and roofs, the high reflective materials can be used, such as titanium dioxide paint (albedo is approximately 0.7-0.9 [652] [653]) and high gloss white paint (albedo is 0.5-0.9 [654] [655]). In this study, the albedo for the cool scenarios have been set as 0.8 [656] [657].

Table 4-3 UHI mitigation strategies scenarios [181]

Strategies	Pavement Albedo	Roof Albedo	Vegetation coverage ratio
Scenario A [658]: Base model	0.1	0.2	2%
Scenario B [181]: Cool pavement model	0.8	0.2	2%
Scenario C [181]: Cool roof model	0.1	0.8	2%
Scenario D [181]: Green space model	0.1	0.2	20%
Scenario E [181]: Integrated model	0.8	0.8	20%
Scenario BC: Cool urban surface model	0.8	0.8	2%
Scenario BD: Cool pavement-Green space model	0.8	0.2	20%
Scenario CD: Cool roof-Green space model	0.1	0.8	20%

Scenario A: Base model: representing the current condition with the albedo of asphalt roads and concrete roofs are 0.1 and 0.2, respectively. Besides, the green coverage ratio is 2%

Scenario B: Cool pavement model: asphalt roads (albedo=0.1) are replaced with concrete pavement (white cement concrete) with higher surface albedo (albedo=0.8) and lower heat capacity.

Scenario C: Cool roof model: concrete roof (albedo=0.2) are changed to high reflective roof (albedo=0.8).

Scenario D: Green space model: increasing a green coverage ratio to 20%. The parameters of trees are reported in Table 4-4. The incremental increase of greening is not considered in this study.

Scenario E: Integrated model: a combination of the three previous UHI mitigation strategies (Scenarios B, C and D).

Scenario BC: Cool urban surface model, asphalt roads and roofs are replaced by white cement concrete, the albedo is 0.8.

Scenario BD: Cool pavement-Green space model: increasing pavement albedo to 0.8, and green coverage to 20%.

Scenario CD: Cool roof-Green space model: increasing roof albedo to 0.8, and green coverage to 20%.

Table 4-4 Parameters of trees employed in the scenarios of Osaka

Tress categories	Tree height (m)	Crown width (m)	Trunk	Leaf area density (LAD)	Applications
Privet	5	5	Medium	High	Roadside, nature space, etc.
Cypress	15	3	Medium	High	Roadside, nature space, etc.
Fescue	0.5	0.3	/	/	Roof

4.3.2 3D urban model for Osaka

To simulate energy consumption for a group of buildings on the city scale, it is essential to achieve an appropriate compromise for modelling accuracy, data availability, and computational costs. Due to computing cost and time saving and combing with the previous studies [181] [650] [671] [672], the research domain for urban microclimate modelling covers an area of $2.5km^2$. This spatial

scale can present the atmospheric circulation for analysing the UHI phenomenon, which consists the typical urban land-use types: residential areas, commercial areas, industrial areas, roads, parks and open spaces.

The data from ArcGIS or building footprints imported into Rhinoceros can represent actual urban objects, such as building space, green space, pavement area, etc. A plugin of Rhinoceros, Lands Design can scan and import 3D buildings from any spot worldwide, with the data of terrain and building height. To be avoided oversimplified the buildings, the detailed building information will be obtained, and machine-learning techniques will use to estimate uncertain building information. Finally, the sensitivity analysis will be performed to understand the impact of uncertainty in building energy modelling. Fig.4-4. shows the research location and area and the 3D model of the research area in Rhinoceros. These steps are typically generalizable to most city centres, with minor differences based on data structures, contexts, and preferences.

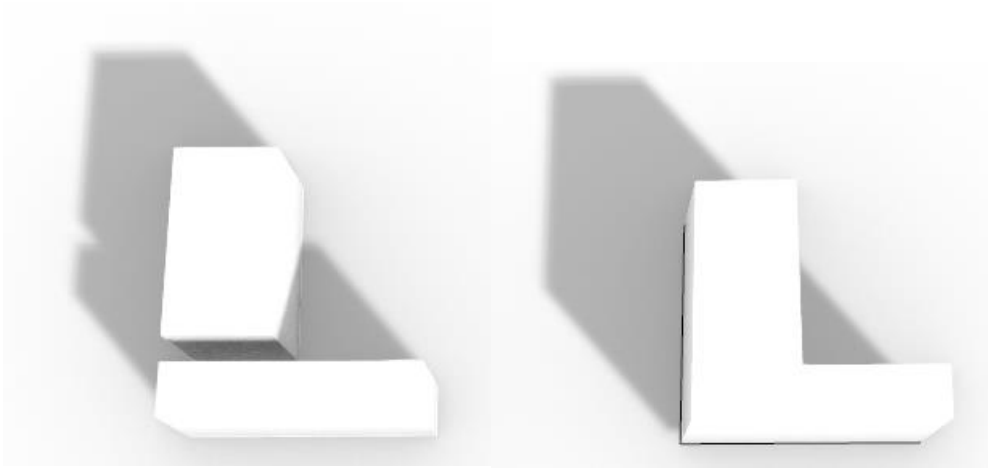

(a) Building polygons simplification (b) Building extrusion

(c) GIS photo for urban research archetype (d) Simplified 3D model in Rhinoceros

Figure 4-4 Polygon dissolution (a) and extrusion (b) for simplified geometry modelling [636]. The archetype of the research area is shown in (c), and its 3D model presents in (d)

4.3.3 Independent and target variables

In this study, 42 building archetypes located in Central Osaka were covered to evaluate the thermal properties of buildings in Osaka. The building blocks have been numbered from No.1 to No.42 in umi (see Fig.4-5. (d)). Each zone in the model represents an individual building determined by the building archetypes. Three types of building archetypes were classified as office buildings, residential buildings and retail buildings.

Every type of building archetype includes the specific independent variables of the building construction, equipment, occupancy schedule and HVAC system. The occupancy schedule has been surveyed by the Statistics Bureau, Ministry of Internal Affairs and Communications [673]. The independent variables are collected based on the law and regulations in Japan, such as Country Report on Building Energy Codes in Japan [674], building standard law [675], Japan Sustainable Building Consortium (JSBC) and Comprehensive Assessment System for Built Environment Efficiency (CASBEE) [676], Japan district design

guide [677], etc. Those independent variables are trained by regression analysis from SPSS to determine the required target data. The range of R^2 from 0.95 to 0.98 indicates the required target variables of building modelling are at an acceptable and reliable level. The post-trained target variables are shown in Table 4-5.

Table 4-5 The initialisation of detailed parameters of buildings and city input

Building Category	Building and city inputs		
	Office building	Residential building	Retail building
Building I.D.s	1,6,7,11,14,15,16,17,20,25,26,27,28,29,30,33,35.	2,3,4,5,10,13,19,22,23,24,31,34,36,37,38,39,40,42.	8,9,12,18,21,32,41.
Lifespan [677]	60 years	60 years	60 years
Window - to-wall-ratio (WWR) [675] [677]	North: 40% South: 40% East: 40% west: 40%	North: 40% South: 40% East: 20% west: 20%	North: 40% South: 40% East: 40% west: 40%
Façade [675] [677]	U-value: 1.51 W/m2 K Clay brick: 60mm, XPS board: 20mm, Concrete block: 150mm, Fiberglass batts: 50mm, Gypsum Plasterboard: 20mm	U-value: 1.51 W/m2 K Clay brick: 60mm, XPS board: 20mm, Concrete block: 150mm, Fiberglass batts: 50mm, Gypsum Plasterboard: 20mm	U-value:1.51 W/m2 K Clay brick: 60mm, XPS board: 20mm, Concrete block: 150m, Fiberglass batts: 50mm, Gypsum Plasterboard: 20mm
Roof [675] [677]	U-value:2.80 W/m2 K XPS board: 100mm, Concrete MC (Lightweight): 150mm, Concrete R.C. (Dense weight): 200 mm, Air floor: 150mm, Gypsum board: 200mm.	U-value: 2.71 W/m2 K Concrete MC (Lightweight): 100m, Plywood board: 20mm, Fiberglass batts: 120mm, Air floor: 100mm, Gypsum Plasterboard: 200mm.	U-value: 2.8 W/m2 K XPS board: 100mm, Concrete MC (Lightweight): 150 mm, Concrete R.C. (Dense weight): 200 mm, Air floor: 150mm, Gypsum board: 200mm.

External floor [675] [677]	U-value:3.52 W/m2 K Concrete R.C. (Dense weight): 150mm, XPS board: 40mm, Cement mortar: 20mm, Urethane carpet: 20mm.	U-value: 3.39 W/m2 K Hardwood general: 20mm, XPS board: 400mm, Plywood board: 20mm, XPS board: 20mm, Wood floor: 2mm.	U-value: 3.52 W/m2 K Concrete R.C. (Dense weight): 150 mm, XPS board: 400mm, Cement mortar: 20m, Urethane carpet: 20m.
Internal floor [675] [677]	U-value: 4.52 W/m2 K Urethane carpet: 20mm, Cement mortar: 20mm, Concrete R.C. (Dense weight): 150mm, Air floor: 150mm, Gypsum Plasterboard: 20mm.	U-value: 4.41W/m2 K Wood floor: 20mm, XPS board:10mm, Plywood board: 2mm, Air floor: 150mm, Gypsum board: 20mm.	U-value: 4.52 W/m2 K Urethane carpet: 20mm, Cement mortar: 20mm, Concrete R.C. (Dense weight): 150mm, Air floor: 150mm, Gypsum board: 20mm.
Partition [675] [677]	U-value: 2.44 W/m2 K Gypsum plaster: 20mm, Softwood general: 20mm, Gypsum plaster: 20mm.	U-value: 2.44 W/m2 K Gypsum plaster: 20mm, Softwood general: 20mm, Gypsum plaster: 20mm.	U-value: 2.44 W/m2 K Gypsum plaster: 20mm, Softwood general: 20m, Gypsum plaster: 20m.
Window [675] [677]	U-value: 3.3 W/m2 K Glass clear 3: 3mm, Air: 6mm.	U-value: 3.3 W/m2 K Glass clear 3: 3mm, Air: 6mm.	U-value: 3.3 W/m2 K Glass clear 3: 3mm, Air: 6mm.
Ventilation [674] [676]	Infiltration rate: 0.35ac/h, Yearly schedule: Off 01.01.2021 to 31.03.2021; 01.11.2021 to 12.31.2021, On 01.04. 2021 to 31.10.2021.	Infiltration rate: 0.35ac/h, Yearly schedule: Off 01.01.2021 to 30.04.2021; 01.11.2021 to 12.31.2021, On 01.05. 2021 to 31.10.2021.	Infiltration rate: 0.35ac/h, Yearly schedule: Off 01.01.2021 to 30.06.2021; 01.10.2021 to 12.31.2021, On 01.07. 2021 to 30.09.2021.
Cooling [674] [676]	Max cooling capacity: 250W/m², Max cool flow: 100m³/s/m², Setpoint temperature: 24°C, COP: 3 Yearly schedule: Off 01.01.2021 to 31.03.2021; 01.10.2021 to 12.31.2021, On 01.04. 2021 to 30.9.2021.	Max cooling capacity 250W/m², Max cool flow: 100m³/s/m², Setpoint temperature: 24°C, COP:3 Yearly schedule: Off 01.01.2021 to 30.06.2021; Off 01.10.2021 to 12.31.2021, On 01.07. 2021 to 30.9.2021.	Max cooling capacity: 250W/m², Max cool flow: 100m³/s/m², Setpoint temperature: 24°C, COP:3 Yearly schedule: Off 01.01.2021 to 30.04.2021; 01.10.2021 to 12.31.2021, On 01.05. 2021 to 30.9.2021.

Heating [674] [676]	Max heating capacity: 200W/M², Max heating flow 100m³/s/m², Setpoint temperature: 20 °C, COP: 2.1 Yearly schedule: On 01.01.2021 to 30.04.2021; 01.10.2021 to 12.31.2021, Off 01.05. 2021 to 30.9.2021.	Max heating capacity: 200W/M², Max heating flow 100m³/s/m², Setpoint temperature: 20 °C, COP: 2.1 Yearly schedule: On 01.01.2021 to 30.04.2021; 01.10.2021 to 12.31.2021, Off 01.05. 2021 to 30.9.2021.	Max heating capacity: 200W/M², Max heating flow 100m³/s/m², Setpoint temperature: 20 °C, COP:2.1 Yearly schedule: On 01.01.2021 to 30.04.2021; 01.10.2021 to 12.31.2021, Off 01.05. 2021 to 30.9.2021.
Domestic Hot water [674] [676]	Supply temperature: 55°C Inlet temperature: 16°C	Supply temperature: 55°C Inlet temperature: 16°C	Supply temperature: 55°C Inlet temperature: 16°C
Occupancy [673]	Occupancy density: 0.55 (P/m²) Occupancy yearly Schedule:01.01.2021 to 31.12.2021	Occupancy density: 0.025 (P/m²) Occupancy yearly Schedule:01.01.2021 to 31.12.2021	Occupancy density: 0.1 (P/m²) Occupancy yearly Schedule:01.01.2021 to 31.12.2021

4.4 Comprehensive meteorological assessment of conventional urban heat island mitigation strategies

The evaluation of UHI mitigation strategies is of great significance, and the assessment of the micro-environmental performance of such strategies is crucial for identifying effective measures. Chapter 2.8 highlights that a combination of hourly annual UHII, sky view factor, net radiation, thermal radiative power, and mean radiation temperature are commonly used indicators for assessing the micro-environment variation of UHI mitigation strategies in the city centre micro-environment. These indicators capture different aspects of the urban energy balance and provide a holistic approach to understanding the urban microclimate.

Hourly annual UHII is a crucial parameter that provides insight into the UHI effect's intensity throughout the year. The parameter measures the temperature difference between urban and rural areas, with higher values indicating more substantial UHI effects. The sky view factor (SVF) represents the fraction of the visible sky from the ground level and is a critical factor in influencing solar radiation and thermal energy exchanges. Higher values of SVF correspond to less obstruction of the sky and can lead to lower temperatures. Net radiation (R_n) is a significant component of the urban energy balance and measures the difference between the incoming and outgoing radiation energy. On the other hand, thermal radiative power (TRP) is a measure of the thermal energy emitted by urban surfaces, which is influenced by surface temperature and emissivity. Mean radiation temperature (MRT) represents the average temperature of all surfaces emitting thermal radiation in an area, including the sky. The combination of these parameters enables the evaluation of the different heat transfer processes in the urban environment, such as the contribution of the urban surfaces' emissivity and absorption to the energy balance.

4.4.1 Sky view factor

The SVF is the fraction at a point in space between the visible sky and a hemisphere centred over the research location. The SVF serves as an index of urban morphology widely used for comparing thermal conditions in different building environments [153]. The average SVF for each simulated scenario is also shown in Fig. 4-6.

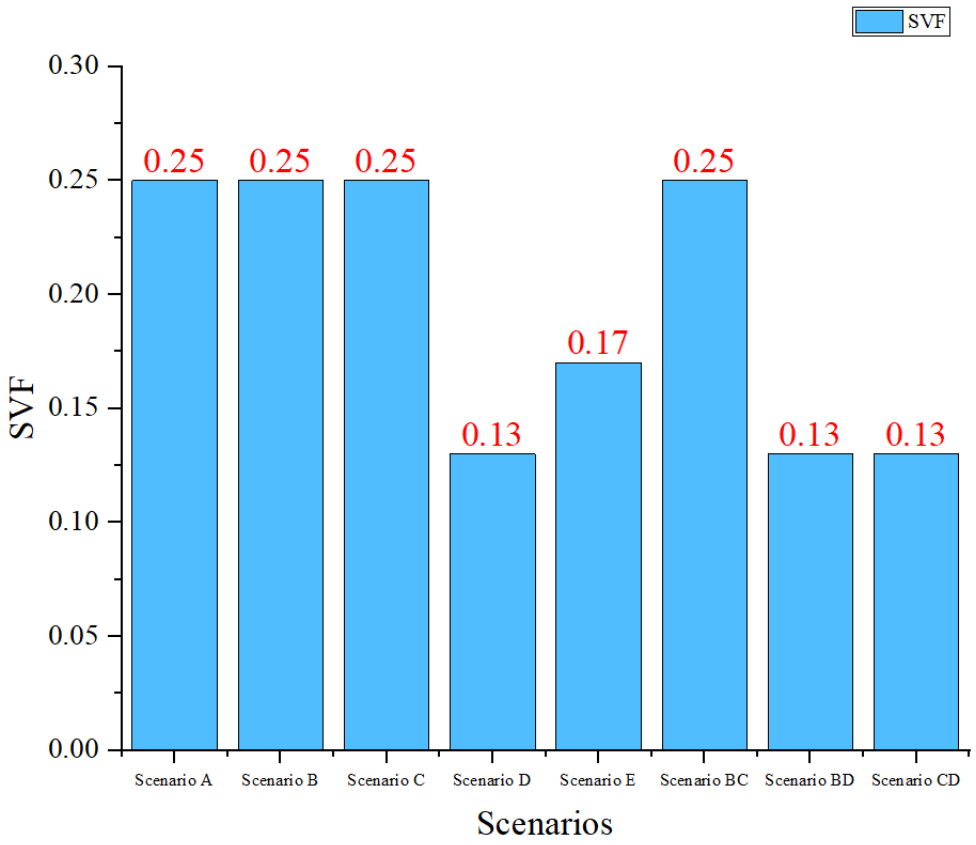

Figure 4-5 Four selected points to assess the SVF and the value of SVF in each scenario

In certain scenarios, the SVF values have demonstrated a lack of change. This phenomenon can be attributed to alterations in the albedo of surfaces not directly impacting the visible sky area. However, an intriguing departure from this trend is evident in scenarios D, BD, and CD. In these cases, the SVF values have notably declined to as low as 0.13. This phenomenon can be attributed to the increased presence of green spaces, which in turn has led to the obstruction and coverage of the available view area towards the sky. This intriguing observation aligns with the broader discourse on the role of green spaces in shaping urban microclimates. The introduction of vegetation introduces an additional dimension to the urban form's intricate relationship with climatic variables. While urban albedo modifications may have minimal influence on SVF, the

incorporation of green spaces emerges as a more dominant factor in reshaping SVF values and, consequently, the thermal and radiative conditions within the urban setting.

4.4.2 Hourly outdoor air temperature and distributions

Fig. 4-6 shows the change in outdoor air temperature (Ta) during the research period for each scenario. The maximum, average, and minimum outdoor air temperatures are T_{a-max}, T_{a-avg}, and T_{a-min} for the scenarios, respectively.

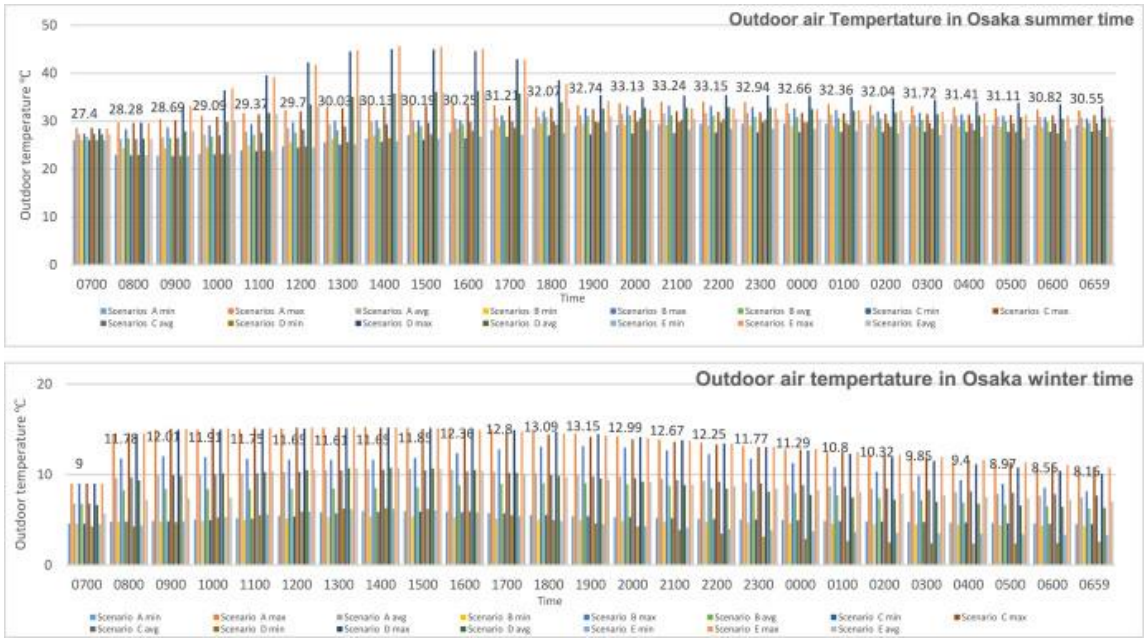

Figure 4-6 The change of T_{a-max}, T_{a-avg}, and T_{a-min} during the research period for each simulated scenario

In the summertime, the maximum T_{a-max} of Scenario A is 35.46 °C, which is close to the record temperature from the meteorological station. The maximum T_{a-max} (45.64 °C) from all scenarios is observed at 12:00 in Scenario E during the research period. Scenario B has the lowest T_{a-max} (33.24 °C), which is the most decreased model. In the wintertime, the maximum Ta is found in Scenario A at 14:00, and the value is 15.21 °C. The minimum T_{a-max} (13.09 °C) have been found in Scenario B at 18:00. Besides, the distribution of Ta is

analysed in this research. Fig. 4-7 and Fig. 4-8 show the distribution of T_{a-max}, for each scenario in summertime and wintertime.

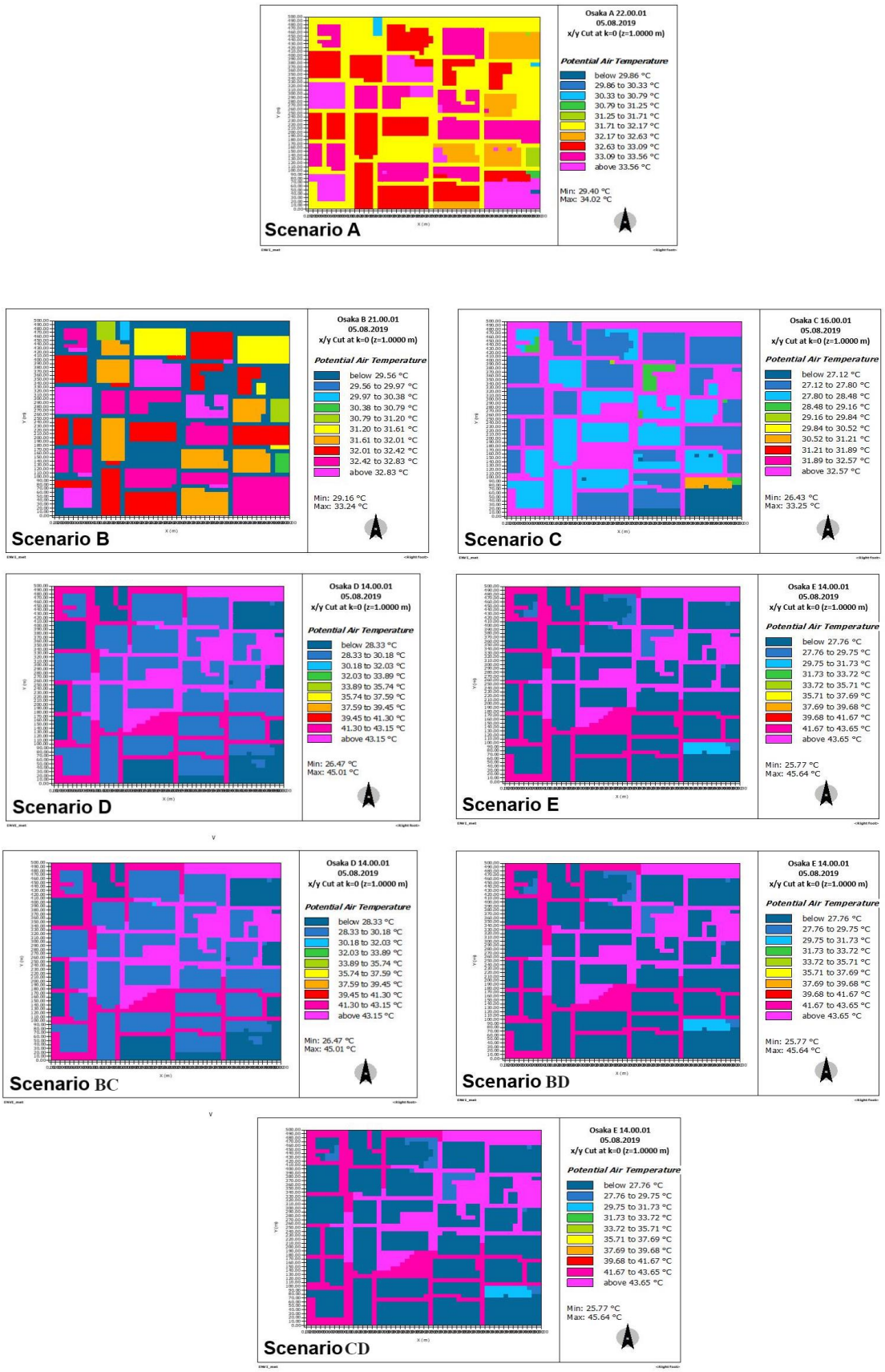

Figure 4-7 The distribution of T_{a-max} for each scenario in the summertime

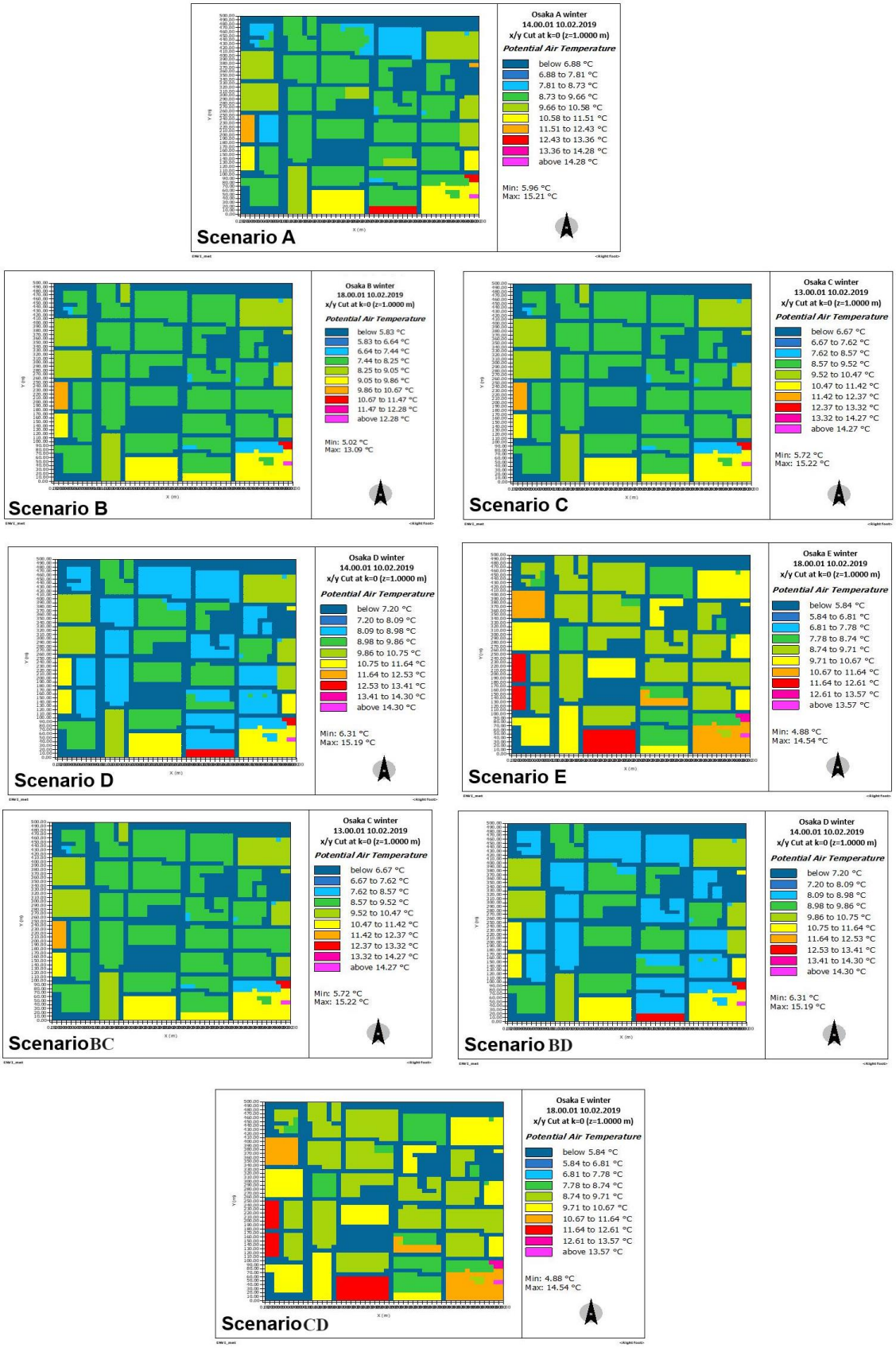

Figure 4-8 The distribution of T_{a-max} for each scenario in the wintertime

Scenario B has a lower temperature distribution outside the building and around

the street. However, scenario E has the highest temperature distribution inside the buildings but higher temperatures around the road and outside the buildings. Fig. 4-9 shows the relative percentage difference in outdoor air temperature compared with Scenario A (base model). In the summertime, the percentages of T_{a-max} significantly increased in Scenario B during the daytime, and it slightly increased during nighttime. Furthermore, the percentages of T_{a-avg} and T_{a-min} have been identified as the highest trend In Scenario C. This implies that Scenario B and Scenario C both are the great efficient model to decrease Ta in the summertime. However, in the wintertime, the most remarkable percentages tendency of the T_{a-max}, T_{a-avg} and T_{a-min} have been found in Scenario B. It indicates that Scenario B has the more efficient ability to decrease Ta in the wintertime. Therefore, Scenario B can be considered the most efficient model to reduce Ta in summer and wintertime.

The results indicate that the performance of Scenario BC is inferior to that of Scenario B. This disparity may be attributed to the higher number of reflective surfaces in Scenario BC, which have the potential to redirect sunlight and heat towards nearby areas, potentially leading to discomfort or increased heat in neighbouring buildings or outdoor spaces. Such a situation can give rise to unintended consequences within the immediate environment. Moreover, an excess of high-albedo surfaces, which emit less thermal radiation compared to darker surfaces, can affect the cooling of outdoor spaces during nighttime hours.

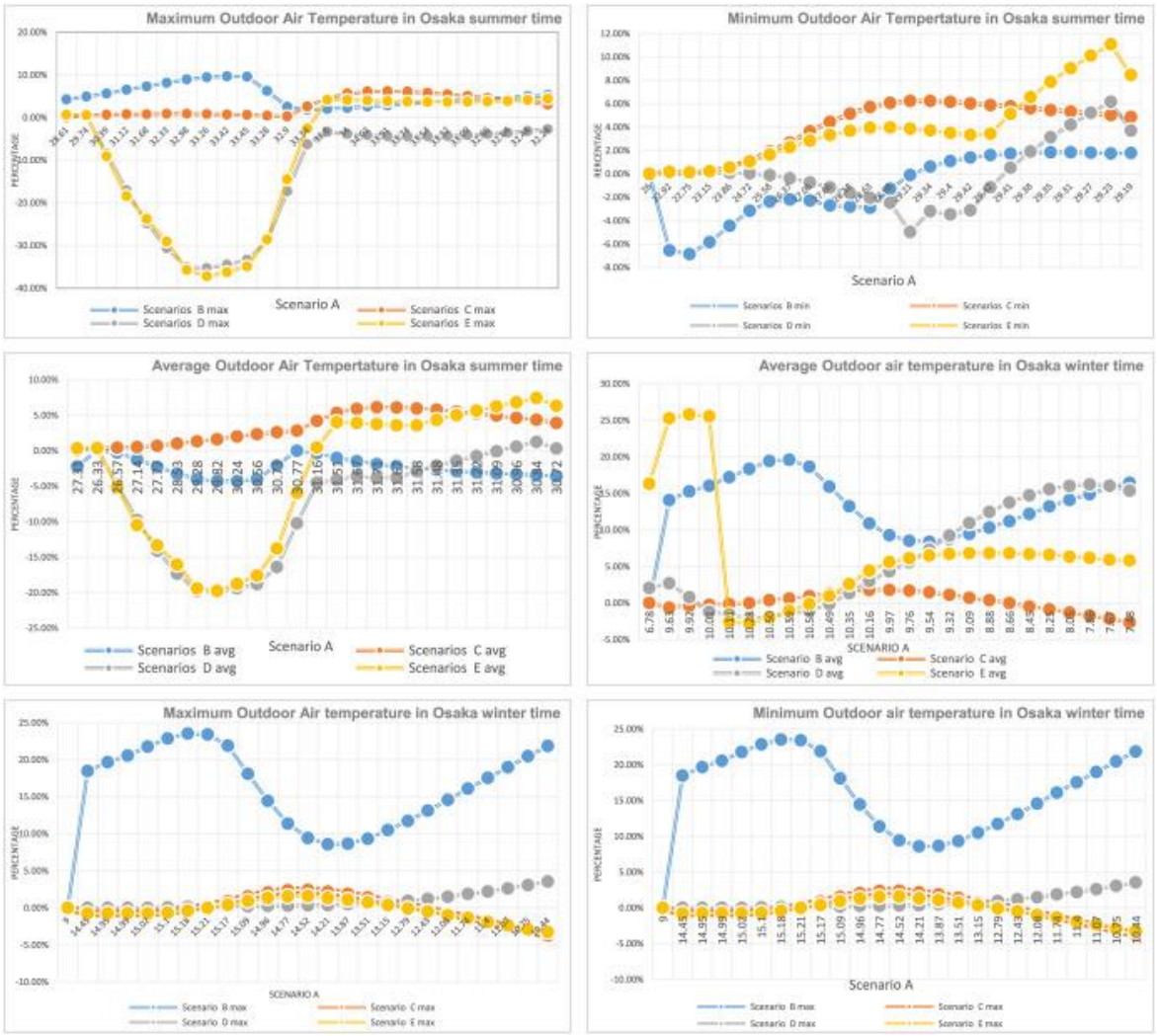

Figure 4-9 The percentages of outdoor air temperature in summer and wintertime

4.4.3 Net radiation

The value of net radiation (R_n) is the difference between incoming and outgoing radiation of both short and long wavelengths. It depends on the temperature and reflectivity of the ground surface exposed to radiative exchange [163]. Fig. 4-10 shows the change in R_n during the research period. The maximum Rn in summertime was found in Scenario A at 11:00, the value is 1936.01 W/ m^2, and that happened at 12:00 in the wintertime; the value is 1257.71 W/ m^2. Besides, the value of R_n in all scenarios significantly decreased from 15:00 p.m. to 06:00 a.m. during sunset and nighttime.

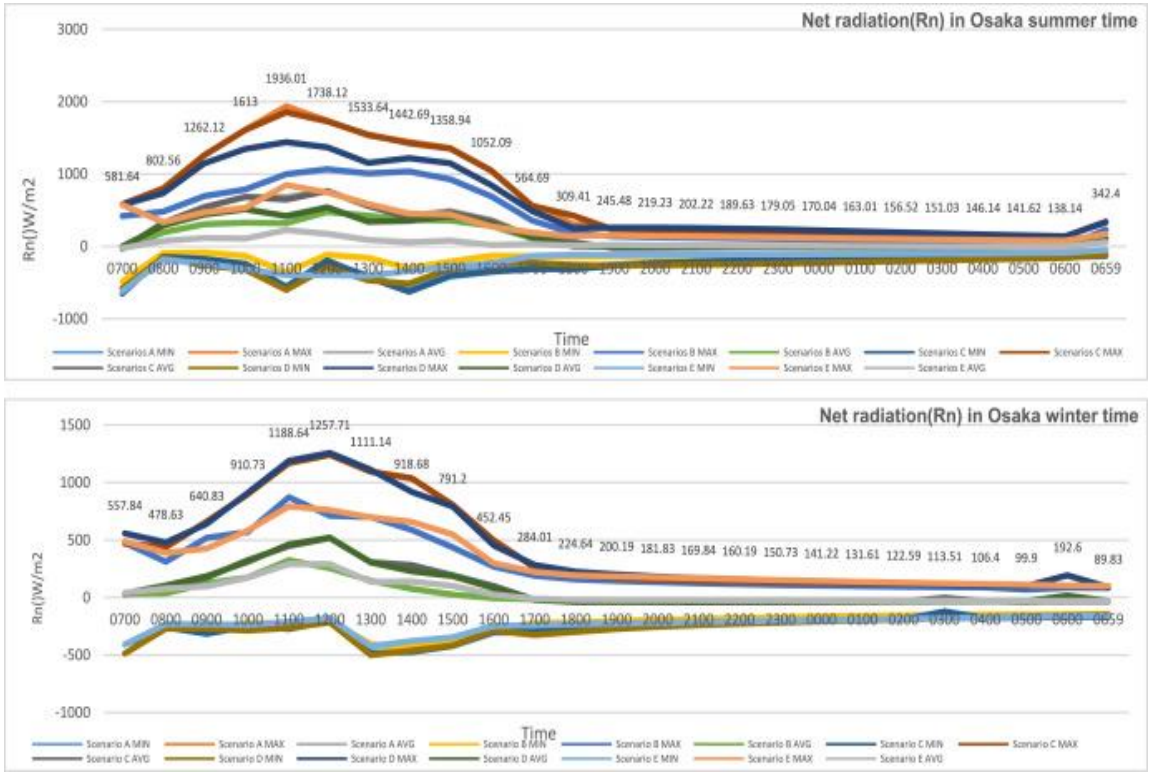

Figure 4-10 The value of Rn for each scenario in summer and wintertime

Fig. 4-11 shows the relative percentage difference of R_n, which is compared with Scenario A. In the summer daytime, Scenario E is the most efficient model to decline R_{n-max}, and Scenario B is the most powerful model to reduce Rn−min. However, in the summer nighttime, Scenario B is more efficient than others to decrease Rn−max, and Scenario E is the most efficient model to decrease Rn−min. Furthermore, in the wintertime, Scenario B generally has the most significant trend to decrease the R_{n-max} and R_{n-min} during the research period. To sum up, Scenario B is considered the most powerful model to reduce net radiation both in summer and wintertime.

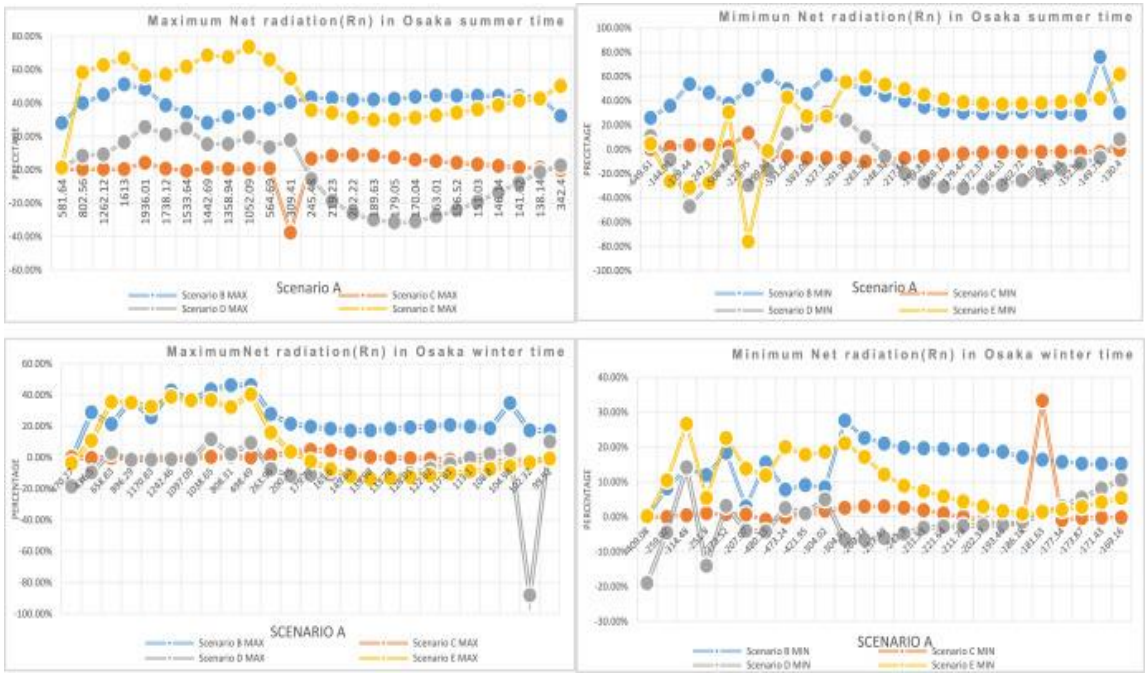

Figure 4-11 The percentages tendency of net radiation

4.4.4 Thermal radiative power

Thermal radiative power (TRP) is used to assess the impact of the solar reflectance of a surface on the UHI effect [167]. According to Stefan-Boltzmann law, the average TRP per m^2 of each element of urban surfaces in each scenario was calculated and shown in Fig. 4-12.

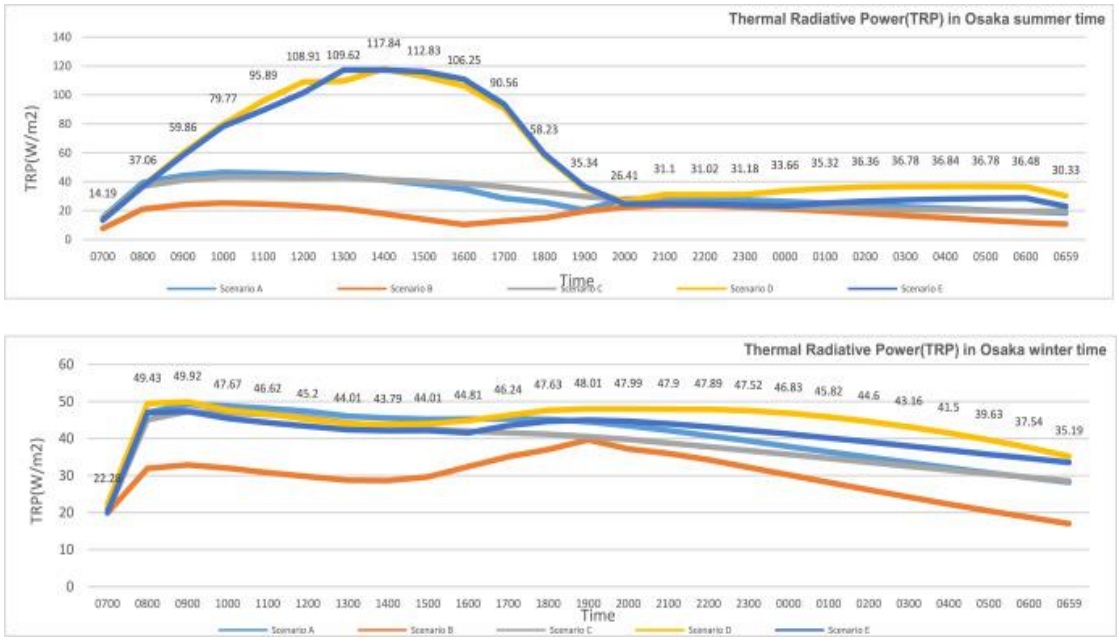

Figure 4-12 The calculated average TRP per m2 of each element of urban

surfaces in each scenario

In the summertime, the values of TRP in Scenario A and C were close during the research period. In Scenario D and Scenario E increased rapidly from 07:00 to 14:00, then decreased until 20:00. The values of TRP in all scenarios are stable during the nighttime. In the wintertime, Scenario B showed the lowest trend of the TRP values. The values of TRP in Scenario C, D and E were close during the research period.

Fig. 4-13 shows the relative percentage difference of TRP, which is compared with the Scenario A base model. The highest percentage trend of TRP is determined in Scenario B in summer and wintertime. It means that Scenario B is the most efficient model to decrease thermal radiative power during the research period.

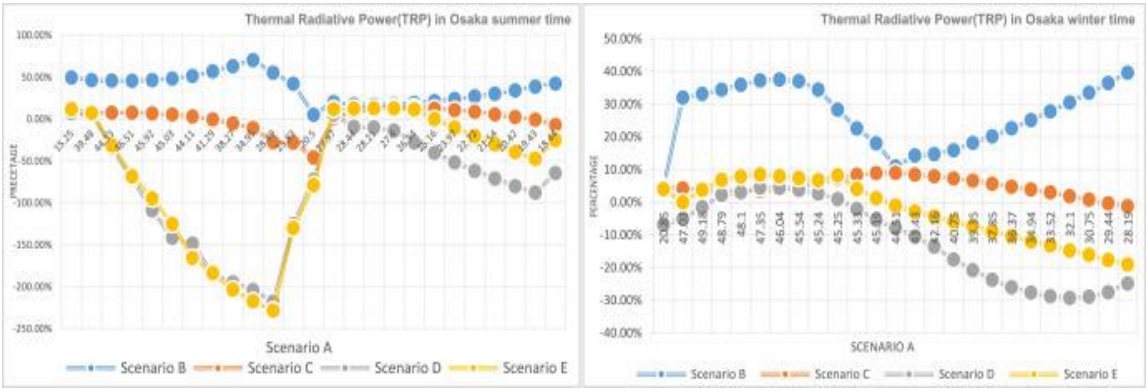

Figure 4-13 The percentages tendency of TRP

4.4.5 Mean radiant temperature

Mean radiant temperature (T_{mrt}) is a crucial parameter for understanding the UHI effect, MRT is defined as the average temperature of all surfaces in a particular environment that is radiating energy. It is an important factor in determining thermal comfort and energy consumption in buildings and urban environments [658]. High MRT values can have negative impacts on human health and energy consumption. Fig. 4-14 shows the change

of $T_{mrt-max}$, $T_{mrt-min}$ and $T_{mrt-avg}$ for the scenarios.

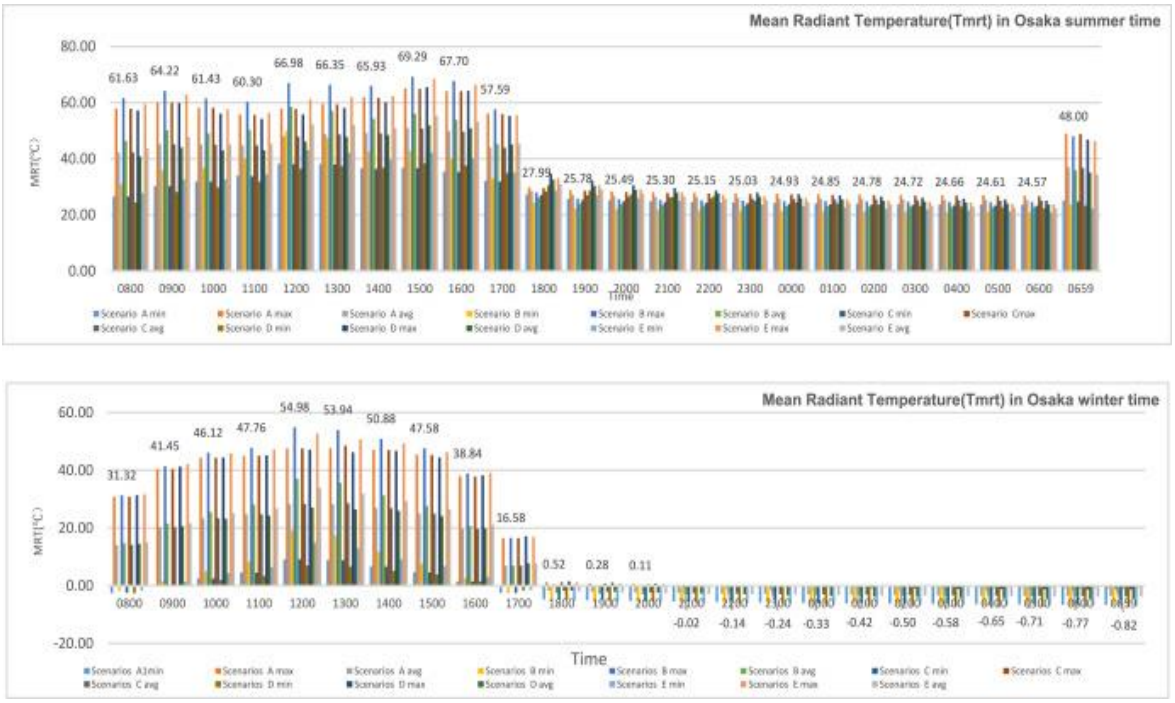

Figure 4-14 The value of $T_{mrt-max}$, $T_{mrt-min}$ and $T_{mrt-avg}$ in the mitigation scenario

The maximum $T_{mrt-max}$ in the summertime of all scenarios was observed in Scenario B at 15:00; the value is 69.29 °C. The minimum value (23.69 °C) of $T_{mrt-max}$ was found at 05:00 in Scenario E. In the wintertime, the maximum $T_{mrt-max}$ has also been found in Scenario B, the value is 54.98 °C.

Fig. 4-15 shows the relative percentage difference of T_{mrt}, which is compared with Scenario A (base model). In the summertime, the stable percentages tendency indicated that Tmrt has decreased insignificantly in Scenario C. Bedside, Scenario B has reduced percentages of Tmrt in summer daytime, however, it has a significate increased Tmrt in the summer nighttime. The results of T_{mrt} reveal that Scenario B has the most efficient ability to decrease Tmrt in the summer nighttime, however, it is unsuitable to decline T_{mrt} in summer daytime. In the wintertime, the percentages of $T_{mrt-max}$ altered to peak during the afternoon winter time in each scenario. However, the percentages of $T_{mrt-max}$ are

all negative during the morning and night time. The results imply that all scenarios can decrease T_{mrt} in winter morning and night time. Scenario B has the highest negative percentages for reducing Tmrt in the wintertime. It shows that T_{mrt} is lowest in Scenario B during the wintertime. In summary, Scenario B is the best model to alter T_{mrt} during the summer daytime and nighttime.

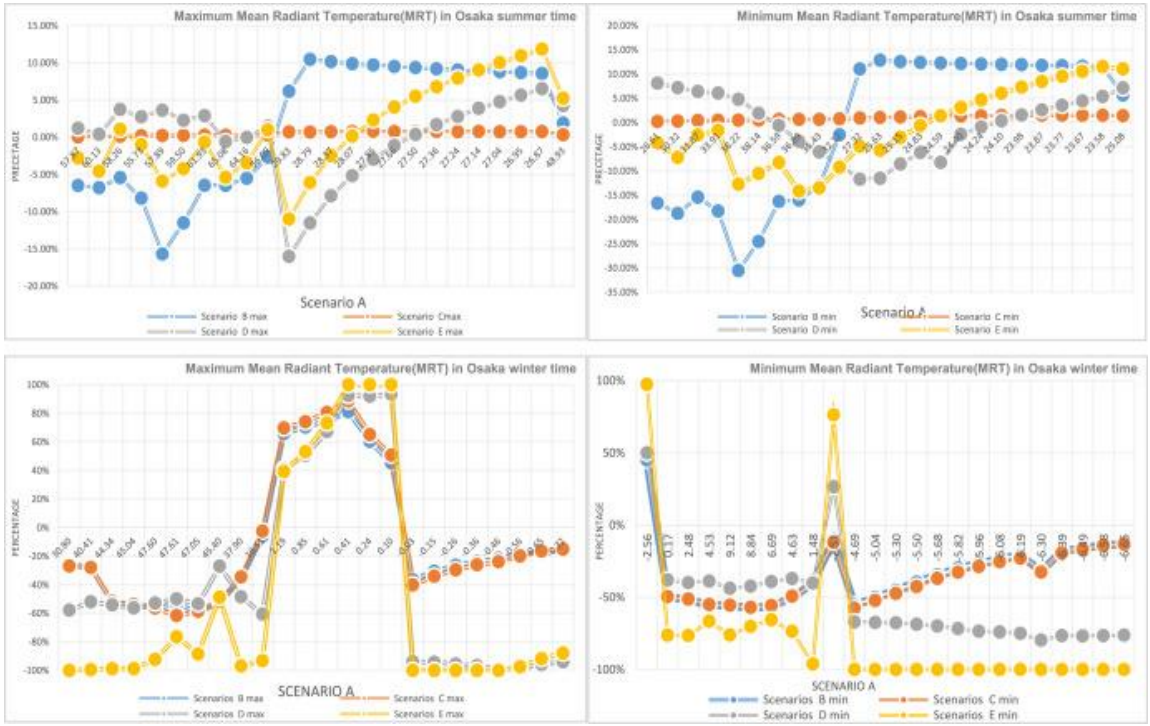

Figure 4-15 The percentage difference of mean radiant temperature in summer and wintertime

4.4.6 Summary

The different mitigation strategies were evaluated using the ENVI-met simulation. Several urban heat island (UHI) mitigation criteria, including outdoor air temperature, sky view factor, net Radiation, thermal radiative power, and mean radiant temperature were employed as standards to assess the efficiency of the UHI mitigation strategies. The simulation results of Scenario A, representing the Base model, were used as the reference value. The relative percentage differences between the UHI mitigation scenarios and Scenario A

were calculated to determine the effectiveness of each strategy.

Based on the simulation results and subsequent discussions, Scenario B, involving the implementation of cool pavement, demonstrated promising results. It was found to effectively decrease outdoor air temperature by approximately 10% in summer and 20% in winter, reduce net radiation by 40% in summer and 20% in winter, lower thermal radiative power by 50% in summer and 40% in winter, and reduce thermal radiant temperature by 10% in summer and 80% in winter.

Furthermore, the study revealed that increasing the albedo of urban fabric material and expanding vegetation coverage ratio were both efficient methods for UHI mitigation. However, it was observed that increasing the albedo of urban fabric material proved to be a more effective mitigation strategy compared to raising the vegetation coverage ratio (Scenario D, green space model), also the integrated and combination scenarios in the urban area. This is because the presence of trees or vegetation that obstruct ventilation in street-level can have several effects that may reduce the cooling potential of the integrated strategy:

(1) Air circulation restriction: Trees and vegetation can act as physical barriers to the movement of air. In urban environments, air circulation is essential for dissipating heat and reducing the urban heat island effect. When trees obstruct airflow, it can lead to stagnant pockets of hot air, impeding the cooling benefits of the increased albedo surfaces.

(2) Shading effect: The excessive shading can hinder the cooling effect of increased albedo surface, resulting in compromising the cooling capacity of the increased albedo surface.

(3)Microclimate alteration: The tree and vegetation can create microclimates in

their immediate surroundings, which can trap heat or enhance cooling through transpiration and shading. If the microclimate generated by the trees counteracts the cooling effect of the albedo surfaces, it may lead the observed underperformance.

To address the issues with tree placement obstructing city ventilation and compromising the performance of integrated and combined UHI mitigation strategies, revaluating the distributing and arrangement of trees and green spaces in the urban area is necessary, aim to maximise airflow and avoid blocking important ventilation pathways. In addition, reconsider the design of streets and roads to promote the better airflow, which could be implemented wider streets or incorporated natural ventilation channels, can improve air movement. Besides, strategically selecting tree species and locations to provide shade without negatively affecting street airflow or obstructing the cooling effects of the increased albedo surfaces.

4.5 Effects of conventional urban heat island mitigation strategies in urban building energy use, carbon emissions, and human thermal comfort

Conventional UHI mitigation strategies in this study include green roofs, cool roofs, cool pavement and green space.

One of the most significant effects of UHI mitigation strategies is their impact on building energy use. For example, cool roofs can reduce total cooling energy consumption by 9.28% due to reducing the amount of cooling energy heat that is transferred through the roof by reflecting sunlight.

UHI mitigation strategies can also have a significant impact on carbon emissions. By reducing the amount of energy needed to cool buildings, these strategies can reduce the amount of carbon emissions associated with energy production.

Finally, UHI mitigation strategies can also have a positive impact on human thermal comfort. By reducing the temperature of urban areas, these strategies can reduce the risk of heat-related illnesses and improve the overall comfort of people living and working in urban environments.

4.5.1 Annual variation of urban heat island intensity

According to chapter 3.3.1, T_g have been generated by UWGE, and the annual UHII for each mitigation strategy has been calculated by Eq. (1). Five difference scales are used to assess the discrepancies of UHII: no UHI (<0℃), minor (0-2℃), moderate (2-4℃), medium (4-6℃), extreme (>6℃) [151]. Fig.4-16. presents the hourly UHII scales occupancy the annual hours (8760 hours) for each scenario.

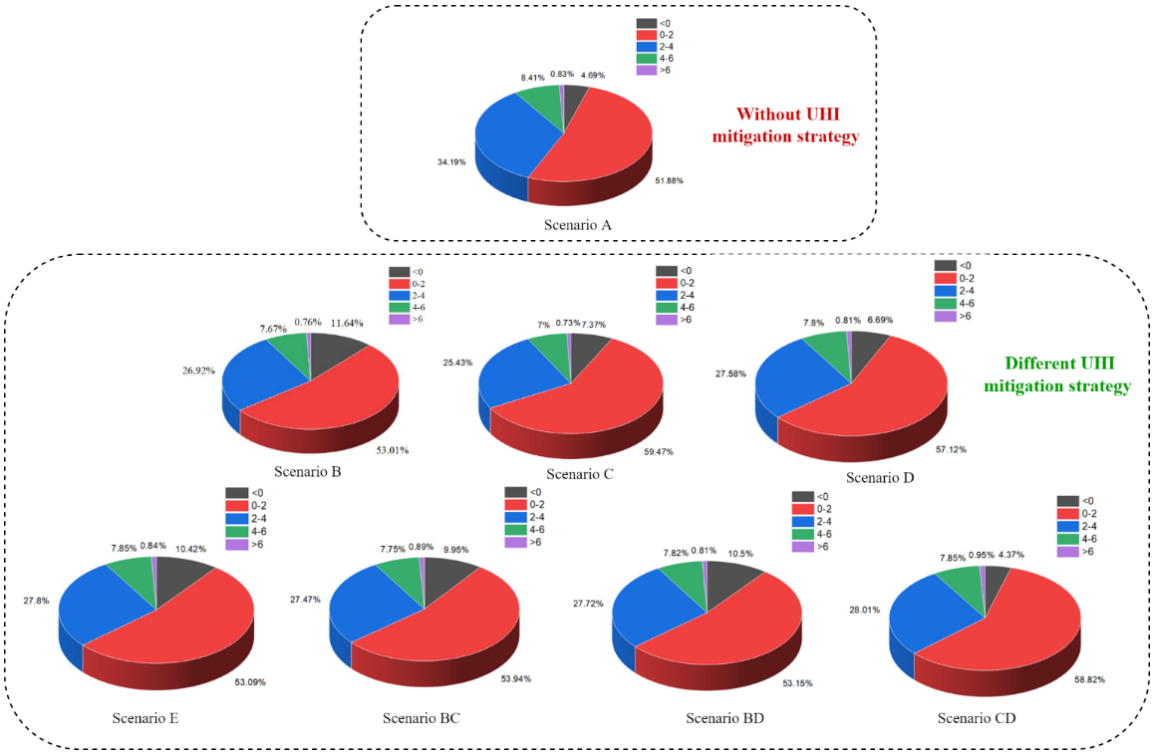

Figure 4-16 Hourly UHII scales occupancy of the annual hours (8760 hours) for each scenario

The percentage difference that the UHII of mitigation strategies have been compared with the benchmark (Scenario A) to determine the ability of UHII reduction for the mitigation strategies. All the scenarios have the ability to reduce the length of the hour for the light and medium UHII. However, Scenario E, BC, and BD increased the hour of strong UHII. Table 4-6 presents the detailed mitigation ability of the mitigation strategies.

Table 4-6 Detailed mitigation ability of the mitigation strategies

Scenario	No UHI (<0°C)	Minor (0-2°C)	Light (2-4°C)	Medium (4-6°C)	Strong (>6°C)
B	150.36%	2.18%	-21.27%	-8.82%	-8.22%
C	57.18%	14.63%	-25.61%	-16.82%	-12.33%
D	42.58%	10.12%	-19.33%	-7.33%	-2.74%

E	122.14%	2.33%	-18.70%	-6.65%	1.37%
BC	-6.88%	13.38%	-18.06%	-6.65%	13.70%
BD	112.17%	3.98%	-19.67%	-7.87%	6.85%
CD	123.84%	2.46%	-18.93%	-7.06%	-2.74%

4.5.2 Building cooling energy use

The cooling energy use is the total energy used for cooling space in the research building. In this study, the maximum cooling capacity for an HVAC system is 100W/m², the maximum cool flow is 100m³/s/m², the setpoint temperature is 24°C and the cooling equipment turns off from 1st January to 3rd March and 1st October to 31st December, turn on from 1st April to 30th September. Fig.4-17. show the range of urban building cooling energy use for the scenarios. All the monthly maximum cooling energy use happened in August, and the minimum cooling energy use is found in September. Besides, Scenario A (with UHI, without mitigation strategy) shows a significant increase in the monthly maximum (209410.80 kWh) and minimum (8457.17kWh) cooling energy use under the UHI phenomenon compared to the cooling energy use under the no UHI phenomenon (top left). On the contrary, all the mitigation strategies have abilities to decrease the maximum and minimum cooling energy use. Scenario C (Cool roof model) shows the lowest monthly maximum (189363.80 kWh) and minimum (7789.40 kWh) cooling energy use. However, Scenario E showed the highest maximum and minimum cooling energy use among the mitigation strategies, which means Scenario E has the highest peak load and cooling energy demand.

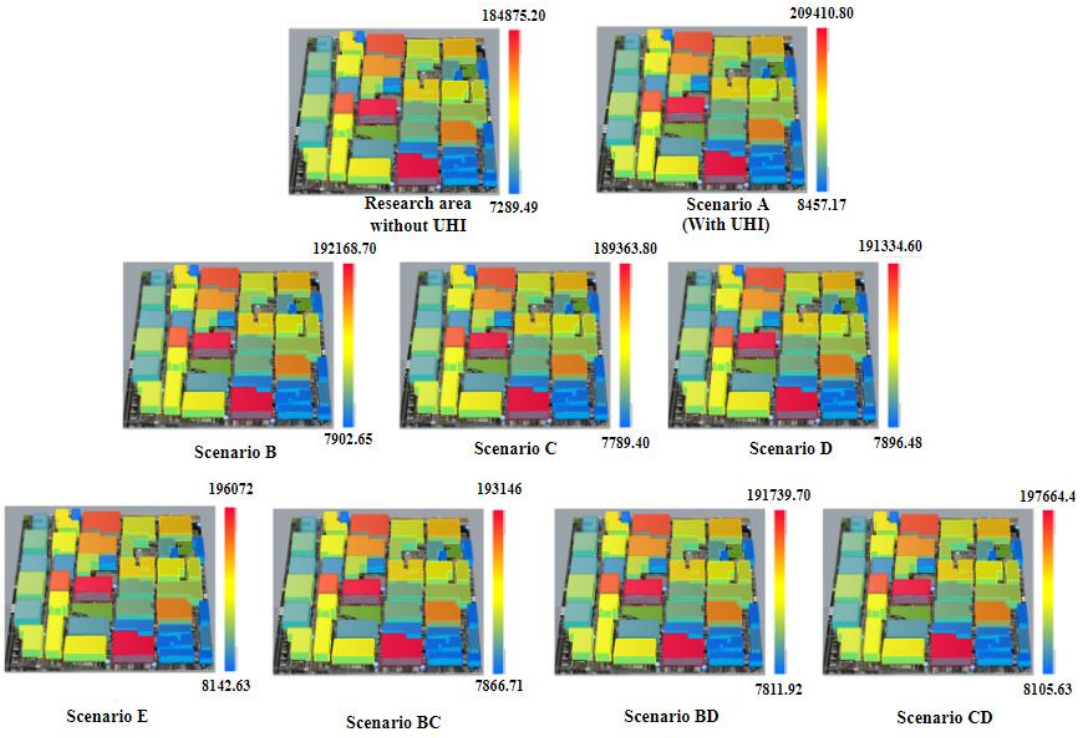

Figure 4-17 The maximum and minimum value of urban building cooling energy use (kWh) in each scenario

The annual cooling energy use value in every mitigation strategy has been compared with the benchmark (Scenario A) to analyse their mitigation ability. Fig.4-18. shows the relative percentage difference in the cooling energy use between the benchmark and the mitigation strategies. All the UHI mitigation strategies have significantly reduced the annual cooling energy use in every type of building and total cooling energy use. The total annual cooling energy use is reduced from 5.65% (Scenario CD) to 9.28% (Scenario C). Moreover, the residential buildings show the greatest reduction in each scenario and the maximum reduction is appeared in Scenario C (11.41%). Office and retail buildings also have big potential for cooling energy saving. The highest reduction in office and retail buildings is Scenario C by 8.66% and 9.18%, respectively. This presents that increasing the roof albedo (Scenario C) is the

prime UHI mitigation strategy for reducing the cooling energy use and also can decrease the peak load of cooling energy demand during the cooling period.

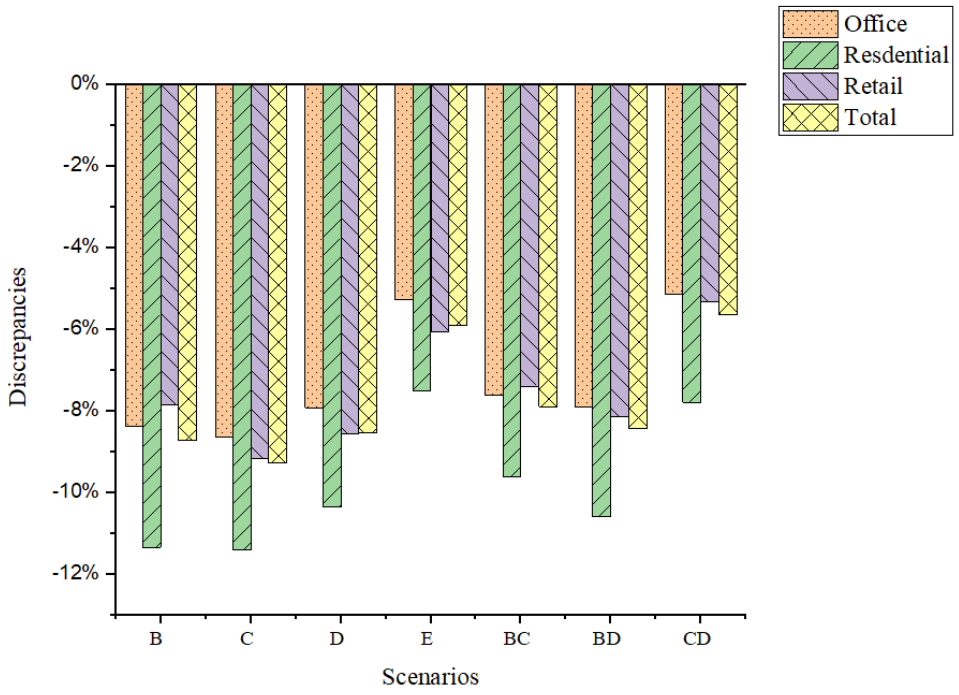

Figure 4-18 The relative percentage difference of the cooling energy use for each mitigation strategy

4.5.3 Indoor thermal comfort

PMV is used to indicate indoor thermal comfort in this study. The annual dissatisfied hour (ADH) is used to indicate the thermal sensation scale. Table 4-7 shows the criteria for scaling indoor thermal comfort [678].

Table 4-7 Annual dissatisfied hour indication

PMV value	Indoor thermal comfort
<-3	Cold
-3 to -2	Cool
-2 to -1	Slightly cool
-1 to 1	Neutral
1 to 2	Slightly warm

2 to3	Warm
>3	Hot

In this study, the range of Slightly warm (1<PMV<2), Warm (2<PMV<3) and Hot (PMV>3) have been chosen to analyse the annual warm hour and avoid heat stress for citizens. The clothing level of human have been set as 1clo and the human is set inside which the metabolic rate is 1met.

The Hot (PMV>3) hour has not been found during the research period. Fig.4-19. presents that the UHI affected the PMV-ADH. When the urban microclimate under the UHI (in scenario A), the annual slightly warm hour in research buildings increased on average by 1.00% and the annual warm hour increased by 2.03%. UHI significantly increases the ADH and that means humans will suffer longer warm hours during the research period.

The annual slightly warm hour is a total of 4181h when in retail buildings without UHI, and 4266h with UHI, which is increased by 0.96%. The warm hour is 1353h (without UHI) and 1538h (with UHI), which is an increase of 2.11%. Besides, in residential buildings, the slightly warm hour is 4112h (without UHI) and 4199h (with UHI), and the warm hour is 1501h (without UHI) and 1679h (with UHI). Moreover, the slightly warm hour in office buildings is 4214h and 4306h, the warm hour is 1131h (without UHI) and 1481h (with UHI).

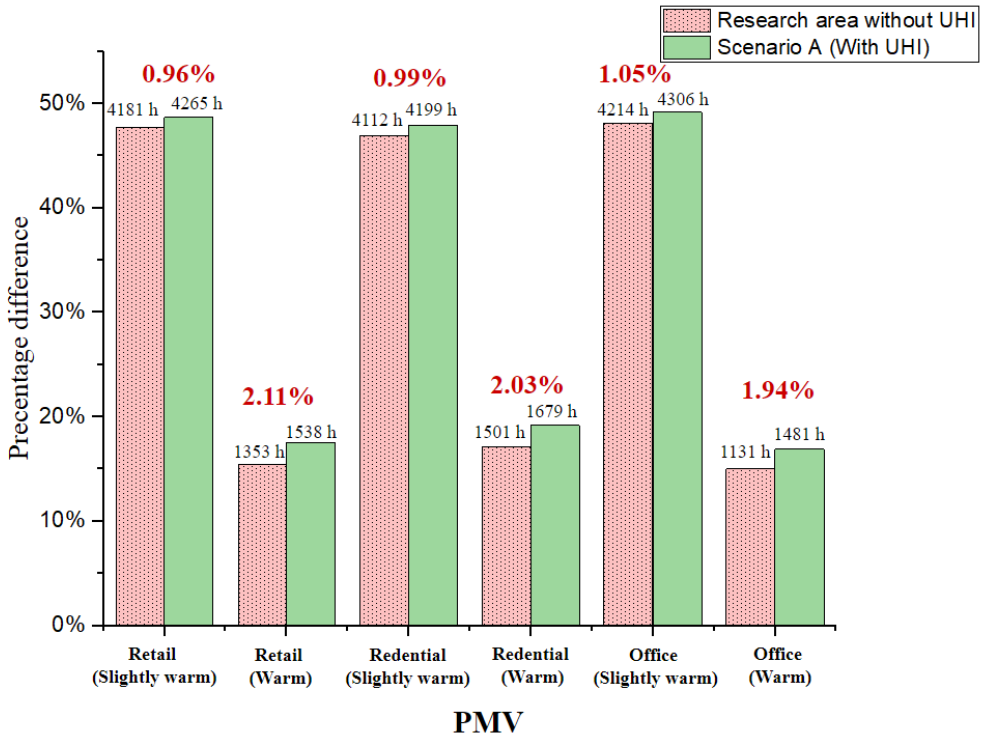

Figure 4-19 The PMV-ADH change in the research area with UHI and without UHI

Fig.4-20 shows the PMV-ADH change in the mitigation strategies, compared with the benchmark (Scenario A). The annual warm hour has been decreased in every mitigation strategy (Scenario B to Scenario CD). The reduction is mostly evident in retail buildings that have the most potential to improve human thermal comfort. Besides, the maximum reduction is found in Scenario C retail buildings model by 0.83%. On the contrary, the slightly warm is increased in every scenario, which means the PMV value in the warm range is down to slightly warm and the urban microclimate is more suitable for citizens.

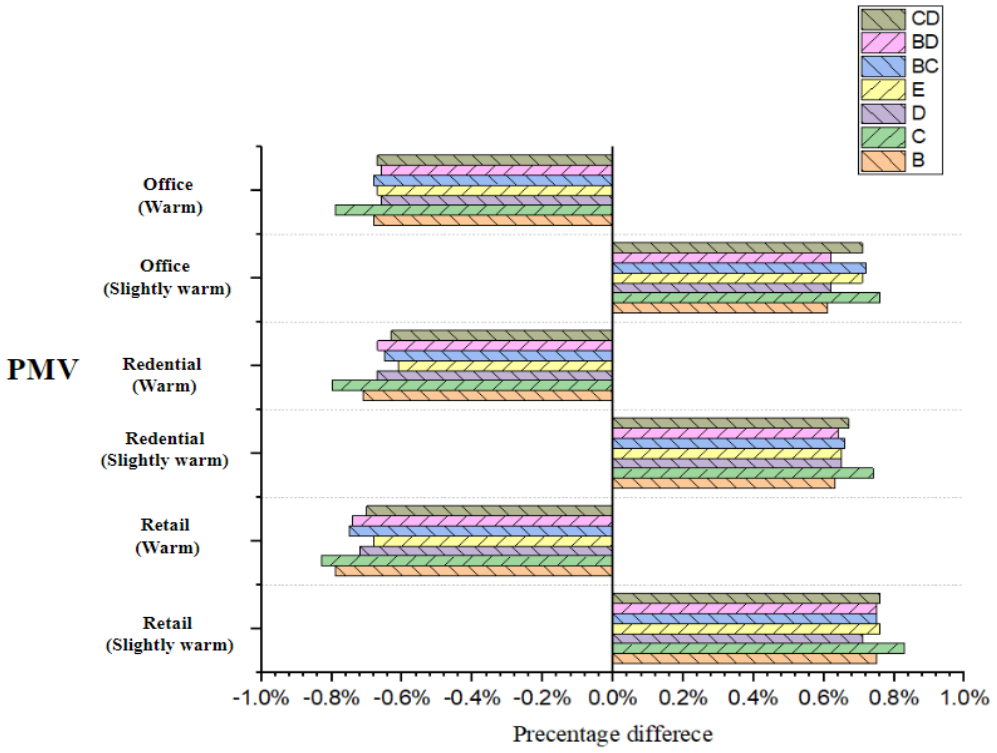

Figure 4-20 PMV-ADH changes in the mitigation strategies, which compared with Scenario A

4.5.4 Outdoor thermal comfort

SET is used to assess outdoor thermal comfort. The scale and temperature threshold have been set in Table 4-8 [679].

Table 4-8 SET indicator scale

SET value (℃)	Indoor thermal comfort
<17	Slightly cool
17-30	Neutral
30-34	Slightly warm
34-37	Warm
>37	Hot

In this study, the range of Slightly warm (30<SET<34), Warm (34<SET<37) and Hot (SET>37) have been chosen to analyse the annual outdoor warm hour and avoid heat stress for citizens. The wind speed 2m above the ground has been simulated, which is the real human wind speed perception. The clothing level has been set as 1clo and the metabolic rate of a person walking outside at 4mph is 3.8met. Fig.4-21. shows that the UHI affected the SET. When the urban microclimate under the UHI (in scenario A), the annual slightly warm hour is decreased by 1.02%, the annual warm hour in research buildings is increased by 0.97% (from 4449h to 4534h) and the annual hot hour is increased by 0.11% (from1902h to1912h). This presents that the SET values for the slightly warm hour are increased to warm and hot ranges. UHI significantly increases the warm and hot hours and humans will suffer longer warm hours during the research period.

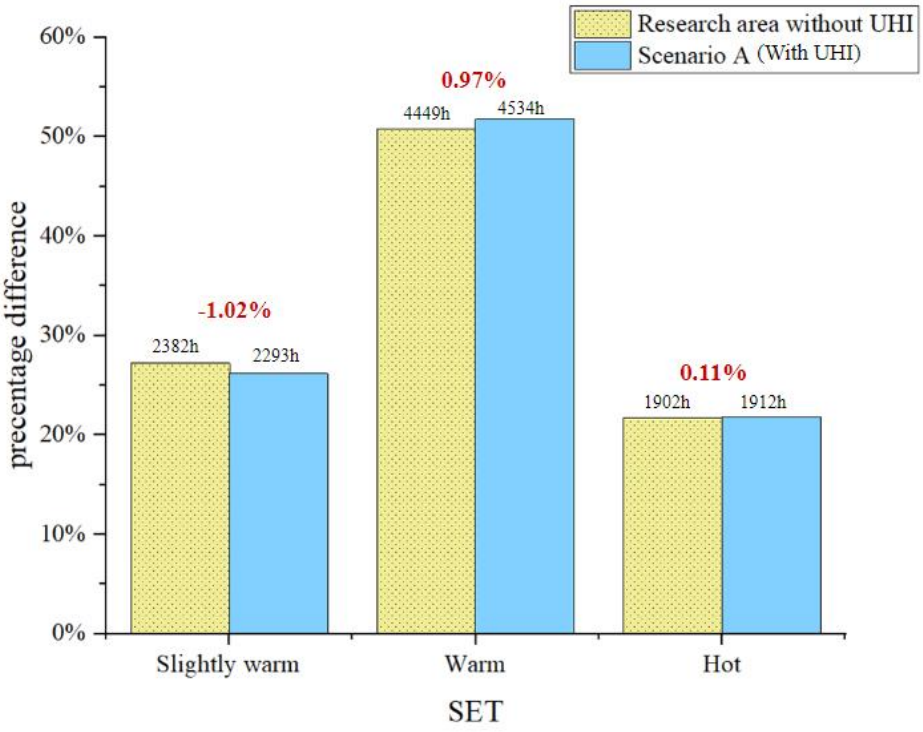

Figure 4-21 SET-ADH change in the research area with UHI and without UHI

Fig.14-22 shows the SET level changes in the mitigation strategies, compared with the benchmark (Scenario A). The hot hours have been decreased in mitigation strategies (Scenario B to Scenario CD), and the annual slightly warm hour has been increased in every mitigation strategy. This presents the SET value in the hot range is down to the warm range and the higher out temperature hour is shorter. Scenario C shows the most significant decline among all the mitigation strategies.

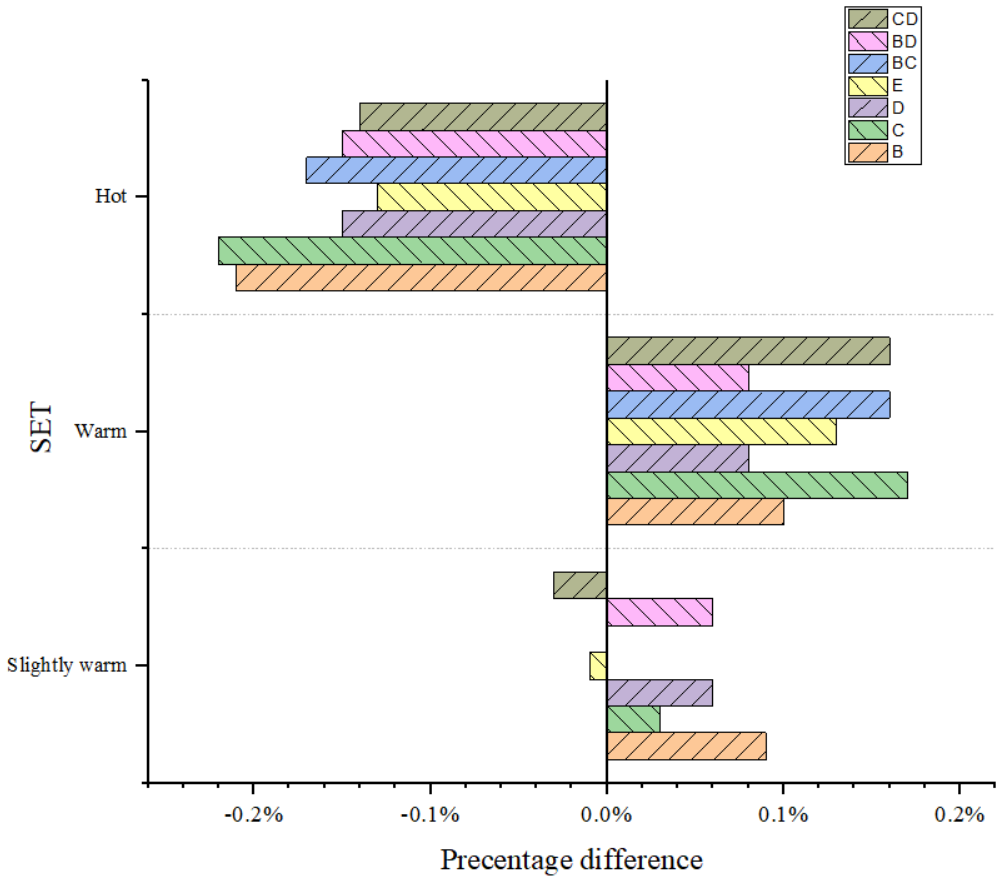

Figure 4-22 SET –ADH changes in the mitigation strategies, which are compared with Scenario A

4.5.5 Urban building carbon emissions

The urban building cumulative carbon emissions in the research area have been calculated by Eq. (7) and Eq. (8) (see CHAPTER.3.3.4.4). The previous a_n is

provided by TEPCO and TEPCO Energy Partner[680], the start year a_n is year 2022.

Besides, due to the UHI significantly increased peak load, cooling demand and use, the carbon emissions for cooling energy use have been used to assess the mitigation ability. The carbon emissions a_{2022} to a_{2060} have been calculated by Eq. (8), which shows in Fig.4-23. Carbon neutrality have been found in 2058. The maximum total carbon emissions are 97.86 Kton in Scenario A is 42.79kton in office buildings, 13.76kton in residential buildings and 25.14kton in retail buildings. For mitigation strategies, Scenario C showed the minimum total carbon emission of 88.78kton, 39.20kton in office buildings, 12.19kton in residential buildings and 22.84kton in retail buildings.

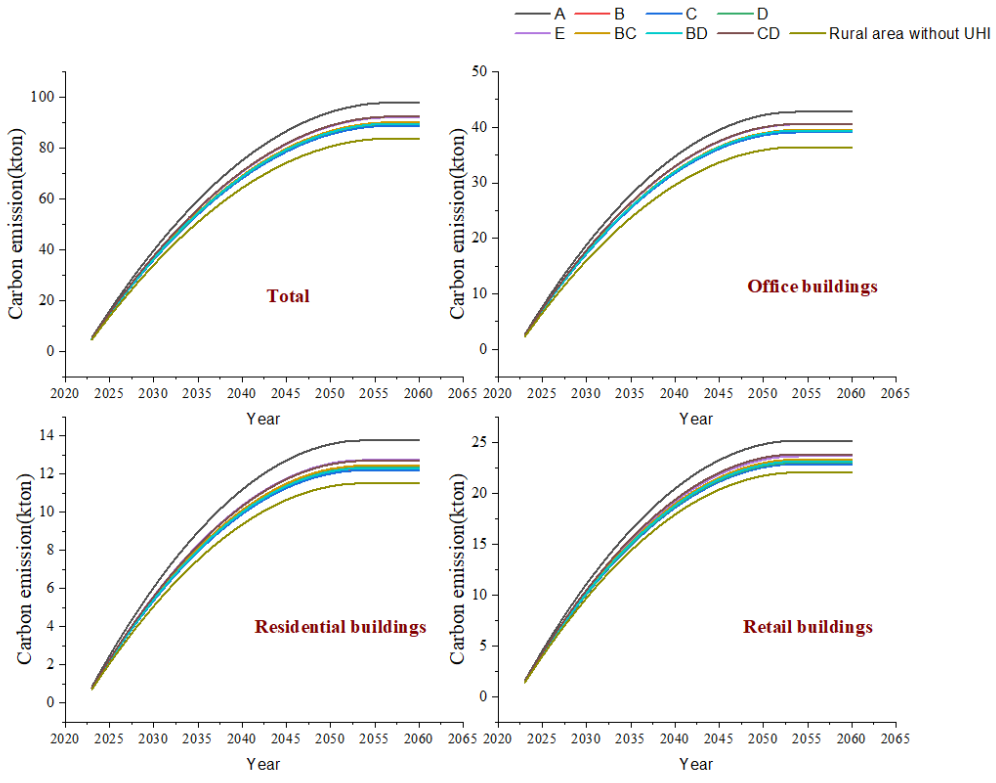

Figure 4-23 The carbon emissions change in conventional UHI mitigation Scenario

4.5.6 Economic analysis

The economic analysis is expected as a function of value in making investment decisions. The market values of interest rate, energy price and the increasing rate for Osaka, Japan are shown in Table 4-9.

Table 4-9 The market values of interest rate, energy price and the increasing rate for Osaka, Japan

	Real discount rate *r* (%)	Electricity price increase rate (%)	Electricity price ($/kWh)
Osaka, Japan	0.99 [681]	0.01 [682]	0.23 [683]

The high reflective print is used to increase the roof and pavement albedo, the cost for high reflective print is $1.76 per m^2[684]. A common street tree in Japan(Japanese maple tree) is used to increase the green space coverage, the cost is $ 15 per m^2[685]. Besides, the installation cost in Japan is $12.64 per hour [686]. According to Eq. (9) (See chapter 3.3.4.5), the initial costs for the conventional mitigation scenarios are shown in Table 4-10.

Table 4-10 Initial costs for the conventional mitigation scenarios

Mitigation strategies	$Cost_{capital}$ ($)	$Cost_{labour}$ ($)	Initial investment ($)
Scenario B	43652.66	343505.50	357158.17
Scenario C	345252.89	2479543.51	2824796.40
Scenario D	676435.92	570001.00	1246445.92
Scenario E	1065341.48	3363059.01	4428400.49

Scenario BC	388905.56	2793049.01	3181954.57
Scenario BD	720088.52	883515.50	1603604.09
Scenario CD	1021688.81	3049553.51	4071242.32

A quick return on investment with the DPP indicator is a significant motivation for UHI mitigation. According to Eq. (10) and Eq. (11) (See chapter 3.3.4.5.), the DPP of all the UHI mitigation strategies have strategies have been calculated and shown in Table 4-11.

Table 4-11 Discounted payback period for each scenario

	Scenario B	Scenario C	Scenario D	Scenario E	Scenario BC	Scenario BD	Scenario CD
DPP (Years)	1	3	2	6	4	2	6

5 CHAPTER V: THERMAL ENERGY STORAGE TECHNOLOGIES IN URBAN HEAT ISLAND MITIGATION STRATEGIES

5.1.1 Thermal energy storage technologies as urban heat island mitigation scenarios

The successful implementation of TES as a UHI mitigation strategy requires careful consideration of various factors to ensure that the system is efficient, cost-effective, safe, and environmentally friendly. There are several factors have been considered that thermal energy storage technologies as urban heat island mitigation scenarios.

Capacity: TES system should have sufficient capacity to meet thermal energy demands during peak hours, also to achieve maximum heat absorption.

Technology: Different types of TES systems should be evaluated for their suitability based on thermal energy demand, operating conditions, and cost-effectiveness.

Cost: TES system cost, including initial investment, installation, and maintenance, should be assessed for economic feasibility.

Environmental Impact: The environmental impact of the TES system, such as materials used, energy consumption, and carbon footprint, should be evaluated.

Safety: Safety measures should be implemented to prevent accidents and ensure the safety of people and the environment.

5.1.1.1 PCM thermal performance algorithm and selection

The properties of the PCMs have been thoroughly studied over the years. Several kinds of paraffin and non-paraffin organic materials have been found to be suitable for cooling storage [659].

The selection of PCMs for building applications is a complex process that requires careful evaluation of the desired thermal performance, environmental factors, and materials properties. One of the key factors to consider is the melting point of the PCM, which should match the average daily temperature range of the target location to ensure proper performance. low-melting point PCMs, such as paraffin wax, are suitable for warm climates [660], while higher-melting point PCMs, such as salt hydrates, may be necessary for cooler climates [661].

Another important factor to consider is the thermal conductivity of the PCM. This property affects the rate at which heat is transferred through the material and can impact the melt and freeze cycles of the PCM. A lower thermal conductivity can reduce heat transfer, but may also lead to longer melt and freeze cycles. It is also important to consider the thermal stability and durability of the PCM over time, especially in outdoor applications where weathering and UV exposure can degrade some materials and reduce their thermal performance.

During the 1980s, several forms of PCM were marketed for active and passive solar applications, including direct gain. Although EnergyPlus is a vastly popular and powerful software, which solves the heat transfer coefficient at a particular point on a surface only considering natural convection, without accounting for no turbulence [662] and less common turbulence [663]. Sensible heat flux refers to the convective heat flux from the building surface to the ambient air can be calculated by Eq. (14).

$$q_s = h_s(T_s - T_a) = h_s \Delta T \quad (14)$$

Where, h_s is the transfer coefficient based on standard convection heat flow relationships (Table 5-1) T_a is the ambient air temperature, Ts is the surface temperature.

Table 5-1 Convective heat flow correlations [662]

Convection type	Range	Nusselt number (Nu)
Natural	$\Delta T>0$, $Ra<10^7$ (laminar)	$0.54Ra^{1/4}$
Natural	$\Delta T>0$, $10^7<Ra<10^{10}$ (turbulent)	$0.15Ra^{1/3}$
Natural	$\Delta T<0$, $10^5<Ra<10^{10}$	$0.27Ra^{1/4}$
Forced	$Re<10^5$ (laminar)	$0.332Re_x^{1/2}Pr^{1/3}$
Forced	$10^5<Re<10^8$ (turbulent)	$0.0296Re_x^{4/5}Pr^{1/3}$

Where, Ra is Rayleigh number, and Re_x is Reynolds number. Combining the natural and forced Nusselt numbers into Eq. (15) to accurate the h_s.

$$h_s = \begin{cases} \beta \frac{k}{L_n} 0.15 Ra_{Ln}^{1/3} + \frac{k}{x} R_f 0.037 Re_x^{4/5} Pr^{1/3}, & when\ T_s - T_a \geq 0 \\ \beta \frac{k}{L_n} 0.27 Ra_{L_n}^{1/4} + \frac{k}{x} R_f 0.66 Re_x^{1/2} Pr^{1/3}, & when\ T_s - T_a < 0\ and\ x < x_c \\ \beta \frac{k}{L_n} 0.27 Ra_{L_n}^{1/4} + \frac{k}{x} R_f \left(0.0037 Re_x^{4/5} - 871\right) Pr^{1/3}, & when\ T_s - T_a < 0\ and\ x > x_c \end{cases} \quad (15)$$

Where β is a function which explains the relationship between the Grashof and Reynolds numbers, can be calculated by Eq. (16).

$$\beta = \frac{1n(1+Gr_{Ln}/Re_x^2)}{1+1n(1+Gr_{ln}/Re_x^2)} \quad (16)$$

where $Re_x = \frac{upx}{\mu}$, Ra $= Gr_{L_n} Pr$ and $Gr_{L_n} = \frac{g\rho^2 L_n^2 \Delta T}{T_f \mu^2}$.

Therefore, the thicknesses or the surface temperature of PCM roof and façade can be calculated by Eq. (117)

$$\text{Thic} = \frac{t_n h_r}{\rho L} (T_{pcm} - T_n) \quad (17)$$

Where Thic is the thickness of the PCM roof or PCM façade, T_n is air temperature, t_n is PCM discharging time, ρ is PCM density, L is the PCM latent heat capacity, and h_r is heat transfer coefficient.

Moreover, Fire resistance is another critical factor to consider for building applications, as the PCM must meet building codes and safety requirements. Some PCMs, such as paraffin wax and salt hydrates, have good fire resistance properties. The cost of the PCM material, as well as the cost of manufacturing and installing the PCM-based systems, must also be considered.

To evaluate the performance of PCMs for building applications, several standardized testing procedures have been developed. For example, the ASTM C1728 standard [664] provides guidelines for testing and evaluating the thermal performance of PCMs used in construction. This standard includes tests for measuring the melting point, thermal conductivity, and thermal stability of PCMs, as well as methods for evaluating their fire resistance.

In conclusion, the selection of PCMs for building applications is a complex process that requires careful consideration of multiple factors, including the desired thermal performance, environmental conditions, materials properties, and cost. Standards such as ASTM C1728 [664]can provide guidance and ensure that the performance of PCMs is properly evaluated, but the specific requirements and constraints of each project must be taken into account to determine the most suitable PCM for a particular application.

Considering the accessibility and the standards mentioned above, and the main disadvantages of inorganic PCMs, such as thermal conductivity mismatch, limited cycle life, environmental concerns, cost, seven organic commercial PCMs have been chosen to use in the PCM roof and PCM façade (Table 5-2)., In pursuit of maximising the potential of phase change material for UHI mitigation, various thicknesses of PCM have been utilised to explore the full range of possibilities. The different thicknesses of each PCM (2cm, 4cm, 6cm,

8cm and 10cm) is used without considering the roof structure safety and PCM leaking risk. By providing insights into the diverse applications of PCM at varying thickness levels, this study contributes valuable knowledge to support evidence-based policies and urban planning initiatives aimed at creating cooler and more resilient urban environments. Besides, by exploring the different PCM thicknesses serves to offer tailored and effective UHI mitigation approaches to policy makers, local authorities, and urban designers.

Table 5-2 Selected PCM as UHI mitigation scenarios

PCM	Type	Phase change temperature (℃)	Density (kg/m^3)	Latent heat capacity (kJ/kg)	Specific heat capacity (kJ/kg K)	Thermal conductivity (W/m K)
A58H	Organic	58	820	240	2.85	0.18
A52	Organic	52	810	220	2.15	0.18
A48	Organic	48	810	230	2.85	0.18
A43	Organic	43	780	280	2.37	0.18
A36H	Organic	36	776	300	2.3	0.22
A32H	Organic	32	820	240	2.2	0.22
A28	Organic	28	789	265	2.22	0.21

5.1.1.2 PVT systems thermal performance algorithm and selection

In this study, the relationship between the UHI phenomenon and PVT systems is analysed by using a flat plate PVT collector, which are sufficient to meet the daily energy storage needs. For building applications, PVT systems can be integrated with roofs, façade, and window structures. Notably the PVT system incorporates solar thermal elements designed to capture and store thermal energy

from solar irradiance. This secondary function distinguishes the PVT system from traditional photovoltaic systems by enabling the utilization of solar heat. This stored thermal energy can be employed across various domains, including space heating, domestic hot water production, and industrial processes, tailoring its use to diverse applications and energy demands.

As an embodiment of thermal energy storage, the PVT system plays a crucial role in accumulating and preserving the captured solar thermal energy. The stored energy is retained within a thermal storage medium, often in the form of a heat storage tank. This feature equips the PVT system with the ability to release stored thermal energy on demand, particularly during periods of limited solar irradiance, ensuring a continuous and reliable supply of thermal energy.

In essence, The performance of the PVT roof can be expressed by a combination of efficiency expressions [420] consisting of thermal efficiency (η_{th}) and electrical efficiency (η_{PV}), which are calculated as the ratio of the useful thermal and electrical gain of the system to the incident solar irradiation on the collector gap within a specific time or period. The analytical parameters of the PVT collector system are presented in Table 5-3. The total PVT efficiency (η_{PVT}) is used to evaluate the overall performance of the system and is calculated in Eq. (18), [665]:

$$\eta_{PVT} = \eta_{th} + \eta_{pv} \quad (18)$$

Table 5-3 analytical parameters of the PVT collector system

Geometric dimensions and optical properties	Abbreviation	Value	Units
Number of the glass cover	N	1	–
Emittance of glass	εg	0.88	–
Emittance of plate	εp	0.95	–

Collector tilt	θ	14	℃
Fluid thermal conductivity	kf	0.613	W/m ℃
Specific heat of the working fluid	Cp	4180	J/kg °C
Back insulation conductivity	kb	0.045	W/m °C
Back insulation thickness	lb	0.05	m
Insulation conductivity	ke	0.045	W/m °C
Edge insulation thickness	le	0.025	m
Absorber conductivity	kabs	51	W/m °C
Absorber thickness	labs	0.002	m
Heat transfer coefficient from cell to absorber	hca	45	W/m °C
Heat transfer inside the tube	hfi	333	W/m °C
Transmittance	τ	0.88	–
Absorptance	α	0.95	–

In this study, the PVT roof system is assumed to be represented as a flat-plate collector with a single glazing sheet. Based on this assumption, the thermal and PV performance of the PVT unit was evaluated by deriving the efficiency parameters based on the Hottel–Whillier equations [666]. The thermal efficiency of a conventional flat-plate solar collector is the ratio of the useful thermal energy (Q_u) to the overall incident solar radiation (S) and can be explained by Eq. (19):

$$\eta_{th} = \frac{Q_u}{S} \tag{19}$$

The useful collected heat absorbed by the flat-plate solar collector can be given as the combined results of the average mass flow rate (ṁ), the heat capacity of the flowing medium (C_p) and the temperature difference at the collector inlet (T_i) and outlet (T_o) and can be calculated by Eq. (20) as:

$$Q_u = \dot{m}C_p(T_0 - T_i) \quad (20)$$

Hottel–Whillier [666] equation can be used to describe the difference between the absorber solar radiation and thermal heat losses and can be expressed as Eq. (21) as follows:

$$Q_u = A_c F_R[G_T(\tau\alpha)_{PV} - U_L(T_i - T_a)] \quad (21)$$

Where, A_c is the collector area, T_a is the ambient temperature, T_i is the inlet temperature, U_L is the overall collector heat loss, $(\tau\alpha)_{PV}$ is the thermal efficiency of PV, G_T is the solar radiation at NOCT, and F_R is the heat removal efficiency factor, which can be calculated by Eq. (22) as follows:

$$F_R = \frac{\dot{m}C_p}{A_c U_L}\left[1 - \exp(-\frac{A_C U_L F'}{\dot{m}C_p})\right] \quad (22)$$

Where F' is the collector efficiency factor, which is calculated by Eq. (23) as follows:

$$F' = \left[\frac{\frac{1}{U_L}}{U_L(D_h+(W-D_h)F)}\right] + \frac{1}{C_b} + \frac{1}{2(a+b)h_{fi}} \quad (23)$$

where a is the duct width, b is the duct height, C_b is the conductance of the bond between the fin and square tube, h_{fi} is the heat-transfer coefficient of the fluid, D_h is the hydraulic diameter, and F is the fin efficiency factor expressed by Eq. (24) as follows:

$$\mathrm{F} = \frac{\tanh(\mathrm{M}\frac{w-D_h}{2})}{\sqrt{M\frac{W-D_h}{2}}} \quad (24)$$

Where

$D_h = \frac{2ab}{(a+b)}$,

$$\text{And M} = \sqrt{\frac{U_L}{k_{abs}l_{abs}+k_{pv}l_{pv}}} \quad (25)$$

where k_{abs} is the absorber thermal conductivity, l_{abs} is the absorber thickness, k_{PV} is the PVT conductivity, and l_{PV} is the PV collector thickness. The U_L is the overall loss coefficient of the collector is the sum of the edge (U_e) and top (U_t) loss coefficients and can be explained by Eq. (26) as follow:

$$U_L = U_e + U_t \tag{26}$$

$$U_e = \frac{k_e p l}{L_c A_c}$$

$$U_t = \left\{ \frac{N}{\frac{C}{T_{pm}}\left[\frac{T_{pm}-T_a}{(N+f)}\right]^e} \frac{1}{h_w} \right\}^{-1} + \frac{\sigma(T_{pm}+T_a)(T_{pm}^2+T_a^2)}{(\varepsilon_p+0.00591 N h_W)^{-1}+\frac{2N+f-1+0.133\varepsilon_p}{\varepsilon_g}-N} \tag{27}$$

Where

$$C = 520(1 - 0.000015\beta^2) \tag{28}$$

$$f = \left(1 + 0.089h_w - 0.1166h_w\varepsilon_p\right)(1 + 0.07866\mathrm{N}) \tag{29}$$

$$e = 0.43\left(1 - \frac{100}{T_{pm}}\right) \tag{30}$$

$$T_m = T_i + \frac{\frac{Q}{A_c}}{F_R U_L}(1 - F_R) \tag{31}$$

where p is the collector perimeter, N is the number of glass covers, σ is the Stefan–Boltzmann constant, ε_p is the plate emittance, ε_g is the glass emittance, β is the collector tilt, T_{pm} is the mean plate temperature, and h_w is the wind heat-transfer coefficient.

5.1.1.3 Thermal energy storage technologies in urban heat island mitigation Scenario

TES greatly absorb the incident solar radiation and emits and absorbs thermal radiation. Transferring heat via charge and discharge processes with the atmospheric air, and their immediate opaque environment, respectively. The

absorbed sensible and latent heat is a function of the heat transfer coefficient and of the temperature difference between the ambient air and the TES system surface [667]. To determine the suitable TES technologies, several factors should be considered to ensure the technology is suitable for the specific application.

To absorb maximum radiation heat and reduce UHII, the energy density of the storage material is a crucial factor, as it determines the amount of energy that can be stored in a given volume. High energy density is desirable for compact storage systems, and materials with high energy densities, such as phase change materials, are often favoured for this reason. The specific heat capacity of the storage material is another important factor, as it determines the amount of heat that can be stored per unit of mass. High specific heat capacities are desirable for storage systems that require a large amount of energy to be stored in a small volume, and materials with high specific heat capacities.

The thermal conductivity of the storage material is an important factor, as it determines the rate at which heat can be transferred into and out of the storage material. High thermal conductivity is desirable for storage systems that require fast charging and discharging times, and materials with high thermal conductivities.

The temperature range of the storage material is a critical factor to select TES, as it determines the maximum and minimum temperatures at which energy can be stored and retrieved. The temperature range of the storage material must be suitable for the intended application, and materials with high temperature ranges. Therefore, seven TES technologies (See Table 5-4) have been selected as UHI mitigation scenarios to analyse the association with UHI:

Table 5-4 TES as UHI mitigation scenarios

Selected TES mitigation scenarios	Description
PCM-Roof model [278]	PCM panels as the uppermost layer are put in the roof, which directly absorb radiation
PCM-Façade model [578]	PCM panels as the outermost layer are put on the south side of the building wall, which absorbs radiation
PCM-Pavement model [253]	Mixing the PCM into asphalt mixture to absorb more radiation heat.
PVT-Roof model [668]	PV layers as the uppermost layer are put in the roof to absorb radiation, and the back side is a solar thermal collector to absorb the heat from PV layers.
PVGT-Window model [669] [687]	PVTG glazing replaced conventional window glazing to absorb radiation.
BIPVT-Façade model [670] [688]	BIPVT panels as the outermost layer are put on the south side of the building external wall.

5.1.2 Outdoor air temperature

The impact of TES technologies on outdoor air temperature has become an important issue in urban planning and design, as excessive heat accumulation in urban areas can have adverse effects on the health and well-being of city dwellers. To evaluate the effects of TES technologies on outdoor air temperature, the advanced UHIMS-ECHE model was used to simulate the complex processes of heat exchange between buildings and the urban environment. All selected TES technologies have analysed the effects on outdoor air temperature by the advanced UHIMS-ECHE model. Hourly outdoor air temperatures for each TES model were generated for all 8760 hours of the research period. By applying Eq.

(6) in Chapter 3.3.4.1, the results show that all selected TES technologies have the ability to reduce outdoor air temperature. Especially in summer seasons, the UHIIs are reduced more obviously. The results showed that all selected TES technologies were effective in reducing outdoor air temperature. In particular, the UHII reduction was more significant during the summer seasons, which are characterised by high temperatures and high humidity.

The reduction in outdoor air temperature observed in this study can be attributed to the ability of TES technologies to store thermal energy during off-peak hours and release it during peak demand periods. By doing so, TES technologies can reduce the need for energy-intensive air conditioning systems during peak periods, thus reducing the amount of heat released into the outdoor environment.

5.1.2.1 PCM-Façade model affects outdoor air temperature

The PCM-façade model has been simulated based on the different thicknesses of selected PCMs. The results show PCM A36H PCM-Façade model (ranging from 2cm to 10cm) has the optimal performance to reduce the UHII, as evidenced by an average annual UHII reduction of 0.65℃ (with PCM A36H-10cm) and a maximum hourly UHII reduction of 4.52 ℃ (with PCM-A36H, 10cm). Further details on the UHII reduction for each PCM façade model are presented in Fig.5-1.

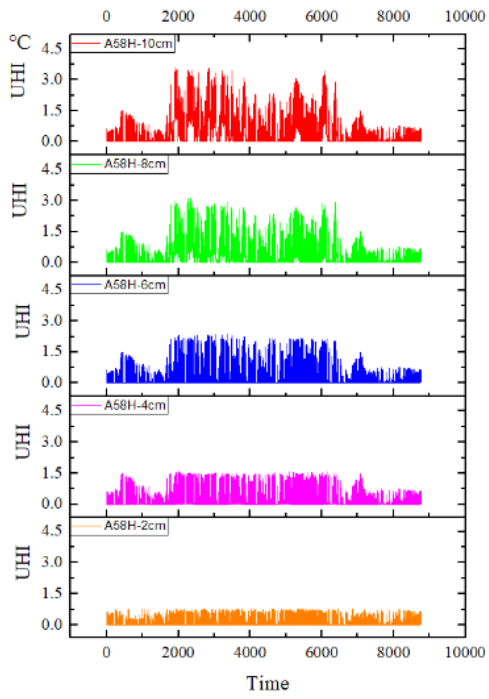

(a) PCM-Facade model-A58H

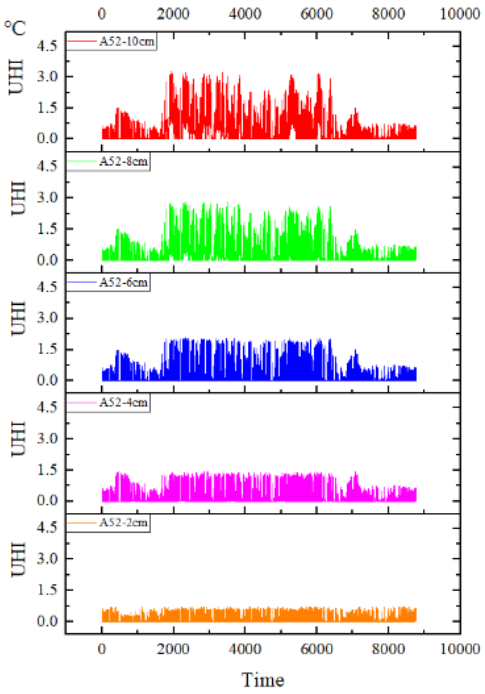

(b) PCM-Facade model-A52

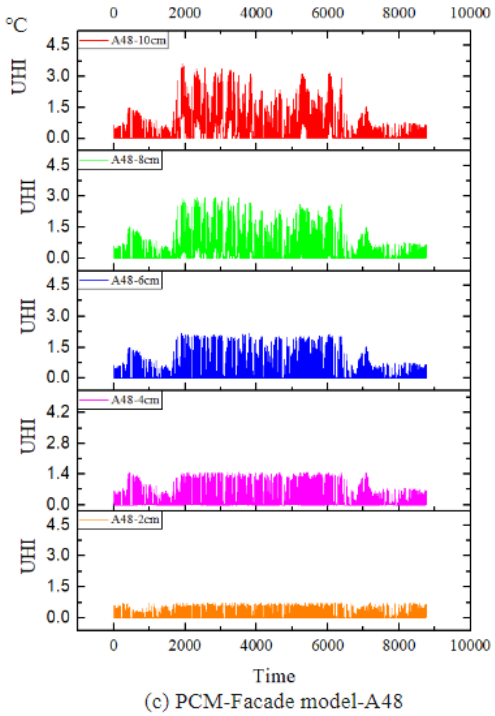

(c) PCM-Facade model-A48

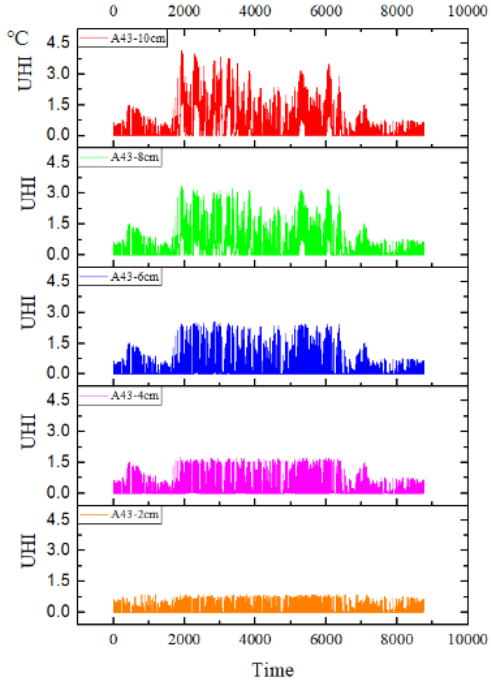

(d) PCM-Facade model-A43

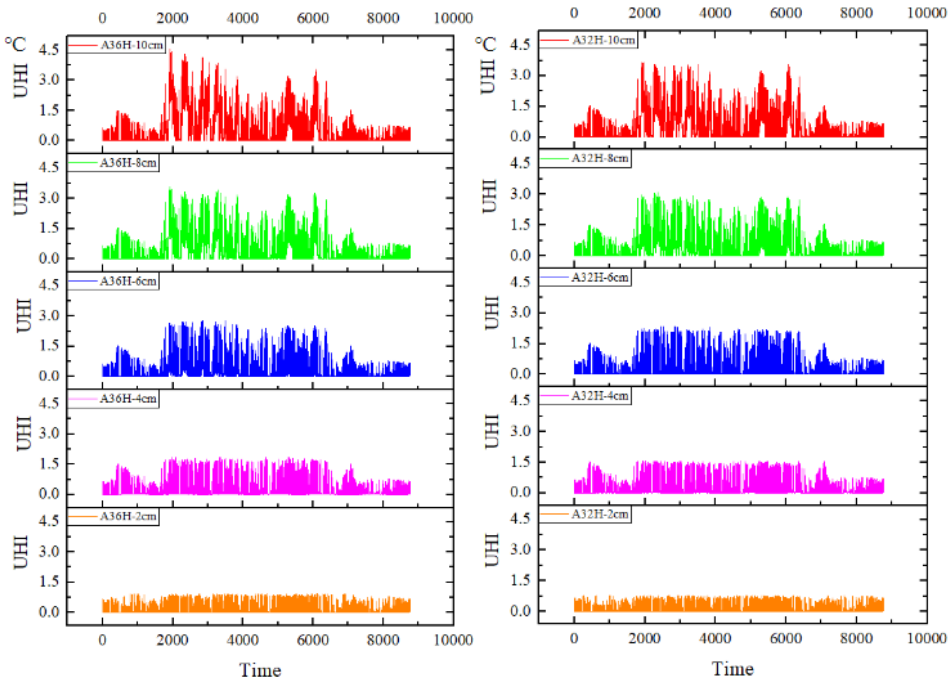

(e) PCM-Facade model-A36H (f) PCM-Facade model-A32H

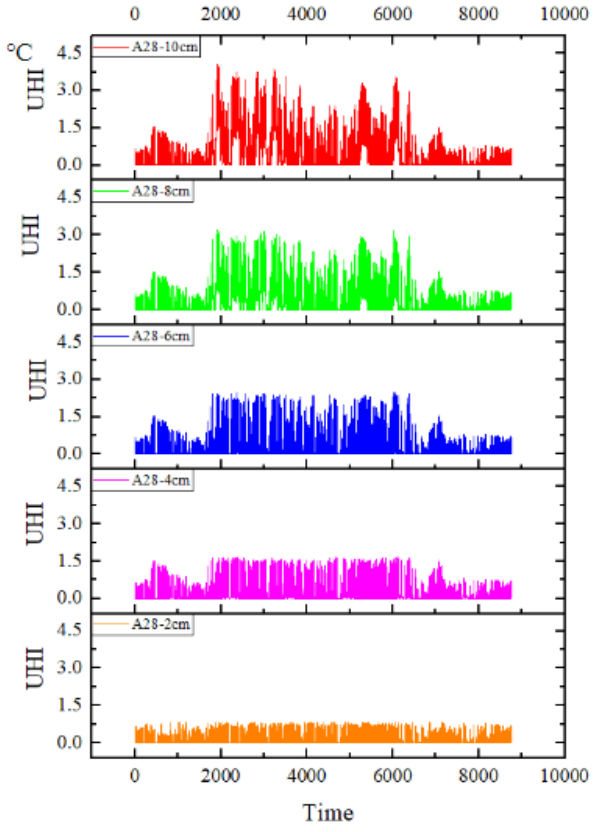

(g) PCM-Facade model-A28

Figure 5-1 UHII decrease for each PCM-façade model

5.1.2.2 PCM–Roof model affects outdoor air temperature

The PCM-roof model was subjected to simulations using the advanced UHIMS-ECHE model, with varying thicknesses of the PCM panel. The simulation results indicate that the use of PCM A28 (ranging from 6cm to 10cm) results in the most effective UHII reduction in the PCM roof model, with an average annual UHII reduction of 0.75℃ (with PCM-A28, 10cm) and a maximum hourly UHII reduction of 7.09℃ (with PCM-A28, 10cm). Additionally, when the thickness of PCM is 2cm and 4cm, the PCM-A36H can reduce the maximum UHII by 2.08℃ and 5.31℃, respectively. Detailed results of UHII mitigation in the PCM roof model are presented in Figure 5-2.

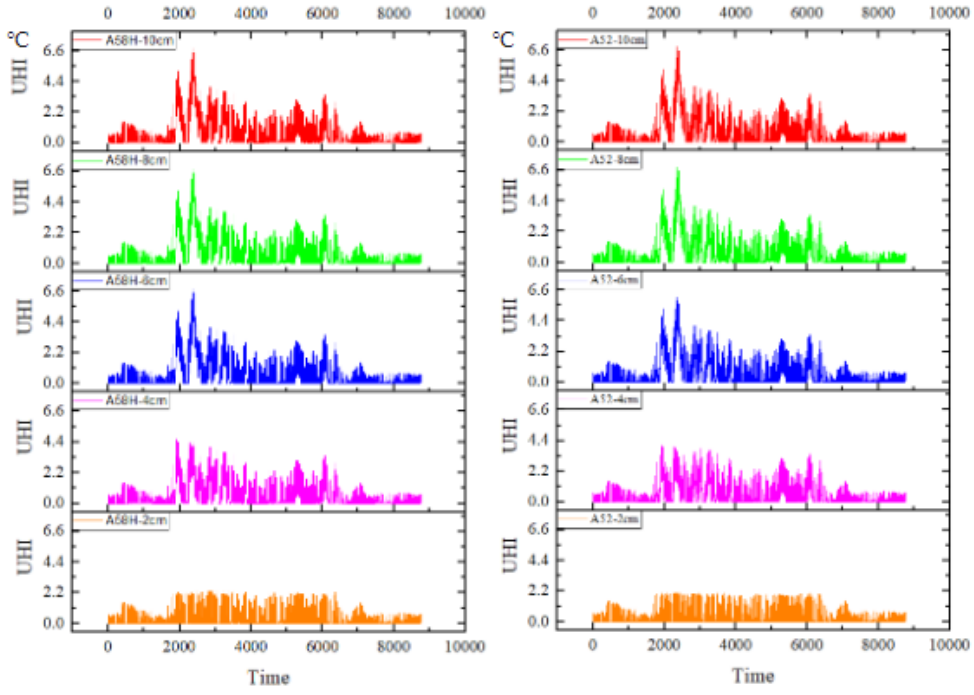

(a) PCM-Roof model-A58H (b) PCM-Roof model-A52

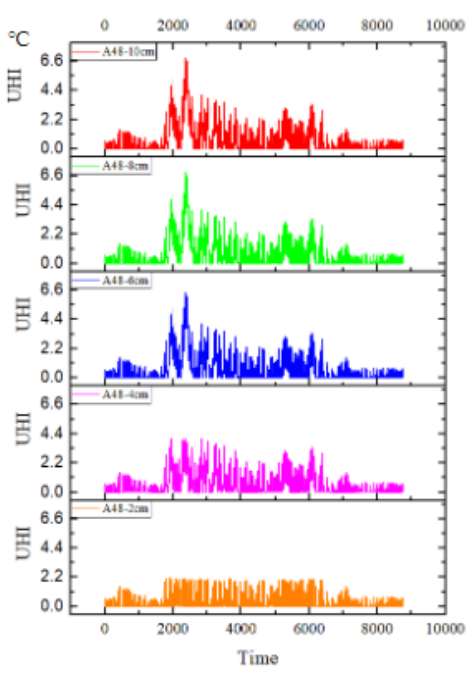

(c) PCM-Roof model-A48

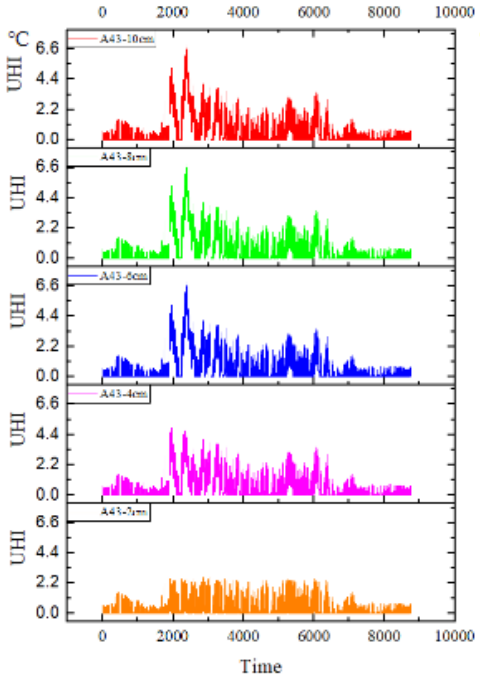

(d) PCM-Roof model-A43

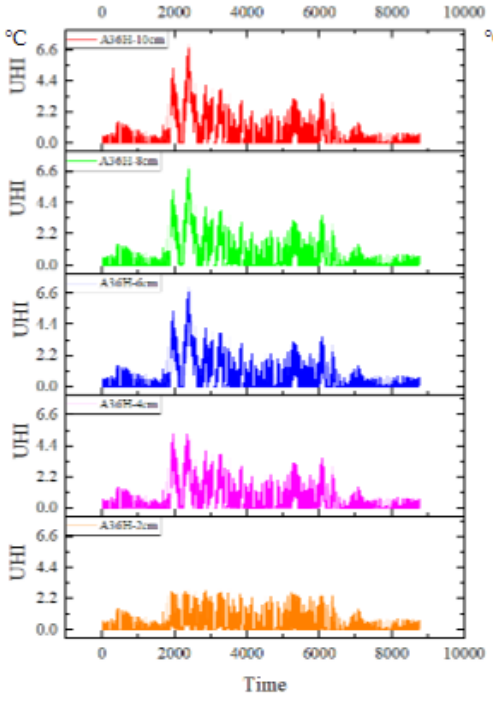

(e) PCM-Roof model-A36H

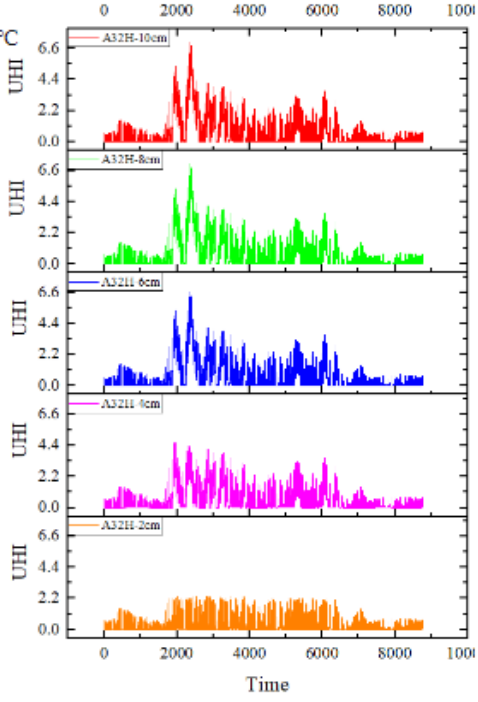

(f) PCM-Roof model-A32H

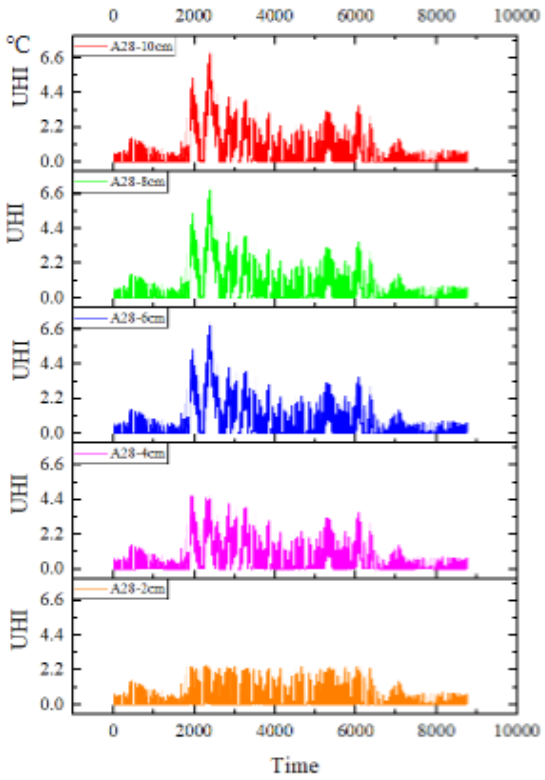

(g) PCM-Roof model-A28

Figure 5-2 UHII decrease for each PCM-Roof model

5.1.2.3 PCM-Pavement model affects outdoor air temperature

The PCM-pavement model was analysed using the advanced UHIMS-ECHE model, considering the varying thicknesses of PCMs. The simulation results indicate that the use of the PCM A36H- pavement model (ranging from 2cm to 10cm) produces the most effective UHII reduction in the PCM pavement model, with an average annual UHII reduction of 0.42℃ (with PCM-A36H, 10cm) and a maximum hourly UHII reduction of 1.73℃ (with PCM-A28, 10cm). A detailed depiction of the UHII mitigation in the PCM-pavement model is shown in Figu.5-3.

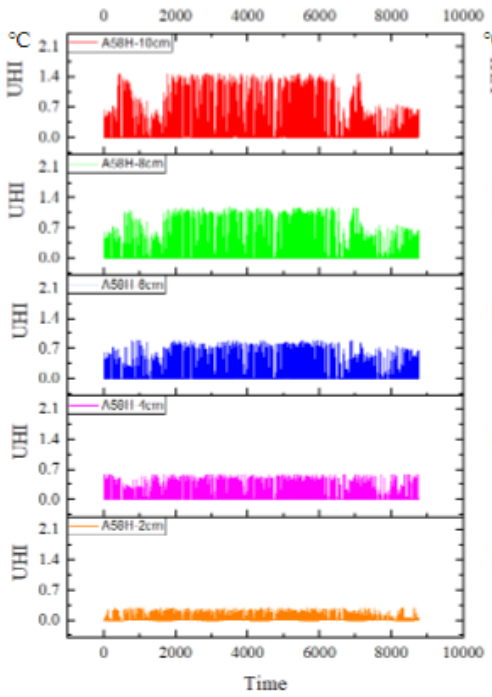

(a) PCM Pavement model-A58H

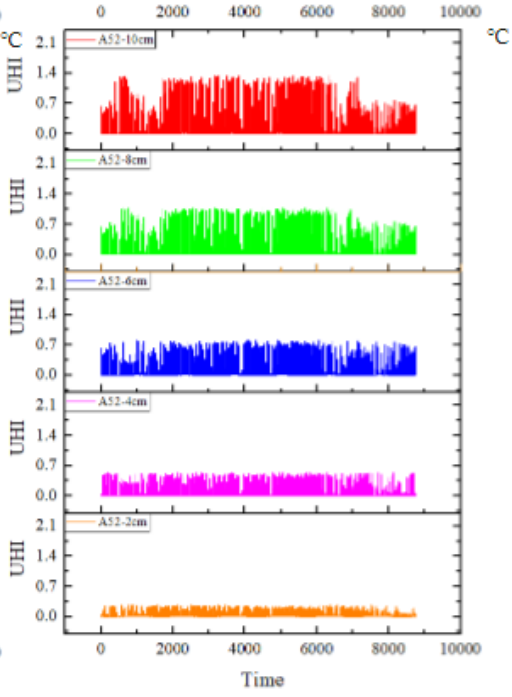

(b) PCM Pavement model-A52

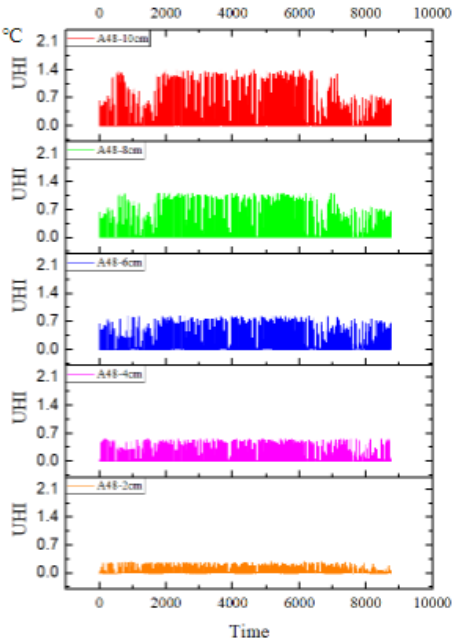

(c) PCM Pavement model-A48

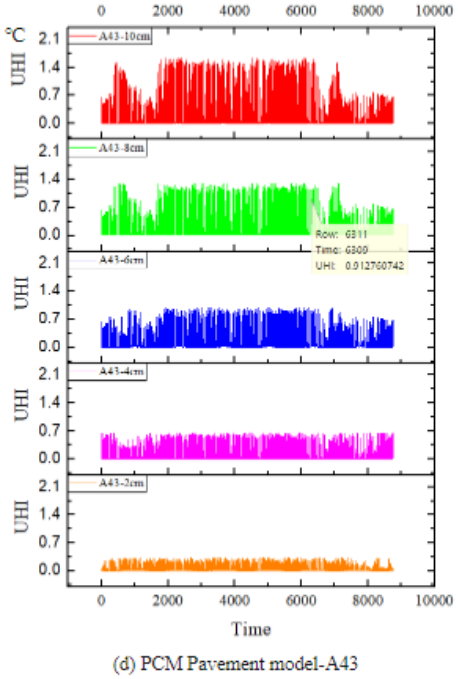

(d) PCM Pavement model-A43

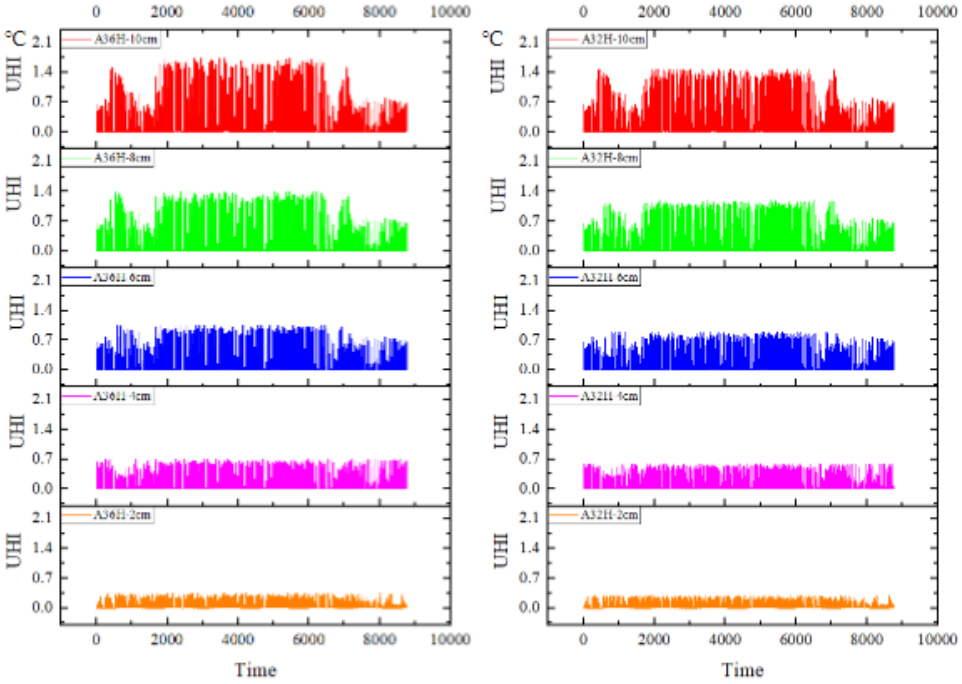

(e) PCM Pavement model-A36H (f) PCM Pavement model-A32H

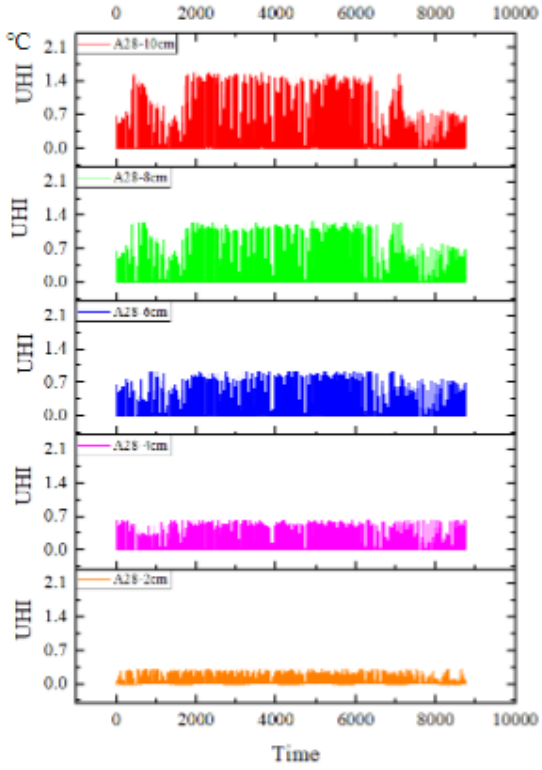

(g) PCM Pavement model-A28

Figure 5-3 UHII decrease for each PCM-Pavement model

5.1.2.4 Effects of PVT models on outdoor air temperature

The PV/T-roof model was analysed using the advanced UHIMS-ECHE model, revealing that the incorporation of PV/T-roof leads to an average annual UHII reduction of 1.23℃ and a maximum hourly UHII reduction of 3.68℃. Figure 5-4 provides a visualization of the UHII decrease in the PV/T-roof model."

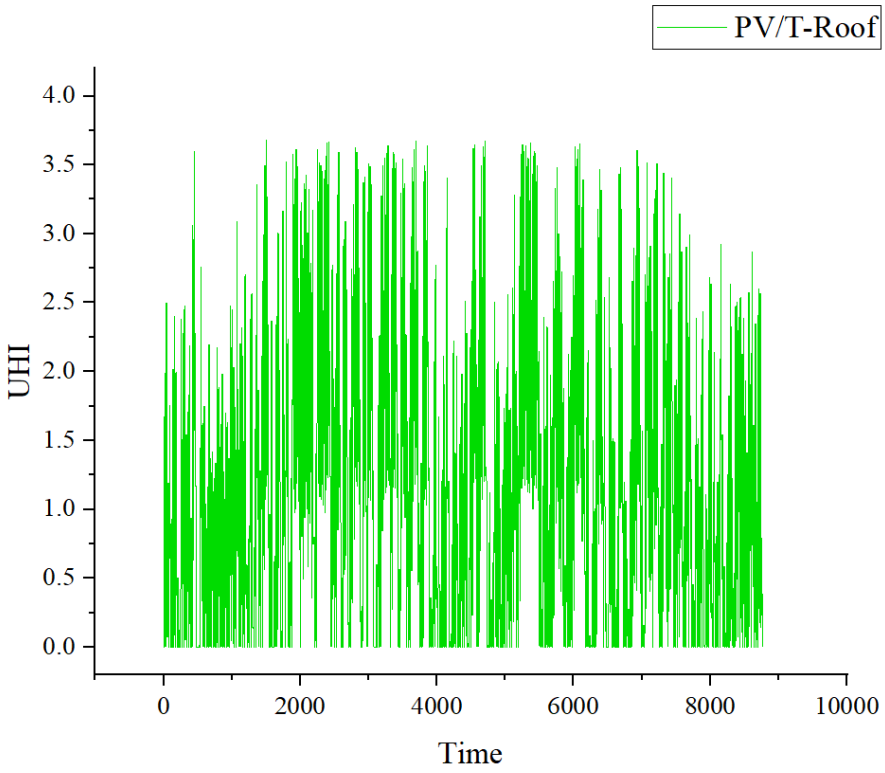

Figure 5-4 UHII decrease in PVT-Roof model

The results of the simulation indicate that the implementation of the PVTG-window model yields a reduction of 0.02℃ in average annual UHII and 0.19℃ in maximum hourly UHII. These findings are visually represented in Fig. 5-5, which depicts the decrease in UHII resulting from the PVG-Window model.

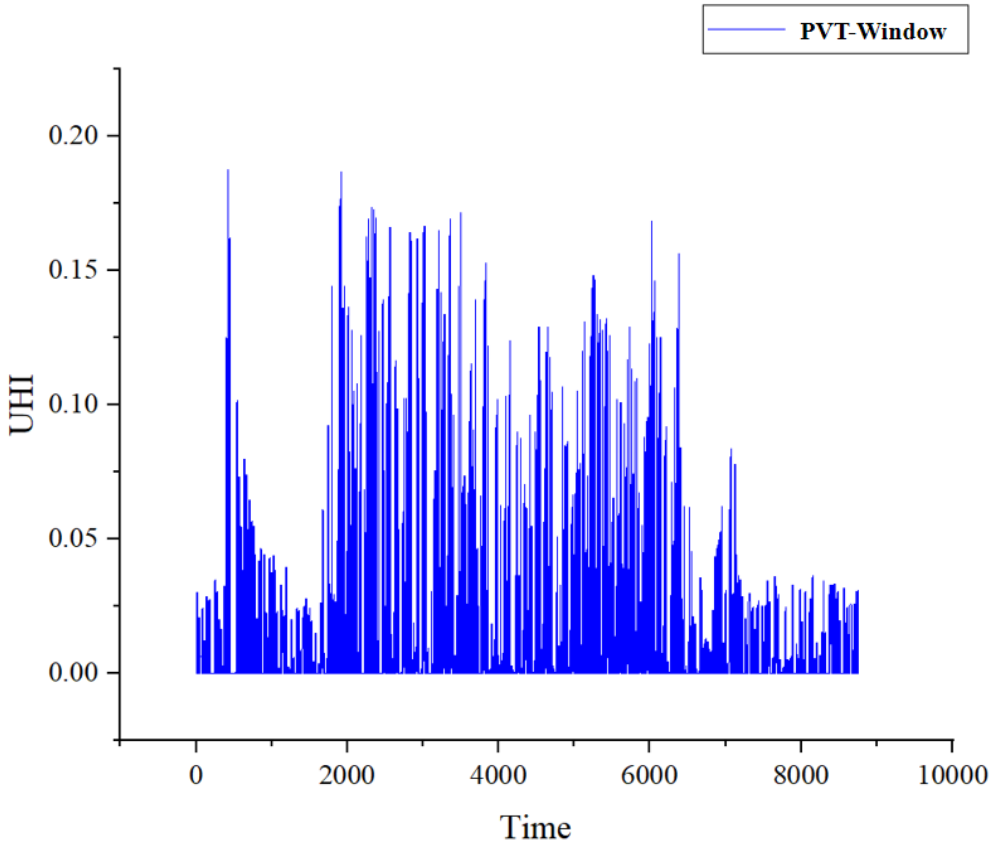

Figure 5-5 UHII decrease in PVG-Window model

The BIPVT-façade model was simulated using the advanced UHIMS-ECHE model. The simulation results demonstrate that the implementation of BIPV-façade technology can reduce the average annual UHII by 0.09℃ and the maximum hourly UHII by 0.76℃. These results are visually presented in Fig. 5-6, which depicts the decrease in UHII resulting from the BIPV-façade model.

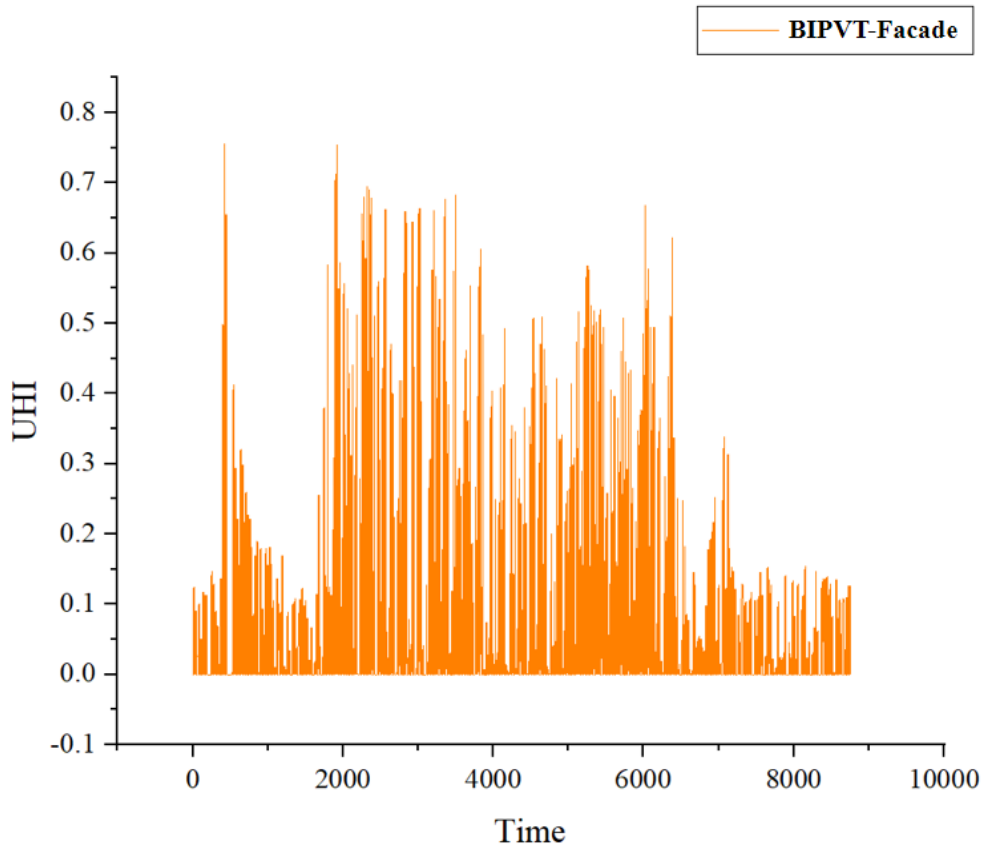

Figure 5-6 UHII decrease in BIPV- Façade model

5.1.2.5 Summary of outdoor air temperature

All selected TES technologies were analysed for the effect of outdoor air temperature to assure the ability of UHII mitigation by simulating with the advanced UHIMS-ECHE model. The simulation results showed that all the TES technologies were capable of effectively reducing the indoor air temperature in the building during hot weather conditions. The efficiency of each technology was found to be dependent on various factors such as the type of material used for thermal storage, the size of the storage unit, and the cooling system design. One of the most promising technologies found was the use of the PCMs-roof model for thermal storage. The simulation results present that PCM A28 (From

6cm to 10cm) has the best performance to reduce the UHII in the PCM roof model, that the average annual UHII reduction is 0.75℃ (PCM-A28, 10cm) and maximum hourly UHII reduction is 7.09℃ (PCM A28-10cm).

This is due to PCMs having a high energy storage capacity and can effectively mitigate the temperature of the outdoor air, providing a comfortable and stable outdoor environment.

It was also observed that the effectiveness of TES technologies increased with the increase in the size of the storage unit. This suggests that larger storage units could potentially provide more stable outdoor air temperatures to citizens.

In conclusion, the use of TES technologies has the potential to mitigate the negative effects of urban heat islands, providing more comfortable and stable outdoor environments. The results of the simulation study highlight the importance of considering various factors such as the type of thermal storage material and the size of the storage unit when designing TES systems for buildings.

5.1.3 Urban building cooling energy use

To evaluate the effectiveness of thermal energy storage (TES) models as UHI mitigation strategies, the advanced UHIMS-ECHE model was employed to analyse their impact on the cooling energy consumption of urban buildings. In this study, the cooling energy use was defined as the total energy required to cool the space in the research buildings. According to Table 3-7, the coefficient of performance (COP) of the HVAC system was determined to be 3. The maximum cooling capacity was 100W/m², the maximum cooling flow was 100m³/s/m², and the setpoint temperature was set at 24°C. The cooling equipment was

programmed to turn off from 1st January to 3rd March and from 1st October to 31st December and to turn on from 1st April to 30th September.

The results of the study indicate that all TES models can improve the energy efficiency of buildings, thereby reducing the amount of heat generated by building operations. By reducing energy consumption, TES systems can help mitigate the UHI effect by decreasing the amount of heat generated by building operations.

5.1.3.1 PCM- Façade model affects building cooling energy use

The PCM-Façade model has been simulated by advanced UHIMS-ECHE. Fig.5-7. show the range of reduction for urban building cooling energy use in the PCM-Façade model. All the monthly maximum cooling energy use happened in August, and the minimum cooling energy use is found in September. In the PCM-Façade model, the A36H-10cm model demonstrated the highest efficacy in reducing annual cooling energy consumption in urban residential buildings, with a reduction of 22.85%. Notably, the A36H-10cm model also exhibited a significant reduction in total cooling energy usage (12.09%).

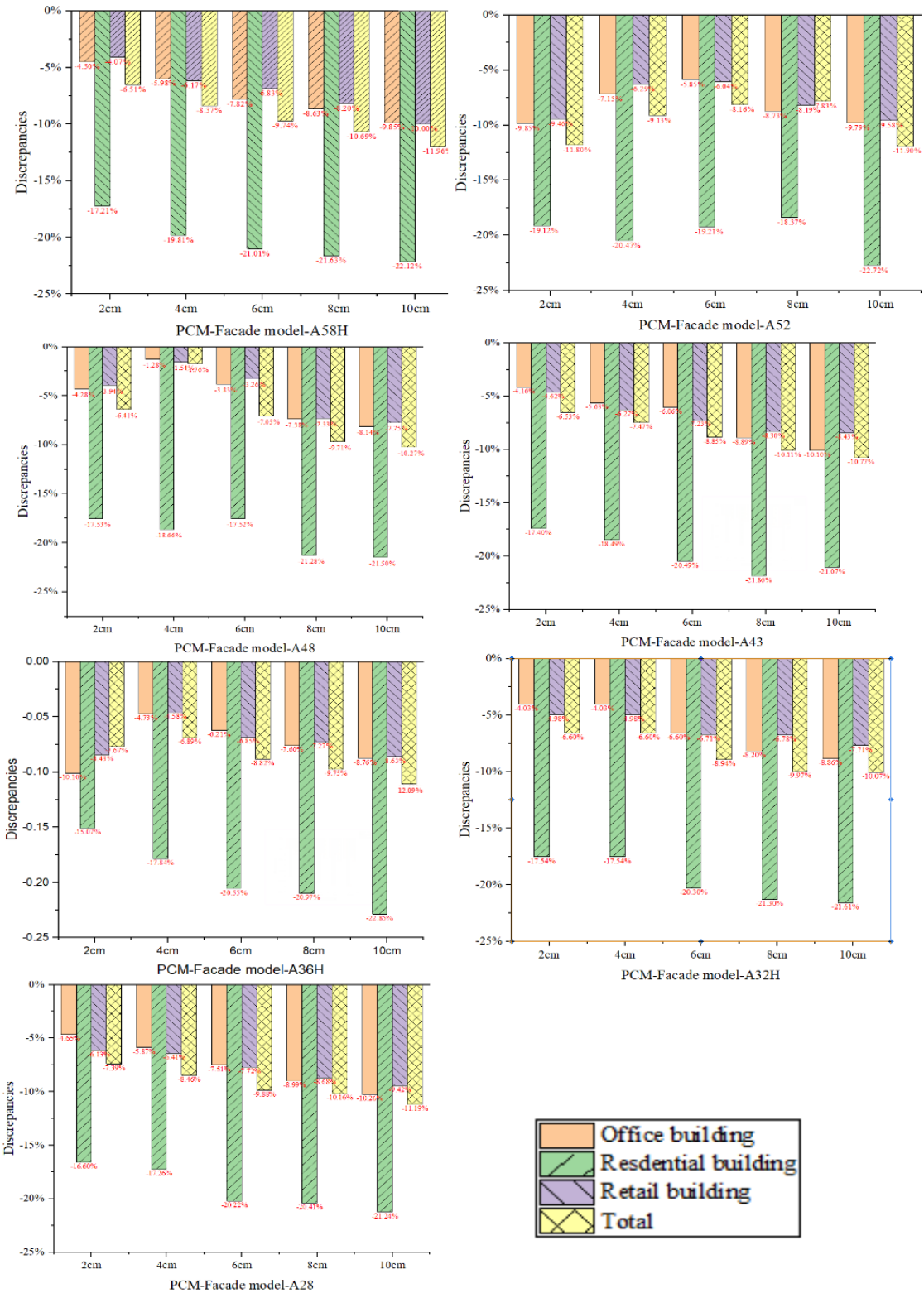

Figure 5-7 Urban building cooling energy use reduction in the PCM-Façade model

5.1.3.2 PCM- Roof model affects building cooling energy use

The PCM-roof model was simulated using the advanced UHIMS-ECHE model, and Fig.5-8 displays the range of reduction in urban building cooling energy use resulting from the PCM-roof model. It was found that the maximum monthly cooling energy use occurred in August, while the minimum cooling energy use was recorded in September. Among the PCM-roof models, the A36H-10cm model demonstrated the most effective performance in reducing annual cooling energy use for urban buildings, with a reduction of 23.68%. Furthermore, the A36H-10cm model exhibited a significant reduction in total cooling energy usage (12.36%).

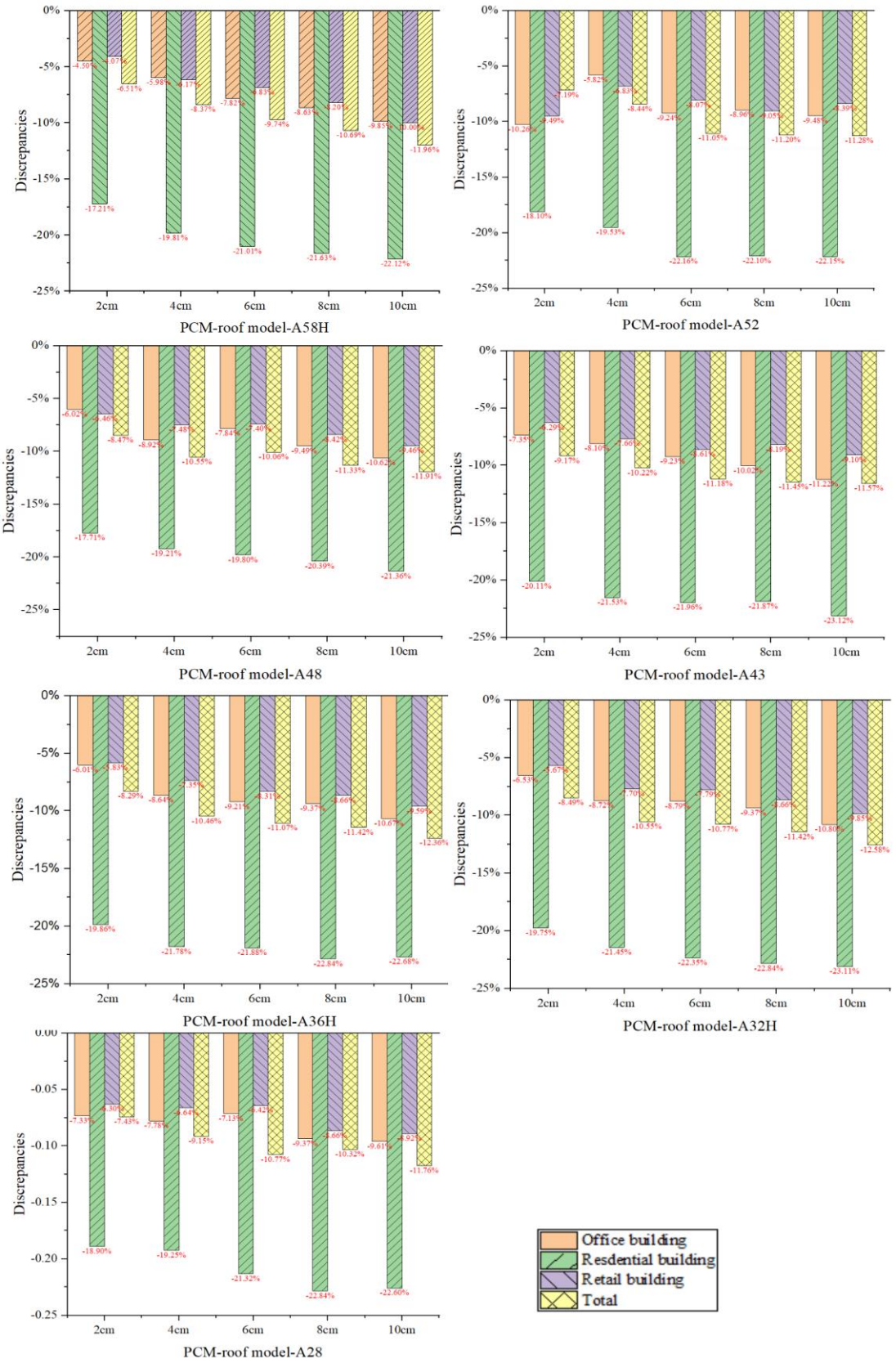

Figure 5-8 Urban building cooling energy use reduction in the PCM-Roof model

5.1.3.3 PCM- Pavement model affects building cooling energy use

The PCM-pavement model was simulated using the advanced UHIMS-ECHE model, and Figure 5-9 presents the range of reduction in urban building cooling energy use resulting from the PCM-pavement model. It was observed that the maximum monthly cooling energy use occurred in August, while the minimum cooling energy use was recorded in September. Among the PCM-pavement models, the A36H-10cm model exhibited the most efficient performance, reducing annual cooling energy consumption for urban buildings by 15.53%. Additionally, the A36H-10cm model exhibited a significant reduction in total cooling energy usage (10.10%).

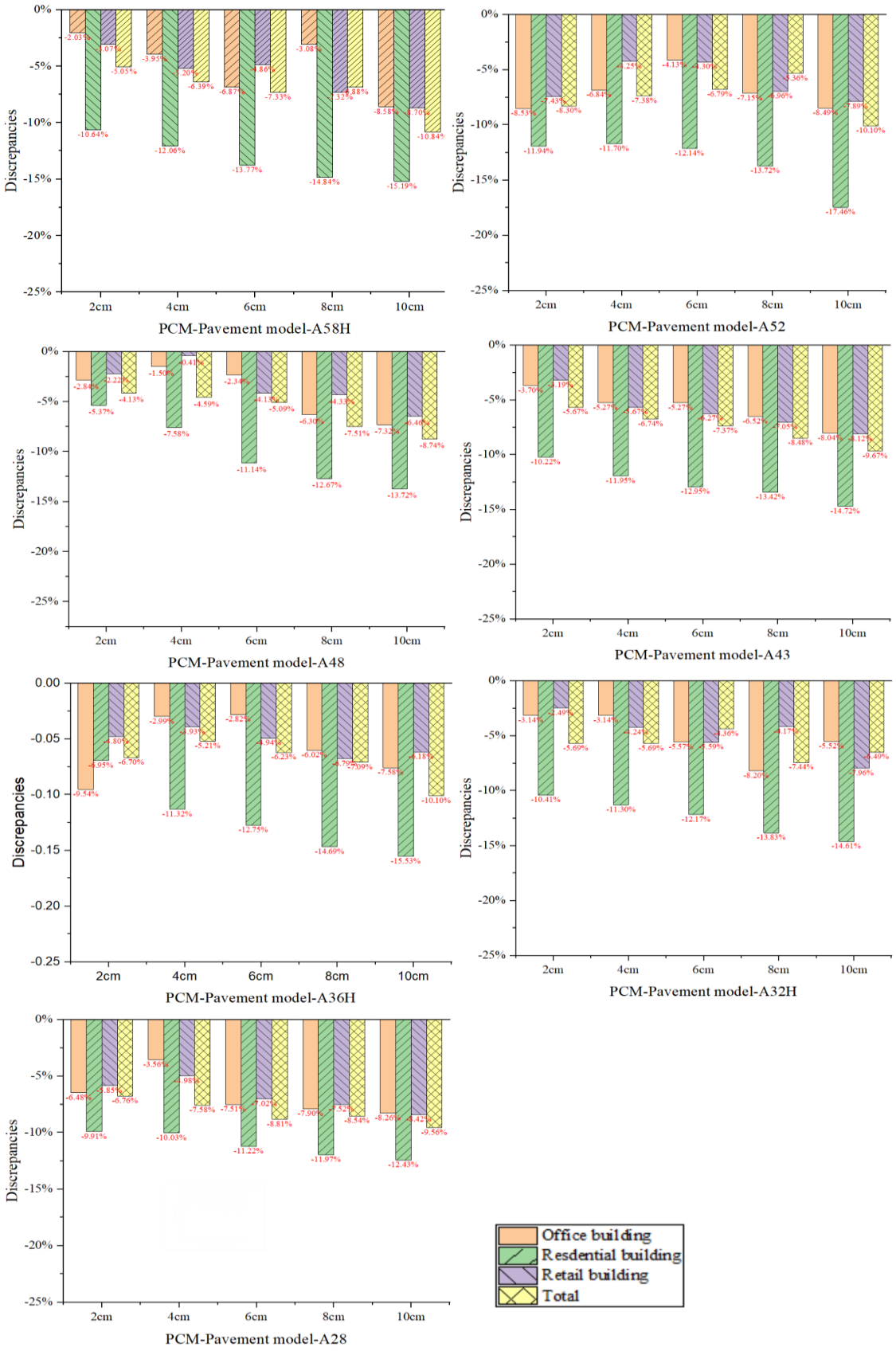

Figure 5-9 Urban building cooling energy use reduction in the PCM-Pavement model

5.1.3.1 Effects of PVT models on building cooling energy use

The PVT-roof model was simulated using the advanced UHIMS-ECHE model, and Figure 5-10 displays the range of reduction for urban building cooling energy use in the PVT-roof model. It was found that the maximum monthly cooling energy use occurred in August, while the minimum cooling energy use was recorded in September. The most efficient performance was observed for the PVT-roof model used in residential buildings, resulting in a reduction percentage of 18.43%. Moreover, the total building cooling was reduced by 13.46%.

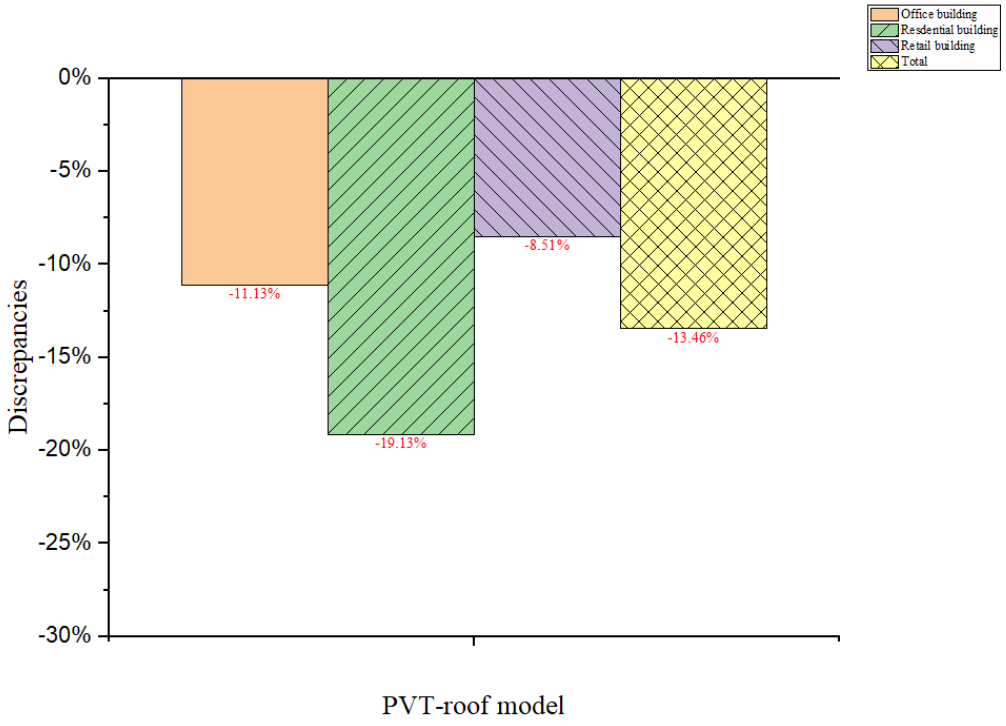

Figure 5-10 The discrepancies of urban building cooling energy use in the PVT-Roof model

The PVTG-Window model was simulated using the advanced UHIMS-ECHE model. The simulation results are presented in Figure 5-11, which illustrates the range of reduction in urban building cooling energy use for the PVG-Window

model. It is worth noting that the monthly maximum cooling energy use occurred in August, while the minimum cooling energy use was recorded in September. The PVG-Window model was found to be most efficient in reducing cooling energy use in residential buildings, with a reduction percentage of 14.82%. Moreover, the total cooling energy use of the building decreased by 4.97%.

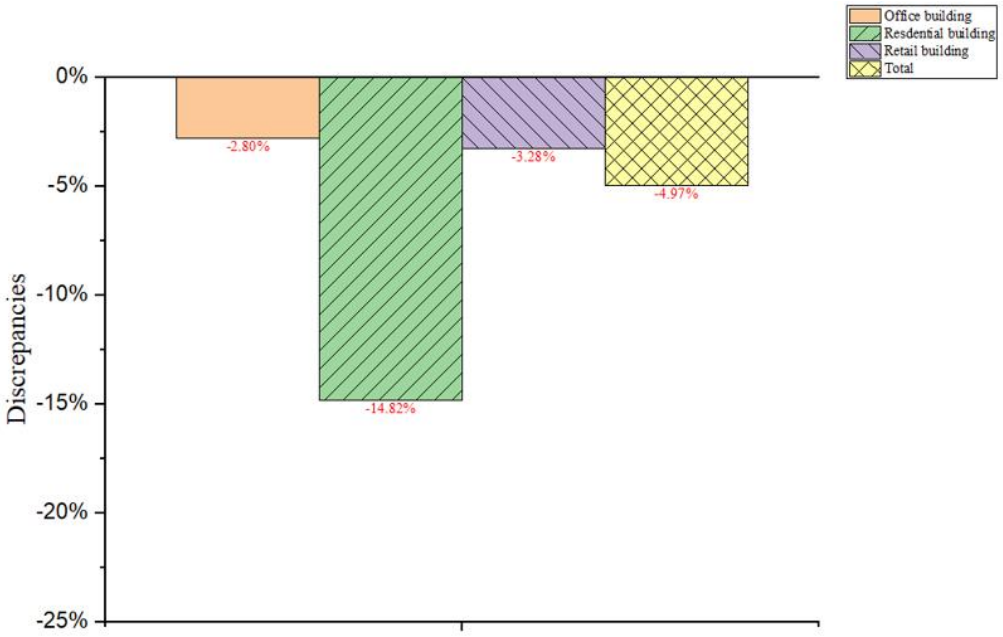

Figure 5-11 The discrepancies of Urban building cooling energy use in the PVTG-Window model

The BIPVT-Façade model has been simulated advanced UHIMS-ECHE. Fig.5-12. show the range of reduction for urban building cooling energy use in the BIPV-Façade model. All the monthly maximum cooling energy use happened in August, and the minimum cooling energy use is found in September. The PVG-Window model was found to be most efficient in reducing cooling energy use in residential buildings, with a reduction percentage of 8.07%. Moreover, the total cooling energy use of the building decreased by 5.79%.

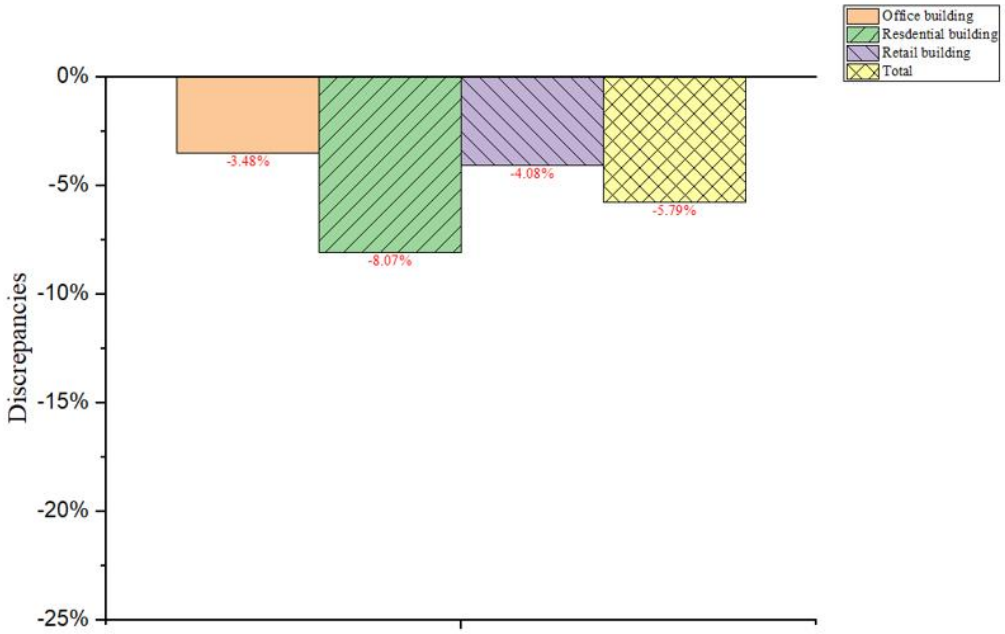

Figure 5-12 The discrepancies of urban building cooling energy use in the BIPVT-Facade model

5.1.3.2 Summary of thermal energy storage in building cooling energy use

This finding has important implications for sustainable building design and energy management, particularly in urban areas where cooling energy consumption is a significant contributor to overall energy usage. The PCM-Roof model, which incorporates phase change materials (PCMs) into building facades, has emerged as a promising approach for reducing energy consumption and improving building performance. The A36H-10cm model has superior performance and it may be a particularly effective design option for residential buildings or total buildings in urban areas.

Furthermore, the use of PCMs in building design has the potential to reduce reliance on traditional cooling systems, which often rely on energy-intensive technologies such as air conditioning units. This shift towards more sustainable building design approaches has become increasingly important as the world

grapples with the challenges of energy saving. The ability of the PCM-Roof model to reduce cooling energy consumption represents a significant step towards achieving these sustainability goals.

5.1.4 Carbon emission

The effectiveness of TES models as UHI mitigation strategies has been analysed using the advanced UHIMS-ECHE model to evaluate their impact on carbon emissions during building cooling applications. The carbon emission levels of each TES model have been compared with an urban base model with UHI effects and no mitigation strategies, as well as a rural area without UHI effects. The results indicate that all TES models can significantly reduce carbon emissions by curbing the amount of cooling energy required. Achieving carbon neutrality is projected to occur in 2057 in each TES mitigation scenario.

5.1.4.1 PCM- Façade model affects carbon emissions

To simulate the performance of PCM-Façade models, the advanced UHIMS-ECHE model has been carried out. Fig.5-13 presents the range of carbon emissions resulting from the cooling energy use of urban buildings. It is observed that PCM integrated with façade structure has the potential to significantly reduce carbon emissions, depending on the specific PCM-Façade model implemented.

Among the various PCM-Façade models that were simulated, the A36H-10cm model demonstrated the highest efficacy in reducing operational carbon emissions. By 2057, this model is projected to result in carbon neutrality of 87.01Kton, highlighting the promising potential of PCM integration for sustainable building design.

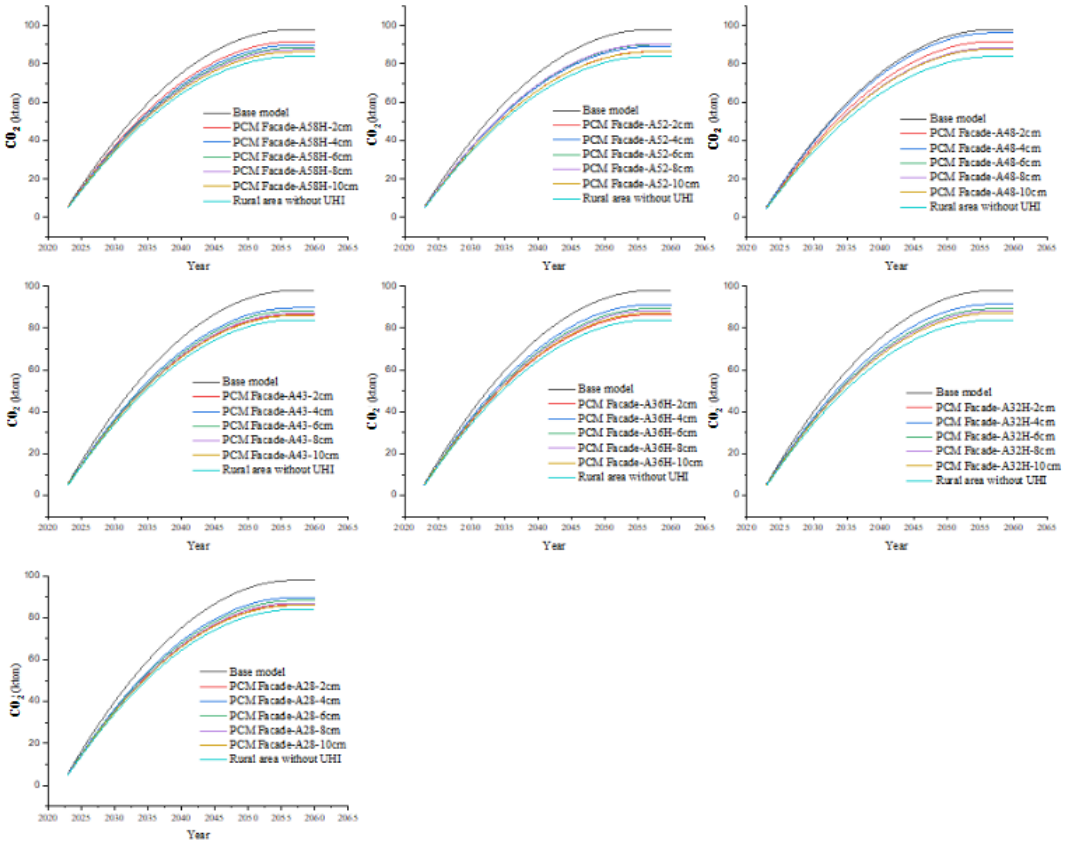

Figure 5-13 The range of carbon emissions reduction resulting from the cooling energy use of urban buildings in the PCM-Façade model

5.1.4.2 PCM- Roof model affects carbon emissions

To simulate the performance of PCM-Roof models, advanced UHIMS-ECHE model have been carried out. Figure 5-14 depicts the range of carbon emissions arising from the cooling energy consumption of urban buildings. The findings indicate that integrating PCM into roof structures has the potential to considerably decrease carbon emissions, contingent on the specific PCM-Roof model utilized.

Of the various PCM-Roof models examined, the A36H-10cm model demonstrated the highest effectiveness in mitigating operational carbon emissions. By 2057, this model is predicted to achieve carbon neutrality of

85.77Kton, underscoring the promising potential of PCM integration for sustainable building design.

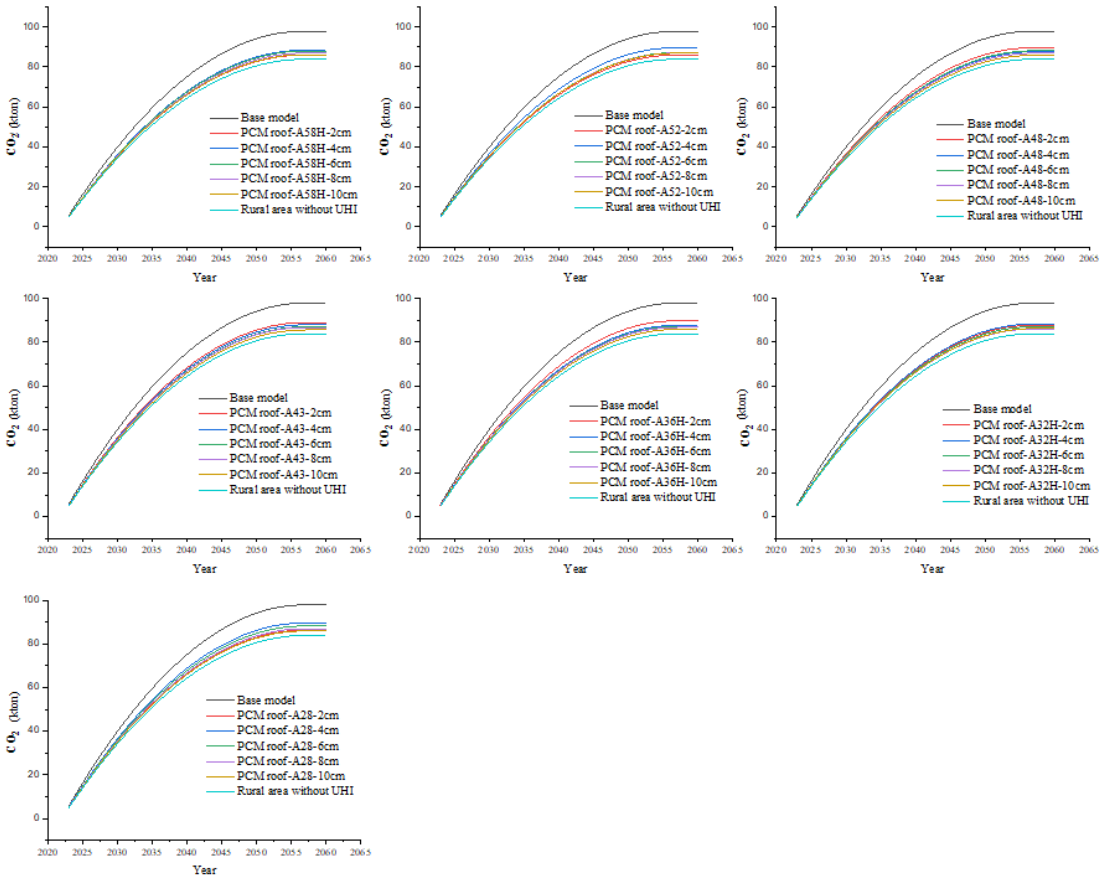

Figure 5-14 The range of carbon emissions reduction resulting from the cooling energy use of urban buildings in the PCM-Roof model

5.1.4.3 PCM- Pavement model affects carbon emissions

To simulate the performance of PCM-Pavement models, advanced UHIMS-ECHE model have been carried out. Figure 5-15 illustrates the range of carbon emissions arising from the cooling energy consumption of urban buildings. The results indicate that incorporating PCM into pavement structures has the potential to considerably decrease carbon emissions, contingent on the specific PCM-Pavement model utilized.

Of the various PCM-Pavement models investigated, the A36H-10cm model exhibited the highest effectiveness in mitigating operational carbon emissions. By 2057, this model is anticipated to achieve carbon neutrality of 89.21Kton.

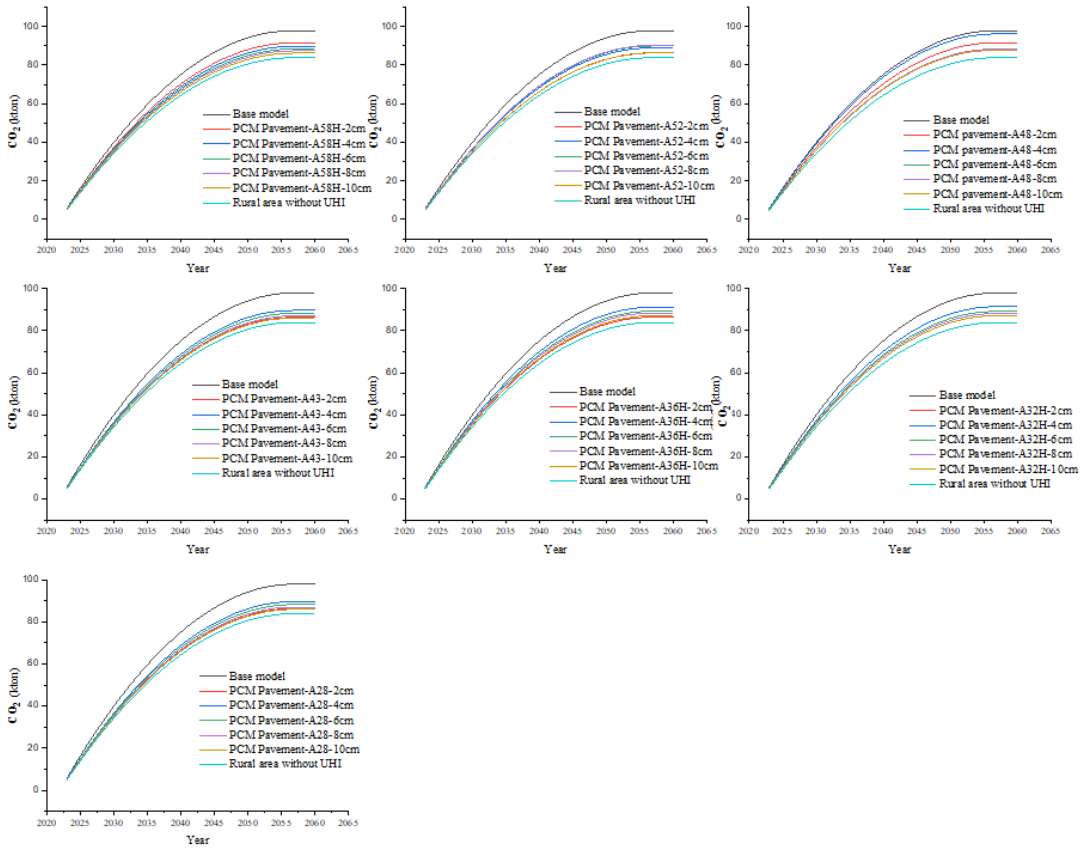

Figure 5-15 The range of carbon emissions reduction resulting from the cooling energy use of urban buildings in the PCM-Pavement model

5.1.4.4 Effects of PVT models on carbon emissions

To simulate the performance of the PV-Roof model, the advanced UHIMS-ECHE model has been used. Fig. 5-16 presents the range of carbon emissions resulting from the cooling energy use of urban buildings. It is observed that a PVT system integrated with a roof structure has the potential to significantly reduce carbon emissions. By 2057, this model is projected to result in a carbon neutrality of 88.06Kton.

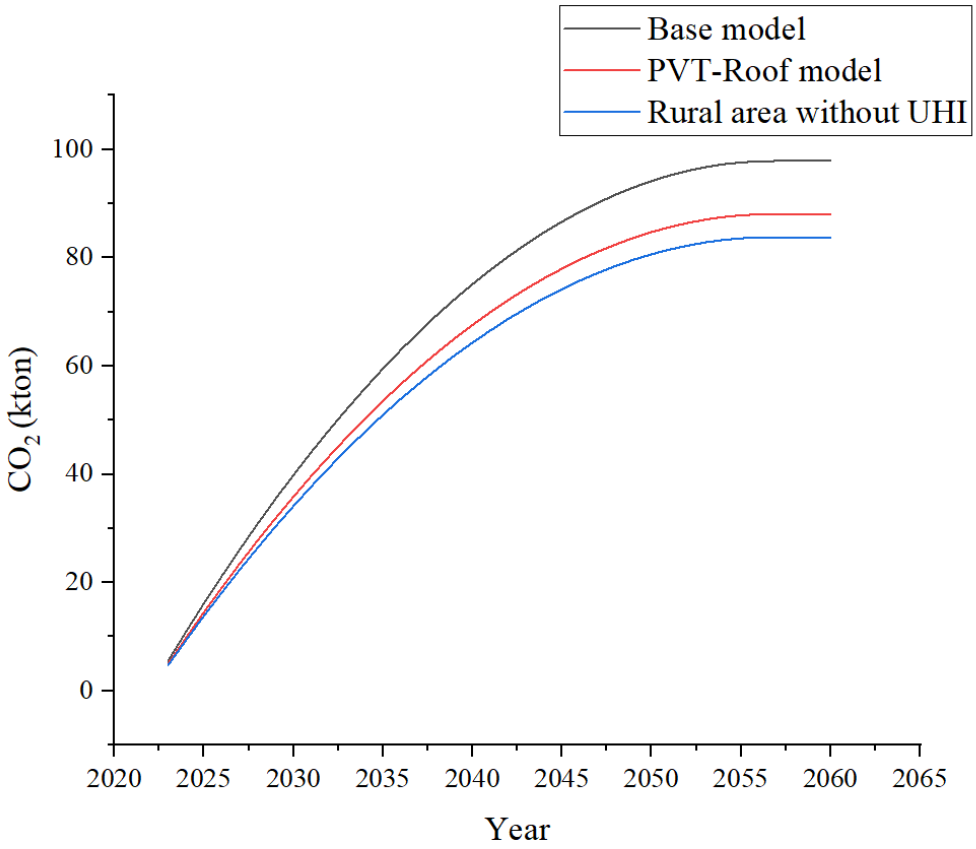

Figure 5-16 The range of carbon emissions reduction resulting from the cooling energy use of urban buildings in the PVT-Roof model

To simulate the performance of the PVTG-Window model, the advanced UHIMS-ECHE model has been used. Fig.5-17 presents the range of carbon emissions resulting from the cooling energy use of urban buildings. It is observed that PVT glazing integrated with window structure has the potential to significantly reduce carbon emissions. By 2057, this model is projected to result in carbon neutrality of 93.00ton,

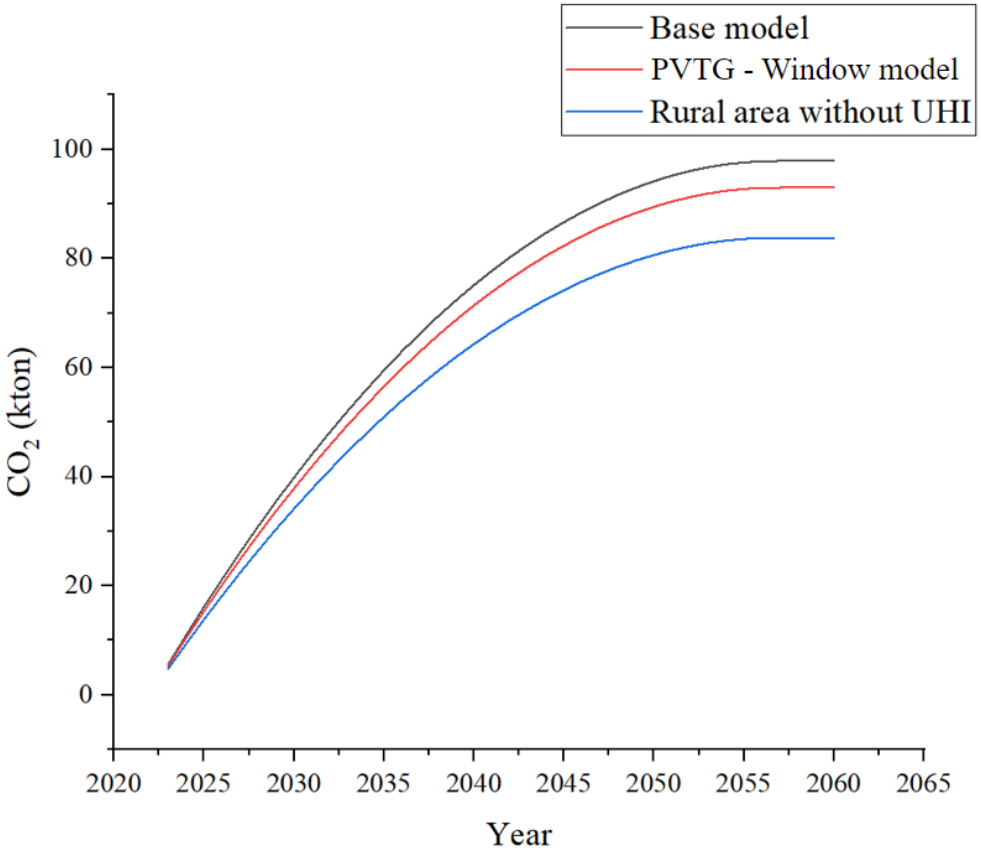

Figure 5-17 The range of carbon emissions reduction resulting from the cooling energy use of urban buildings in PVTG- Window model

The advanced UHIMS-ECHE model has been used to simulate the performance of the BIPVT-Facade model. Fig. 5-18 illustrates the range of carbon emissions arising from the cooling energy consumption of urban buildings. The findings indicate that integrating BIPV systems into facade structures has the potential to significantly decrease carbon emissions. By 2057, this model is predicted to achieve carbon neutrality of 92.20ton.

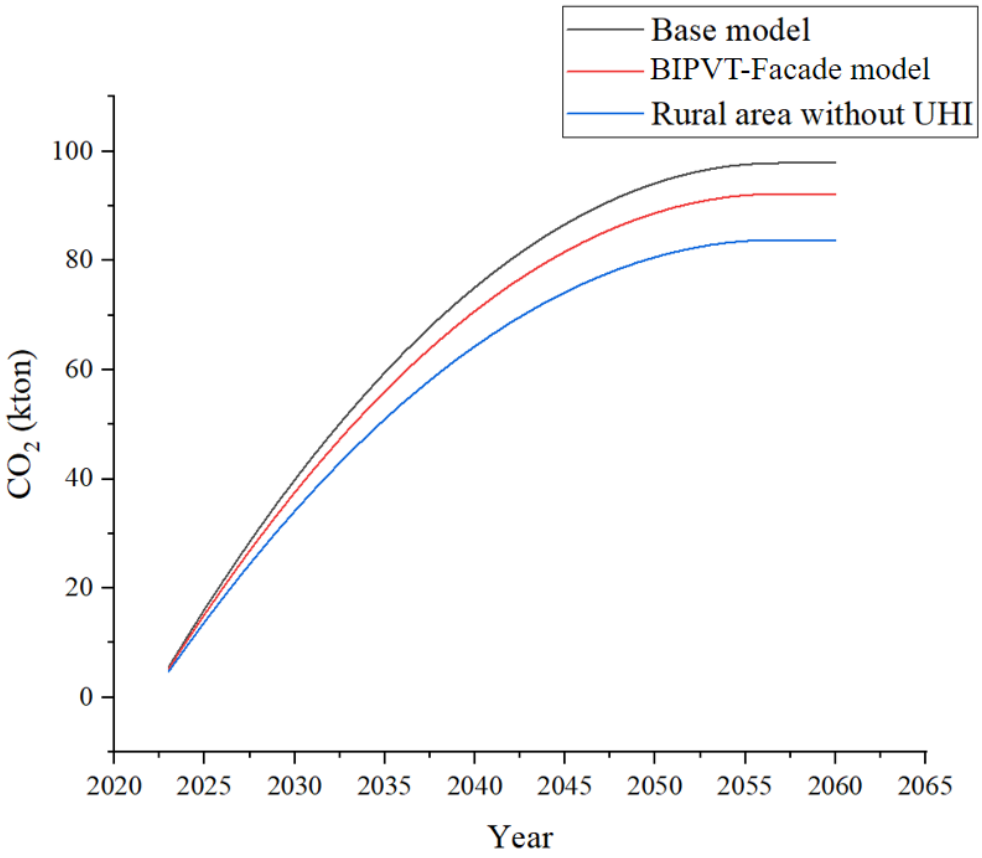

Figure 5-18 The range of carbon emissions reduction resulting from the cooling energy use of urban buildings in the BIPVT-Façade model

5.1.4.5 Summary of thermal energy storage in carbon emissions

The application of TES models has great promise for mitigating carbon emissions and then reducing dependence on fossil fuel-based power generation. Specifically, the implementation of a PCM-Roof model, designated as A36H-10cm, has been shown to offer significant benefits in terms of reducing carbon emissions. This model has the potential to reduce carbon emissions to as low as 85.77Kton by the year 2057, thereby achieving carbon neutrality.

The use of TES models represents a promising approach for addressing the critical challenge of reducing carbon emissions associated with space cooling. These models leverage the ability to store and release energy, which enables

them to reduce the demand for energy during peak periods when electricity is typically generated through the burning of fossil fuels. By using PCM roof models, in particular, it is possible to harness the thermal properties of the roof itself to reduce the overall energy demand, thereby reducing carbon emissions.

The implementation of the PCM roof model A36H-10cm has been shown to be particularly effective in this regard. This model has been found to be capable of reducing carbon emissions by a considerable amount and is therefore a promising option for achieving carbon neutrality. By harnessing the thermal properties of the roof in this way, it is possible to achieve significant reductions in carbon emissions over the long term, thereby contributing to the global effort to combat climate change.

5.1.5 Human thermal comfort

By adopting the advanced UHIMS-ECHE model, TES models have been analysed to determine the effects on human thermal comfort. The results present that TES technologies as UHI mitigation strategies can reduce indoor and outdoor air temperature, thus affecting human thermal comfort by regulating temperature and humidity levels. TES systems can help to maintain a more consistent air temperature, reducing temperature fluctuations that can be uncomfortable for humans. By storing thermal energy during off-peak periods and releasing it during peak periods, TES systems can reduce temperature fluctuations and maintain a more consistent air temperature, which can help to improve human thermal comfort. TES systems can also be designed to control humidity levels, which can help to improve indoor air quality and human health.

5.1.5.1 Indoor thermal comfort

The PMV-ADS for each TES model were calculated and evaluated using Table 4-11. Using this data, the PMV-ADS for each model was calculated and compared to the benchmark scenario (Scenario A). The results are shown in Fig. 5-19.

It is evident from Fig. 45-19 that all TES models led to a reduction in the annual warm hour. This is a significant finding since prolonged exposure to high temperatures can have negative effects on human health, particularly in vulnerable populations such as the elderly and children. Among the various TES models, the PCM-Roof model-A36H-10cm demonstrated the highest reduction in the annual warm hour of 0.90%. This indicates that this model is the most effective in reducing the impact of urban heat islands and improving thermal comfort for residents.

In contrast, the slightly warm values increased in all TES models. This suggests that the PMV value in the warm range has shifted towards the slightly warm category, resulting in a more comfortable urban microclimate for citizens. This is a positive outcome, as it indicates that TES models can help mitigate the effects of urban heat islands and improve thermal comfort for residents.

Overall, the findings suggest that TES models have the potential to significantly improve indoor thermal comfort. The PCM-Roof model-A36H-10cm demonstrated the highest reduction in the annual warm hour and achieved the

most significant reduction in carbon emissions. Therefore, this model is a promising approach to sustainable building design in urban areas.

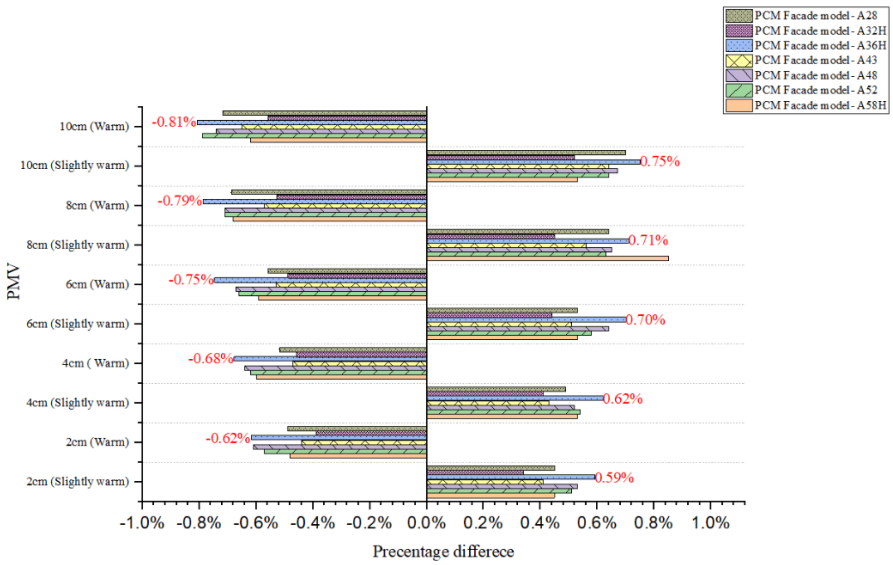

(a) PCM Façade models

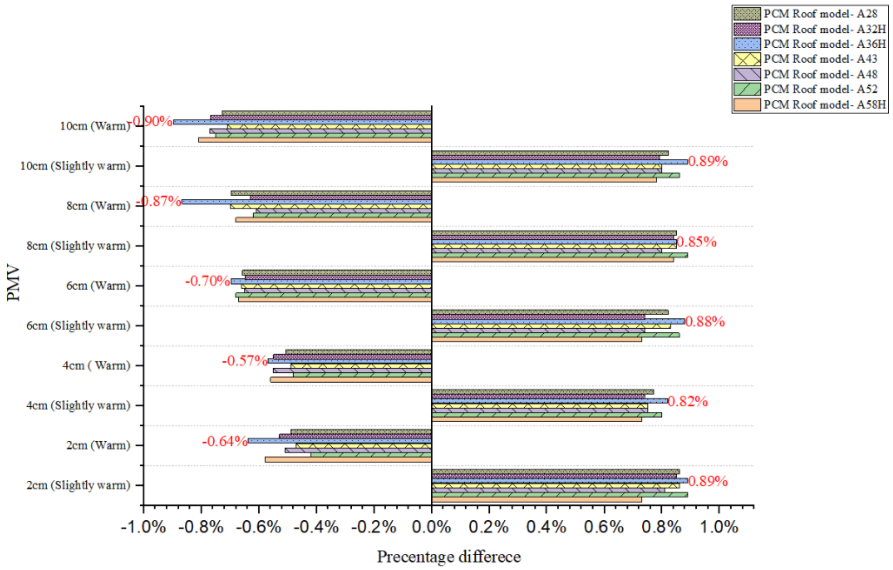

(b) PCM Roof mdoels

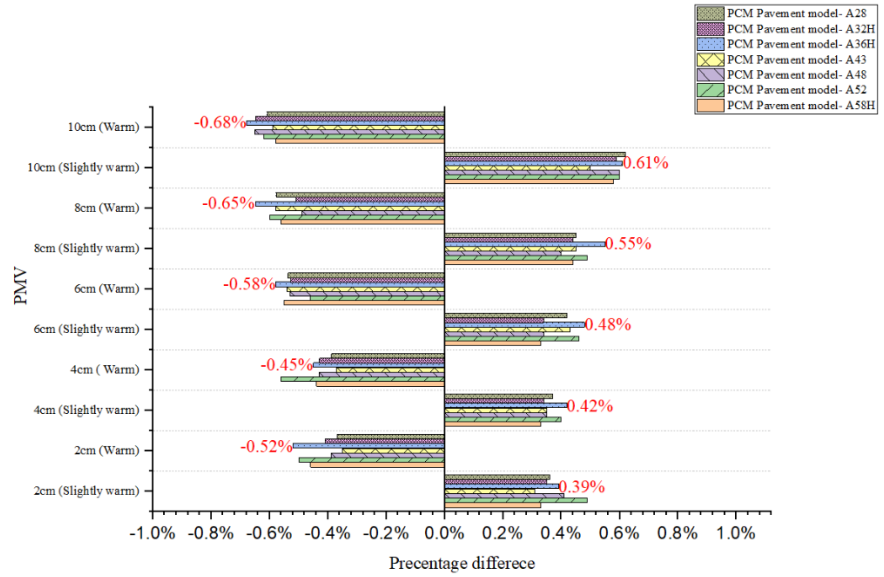

(c) PCM Pavement models

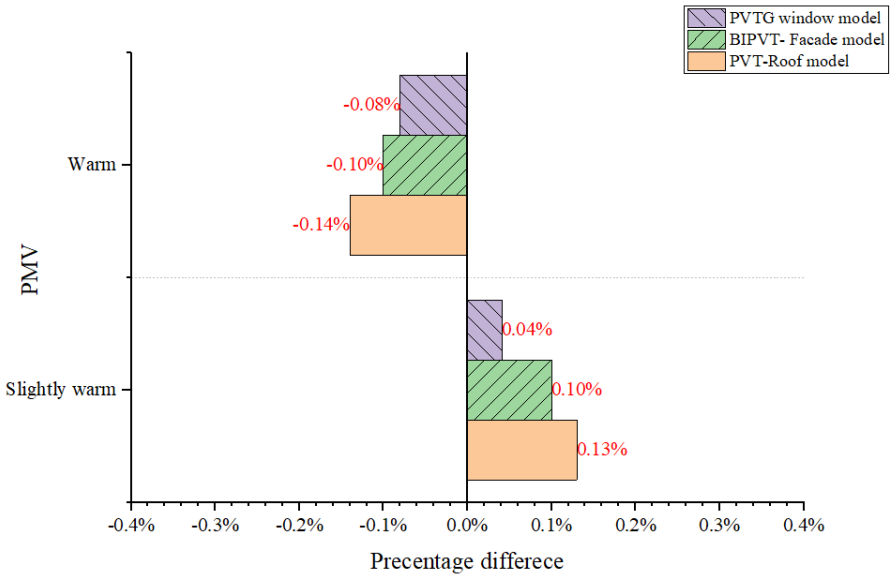

(d) PVT models

Figure 5-19 PMV-ADH change in the TES mitigation scenarios

5.1.5.2 Outdoor thermal comfort

By applying the data in Table 4-12, the SET values for each TES mitigation scenario have been calculated and evaluated. The changes in SET values for the TES models, as compared to the benchmark (Scenario A).

Notably, all TES models resulted in a decrease in the annual outdoor warm level. Figs. 5-20 to 5-23 illustrate the changes in SET levels for the TES models when compared to the benchmark (Scenario A). The number of hot hours was reduced, while the annual slightly warm hour increased for each TES model. This suggests that the SET value for the hot range was shifted towards the warm range, and the higher outdoor air temperature hour became shorter. The findings suggest that the PCM-Roof model-A36H-10cm (with a reduction of 0.20%) may

be the most effective TES model in this context, as it exhibited the most significant enhancement in outdoor thermal comfort.

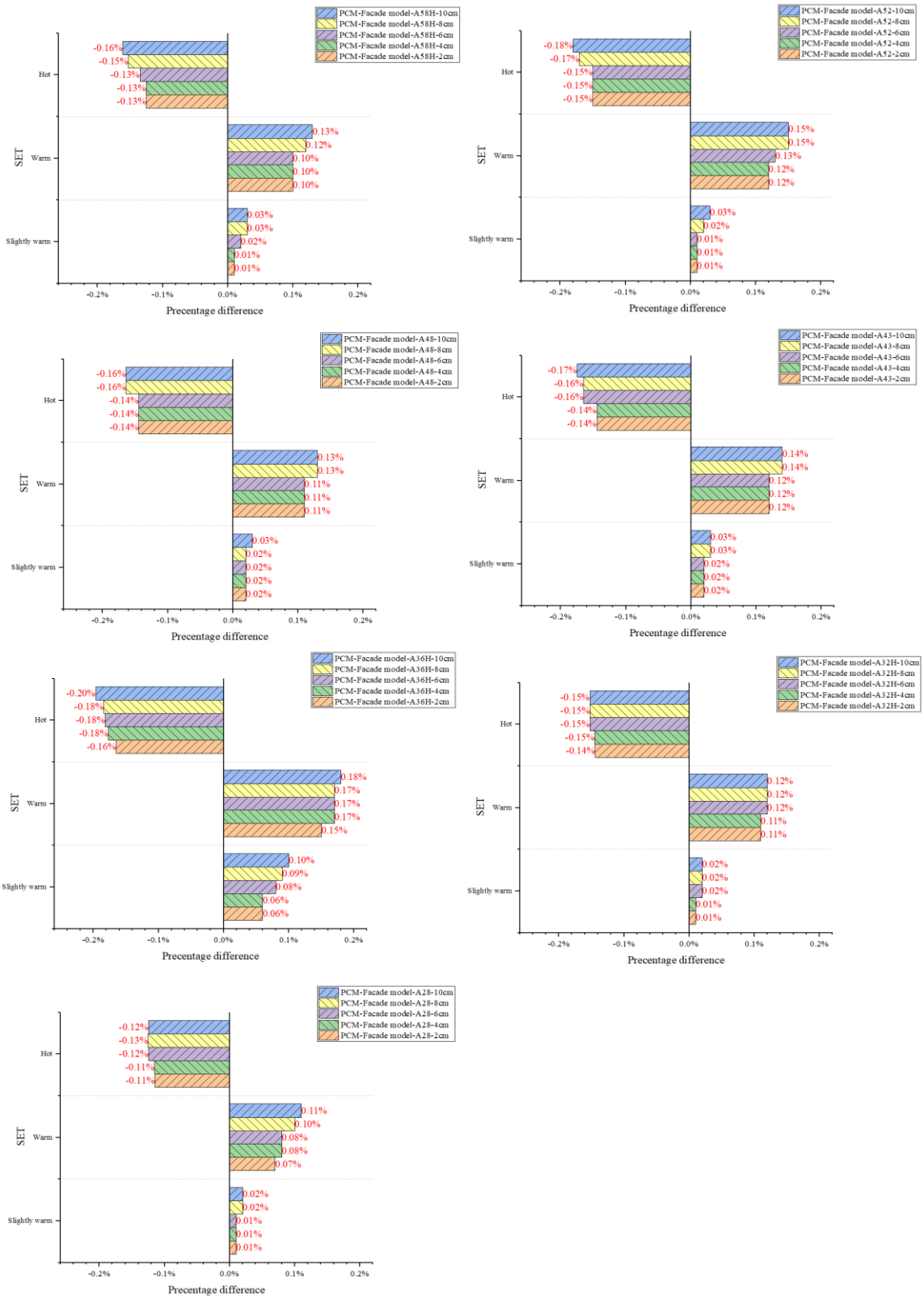

Figure 5-20 SET change in PCM-Facade model

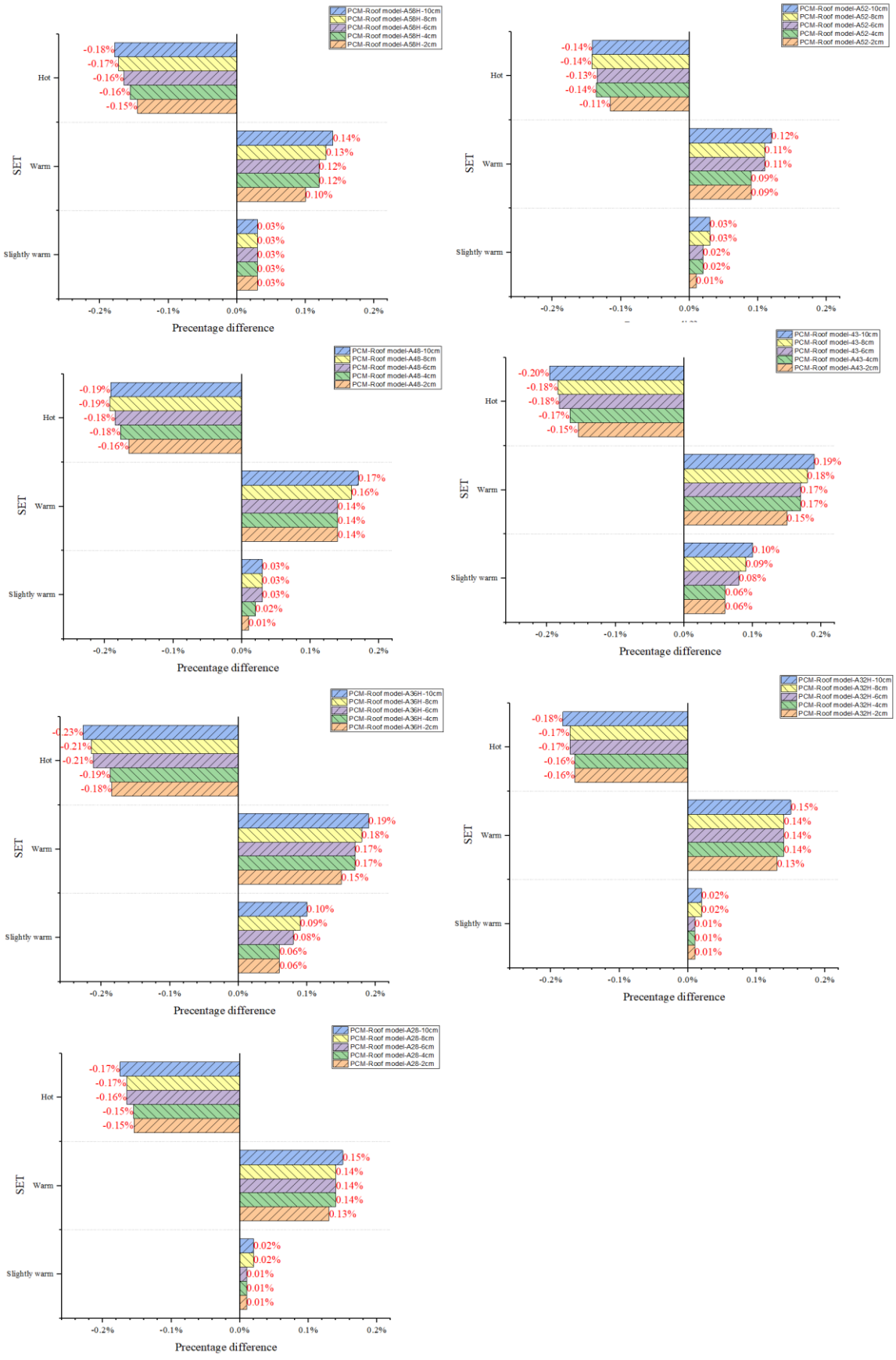

Figure 5-21 SET change in PCM-Roof model

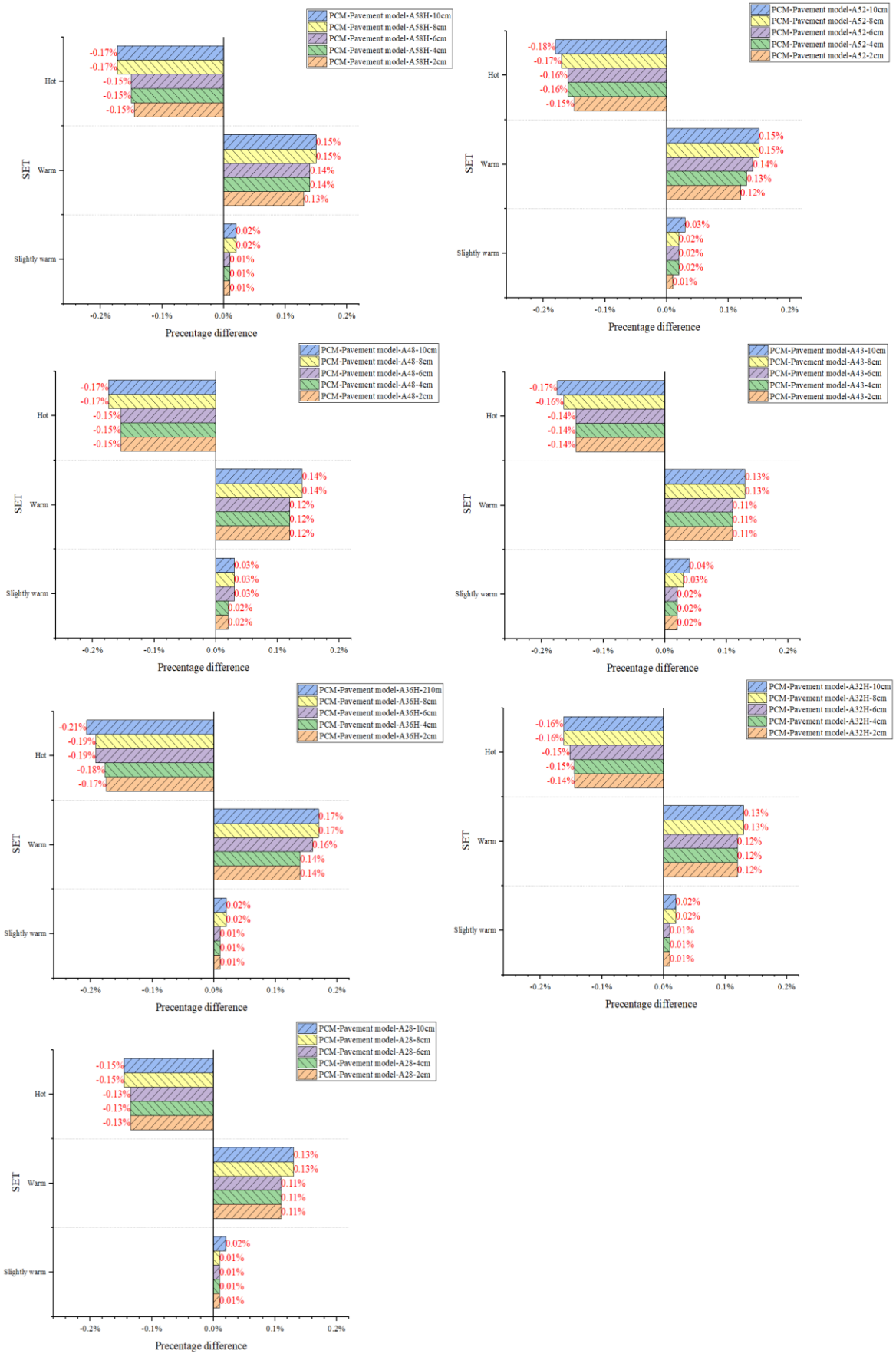

Figure 5-22 SET change in PCM-Pavement model

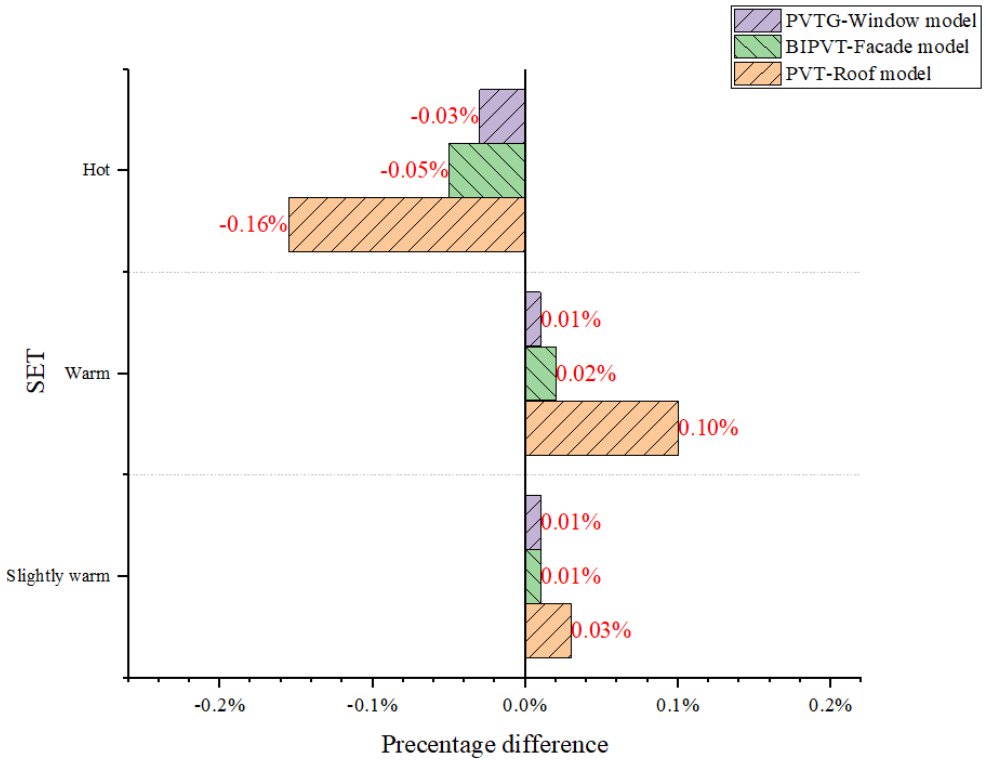

Figure 5-23 SET change in PV models

5.1.5.3 Summary of thermal comfort

This section explores the impact of TES technologies as UHI mitigation strategies on human thermal comfort. Simulation results demonstrate that TES models have the potential to decrease indoor and outdoor air temperatures and enhance human thermal comfort. Various TES models were assessed using PMV-ADS and SET values, revealing that all models resulted in a reduction in the annual warm hour. The PCM-Roof model-A36H-10cm emerged as the most effective in enhancing thermal comfort for occupants, achieving the highest reduction in the annual warm hour and SET value. In summary, TES systems offer a promising approach to alleviate the consequences of UHIs and promote human thermal comfort.

6 CHAPTER VI: CONCLUSIONS, RECOMMENDATIONS AND FUTURE WORKS

6.1 Conclusions

In this research study, an evaluation was conducted on urban heat island mitigation strategies within a subtropical urban region. The aim and objectives of this study were to provide valuable insights that could inform the development of effective UHI mitigation strategies to ensure that the living conditions of subtropical residents are conducive to their well-being. Furthermore, the findings of this study could inform the development of sustainable subtropical cities in the future.

The significance of this research lies in the fact that subtropical regions are often characterised by high temperatures, which can have negative impacts on the health and well-being of residents. The urban heat island effect exacerbates this issue, resulting in higher temperatures within urban areas than in their rural surroundings. Therefore, the development of effective UHI mitigation strategies is crucial for ensuring the comfort and well-being of residents in subtropical cities.

The methodology employed in this study involved a comprehensive assessment of UHI mitigation strategies within a subtropical urban region. Data was collected through various means, including surveys, and on-site measurements. The data collected was then analysed using the software ENVI-met and an innovation model UHIMS-ECHE.

The findings of this study revealed that various UHI mitigation strategies were effective in reducing temperatures, energy use, carbon emission and improving

human thermal comfort in subtropical areas. These included conventional strategies (green roofs, cool roofs, green space, etc.) and novel strategies (TES technologies), among others. The study also identified some challenges and limitations associated with the implementation of these strategies for future work. Overall, the results of this study provide valuable guidance for the development of effective UHI mitigation strategies within subtropical urban areas. The findings also highlight the importance of considering the unique characteristics of subtropical regions when designing such strategies. This study contributes to the growing body of knowledge on UHI mitigation strategies and can inform the development of sustainable subtropical cities for the future.

6.1.1 Meteorological assessment

The different mitigation strategies were analysed by a simulation ENVI-met. In this study, outdoor air temperature , sky view factor, Net Radiation , thermal radiative power and mean radiant temperature as urban heat island mitigation criteria are standards for evaluating the efficiency of UHI mitigation strategies. The simulation results of Scenario A (Base model) are considered as the reference value. The relative percentage differences between UHI mitigation scenarios with Scenario A are determined. According to the simulation results and discussion, Scenario B cool pavement can approximately decrease the outdoor air temperature (10% in summer, 20% in winter); net radiation (40% in summer, 20% in winter; thermal radiative power (50% in summer, 40% in winter) and thermal radiant temperature (10% in summer, 80% in winter).

The findings of this part underscore the efficacy of certain strategies in mitigating the UHI effect. Notably, both augmenting the albedo of urban fabric materials and expanding the ratio of vegetation coverage have demonstrated

their potential in effectively addressing UHI concerns.

Specifically, the augmentation of urban albedo emerges as a robust mitigation strategy. Elevating the albedo of urban fabric materials proves to be a particularly effective measure in curbing UHI. This strategy, encompassing the modification of surface reflectivity, directly influences the absorption and reflection of solar radiation. Consequently, it contributes significantly to ameliorating the heat accumulation within urban environments and subsequently attenuating the UHI effect. Furthermore, the study reveals that an expanded vegetation coverage ratio can also contribute to UHI mitigation. However, an intriguing insight arises from the comparison with Scenario D, the green space model. The results suggest that while this approach introduces positive effects by enhancing greenery, it can concurrently impose challenges related to city ventilation. This paradoxical relationship highlights the intricate balance that needs to be struck between green space expansion and ensuring optimal airflow dynamics within urban areas.

In light of these observations, it becomes evident that indiscriminate escalation of vegetation coverage might not yield the desired outcomes in mitigating UHI in subtropical city centres. The potential drawbacks associated with decreased city ventilation, arising from excessive vegetation, warrant a nuanced approach in the deployment of this strategy.

Conversely, the outcomes firmly advocate for prioritizing the augmentation of urban albedo as a more effective and manageable UHI mitigation strategy. The balance between reflective surfaces and vegetated areas can be manipulated to ensure both efficient heat reflection and adequate ventilation. This approach underscores the importance of comprehensively evaluating not only the specific mitigation techniques but also their interplay with broader urban climatic

dynamics.

6.1.2 Conventional UHI mitigation scenario in energy use, carbon emissions and human thermal comfort

Several studies have attempted to address the challenge of accurately predicting urban building energy consumption, thermal comfort, and carbon emissions through the incorporation of urban heat island mitigation strategies. However, there remains a dearth of research that investigates the relationship between these variables comprehensively. Therefore, this research proposes an innovative model, namely the UHIMS-ECHE, which analyses the interplay between UHI mitigation strategies, urban building energy computation, thermal comfort, and carbon emissions. The notable merits of the model include the ability to calculate UHI intensity, accurately model building energy use by accounting for UHI effects, easily simulate carbon emissions and human comfort, provide direct visualization of simulation results, and save on computational time.

A case study in subtropical was conducted, analysing the performance of urban building energy use, carbon emissions, and thermal comfort regarding UHI mitigation strategies. The accuracy of the UHIMS-ECHE model was verified through cross-validation, affirming the reliability.

The results of the case study show that the Scenario C cool roof model (increase the albedo to 0.8 in roof areas) is the most effective way to reduce annual outdoor air temperature, urban building cooling energy use, and carbon emission and improve human thermal comfort in subtropical area.

The effect of increased pavement albedo (Scenario B) on reducing outdoor temperature is due to the increased reflection of solar radiation during the daytime hours, which results in a reduction in the amount of energy absorbed by

the pavement. However, in the annual variation, increasing roof albedo has a more significant effect on reducing outdoor temperature compared to increasing pavement albedo, as roofs are exposed to solar radiation throughout the year. This effect is especially pronounced during summer months and at night when stored heat is slowly released. Roofs have a higher potential to radiate heat back into the atmosphere than pavements, resulting in a more substantial reduction in energy absorbed by the urban environment and lower air temperatures. Therefore, in the diurnal variation, increasing pavement albedo has a more pronounced effect during the day, while increasing roof albedo has a more significant effect in an annual simulation model due to its cumulative effect on the surface energy balance.

Furthermore, it is possible that increasing both pavement and roof albedo (Scenario BC) may not show the greatest reduction in outdoor temperature, even if all other conditions are kept the same. This is because the relationship between surface albedo and outdoor temperature is not linear, and there may be a point of diminishing returns where further increases in albedo do not result in significant temperature reductions. Another factor to consider is that while increasing albedo can reduce the amount of solar radiation absorbed by the surface, it can also increase the amount of solar radiation reflected back into the atmosphere. This can potentially lead to higher atmospheric temperatures and can offset some of the cooling effects of increased albedo.

6.1.3 Thermal energy storage as urban heat island mitigation strategies

By applying advanced models like the UHIMS-ECHE mode, thermal energy storage models have emerged as a promising solution to reduce the intensity of urban heat islands, the cooling energy use of buildings and carbon emissions. In

particular, TES models have shown great potential to improve human thermal comfort. The simulation results suggest that the PCM-Roof model-A36H-10cm is the most effective model to achieve these goals.

One of the most significant advantages of thermal energy storage models is their ability to store energy when it is abundant and release it when it is needed. This process helps to reduce peak energy demand, which is one of the main contributors to high energy consumption and carbon emissions in urban areas. By reducing peak demand, thermal energy storage models can lower the strain on the power grid and prevent blackouts, which can be critical in extreme weather conditions. Moreover, the use of thermal energy storage models can improve the thermal comfort of building occupants both indoors and outdoors.

The PCM-Roof model is an ideal thermal energy storage model that combines a phase change material (PCM) with a heat exchanger. The PCM absorbs heat during the day and releases it at night, while the heat exchanger improves the efficiency of heat transfer. This model has been shown to be effective in reducing the cooling energy use of buildings and decreasing carbon emissions.

Among the various PCM-Roof models studied, simulation results have demonstrated that the PCM-Roof model-A36H-10cm is the most effective model for reducing urban building cooling energy use, and carbon emissions and improve human thermal comfort. This model uses a PCM layer with a thickness of 10cm and is installed on the roof of the building. The PCM layer absorbs heat during the day and releases it at night, reducing the need for air conditioning and decreasing energy consumption. Additionally, the PCM layer helps to regulate the temperature inside the building, improving thermal comfort for occupants.

In conclusion, thermal energy storage models have significant potential to reduce

the energy consumption of buildings and decrease carbon emissions. By adopting advanced TES models like the PCM-Roof model-A36H-10cm, urban building cooling energy usage can be reduced while improving human thermal comfort. The adoption of thermal energy storage models can help mitigate the effects of climate change and contribute to a sustainable future. It is worth to notice that adding 10cm thick layer of PCM is not practical in the real situation. There are some way to can achieve this aim in practical. This includes exploring new lighter phase-change materials and heat transfer fluids to optimise the energy storage and release process and developing new designs for the PCM panel systems to achieve the 10cm thick layer can be installed in building application.

6.2 Limitation, recommendations and future work

The excessive heat generated by the UHI effect can lead to numerous negative consequences such as increased energy consumption, decreased air quality, and adverse health effects. To mitigate the UHI effect in urban areas, various strategies have been proposed, including the use of conventional mitigation strategies and thermal energy storage (TES) systems. To evaluate the effectiveness of TES systems in mitigating the UHI effect, an analysis was conducted using the advanced Urban Heat Island Mitigation Energy use, Carbon emissions, and Human thermal comfort and economic (UHIMS-ECHE) model.

6.2.1 UHIMS-ECHE model

To further upgrade the research on the UHIMS-ECHE model, it is important to address several limitations that were identified in the study. The four limitations that should be addressed in further research are discussed below:

Firstly, the UHIMS-ECHE model primarily focuses on urban building energy consumption, but it does not take into account the influence of urban transportation and infrastructure energy use. Therefore, future work should aim to consider these factors to develop a more comprehensive understanding of urban energy consumption.

Secondly, the study presented limited and simplified UHI (Urban Heat Island) mitigation strategies. To achieve more precise predictions, it is recommended that an in-depth variation investigation of UHI mitigation strategies is conducted. This will enable researchers to understand the varying effects of different mitigation strategies on urban energy consumption and temperature.

Thirdly, the calculation of urban building carbon emissions and economic analysis is currently conducted using equations. In the next step, the researcher should consider adding an automatic calculation to the model. This will improve the accuracy and efficiency of the calculations, as well as reduce the potential for errors that may occur when using manual calculations.

Finally, it is important to note that the UHIMS-ECHE model was developed and tested in a specific geographical region. Future research should consider testing the model in different regions to evaluate its applicability and effectiveness in diverse urban environments.

In conclusion, addressing these limitations will enhance the accuracy and scope of the UHIMS-ECHE model, and further advance our understanding of urban energy consumption and UHI mitigation strategies.

6.2.2 Modelling limitation

In the scope of this thesis, which conducted PCM modelling for UHI mitigation, it is important to recognise and address certain inherent limitations and

simplifications. The PCM acts as a daytime heat absorber and prevents rapid outdoor temperature increases by melting during the day. However, at night, it releases absorbed heat, necessitating active systems to transfer heat during PCM solidification. The research focuses only on daytime effects and simplifies calculations by neglecting thermal resistance between the PCM and its surroundings, which may not fully represent real-world scenarios. In the future work, the day and night cycle should be considered in research modelling.

Besides, the one-dimensional heat transfer assumptions have been employed for computational efficiency, yet this may not fully capture multidimensional heat transfer in real-world PCM systems. Constant material property assumptions simplify calculations but may not account for dynamic property changes with temperature and phase transitions. The isothermal assumption during PCM phase change simplifies modelling but overlooks temperature gradients within the PCM. Neglecting natural convection can lead to discrepancies in temperature profiles, especially with substantial temperature differences or larger PCM volumes. Idealised geometries for PCM containers may not represent real-world scenarios accurately, and ignoring thermal resistance between PCM and containers can affect heat transfer rates. Addressing these limitations will enhance the accuracy and practicality of PCM models.

6.2.3 Materials and design optimisation

Developing new materials and designing TES systems with optimal configurations can improve their efficiency and effectiveness. This includes exploring new phase-change materials and heat transfer fluids to optimise the energy storage and release process and developing new designs for the TES systems to maximise heat transfer efficiency and storage capacity. Besides, TES systems can be expensive to internal,

install and maintain cost. High costs can also limit the adoption of TES systems, which can slow down the development of the technology. Future research can focus on developing cost-benefit analysis models for TES systems.

7 REFERENCES

[1] Howard L. The climate of London. London Harvey Dorton. 2022;2:1818-20.
[2] Oke T. The energetic basis of urban heat island. Quarterly Journal of the Royal Meteorological Society. 1982;108:1-24.
[3] organization Wm. urban heat island. 2020.
[4] IPCC. Climate Change 2022: Mitigation of Climate Change. 2022.
[5] Sharlach M. Solutions to urban heat differ between tropical and drier climes. 2019.
[6] O'Malley C, Piroozfar P, Farr ERP, Pomponi F. Urban Heat Island (UHI) mitigating strategies: A case-based comparative analysis. Sustainable Cities and Society. 2015;19:222-35.
[7] Wang Y, Berardi U, Akbari H. Comparing the effects of urban heat island mitigation strategies for Toronto, Canada. Energy and Buildings. 2016;114:2-19.
[8] Benrazavi RS, Dola KB, Ujang N, Benrazavi NS. Effect of pavement materials on surface temperatures in tropical environment. Sustainable Cities and Society. 2016;22:94-103.
[9] Chen X-L, Zhao H-M, Li P-X, Yin Z-Y. Remote sensing image-based analysis of the relationship between urban heat island and land use/cover changes. Remote sensing of environment. 2006;104(2):133-46.
[10] Li H, Meier F, Lee X, Chakraborty T, Liu J, Schaap M, et al. Interaction between urban heat island and urban pollution island during summer in Berlin. Science of The Total Environment. 2018;636:818-28.
[11] Oke TR. The distinction between canopy and boundary-layer urban heat islands. Atmosphere. 1976;14(4):268-77.
[12] Ramakreshnan L, Aghamohammadi N, Fong CS, Ghaffarianhoseini A, Ghaffarianhoseini A, Wong LP, et al. A critical review of urban heat island phenomenon in the context of greater Kuala Lumpur, Malaysia. Sustainable Cities and Society. 2018;39:99-113.
[13] Oke TR. The energetic basis of the urban heat island. Quarterly Journal of the Royal Meteorological Society. 1982;108(455):1-24.
[14] Emmanuel R, Krüger E. Urban heat island and its impact on climate change resilience in a shrinking city: The case of Glasgow, UK. Building and Environment. 2012;53:137-49.
[15] Oke TR. Boundary layer climates: Routledge, 2002.
[16] Mohajerani A, Bakaric J, Jeffrey-Bailey T. The urban heat island effect, its causes, and mitigation, with reference to the thermal properties of asphalt concrete. Journal of Environmental Management. 2017;197:522-38.
[17] Fernández FJ, Alvarez-Vázquez LJ, García-Chan N, Martínez A, Vázquez-Méndez ME. Optimal location of green zones in metropolitan areas to control the urban heat island. Journal of Computational and Applied Mathematics. 2015;289:412-25.
[18] AIA_Asphalt. Key Facts. 2022.
[19] Association NAP. FAST FACTS. 2022.
[20] Higashiyama H, Sano M, Nakanishi F, Takahashi O, Tsukuma S. Field measurements of road surface temperature of several asphalt pavements with temperature rise reducing function. Case Studies in Construction Materials. 2016;4:73-80.
[21] Santamouris M. Using cool pavements as a mitigation strategy to fight urban heat island—A review of the actual developments. Renewable and Sustainable Energy Reviews. 2013;26:224-40.

[22] Bobes-Jesus V, Pascual-Muñoz P, Castro-Fresno D, Rodriguez-Hernandez J. Asphalt solar collectors: A literature review. Applied Energy. 2013;102:962-70.
[23] Susca T, Gaffin SR, Dell'Osso GR. Positive effects of vegetation: Urban heat island and green roofs. Environmental Pollution. 2011;159(8):2119-26.
[24] Jáuregui E. Influence of a large urban park on temperature and convective precipitation in a tropical city. Energy and buildings. 1990;15(3-4):457-63.
[25] Wong NH, Yu C. Study of green areas and urban heat island in a tropical city. Habitat International. 2005;29(3):547-58.
[26] Xiao XD, Dong L, Yan H, Yang N, Xiong Y. The influence of the spatial characteristics of urban green space on the urban heat island effect in Suzhou Industrial Park. Sustainable Cities and Society. 2018;40:428-39.
[27] Bärring L, Mattsson JO, Lindqvist S. Canyon geometry, street temperatures and urban heat island in malmö, sweden. Journal of Climatology. 1985;5(4):433-44.
[28] Ahmad K, Khare M, Chaudhry KK. Wind tunnel simulation studies on dispersion at urban street canyons and intersections—a review. Journal of Wind Engineering and Industrial Aerodynamics. 2005;93(9):697-717.
[29] Rizwan AM, Dennis LYC, Liu C. A review on the generation, determination and mitigation of Urban Heat Island. Journal of Environmental Sciences. 2008;20(1):120-8.
[30] Oke TR. City size and the urban heat island. Atmospheric Environment (1967). 1973;7(8):769-79.
[31] Kotharkar R, Surawar M. Land Use, Land Cover, and Population Density Impact on the Formation of Canopy Urban Heat Islands through Traverse Survey in the Nagpur Urban Area, India. Journal of Urban Planning and Development. 2016;142(1):04015003.
[32] Manoli G, Fatichi S, Schläpfer M, Yu K, Crowther TW, Meili N, et al. Magnitude of urban heat islands largely explained by climate and population. Nature. 2019;573(7772):55-60.
[33] Affairs DoEaS. World Population Prospects 2022:Summary of Results. UN DESA/POP/2022/TR/NO 32022.
[34] Beck HE, Zimmermann NE, McVicar TR, Vergopolan N, Berg A, Wood EF. Present and future Köppen-Geiger climate classification maps at 1-km resolution. Scientific data. 2018;5(1):1-12.
[35] Yang L, Qian F, Song D-X, Zheng K-J. Research on Urban Heat-Island Effect. Procedia Engineering. 2016;169:11-8.
[36] Kolokotroni M, Ren X, Davies M, Mavrogianni A. London's urban heat island: Impact on current and future energy consumption in office buildings. Energy and Buildings. 2012;47:302-11.
[37] Zhao H-x, Magoulès F. A review on the prediction of building energy consumption. Renewable and Sustainable Energy Reviews. 2012;16(6):3586-92.
[38] Yang Z, Ghahramani A, Becerik-Gerber B. Building occupancy diversity and HVAC (heating, ventilation, and air conditioning) system energy efficiency. Energy. 2016;109:641-9.
[39] Ürge-Vorsatz D, Cabeza LF, Serrano S, Barreneche C, Petrichenko K. Heating and cooling energy trends and drivers in buildings. Renewable and Sustainable Energy Reviews. 2015;41:85-98.
[40] Kolokotroni M, Giannitsaris I, Watkins R. The effect of the London urban heat island on building summer cooling demand and night ventilation strategies. Solar Energy. 2006;80(4):383-92.
[41] Santamouris M, Haddad S, Saliari M, Vasilakopoulou K, Synnefa A, Paolini R, et al. On the energy impact of urban heat island in Sydney:

Climate and energy potential of mitigation technologies. Energy and Buildings. 2018;166:154-64.
[42] Santamouris M, Cartalis C, Synnefa A, Kolokotsa D. On the impact of urban heat island and global warming on the power demand and electricity consumption of buildings—A review. Energy and Buildings. 2015;98:119-24.
[43] Parkpoom S, Harrison GP. Analyzing the Impact of Climate Change on Future Electricity Demand in Thailand. IEEE Transactions on Power Systems. 2008;23(3):1441-8.
[44] Giannakopoulos C, Psiloglou BE. Trends in energy load demand for Athens, Greece: weather and non-weather related factors. Climate research. 2006;31(1):97-108.
[45] Rosenfeld AH, Akbari H, Bretz S, Fishman BL, Kurn DM, Sailor D, et al. Mitigation of urban heat islands: materials, utility programs, updates. Energy and buildings. 1995;22(3):255-65.
[46] Fung WY, Lam KS, Hung WT, Pang SW, Lee YL. Impact of urban temperature on energy consumption of Hong Kong. Energy. 2006;31(14):2623-37.
[47] Wong SL, Wan KKW, Li DHW, Lam JC. Impact of climate change on residential building envelope cooling loads in subtropical climates. Energy and Buildings. 2010;42(11):2098-103.
[48] Hayhoe K, Robson M, Rogula J, Auffhammer M, Miller N, VanDorn J, et al. An integrated framework for quantifying and valuing climate change impacts on urban energy and infrastructure: A Chicago case study. Journal of Great Lakes Research. 2010;36:94-105.
[49] Amato AD, Ruth M, Kirshen P, Horwitz J. Regional energy demand responses to climate change: methodology and application to the commonwealth of Massachusetts. Climatic Change. 2005;71(1):175-201.
[50] Wilby RL. Constructing climate change scenarios of urban heat island intensity and air quality. Environment and planning B: Planning and Design. 2008;35(5):902-19.
[51] Coates J, Mar KA, Ojha N, Butler TM. The influence of temperature on ozone production under varying NO x conditions–a modelling study. Atmospheric Chemistry and Physics. 2016;16(18):11601-15.
[52] Pyrgou A, Hadjinicolaou P, Santamouris M. Enhanced near-surface ozone under heatwave conditions in a Mediterranean island. Scientific reports. 2018;8(1):1-10.
[53] Stathopoulou E, Mihalakakou G, Santamouris M, Bagiorgas HS. On the impact of temperature on tropospheric ozone concentration levels in urban environments. Journal of Earth System Science. 2008;117(3):227-36.
[54] Beaney G, Gough WA. The influence of tropospheric ozone on the air temperature of the city of Toronto, Ontario, Canada. Atmospheric environment. 2002;36(14):2319-25.
[55] Ryu Y-H, Baik J-J, Lee S-H. Effects of anthropogenic heat on ozone air quality in a megacity. Atmospheric environment. 2013;80:20-30.
[56] Jenkin ME, Clemitshaw KC. Ozone and other secondary photochemical pollutants: chemical processes governing their formation in the planetary boundary layer. Atmospheric Environment. 2000;34(16):2499-527.
[57] Wang Y, Du H, Xu Y, Lu D, Wang X, Guo Z. Temporal and spatial variation relationship and influence factors on surface urban heat island and ozone pollution in the Yangtze River Delta, China. Science of the Total Environment. 2018;631:921-33.
[58] Diem JE, Stauber CE, Rothenberg R. Heat in the southeastern United States: Characteristics, trends, and potential health impact. PloS one. 2017;12(5):e0177937.

[59] Li J, Georgescu M, Hyde P, Mahalov A, Moustaoui M. Achieving accurate simulations of urban impacts on ozone at high resolution. Environmental Research Letters. 2014;9(11):114019.
[60] Wang XM, Lin WS, Yang LM, Deng RR, Lin H. A numerical study of influences of urban land-use change on ozone distribution over the Pearl River Delta region, China. Tellus B: Chemical and Physical Meteorology. 2007;59(3):633-41.
[61] Yoshikado H, Tsuchida M. High levels of winter air pollution under the influence of the urban heat island along the shore of Tokyo Bay. Journal of Applied Meteorology and Climatology. 1996;35(10):1804-13.
[62] Aw J, Kleeman MJ. Evaluating the first-order effect of intraannual temperature variability on urban air pollution. Journal of Geophysical Research: Atmospheres. 2003;108(D12).
[63] Yang Y, Zheng Z, Yim SYL, Roth M, Ren G, Gao Z, et al. PM2. 5 pollution modulates wintertime urban heat island intensity in the Beijing-Tianjin-Hebei Megalopolis, China. Geophysical Research Letters. 2020;47(1):e2019GL084288.
[64] Yang G, Ren G, Zhang P, Xue X, Tysa SK, Jia W, et al. PM2. 5 influence on Urban Heat Island (UHI) effect in Beijing and the possible mechanisms. Journal of Geophysical Research: Atmospheres. 2021;126(17):e2021JD035227.
[65] Jacob DJ, Winner DA. Effect of climate change on air quality. Atmospheric environment. 2009;43(1):51-63.
[66] Pylsy P, Lylykangas K, Kurnitski J. Buildings' energy efficiency measures effect on CO2 emissions in combined heating, cooling and electricity production. Renewable and Sustainable Energy Reviews. 2020;134:110299.
[67] Kleerekoper L, van Esch M, Salcedo TB. How to make a city climate-proof, addressing the urban heat island effect. Resources, Conservation and Recycling. 2012;64:30-8.
[68] Roxon J, Ulm FJ, Pellenq RJM. Urban heat island impact on state residential energy cost and CO2 emissions in the United States. Urban Climate. 2020;31:100546.
[69] George K, Ziska LH, Bunce JA, Quebedeaux B. Elevated atmospheric CO2 concentration and temperature across an urban–rural transect. Atmospheric Environment. 2007;41(35):7654-65.
[70] Baccini M, Biggeri A, Accetta G, Kosatsky T, Katsouyanni K, Analitis A, et al. Heat effects on mortality in 15 European cities. Epidemiology. 2008:711-9.
[71] Gasparrini A, Guo Y, Hashizume M, Lavigne E, Zanobetti A, Schwartz J, et al. Mortality risk attributable to high and low ambient temperature: a multicountry observational study. The lancet. 2015;386(9991):369-75.
[72] Arghavani S, Malakooti H, Ali Akbari Bidokhti A-A. Numerical assessment of the urban green space scenarios on urban heat island and thermal comfort level in Tehran Metropolis. Journal of Cleaner Production. 2020;261:121183.
[73] Heaviside C, Macintyre H, Vardoulakis S. The Urban Heat Island: Implications for Health in a Changing Environment. Current Environmental Health Reports. 2017;4(3):296-305.
[74] Lowe SA. An energy and mortality impact assessment of the urban heat island in the US. Environmental Impact Assessment Review. 2016;56:139-44.
[75] Laaidi K, Zeghnoun A, Dousset B, Bretin P, Vandentorren S, Giraudet E, et al. The impact of heat islands on mortality in Paris during the August 2003 heat wave. Environmental health perspectives. 2012;120(2):254-9.
[76] Uejio CK, Wilhelmi OV, Golden JS, Mills DM, Gulino SP, Samenow JP. Intra-urban societal vulnerability to extreme heat: the role of heat

exposure and the built environment, socioeconomics, and neighborhood stability. Health & place. 2011;17(2):498-507.
[77] Heaviside C, Vardoulakis S, Cai X-M. Attribution of mortality to the urban heat island during heatwaves in the West Midlands, UK. Environmental health. 2016;15(1):49-59.
[78] Burkart K, Meier F, Schneider A, Breitner S, Canário P, Alcoforado MJ, et al. Modification of heat-related mortality in an elderly urban population by vegetation (urban green) and proximity to water (urban blue): evidence from Lisbon, Portugal. Environmental health perspectives. 2016;124(7):927-34.
[79] Gronlund CJ, Berrocal VJ, White-Newsome JL, Conlon KC, O'Neill MS. Vulnerability to extreme heat by socio-demographic characteristics and area green space among the elderly in Michigan, 1990–2007. Environmental research. 2015;136:449-61.
[80] Gabriel KMA, Endlicher WR. Urban and rural mortality rates during heat waves in Berlin and Brandenburg, Germany. Environmental Pollution. 2011;159(8):2044-50.
[81] Taylor J, Wilkinson P, Davies M, Armstrong B, Chalabi Z, Mavrogianni A, et al. Mapping the effects of urban heat island, housing, and age on excess heat-related mortality in London. Urban Climate. 2015;14:517-28.
[82] Tan J, Zheng Y, Tang X, Guo C, Li L, Song G, et al. The urban heat island and its impact on heat waves and human health in Shanghai. International journal of biometeorology. 2010;54(1):75-84.
[83] Robine J-M, Cheung SLK, Le Roy S, Van Oyen H, Griffiths C, Michel J-P, et al. Death toll exceeded 70,000 in Europe during the summer of 2003. Comptes Rendus Biologies. 2008;331(2):171-8.
[84] Santamouris M. Recent progress on urban overheating and heat island research. Integrated assessment of the energy, environmental, vulnerability and health impact. Synergies with the global climate change. Energy and Buildings. 2020;207:109482.
[85] Weber S, Sadoff N, Zell E, de Sherbinin A. Policy-relevant indicators for mapping the vulnerability of urban populations to extreme heat events: A case study of Philadelphia. Applied Geography. 2015;63:231-43.
[86] Harlan SL, Brazel AJ, Prashad L, Stefanov WL, Larsen L. Neighborhood microclimates and vulnerability to heat stress. Social science & medicine. 2006;63(11):2847-63.
[87] Leal Filho W, Icaza LE, Neht A, Klavins M, Morgan EA. Coping with the impacts of urban heat islands. A literature based study on understanding urban heat vulnerability and the need for resilience in cities in a global climate change context. Journal of Cleaner Production. 2018;171:1140-9.
[88] Schinasi LH, Benmarhnia T, De Roos AJ. Modification of the association between high ambient temperature and health by urban microclimate indicators: A systematic review and meta-analysis. Environmental research. 2018;161:168-80.
[89] Rosenthal JK, Kinney PL, Metzger KB. Intra-urban vulnerability to heat-related mortality in New York City, 1997–2006. Health & place. 2014;30:45-60.
[90] Santamouris M, Alevizos SM, Aslanoglou L, Mantzios D, Milonas P, Sarelli I, et al. Freezing the poor—Indoor environmental quality in low and very low income households during the winter period in Athens. Energy and Buildings. 2014;70:61-70.
[91] Gouveia JP, Seixas J, Long G. Mining households' energy data to disclose fuel poverty: Lessons for Southern Europe. Journal of Cleaner Production. 2018;178:534-50.
[92] Santamouris M. Innovating to zero the building sector in Europe: Minimising the energy consumption, eradication of the energy poverty and mitigating the local climate change. Solar Energy. 2016;128:61-94.

[93] Goggins WB, Chan EYY, Ng E, Ren C, Chen L. Effect modification of the association between short-term meteorological factors and mortality by urban heat islands in Hong Kong. PloS one. 2012;7(6):e38551.
[94] Harlan SL, Declet-Barreto JH, Stefanov WL, Petitti DB. Neighborhood effects on heat deaths: social and environmental predictors of vulnerability in Maricopa County, Arizona. Environmental health perspectives. 2013;121(2):197-204.
[95] Vaneckova P, Beggs PJ, Jacobson CR. Spatial analysis of heat-related mortality among the elderly between 1993 and 2004 in Sydney, Australia. Social science & medicine. 2010;70(2):293-304.
[96] Ribeiro Sobral H. Heat island in São Paulo, Brazil: effects on health. Critical Public Health. 2005;15(2):147-56.
[97] Aflaki A, Mirnezhad M, Ghaffarianhoseini A, Ghaffarianhoseini A, Omrany H, Wang Z-H, et al. Urban heat island mitigation strategies: A state-of-the-art review on Kuala Lumpur, Singapore and Hong Kong. Cities. 2017;62:131-45.
[98] Mirzaei PA, Haghighat F. Approaches to study urban heat island–abilities and limitations. Building and environment. 2010;45(10):2192-201.
[99] Voogt JA, Oke TR. Thermal remote sensing of urban climates. Remote sensing of environment. 2003;86(3):370-84.
[100] Uehara K, Murakami S, Oikawa S, Wakamatsu S. Wind tunnel experiments on how thermal stratification affects flow in and above urban street canyons. Atmospheric Environment. 2000;34(10):1553-62.
[101] Giannaros TM, Melas D, Daglis IA, Keramitsoglou I, Kourtidis K. Numerical study of the urban heat island over Athens (Greece) with the WRF model. Atmospheric Environment. 2013;73:103-11.
[102] Wang X, Li Y. Predicting urban heat island circulation using CFD. Building and Environment. 2016;99:82-97.
[103] Li H, Zhou Y, Wang X, Zhou X, Zhang H, Sodoudi S. Quantifying urban heat island intensity and its physical mechanism using WRF/UCM. Science of The Total Environment. 2019;650:3110-9.
[104] Aghamolaei R, Fallahpour M, Mirzaei PA. Tempo-spatial thermal comfort analysis of urban heat island with coupling of CFD and building energy simulation. Energy and Buildings. 2021;251:111317.
[105] Powers JG, Klemp JB, Skamarock WC, Davis CA, Dudhia J, Gill DO, et al. The weather research and forecasting model: Overview, system efforts, and future directions. Bulletin of the American Meteorological Society. 2017;98(8):1717-37.
[106] Skamarock WC, Klemp JB, Dudhia J, Gill DO, Liu Z, Berner J, et al. A description of the advanced research WRF model version 4. National Center for Atmospheric Research: Boulder, CO, USA. 2019;145(145):550.
[107] Litta AJ, Mohanty UC, Das S, Idicula SM. Numerical simulation of severe local storms over east India using WRF-NMM mesoscale model. Atmospheric Research. 2012;116:161-84.
[108] Torn RD, Hakim GJ, Snyder C. Boundary conditions for limited-area ensemble Kalman filters. Monthly weather review. 2006;134(9):2490-502.
[109] Ruiz JJ, Saulo C, Nogués-Paegle J. WRF model sensitivity to choice of parameterization over South America: validation against surface variables. Monthly weather review. 2010;138(8):3342-55.
[110] Blocken B. Computational Fluid Dynamics for urban physics: Importance, scales, possibilities, limitations and ten tips and tricks towards accurate and reliable simulations. Building and Environment. 2015;91:219-45.
[111] Mirzaei PA, Haghighat F. Approaches to study Urban Heat Island – Abilities and limitations. Building and Environment. 2010;45(10):2192-201.

[112] Rizwan AM, Dennis LYC, Chunho LIU. A review on the generation, determination and mitigation of Urban Heat Island. Journal of environmental sciences. 2008;20(1):120-8.
[113] Jonsson P. Vegetation as an urban climate control in the subtropical city of Gaborone, Botswana. International Journal of Climatology: A Journal of the Royal Meteorological Society. 2004;24(10):1307-22.
[114] Roth M. Review of urban climate research in (sub) tropical regions. International Journal of Climatology: A Journal of the Royal Meteorological Society. 2007;27(14):1859-73.
[115] Chakraborty T, Sarangi C, Tripathi SN. Understanding diurnality and inter-seasonality of a sub-tropical urban heat island. Boundary-Layer Meteorology. 2017;163(2):287-309.
[116] Hartz DA, Prashad L, Hedquist BC, Golden J, Brazel AJ. Linking satellite images and hand-held infrared thermography to observed neighborhood climate conditions. Remote sensing of environment. 2006;104(2):190-200.
[117] Stathopoulou M, Cartalis C. Downscaling AVHRR land surface temperatures for improved surface urban heat island intensity estimation. Remote Sensing of Environment. 2009;113(12):2592-605.
[118] van Hove LWA, Jacobs CMJ, Heusinkveld BG, Elbers JA, van Driel BL, Holtslag AAM. Temporal and spatial variability of urban heat island and thermal comfort within the Rotterdam agglomeration. Building and Environment. 2015;83:91-103.
[119] Moyer AN, Hawkins TW. River effects on the heat island of a small urban area. Urban Climate. 2017;21:262-77.
[120] Yao R, Luo Q, Luo Z, Jiang L, Yang Y. An integrated study of urban microclimates in Chongqing, China: Historical weather data, transverse measurement and numerical simulation. Sustainable Cities and Society. 2015;14:187-99.
[121] Zinzi M, Carnielo E. Impact of urban temperatures on energy performance and thermal comfort in residential buildings. The case of Rome, Italy. Energy and Buildings. 2017;157:20-9.
[122] Lin P, Lau SSY, Qin H, Gou Z. Effects of urban planning indicators on urban heat island: a case study of pocket parks in high-rise high-density environment. Landscape and Urban Planning. 2017;168:48-60.
[123] Liu L, Lin Y, Liu J, Wang L, Wang D, Shui T, et al. Analysis of local-scale urban heat island characteristics using an integrated method of mobile measurement and GIS-based spatial interpolation. Building and Environment. 2017;117:191-207.
[124] Kim M, Lee K, Cho G-H. Temporal and spatial variability of urban heat island by geographical location: A case study of Ulsan, Korea. Building and Environment. 2017;126:471-82.
[125] Wolters D, Brandsma T. Estimating the urban heat island in residential areas in the Netherlands using observations by weather amateurs. Journal of Applied Meteorology and Climatology. 2012;51(4):711-21.
[126] Arifwidodo S, Chandrasiri O. Urban heat island and household energy consumption in Bangkok, Thailand. Energy Procedia. 2015;79:189-94.
[127] Yadav N, Sharma C, Peshin SK, Masiwal R. Study of intra-city urban heat island intensity and its influence on atmospheric chemistry and energy consumption in Delhi. Sustainable Cities and Society. 2017;32:202-11.
[128] Li X-X, Norford LK. Evaluation of cool roof and vegetations in mitigating urban heat island in a tropical city, Singapore. Urban Climate. 2016;16:59-74.
[129] Ooi MCG, Chan A, Ashfold MJ, Morris KI, Oozeer MY, Salleh SA. Numerical study on effect of urban heating on local climate during calm

inter-monsoon period in greater Kuala Lumpur, Malaysia. Urban Climate. 2017;20:228-50.
[130] Liu X, Tian G, Feng J, Wang J, Kong L. Assessing summertime urban warming and the cooling efficacy of adaptation strategy in the Chengdu-Chongqing metropolitan region of China. Science of The Total Environment. 2018;610-611:1092-102.
[131] Kohler M, Tannier C, Blond N, Aguejdad R, Clappier A. Impacts of several urban-sprawl countermeasures on building (space heating) energy demands and urban heat island intensities. A case study. Urban Climate. 2017;19:92-121.
[132] Lauwaet D, De Ridder K, Saeed S, Brisson E, Chatterjee F, van Lipzig NPM, et al. Assessing the current and future urban heat island of Brussels. Urban Climate. 2016;15:1-15.
[133] Bernard J, Musy M, Calmet I, Bocher E, Keravec P. Urban heat island temporal and spatial variations: Empirical modeling from geographical and meteorological data. Building and Environment. 2017;125:423-38.
[134] Afshari A, Liu N. Inverse modeling of the urban energy system using hourly electricity demand and weather measurements, Part 2: Gray-box model. Energy and Buildings. 2017;157:139-56.
[135] Santos LGR, Afshari A, Norford LK, Mao J. Evaluating approaches for district-wide energy model calibration considering the Urban Heat Island effect. Applied Energy. 2018;215:31-40.
[136] Roberge F, Sushama L. Urban heat island in current and future climates for the island of Montreal. Sustainable Cities and Society. 2018;40:501-12.
[137] Gu Y, Li D. A modeling study of the sensitivity of urban heat islands to precipitation at climate scales. Urban Climate. 2018;24:982-93.
[138] Guo G, Wu Z, Xiao R, Chen Y, Liu X, Zhang X. Impacts of urban biophysical composition on land surface temperature in urban heat island clusters. Landscape and Urban Planning. 2015;135:1-10.
[139] Bektaş Balçik F. Determining the impact of urban components on land surface temperature of Istanbul by using remote sensing indices. Environmental monitoring and assessment. 2014;186:859-72.
[140] Shatnawi N, Abu Qdais H. Mapping urban land surface temperature using remote sensing techniques and artificial neural network modelling. International Journal of Remote Sensing. 2019;40(10):3968-83.
[141] Tomlinson CJ, Chapman L, Thornes JE, Baker C. Remote sensing land surface temperature for meteorology and climatology: A review. Meteorological Applications. 2011;18(3):296-306.
[142] Pongracz R, Bartholy J, Dezso Z. Remotely sensed thermal information applied to urban climate analysis. Advances in Space Research. 2006;37(12):2191-6.
[143] Stathopoulou M, Cartalis C. Daytime urban heat islands from Landsat ETM+ and Corine land cover data: An application to major cities in Greece. Solar Energy. 2007;81(3):358-68.
[144] Pongrácz R, Bartholy J, Dezső Z. Application of remotely sensed thermal information to urban climatology of Central European cities. Physics and Chemistry of the Earth, Parts A/B/C. 2010;35(1):95-9.
[145] Li Y-y, Zhang H, Kainz W. Monitoring patterns of urban heat islands of the fast-growing Shanghai metropolis, China: Using time-series of Landsat TM/ETM+ data. International Journal of Applied Earth Observation and Geoinformation. 2012;19:127-38.
[146] Klok L, Zwart S, Verhagen H, Mauri E. The surface heat island of Rotterdam and its relationship with urban surface characteristics. Resources, Conservation and Recycling. 2012;64:23-9.

[147] Hu L, Brunsell NA. The impact of temporal aggregation of land surface temperature data for surface urban heat island (SUHI) monitoring. Remote Sensing of Environment. 2013;134:162-74.
[148] Anniballe R, Bonafoni S, Pichierri M. Spatial and temporal trends of the surface and air heat island over Milan using MODIS data. Remote Sensing of Environment. 2014;150:163-71.
[149] Mathew A, Khandelwal S, Kaul N. Spatial and temporal variations of urban heat island effect and the effect of percentage impervious surface area and elevation on land surface temperature: Study of Chandigarh city, India. Sustainable Cities and Society. 2016;26:264-77.
[150] Göndöcs J, Breuer H, Pongrácz R, Bartholy J. Urban heat island mesoscale modelling study for the Budapest agglomeration area using the WRF model. Urban Climate. 2017;21:66-86.
[151] Meng Q, Zhang L, Sun Z, Meng F, Wang L, Sun Y. Characterizing spatial and temporal trends of surface urban heat island effect in an urban main built-up area: A 12-year case study in Beijing, China. Remote Sensing of Environment. 2018;204:826-37.
[152] Cheval S, Dumitrescu A, Irașoc A, Paraschiv M-G, Perry M, Ghent D. MODIS-based climatology of the Surface Urban Heat Island at country scale (Romania). Urban Climate. 2022;41:101056.
[153] Miao C, Yu S, Hu Y, Zhang H, He X, Chen W. Review of methods used to estimate the sky view factor in urban street canyons. Building and Environment. 2020;168:106497.
[154] Chatzipoulka C, Compagnon R, Kaempf J, Nikolopoulou M. Sky view factor as predictor of solar availability on building façades. Solar Energy. 2018;170:1026-38.
[155] Svensson MK. Sky view factor analysis–implications for urban air temperature differences. Meteorological applications. 2004;11(3):201-11.
[156] Lyu T, Buccolieri R, Gao Z. A numerical study on the correlation between sky view factor and summer microclimate of local climate zones. Atmosphere. 2019;10(8):438.
[157] Dirksen M, Ronda RJ, Theeuwes NE, Pagani GA. Sky view factor calculations and its application in urban heat island studies. Urban Climate. 2019;30:100498.
[158] Middel A, Lukasczyk J, Maciejewski R, Demuzere M, Roth M. Sky View Factor footprints for urban climate modeling. Urban Climate. 2018;25:120-34.
[159] Theeuwes NE, Steeneveld G-J, Ronda RJ, Holtslag AAM. A diagnostic equation for the daily maximum urban heat island effect for cities in northwestern Europe. International Journal of Climatology. 2017;37(1):443-54.
[160] Gong F-Y, Zeng Z-C, Zhang F, Li X, Ng E, Norford LK. Mapping sky, tree, and building view factors of street canyons in a high-density urban environment. Building and Environment. 2018;134:155-67.
[161] Sobel I, Feldman G. A 3x3 isotropic gradient operator for image processing. a talk at the Stanford Artificial Project in. 1968:271-2.
[162] Middel A, Lukasczyk J, Maciejewski R. Sky view factors from synthetic fisheye photos for thermal comfort routing—a case study in Phoenix, Arizona. 2017.
[163] An N, Hemmati S, Cui Y-J. Assessment of the methods for determining net radiation at different time-scales of meteorological variables. Journal of Rock Mechanics and Geotechnical Engineering. 2017;9(2):239-46.
[164] Takebayashi H, Moriyama M. Surface heat budget on green roof and high reflection roof for mitigation of urban heat island. Building and Environment. 2007;42(8):2971-9.

[165] Wang Y, Berardi U, Akbari H. The Urban Heat Island Effect in the City of Toronto. Procedia Engineering. 2015;118:137-44.
[166] Wille F, Nehrig M, Feldkamp M. 8 - Thermal performance of transportation packages for radioactive materials. In: Sorenson KB, editor. Safe and Secure Transport and Storage of Radioactive Materials. Oxford: Woodhead Publishing; 2015. p. 107-21.
[167] Wang Y, Akbari H. Development and application of 'thermal radiative power' for urban environmental evaluation. Sustainable Cities and Society. 2015;14:316-22.
[168] Coccolo S, Kämpf J, Scartezzini J-L, Pearlmutter D. Outdoor human comfort and thermal stress: A comprehensive review on models and standards. Urban Climate. 2016;18:33-57.
[169] He B-J, Ding L, Prasad D. Relationships among local-scale urban morphology, urban ventilation, urban heat island and outdoor thermal comfort under sea breeze influence. Sustainable Cities and Society. 2020;60:102289.
[170] Ashrae AP. Standard 55-Thermal environmental conditions for human occupancy. 2017.
[171] Höppe P. Different aspects of assessing indoor and outdoor thermal comfort. Energy and Buildings. 2002;34(6):661-5.
[172] Atmaca I, Kaynakli O, Yigit A. Effects of radiant temperature on thermal comfort. Building and Environment. 2007;42(9):3210-20.
[173] Li H. Chapter 13 - Impacts of Pavement Strategies on Human Thermal Comfort. In: Li H, editor. Pavement Materials for Heat Island Mitigation. Boston: Butterworth-Heinemann; 2016. p. 281-306.
[174] Kántor N, Unger J. The most problematic variable in the course of human-biometeorological comfort assessment—the mean radiant temperature. Central European Journal of Geosciences. 2011;3(1):90-100.
[175] Höppe P. The physiological equivalent temperature–a universal index for the biometeorological assessment of the thermal environment. International journal of Biometeorology. 1999;43:71-5.
[176] Zare S, Hasheminejad N, Shirvan HE, Hemmatjo R, Sarebanzadeh K, Ahmadi S. Comparing Universal Thermal Climate Index (UTCI) with selected thermal indices/environmental parameters during 12 months of the year. Weather and Climate Extremes. 2018;19:49-57.
[177] Yau YH, Chew BT. A review on predicted mean vote and adaptive thermal comfort models. Building Services Engineering Research and Technology. 2014;35(1):23-35.
[178] Churkina G. The Role of Urbanization in the Global Carbon Cycle. Frontiers in Ecology and Evolution. 2016;3.
[179] Seto Karen C, Güneralp B, Hutyra Lucy R. Global forecasts of urban expansion to 2030 and direct impacts on biodiversity and carbon pools. Proceedings of the National Academy of Sciences. 2012;109(40):16083-8.
[180] Avtar R, Tripathi S, Aggarwal AK, Kumar P. Population–urbanization–energy nexus: a review. Resources. 2019;8(3):136.
[181] Zheng T, Qu K, Darkwa J, Calautit JK. Evaluating urban heat island mitigation strategies for a subtropical city centre (a case study in Osaka, Japan). Energy. 2022;250:123721.
[182] Singh M, Sharston R. Quantifying the dualistic nature of urban heat Island effect (UHI) on building energy consumption. Energy and Buildings. 2022;255:111649.
[183] Santamouris M. On the energy impact of urban heat island and global warming on buildings. Energy and Buildings. 2014;82:100-13.
[184] Buchin O, Hoelscher M-T, Meier F, Nehls T, Ziegler F. Evaluation of the health-risk reduction potential of countermeasures to urban heat islands. Energy and Buildings. 2016;114:27-37.

[185] Chandramowli SN, Felder FA. Impact of climate change on electricity systems and markets–a review of models and forecasts. Sustainable Energy Technologies and Assessments. 2014;5:62-74.
[186] Dirks JA, Gorrissen WJ, Hathaway JH, Skorski DC, Scott MJ, Pulsipher TC, et al. Impacts of climate change on energy consumption and peak demand in buildings: A detailed regional approach. Energy. 2015;79:20-32.
[187] Guattari C, Evangelisti L, Balaras CA. On the assessment of urban heat island phenomenon and its effects on building energy performance: A case study of Rome (Italy). Energy and Buildings. 2018;158:605-15.
[188] Salvati A, Coch Roura H, Cecere C. Assessing the urban heat island and its energy impact on residential buildings in Mediterranean climate: Barcelona case study. Energy and Buildings. 2017;146:38-54.
[189] Kolokotsa D, Santamouris M, Zerefos SC. Green and cool roofs' urban heat island mitigation potential in European climates for office buildings under free floating conditions. Solar Energy. 2013;95:118-30.
[190] Hassid S, Santamouris M, Papanikolaou N, Linardi A, Klitsikas N, Georgakis C, et al. The effect of the Athens heat island on air conditioning load. Energy and Buildings. 2000;32(2):131-41.
[191] Hirano Y, Fujita T. Evaluation of the impact of the urban heat island on residential and commercial energy consumption in Tokyo. Energy. 2012;37(1):371-83.
[192] Street M, Reinhart C, Norford L, Ochsendorf J. Urban heat island in Boston–An evaluation of urban air-temperature models for predicting building energy use. Conference Urban heat island in Boston–An evaluation of urban air-temperature models for predicting building energy use. p. 1022-9.
[193] Ignatius M, Wong NH, Jusuf SK. The significance of using local predicted temperature for cooling load simulation in the tropics. Energy and Buildings. 2016;118:57-69.
[194] Palme M, Inostroza L, Villacreses G, Lobato-Cordero A, Carrasco C. From urban climate to energy consumption. Enhancing building performance simulation by including the urban heat island effect. Energy and Buildings. 2017;145:107-20.
[195] Sun Y, Augenbroe G. Urban heat island effect on energy application studies of office buildings. Energy and Buildings. 2014;77:171-9.
[196] Wangpattarapong K, Maneewan S, Ketjoy N, Rakwichian W. The impacts of climatic and economic factors on residential electricity consumption of Bangkok Metropolis. Energy and Buildings. 2008;40(8):1419-25.
[197] Hong T, Chen Y, Luo X, Luo N, Lee SH. Ten questions on urban building energy modeling. Building and Environment. 2020;168:106508.
[198] Swan LG, Ugursal VI. Modeling of end-use energy consumption in the residential sector: A review of modeling techniques. Renewable and Sustainable Energy Reviews. 2009;13(8):1819-35.
[199] Ferrando M, Causone F, Hong T, Chen Y. Urban building energy modeling (UBEM) tools: A state-of-the-art review of bottom-up physics-based approaches. Sustainable Cities and Society. 2020;62.
[200] Böhringer C, Rutherford TF. Integrated assessment of energy policies: Decomposing top-down and bottom-up. Journal of Economic Dynamics and Control. 2009;33(9):1648-61.
[201] Rault T, Bouabdallah A, Challal Y. Energy efficiency in wireless sensor networks: A top-down survey. Computer networks. 2014;67:104-22.
[202] Trotta G. The determinants of energy efficient retrofit investments in the English residential sector. Energy Policy. 2018;120:175-82.

[203] Li W, Zhou Y, Cetin K, Eom J, Wang Y, Chen G, et al. Modeling urban building energy use: A review of modeling approaches and procedures. Energy. 2017;141:2445-57.
[204] Reinhart CF, Cerezo Davila C. Urban building energy modeling – A review of a nascent field. Building and Environment. 2016;97:196-202.
[205] Fathi S, Srinivasan R, Fenner A, Fathi S. Machine learning applications in urban building energy performance forecasting: A systematic review. Renewable and Sustainable Energy Reviews. 2020;133:110287.
[206] Abbasabadi N, Ashayeri M, Azari R, Stephens B, Heidarinejad M. An integrated data-driven framework for urban energy use modeling (UEUM). Applied Energy. 2019;253:113550.
[207] Ahmad T, Chen H, Guo Y, Wang J. A comprehensive overview on the data driven and large scale based approaches for forecasting of building energy demand: A review. Energy and Buildings. 2018;165:301-20.
[208] Deb C, Schlueter A. Review of data-driven energy modelling techniques for building retrofit. Renewable and Sustainable Energy Reviews. 2021;144:110990.
[209] Li Y, O'Neill Z, Zhang L, Chen J, Im P, DeGraw J. Grey-box modeling and application for building energy simulations - A critical review. Renewable and Sustainable Energy Reviews. 2021;146:111174.
[210] Li J, Jin R, Hang ZY. Integration of physically-based and data-driven approaches for thermal field prediction in additive manufacturing. Materials & Design. 2018;139:473-85.
[211] Yang Xe, Liu S, Zou Y, Ji W, Zhang Q, Ahmed A, et al. Energy-saving potential prediction models for large-scale building: A state-of-the-art review. Renewable and Sustainable Energy Reviews. 2022;156:111992.
[212] Brøgger M, Bacher P, Wittchen KB. A hybrid modelling method for improving estimates of the average energy-saving potential of a building stock. Energy and Buildings. 2019;199:287-96.
[213] Dong B, Li Z, Rahman SMM, Vega R. A hybrid model approach for forecasting future residential electricity consumption. Energy and Buildings. 2016;117:341-51.
[214] Zhao F, Martinez-Moyano IJ, Augenbroe G. Agent-based modeling of commercial building stocks for policy support. Conference Agent-based modeling of commercial building stocks for policy support. p. 2385-92.
[215] Nouvel R, Brassel K-H, Bruse M, Duminil E, Coors V, Eicker U, et al. SimStadt, a new workflow-driven urban energy simulation platform for CityGML city models. Conference SimStadt, a new workflow-driven urban energy simulation platform for CityGML city models. LESO-PB, EPFL, p. 889-94.
[216] Kaden R, Kolbe TH. City-wide total energy demand estimation of buildings using semantic 3D city models and statistical data. Conference City-wide total energy demand estimation of buildings using semantic 3D city models and statistical data.
[217] Remmen P, Lauster M, Mans M, Fuchs M, Osterhage T, Müller D. TEASER: an open tool for urban energy modelling of building stocks. Journal of Building Performance Simulation. 2018;11(1):84-98.
[218] Fonseca JA, Nguyen T-A, Schlueter A, Marechal F. City Energy Analyst (CEA): Integrated framework for analysis and optimization of building energy systems in neighborhoods and city districts. Energy and Buildings. 2016;113:202-26.
[219] Baetens R, De Coninck R, Jorissen F, Picard D, Helsen L, Saelens D. Openideas-an open framework for integrated district energy simulations. Conference Openideas-an open framework for integrated district energy simulations.

[220] Hong T, Chen Y, Lee SH, Piette MA. CityBES: A web-based platform to support city-scale building energy efficiency. Urban Computing. 2016;14:2016.
[221] Robinson D, Haldi F, Leroux P, Perez D, Rasheed A, Wilke U. CITYSIM: Comprehensive Micro-Simulation of Resource Flows for Sustainable Urban Planning. p. 1083-90--90.
[222] Bollinger LA, Evins R. HUES: A holistic urban energy simulation platform for effective model integration. Conference HUES: A holistic urban energy simulation platform for effective model integration. LESO-PB, EPFL, p. 841-6.
[223] Cerezo Davila C, Reinhart CF, Bemis JL. Modeling Boston: A workflow for the efficient generation and maintenance of urban building energy models from existing geospatial datasets. Energy. 2016;117:237-50.
[224] Reinhart C, Dogan T, Jakubiec JA, Rakha T, Sang A. Umi-an urban simulation environment for building energy use, daylighting and walkability. Conference Umi-an urban simulation environment for building energy use, daylighting and walkability, vol. 1. p. 476-83.
[225] Ali U, Shamsi MH, Hoare C, Mangina E, O'Donnell J. Review of urban building energy modeling (UBEM) approaches, methods and tools using qualitative and quantitative analysis. Energy and Buildings. 2021;246:111073.
[226] Chong A, Gu Y, Jia H. Calibrating building energy simulation models: A review of the basics to guide future work. Energy and Buildings. 2021;253:111533.
[227] Lim H, Zhai ZJ. Comprehensive evaluation of the influence of meta-models on Bayesian calibration. Energy and Buildings. 2017;155:66-75.
[228] Hou D, Hassan IG, Wang L. Review on building energy model calibration by Bayesian inference. Renewable and Sustainable Energy Reviews. 2021;143:110930.
[229] Yang T, Pan Y, Mao J, Wang Y, Huang Z. An automated optimization method for calibrating building energy simulation models with measured data: Orientation and a case study. Applied Energy. 2016;179:1220-31.
[230] Lomas KJ, Eppel H, Martin CJ, Bloomfield DP. Empirical validation of building energy simulation programs. Energy and Buildings. 1997;26(3):253-75.
[231] Schwartz Y, Raslan R. Variations in results of building energy simulation tools, and their impact on BREEAM and LEED ratings: A case study. Energy and Buildings. 2013;62:350-9.
[232] Yaghoobian N, Kleissl J. An indoor–outdoor building energy simulator to study urban modification effects on building energy use – Model description and validation. Energy and Buildings. 2012;54:407-17.
[233] Oquendo-Di Cosola V, Olivieri F, Ruiz-García L. A systematic review of the impact of green walls on urban comfort: temperature reduction and noise attenuation. Renewable and Sustainable Energy Reviews. 2022;162:112463.
[234] Djongyang N, Tchinda R, Njomo D. Thermal comfort: A review paper. Renewable and Sustainable Energy Reviews. 2010;14(9):2626-40.
[235] Ye G, Yang C, Chen Y, Li Y. A new approach for measuring predicted mean vote (PMV) and standard effective temperature (SET∗). Building and Environment. 2003;38(1):33-44.
[236] Humphreys MA, Fergus Nicol J. The validity of ISO-PMV for predicting comfort votes in every-day thermal environments. Energy and Buildings. 2002;34(6):667-84.
[237] IPCC. AR6 Synthesis Report: Climate Change 2023. 2022.
[238] Hirano Y, Ihara T, Gomi K, Fujita T. Simulation-Based Evaluation of the Effect of Green Roofs in Office Building Districts on Mitigating the Urban Heat Island Effect and Reducing CO2 Emissions. Sustainability2019.

[239] Zhang B, Xie G-d, Gao J-x, Yang Y. The cooling effect of urban green spaces as a contribution to energy-saving and emission-reduction: A case study in Beijing, China. Building and Environment. 2014;76:37-43.
[240] Pan W, Li K, Teng Y. Rethinking system boundaries of the life cycle carbon emissions of buildings. Renewable and Sustainable Energy Reviews. 2018;90:379-90.
[241] Roh S, Tae S, Suk SJ, Ford G, Shin S. Development of a building life cycle carbon emissions assessment program (BEGAS 2.0) for Korea′s green building index certification system. Renewable and Sustainable Energy Reviews. 2016;53:954-65.
[242] Chau CK, Leung TM, Ng WY. A review on Life Cycle Assessment, Life Cycle Energy Assessment and Life Cycle Carbon Emissions Assessment on buildings. Applied Energy. 2015;143:395-413.
[243] Köne AÇ, Büke T. Forecasting of CO2 emissions from fuel combustion using trend analysis. Renewable and Sustainable Energy Reviews. 2010;14(9):2906-15.
[244] Claus K, Rousseau S. Public versus private incentives to invest in green roofs: A cost benefit analysis for Flanders. Urban Forestry & Urban Greening. 2012;11(4):417-25.
[245] Bianchini F, Hewage K. Probabilistic social cost-benefit analysis for green roofs: A lifecycle approach. Building and Environment. 2012;58:152-62.
[246] Bhandari SB. Discounted payback period-some extensions. Journal of Business and Behavioral Sciences. 2009;21(1):28-38.
[247] Synnefa A, Dandou A, Santamouris M, Tombrou M, Soulakellis N. On the use of cool materials as a heat island mitigation strategy. Journal of Applied Meteorology and Climatology. 2008;47(11):2846-56.
[248] Karlessi T, Santamouris M, Apostolakis K, Synnefa A, Livada I. Development and testing of thermochromic coatings for buildings and urban structures. Solar Energy. 2009;83(4):538-51.
[249] Park J, Kim J-H, Lee DK, Park CY, Jeong SG. The influence of small green space type and structure at the street level on urban heat island mitigation. Urban forestry & urban greening. 2017;21:203-12.
[250] Susca T, Gaffin SR, Dell'Osso GR. Positive effects of vegetation: Urban heat island and green roofs. Environmental pollution. 2011;159(8-9):2119-26.
[251] Zhang Y, Murray AT, Turner Ii BL. Optimizing green space locations to reduce daytime and nighttime urban heat island effects in Phoenix, Arizona. Landscape and Urban Planning. 2017;165:162-71.
[252] Karlessi T, Santamouris M, Synnefa A, Assimakopoulos D, Didaskalopoulos P, Apostolakis K. Development and testing of PCM doped cool colored coatings to mitigate urban heat island and cool buildings. Building and environment. 2011;46(3):570-6.
[253] Guan B, Ma B, Qin F. Application of asphalt pavement with phase change materials to mitigate urban heat island effect. Conference Application of asphalt pavement with phase change materials to mitigate urban heat island effect, vol. 3. IEEE, p. 2389-92.
[254] Salamanca F, Georgescu M, Mahalov A, Moustaoui M, Wang M, Svoma BM. Assessing summertime urban air conditioning consumption in a semiarid environment. Environmental Research Letters. 2013;8(3):034022.
[255] Wang Y, Chen L, Kubota J. The relationship between urbanization, energy use and carbon emissions: evidence from a panel of Association of Southeast Asian Nations (ASEAN) countries. Journal of Cleaner Production. 2016;112:1368-74.

[256] Hassan AM, Elmokadem AA, Megahed NA, Eleinen OMA. Urban morphology as a passive strategy in promoting outdoor air quality. Journal of Building Engineering. 2020;29:101204.
[257] Akbari H, Levinson R, Rainer L. Monitoring the energy-use effects of cool roofs on California commercial buildings. Energy and Buildings. 2005;37(10):1007-16.
[258] Akbari H, Cartalis C, Kolokotsa D, Muscio A, Pisello AL, Rossi F, et al. Local climate change and urban heat island mitigation techniques–the state of the art. Journal of Civil Engineering and Management. 2016;22(1):1-16.
[259] Seiwert A, Rößler S. Understanding the term green infrastructure: origins, rationales, semantic content and purposes as well as its relevance for application in spatial planning. Land Use Policy. 2020;97:104785.
[260] Shafique M, Kim R, Rafiq M. Green roof benefits, opportunities and challenges – A review. Renewable and Sustainable Energy Reviews. 2018;90:757-73.
[261] Stovin V, Vesuviano G, Kasmin H. The hydrological performance of a green roof test bed under UK climatic conditions. Journal of Hydrology. 2012;414-415:148-61.
[262] Marando F, Salvatori E, Sebastiani A, Fusaro L, Manes F. Regulating ecosystem services and green infrastructure: Assessment of urban heat island effect mitigation in the municipality of Rome, Italy. Ecological Modelling. 2019;392:92-102.
[263] Herath H, Halwatura RU, Jayasinghe GY. Evaluation of green infrastructure effects on tropical Sri Lankan urban context as an urban heat island adaptation strategy. Urban Forestry & Urban Greening. 2018;29:212-22.
[264] Aboelata A, Sodoudi S. Evaluating urban vegetation scenarios to mitigate urban heat island and reduce buildings' energy in dense built-up areas in Cairo. Building and Environment. 2019;166:106407.
[265] Chun B, Guldmann J-M. Impact of greening on the urban heat island: Seasonal variations and mitigation strategies. Computers, Environment and Urban Systems. 2018;71:165-76.
[266] Kim H, Gu D, Kim HY. Effects of Urban Heat Island mitigation in various climate zones in the United States. Sustainable Cities and Society. 2018;41:841-52.
[267] Razzaghmanesh M, Beecham S, Salemi T. The role of green roofs in mitigating Urban Heat Island effects in the metropolitan area of Adelaide, South Australia. Urban Forestry & Urban Greening. 2016;15:89-102.
[268] Bianchini F, Hewage K. How "green" are the green roofs? Lifecycle analysis of green roof materials. Building and Environment. 2012;48:57-65.
[269] Kosareo L, Ries R. Comparative environmental life cycle assessment of green roofs. Building and Environment. 2007;42(7):2606-13.
[270] Jeanjean APR, Buccolieri R, Eddy J, Monks PS, Leigh RJ. Air quality affected by trees in real street canyons: The case of Marylebone neighbourhood in central London. Urban Forestry & Urban Greening. 2017;22:41-53.
[271] Ignatius M, Wong NH, Jusuf SK. Urban microclimate analysis with consideration of local ambient temperature, external heat gain, urban ventilation, and outdoor thermal comfort in the tropics. Sustainable Cities and Society. 2015;19:121-35.
[272] Cheng V, Ng E, Chan C, Givoni B. Outdoor thermal comfort study in a sub-tropical climate: a longitudinal study based in Hong Kong. International journal of biometeorology. 2012;56(1):43-56.
[273] Erell E, Pearlmutter D, Williamson T. Urban microclimate: designing the spaces between buildings: Routledge, 2012.

[274] Synnefa A, Santamouris M. Advances on technical, policy and market aspects of cool roof technology in Europe: The Cool Roofs project. Energy and Buildings. 2012;55:35-41.
[275] Kolokotsa D, Maravelaki-Kalaitzaki P, Papantoniou S, Vangeloglou E, Saliari M, Karlessi T, et al. Development and analysis of mineral based coatings for buildings and urban structures. Solar energy. 2012;86(5):1648-59.
[276] Hodo-Abalo S, Banna M, Zeghmati B. Performance analysis of a planted roof as a passive cooling technique in hot-humid tropics. Renewable Energy. 2012;39(1):140-8.
[277] Zingre KT, Wan MP, Tong S, Li H, Chang VWC, Wong SK, et al. Modeling of cool roof heat transfer in tropical climate. Renewable Energy. 2015;75:210-23.
[278] Li D, Zheng Y, Liu C, Wu G. Numerical analysis on thermal performance of roof contained PCM of a single residential building. Energy Conversion and Management. 2015;100:147-56.
[279] Chou H-M, Chen C-R, Nguyen V-L. A new design of metal-sheet cool roof using PCM. Energy and Buildings. 2013;57:42-50.
[280] Pasupathy A, Velraj R. Effect of double layer phase change material in building roof for year round thermal management. Energy and Buildings. 2008;40(3):193-203.
[281] Yang J, Mohan Kumar Dl, Pyrgou A, Chong A, Santamouris M, Kolokotsa D, et al. Green and cool roofs' urban heat island mitigation potential in tropical climate. Solar Energy. 2018;173:597-609.
[282] Chung MH, Park JC. Development of PCM cool roof system to control urban heat island considering temperate climatic conditions. Energy and Buildings. 2016;116:341-8.
[283] Roman KK, O'Brien T, Alvey JB, Woo O. Simulating the effects of cool roof and PCM (phase change materials) based roof to mitigate UHI (urban heat island) in prominent US cities. Energy. 2016;96:103-17.
[284] Yang YK, Kang IS, Chung MH, Kim S, Park JC. Effect of PCM cool roof system on the reduction in urban heat island phenomenon. Building and Environment. 2017;122:411-21.
[285] Meng E, Wang J, Yu H, Cai R, Chen Y, Zhou B. Experimental study of the thermal protection performance of the high reflectivity-phase change material (PCM) roof in summer. Building and Environment. 2019;164:106381.
[286] Anting N, Din MFM, Iwao K, Ponraj M, Jungan K, Yong LY, et al. Experimental evaluation of thermal performance of cool pavement material using waste tiles in tropical climate. Energy and buildings. 2017;142:211-9.
[287] Doulos L, Santamouris M, Livada I. Passive cooling of outdoor urban spaces. The role of materials. Solar energy. 2004;77(2):231-49.
[288] Qin Y. A review on the development of cool pavements to mitigate urban heat island effect. Renewable and sustainable energy reviews. 2015;52:445-59.
[289] Wang C, Wang Z-H, Kaloush KE, Shacat J. Cool pavements for urban heat island mitigation: A synthetic review. Renewable and Sustainable Energy Reviews. 2021;146:111171.
[290] Takebayashi H, Moriyama M. Relationships between the properties of an urban street canyon and its radiant environment: Introduction of appropriate urban heat island mitigation technologies. Solar Energy. 2012;86(9):2255-62.
[291] Wang J, Meng Q, Tan K, Zhang L, Zhang Y. Experimental investigation on the influence of evaporative cooling of permeable pavements on outdoor thermal environment. Building and Environment. 2018;140:184-93.

[292] Santamouris M, Gaitani N, Spanou A, Saliari M, Giannopoulou K, Vasilakopoulou K, et al. Using cool paving materials to improve microclimate of urban areas–Design realization and results of the flisvos project. Building and Environment. 2012;53:128-36.
[293] Sen S, Roesler J, Ruddell B, Middel A. Cool Pavement Strategies for Urban Heat Island Mitigation in Suburban Phoenix, Arizona. Sustainability2019.
[294] Taleghani M, Berardi U. The effect of pavement characteristics on pedestrians' thermal comfort in Toronto. Urban Climate. 2018;24:449-59.
[295] Li H, Harvey JT, Holland TJ, Kayhanian M. The use of reflective and permeable pavements as a potential practice for heat island mitigation and stormwater management. Environmental Research Letters. 2013;8(1):015023.
[296] Chen J, Chu R, Wang H, Zhang L, Chen X, Du Y. Alleviating urban heat island effect using high-conductivity permeable concrete pavement. Journal of Cleaner Production. 2019;237:117722.
[297] Liu Y, Li T, Peng H. A new structure of permeable pavement for mitigating urban heat island. Science of The Total Environment. 2018;634:1119-25.
[298] Athukorallage B, Dissanayaka T, Senadheera S, James D. Performance analysis of incorporating phase change materials in asphalt concrete pavements. Construction and Building Materials. 2018;164:419-32.
[299] Bo G, Biao M, Fang Q. Application of asphalt pavement with phase change materials to mitigate urban heat island effect. Conference Application of asphalt pavement with phase change materials to mitigate urban heat island effect, vol. 3. p. 2389-92.
[300] Ratti C, Raydan D, Steemers K. Building form and environmental performance: archetypes, analysis and an arid climate. Energy and buildings. 2003;35(1):49-59.
[301] Farhadi H, Faizi M, Sanaieian H. Mitigating the urban heat island in a residential area in Tehran: Investigating the role of vegetation, materials, and orientation of buildings. Sustainable Cities and Society. 2019;46:101448.
[302] Behzadi A, Holmberg S, Duwig C, Haghighat F, Ooka R, Sadrizadeh S. Smart design and control of thermal energy storage in low-temperature heating and high-temperature cooling systems: A comprehensive review. Renewable and Sustainable Energy Reviews. 2022;166:112625.
[303] Klemeš JJ, Jiang P, Fan YV, Bokhari A, Wang X-C. COVID-19 pandemics Stage II – Energy and environmental impacts of vaccination. Renewable and Sustainable Energy Reviews. 2021;150:111400.
[304] Adebayo TS, AbdulKareem HKK, Bilal, Kirikkaleli D, Shah MI, Abbas S. CO2 behavior amidst the COVID-19 pandemic in the United Kingdom: The role of renewable and non-renewable energy development. Renewable Energy. 2022;189:492-501.
[305] Razmi AR, Soltani M, Ardehali A, Gharali K, Dusseault MB, Nathwani J. Design, thermodynamic, and wind assessments of a compressed air energy storage (CAES) integrated with two adjacent wind farms: A case study at Abhar and Kahak sites, Iran. Energy. 2021;221:119902.
[306] Ding Z, Wu W, Leung M. Advanced/hybrid thermal energy storage technology: material, cycle, system and perspective. Renewable and Sustainable Energy Reviews. 2021;145:111088.
[307] O'Malley C, Kikumoto H. An investigation into heat storage by adopting local climate zones and nocturnal-diurnal urban heat island differences in the Tokyo Prefecture. Sustainable Cities and Society. 2022;83:103959.

[308] Hrisko J, Ramamurthy P, Gonzalez JE. Estimating heat storage in urban areas using multispectral satellite data and machine learning. Remote Sensing of Environment. 2021;252:112125.
[309] Wang D, Shi Y, Chen G, Zeng L, Hang J, Wang Q. Urban thermal environment and surface energy balance in 3D high-rise compact urban models: Scaled outdoor experiments. Building and Environment. 2021;205:108251.
[310] Hoelscher M-T, Nehls T, Jänicke B, Wessolek G. Quantifying cooling effects of facade greening: Shading, transpiration and insulation. Energy and Buildings. 2016;114:283-90.
[311] Santamouris M. Cooling the cities – A review of reflective and green roof mitigation technologies to fight heat island and improve comfort in urban environments. Solar Energy. 2014;103:682-703.
[312] Sharma M, Whaley M, Chamberlain J, Oswald T, Schroden R, Graham A, et al. Evaluation of thermochromic elastomeric roof coatings for low-slope roofs. Energy and Buildings. 2017;155:459-66.
[313] Santamouris M, Yun GY. Recent development and research priorities on cool and super cool materials to mitigate urban heat island. Renewable Energy. 2020;161:792-807.
[314] Xie N, Li H, Abdelhady A, Harvey J. Laboratorial investigation on optical and thermal properties of cool pavement nano-coatings for urban heat island mitigation. Building and Environment. 2019;147:231-40.
[315] Habibi S, Obonyo EA, Memari AM. Design and development of energy efficient re-roofing solutions. Renewable Energy. 2020;151:1209-19.
[316] Gartland LM. Heat islands: understanding and mitigating heat in urban areas: Routledge, 2012.
[317] Eleni PN, Katsavou I, Krokida MK, Polyzois GL, Gettleman L. Mechanical behavior of facial prosthetic elastomers after outdoor weathering. Dental Materials. 2009;25(12):1493-502.
[318] Bretz S, Akbari H, Rosenfeld A. Practical issues for using solar-reflective materials to mitigate urban heat islands. Atmospheric Environment. 1998;32(1):95-101.
[319] Gaffin SR, Imhoff M, Rosenzweig C, Khanbilvardi R, Pasqualini A, Kong AYY, et al. Bright is the new black—multi-year performance of high-albedo roofs in an urban climate. Environmental Research Letters. 2012;7(1):014029.
[320] Li G. Sensible heat thermal storage energy and exergy performance evaluations. Renewable and Sustainable Energy Reviews. 2016;53:897-923.
[321] Olivkar PR, Katekar VP, Deshmukh SS, Palatkar SV. Effect of sensible heat storage materials on the thermal performance of solar air heaters: State-of-the-art review. Renewable and Sustainable Energy Reviews. 2022;157:112085.
[322] Khan Z, Khan Z, Ghafoor A. A review of performance enhancement of PCM based latent heat storage system within the context of materials, thermal stability and compatibility. Energy Conversion and Management. 2016;115:132-58.
[323] Tao YB, He Y-L. A review of phase change material and performance enhancement method for latent heat storage system. Renewable and Sustainable Energy Reviews. 2018;93:245-59.
[324] Zeinelabdein R, Omer S, Gan G. Critical review of latent heat storage systems for free cooling in buildings. Renewable and Sustainable Energy Reviews. 2018;82:2843-68.
[325] Hu N, Li Z-R, Xu Z-W, Fan L-W. Rapid charging for latent heat thermal energy storage: A state-of-the-art review of close-contact melting. Renewable and Sustainable Energy Reviews. 2022;155:111918.

[326] N'Tsoukpoe KE, Kuznik F. A reality check on long-term thermochemical heat storage for household applications. Renewable and Sustainable Energy Reviews. 2021;139:110683.
[327] Gbenou TRS, Fopah-Lele A, Wang K. Macroscopic and microscopic investigations of low-temperature thermochemical heat storage reactors: A review. Renewable and Sustainable Energy Reviews. 2022;161:112152.
[328] Li W, Klemeš JJ, Wang Q, Zeng M. Salt hydrate–based gas-solid thermochemical energy storage: Current progress, challenges, and perspectives. Renewable and Sustainable Energy Reviews. 2022;154:111846.
[329] Marín PE, Milian Y, Ushak S, Cabeza LF, Grágeda M, Shire GSF. Lithium compounds for thermochemical energy storage: A state-of-the-art review and future trends. Renewable and Sustainable Energy Reviews. 2021;149:111381.
[330] Han X, Wang L, Ling H, Ge Z, Lin X, Dai X, et al. Critical review of thermochemical energy storage systems based on cobalt, manganese, and copper oxides. Renewable and Sustainable Energy Reviews. 2022;158:112076.
[331] Bennici S, Polimann T, Ondarts M, Gonze E, Vaulot C, Le Pierrès N. Long-term impact of air pollutants on thermochemical heat storage materials. Renewable and Sustainable Energy Reviews. 2020;117:109473.
[332] Ahmed N, Elfeky KE, Lu L, Wang QW. Thermal and economic evaluation of thermocline combined sensible-latent heat thermal energy storage system for medium temperature applications. Energy Conversion and Management. 2019;189:14-23.
[333] Tatsidjodoung P, Le Pierrès N, Luo L. A review of potential materials for thermal energy storage in building applications. Renewable and Sustainable Energy Reviews. 2013;18:327-49.
[334] Fallahi A, Guldentops G, Tao M, Granados-Focil S, Van Dessel S. Review on solid-solid phase change materials for thermal energy storage: Molecular structure and thermal properties. Applied Thermal Engineering. 2017;127:1427-41.
[335] Mohamed SA, Al-Sulaiman FA, Ibrahim NI, Zahir MH, Al-Ahmed A, Saidur R, et al. A review on current status and challenges of inorganic phase change materials for thermal energy storage systems. Renewable and Sustainable Energy Reviews. 2017;70:1072-89.
[336] Prieto C, Cooper P, Fernández AI, Cabeza LF. Review of technology: Thermochemical energy storage for concentrated solar power plants. Renewable and Sustainable Energy Reviews. 2016;60:909-29.
[337] Khalilpour R, Vassallo A. Planning and operation scheduling of PV-battery systems: A novel methodology. Renewable and Sustainable Energy Reviews. 2016;53:194-208.
[338] Han X, Garrison J, Hug G. Techno-economic analysis of PV-battery systems in Switzerland. Renewable and Sustainable Energy Reviews. 2022;158:112028.
[339] Freitas Gomes IS, Perez Y, Suomalainen E. Coupling small batteries and PV generation: A review. Renewable and Sustainable Energy Reviews. 2020;126:109835.
[340] Shubbak MH. Advances in solar photovoltaics: Technology review and patent trends. Renewable and Sustainable Energy Reviews. 2019;115:109383.
[341] Jurasz J, Ceran B, Orłowska A. Component degradation in small-scale off-grid PV-battery systems operation in terms of reliability, environmental impact and economic performance. Sustainable Energy Technologies and Assessments. 2020;38:100647.
[342] Mehrabankhomartash M, Rayati M, Sheikhi A, Ranjbar AM. Practical battery size optimization of a PV system by considering individual customer

damage function. Renewable and Sustainable Energy Reviews. 2017;67:36-50.
[343] Gonzalez-Moreno A, Marcos J, de la Parra I, Marroyo L. A PV ramp-rate control strategy to extend battery lifespan using forecasting. Applied Energy. 2022;323:119546.
[344] Zia MF, Nasir M, Elbouchikhi E, Benbouzid M, Vasquez JC, Guerrero JM. Energy management system for a hybrid PV-Wind-Tidal-Battery-based islanded DC microgrid: Modeling and experimental validation. Renewable and Sustainable Energy Reviews. 2022;159:112093.
[345] Shabani M, Dahlquist E, Wallin F, Yan J. Techno-economic impacts of battery performance models and control strategies on optimal design of a grid-connected PV system. Energy Conversion and Management. 2021;245:114617.
[346] Ibrahim KH, Hassan AY, AbdElrazek AS, Saleh SM. Economic analysis of stand-alone PV-battery system based on new power assessment configuration in Siwa Oasis – Egypt. Alexandria Engineering Journal. 2023;62:181-91.
[347] Bergner J, Weniger J, Tjaden T, Quaschning V. Feed-in power limitation of grid-connected PV battery systems with autonomous forecast-based operation strategies. Conference Feed-in power limitation of grid-connected PV battery systems with autonomous forecast-based operation strategies. p. 2363-70.
[348] Fernández-Yáñez P, Romero V, Armas O, Cerretti G. Thermal management of thermoelectric generators for waste energy recovery. Applied Thermal Engineering. 2021;196:117291.
[349] Jaziri N, Boughamoura A, Müller J, Mezghani B, Tounsi F, Ismail M. A comprehensive review of Thermoelectric Generators: Technologies and common applications. Energy Reports. 2020;6:264-87.
[350] Siddique ARM, Mahmud S, Heyst BV. A review of the state of the science on wearable thermoelectric power generators (TEGs) and their existing challenges. Renewable and Sustainable Energy Reviews. 2017;73:730-44.
[351] Twaha S, Zhu J, Yan Y, Li B. A comprehensive review of thermoelectric technology: Materials, applications, modelling and performance improvement. Renewable and Sustainable Energy Reviews. 2016;65:698-726.
[352] Wang Y, Li S, Zhang Y, Yang X, Deng Y, Su C. The influence of inner topology of exhaust heat exchanger and thermoelectric module distribution on the performance of automotive thermoelectric generator. Energy Conversion and Management. 2016;126:266-77.
[353] Tian H, Sun X, Jia Q, Liang X, Shu G, Wang X. Comparison and parameter optimization of a segmented thermoelectric generator by using the high temperature exhaust of a diesel engine. Energy. 2015;84:121-30.
[354] Bai S, Lu H, Wu T, Yin X, Shi X, Chen L. Numerical and experimental analysis for exhaust heat exchangers in automobile thermoelectric generators. Case Studies in Thermal Engineering. 2014;4:99-112.
[355] Karri MA, Thacher EF, Helenbrook BT. Exhaust energy conversion by thermoelectric generator: Two case studies. Energy Conversion and Management. 2011;52(3):1596-611.
[356] Liu C, Pan X, Zheng X, Yan Y, Li W. An experimental study of a novel prototype for two-stage thermoelectric generator from vehicle exhaust. Journal of the Energy Institute. 2016;89(2):271-81.
[357] Du Q, Diao H, Niu Z, Zhang G, Shu G, Jiao K. Effect of cooling design on the characteristics and performance of thermoelectric generator used for internal combustion engine. Energy Conversion and Management. 2015;101:9-18.

[358] Thielen M, Sigrist L, Magno M, Hierold C, Benini L. Human body heat for powering wearable devices: From thermal energy to application. Energy Conversion and Management. 2017;131:44-54.
[359] Siddique ARM, Rabari R, Mahmud S, Heyst BV. Thermal energy harvesting from the human body using flexible thermoelectric generator (FTEG) fabricated by a dispenser printing technique. Energy. 2016;115:1081-91.
[360] Qing S, Rezania A, Rosendahl LA, Gou X. Design of flexible thermoelectric generator as human body sensor. Materials Today: Proceedings. 2018;5(4, Part 1):10338-46.
[361] Guan M, Wang K, Xu D, Liao W-H. Design and experimental investigation of a low-voltage thermoelectric energy harvesting system for wireless sensor nodes. Energy Conversion and Management. 2017;138:30-7.
[362] Iezzi B, Ankireddy K, Twiddy J, Losego MD, Jur JS. Printed, metallic thermoelectric generators integrated with pipe insulation for powering wireless sensors. Applied Energy. 2017;208:758-65.
[363] Parás-Hernández FU, Fabián-Mijangos A, Cardona-Castro MA, Alvarez-Quintana J. Enhanced performance nanostructured thermoelectric converter for self-powering health sensors. Nano Energy. 2020;74:104854.
[364] Li G, Shittu S, Diallo TMO, Yu M, Zhao X, Ji J. A review of solar photovoltaic-thermoelectric hybrid system for electricity generation. Energy. 2018;158:41-58.
[365] Tuoi TTK, Toan NV, Ono T. Theoretical and experimental investigation of a thermoelectric generator (TEG) integrated with a phase change material (PCM) for harvesting energy from ambient temperature changes. Energy Reports. 2020;6:2022-9.
[366] Byon Y-S, Jeong J-W. Phase change material-integrated thermoelectric energy harvesting block as an independent power source for sensors in buildings. Renewable and Sustainable Energy Reviews. 2020;128:109921.
[367] Cui T, Xuan Y, Li Q. Design of a novel concentrating photovoltaic–thermoelectric system incorporated with phase change materials. Energy Conversion and Management. 2016;112:49-60.
[368] Riffat SB, Ma X. Thermoelectrics: a review of present and potential applications. Applied thermal engineering. 2003;23(8):913-35.
[369] Bjørk R, Nielsen KK. The maximum theoretical performance of unconcentrated solar photovoltaic and thermoelectric generator systems. Energy Conversion and Management. 2018;156:264-8.
[370] Ju X, Wang Z, Flamant G, Li P, Zhao W. Numerical analysis and optimization of a spectrum splitting concentration photovoltaic–thermoelectric hybrid system. Solar Energy. 2012;86(6):1941-54.
[371] Kraemer D, Hu L, Muto A, Chen X, Chen G, Chiesa M. Photovoltaic-thermoelectric hybrid systems: A general optimization methodology. Applied Physics Letters. 2008;92(24):243503.
[372] Wang N, Han L, He H, Park N-H, Koumoto K. A novel high-performance photovoltaic–thermoelectric hybrid device. Energy & Environmental Science. 2011;4(9):3676-9.
[373] Babu C, Ponnambalam P. The theoretical performance evaluation of hybrid PV-TEG system. Energy Conversion and Management. 2018;173:450-60.
[374] Zhang H, Yue H, Huang J, Liang K, Chen H. Experimental studies on a low concentrating photovoltaic/thermal (LCPV/T) collector with a thermoelectric generator (TEG) module. Renewable Energy. 2021;171:1026-40.
[375] Alian Fini M, Gharapetian D, Asgari M. Efficiency improvement of hybrid PV-TEG system based on an energy, exergy, energy-economic and

environmental analysis; experimental, mathematical and numerical approaches. Energy Conversion and Management. 2022;265:115767.
[376] Bjørk R, Nielsen KK. The performance of a combined solar photovoltaic (PV) and thermoelectric generator (TEG) system. Solar Energy. 2015;120:187-94.
[377] Ko J, Jeong J-W. Annual performance evaluation of thermoelectric generator-assisted building-integrated photovoltaic system with phase change material. Renewable and Sustainable Energy Reviews. 2021;145:111085.
[378] Shaikh FK, Zeadally S. Energy harvesting in wireless sensor networks: A comprehensive review. Renewable and Sustainable Energy Reviews. 2016;55:1041-54.
[379] Liu A, Zou J, Wu Z, Wang Y, Tian Y, Xie H. Enhancing the performance of TEG system coupled with PCMs by regulating the interfacial thermal conduction. Energy Reports. 2020;6:1942-9.
[380] Yin E, Li Q, Li D, Xuan Y. Experimental investigation on effects of thermal resistances on a photovoltaic-thermoelectric system integrated with phase change materials. Energy. 2019;169:172-85.
[381] Darkwa J, Calautit J, Du D, Kokogianakis G. A numerical and experimental analysis of an integrated TEG-PCM power enhancement system for photovoltaic cells. Applied Energy. 2019;248:688-701.
[382] Dincer I, Dost S, Li X. Performance analyses of sensible heat storage systems for thermal applications. International Journal of Energy Research. 1997;21(12):1157-71.
[383] Joshi SS, Dhoble AS. Photovoltaic -Thermal systems (PVT): Technology review and future trends. Renewable and Sustainable Energy Reviews. 2018;92:848-82.
[384] Kumar A, Baredar P, Qureshi U. Historical and recent development of photovoltaic thermal (PVT) technologies. Renewable and Sustainable Energy Reviews. 2015;42:1428-36.
[385] Sathe TM, Dhoble AS. A review on recent advancements in photovoltaic thermal techniques. Renewable and Sustainable Energy Reviews. 2017;76:645-72.
[386] Tiwari A, Sodha MS. Performance evaluation of solar PV/T system: an experimental validation. Solar energy. 2006;80(7):751-9.
[387] Sohel MI, Ma Z, Cooper P, Adams J, Scott R. A dynamic model for air-based photovoltaic thermal systems working under real operating conditions. Applied Energy. 2014;132:216-25.
[388] Ibrahim A, Fudholi A, Sopian K, Othman MY, Ruslan MH. Efficiencies and improvement potential of building integrated photovoltaic thermal (BIPVT) system. Energy Conversion and Management. 2014;77:527-34.
[389] Yu G, Yang H, Yan Z, Kyeredey Ansah M. A review of designs and performance of façade-based building integrated photovoltaic-thermal (BIPVT) systems. Applied Thermal Engineering. 2021;182:116081.
[390] Xu L, Luo K, Ji J, Yu B, Li Z, Huang S. Study of a hybrid BIPV/T solar wall system. Energy. 2020;193:116578.
[391] Koyunbaba BK, Yilmaz Z, Ulgen K. An approach for energy modeling of a building integrated photovoltaic (BIPV) Trombe wall system. Energy and Buildings. 2013;67:680-8.
[392] Hu Z, He W, Ji J, Hu D, Lv S, Chen H, et al. Comparative study on the annual performance of three types of building integrated photovoltaic (BIPV) Trombe wall system. Applied Energy. 2017;194:81-93.
[393] Wajs J, Golabek A, Bochniak R, Mikielewicz D. Air-cooled photovoltaic roof tile as an example of the BIPVT system – An experimental study on the energy and exergy performance. Energy. 2020;197:117255.

[394] Tiwari GN, Saini H, Tiwari A, Deo A, Gupta N, Saini PS. Periodic theory of building integrated photovoltaic thermal (BiPVT) system. Solar Energy. 2016;125:373-80.
[395] Chen F, Yin H. Fabrication and laboratory-based performance testing of a building-integrated photovoltaic-thermal roofing panel. Applied Energy. 2016;177:271-84.
[396] Barman S, Chowdhury A, Mathur S, Mathur J. Assessment of the efficiency of window integrated CdTe based semi-transparent photovoltaic module. Sustainable Cities and Society. 2018;37:250-62.
[397] Do SL, Shin M, Baltazar J-C, Kim J. Energy benefits from semi-transparent BIPV window and daylight-dimming systems for IECC code-compliance residential buildings in hot and humid climates. Solar Energy. 2017;155:291-303.
[398] Ghosh A, Sarmah N, Sundaram S, Mallick TK. Numerical studies of thermal comfort for semi-transparent building integrated photovoltaic (BIPV)-vacuum glazing system. Solar Energy. 2019;190:608-16.
[399] Ghosh A, Sundaram S, Mallick TK. Colour properties and glazing factors evaluation of multicrystalline based semi-transparent Photovoltaic-vacuum glazing for BIPV application. Renewable Energy. 2019;131:730-6.
[400] Akbari Paydar M. Optimum design of building integrated PV module as a movable shading device. Sustainable Cities and Society. 2020;62:102368.
[401] Hong T, Koo C, Oh J, Jeong K. Nonlinearity analysis of the shading effect on the technical–economic performance of the building-integrated photovoltaic blind. Applied Energy. 2017;194:467-80.
[402] Jayathissa P, Luzzatto M, Schmidli J, Hofer J, Nagy Z, Schlueter A. Optimising building net energy demand with dynamic BIPV shading. Applied Energy. 2017;202:726-35.
[403] Buonomano A, Calise F, Palombo A, Vicidomini M. BIPVT systems for residential applications: An energy and economic analysis for European climates. Applied Energy. 2016;184:1411-31.
[404] Sharples S, Radhi H. Assessing the technical and economic performance of building integrated photovoltaics and their value to the GCC society. Renewable Energy. 2013;55:150-9.
[405] Eltawil MA, Zhao Z. Grid-connected photovoltaic power systems: Technical and potential problems—A review. Renewable and Sustainable Energy Reviews. 2010;14(1):112-29.
[406] Ortega MJ, Hernández JC, García OG. Measurement and assessment of power quality characteristics for photovoltaic systems: Harmonics, flicker, unbalance, and slow voltage variations. Electric Power Systems Research. 2013;96:23-35.
[407] Karimi M, Mokhlis H, Naidu K, Uddin S, Bakar AHA. Photovoltaic penetration issues and impacts in distribution network – A review. Renewable and Sustainable Energy Reviews. 2016;53:594-605.
[408] Azadian F, Radzi MAM. A general approach toward building integrated photovoltaic systems and its implementation barriers: A review. Renewable and Sustainable Energy Reviews. 2013;22:527-38.
[409] Tsantopoulos G, Arabatzis G, Tampakis S. Public attitudes towards photovoltaic developments: Case study from Greece. Energy Policy. 2014;71:94-106.
[410] Curtius HC. The adoption of building-integrated photovoltaics: barriers and facilitators. Renewable Energy. 2018;126:783-90.
[411] Azarova V, Cohen J, Friedl C, Reichl J. Designing local renewable energy communities to increase social acceptance: Evidence from a choice experiment in Austria, Germany, Italy, and Switzerland. Energy Policy. 2019;132:1176-83.

[412] Heras-Saizarbitoria I, Cilleruelo E, Zamanillo I. Public acceptance of renewables and the media: an analysis of the Spanish PV solar experience. Renewable and Sustainable Energy Reviews. 2011;15(9):4685-96.
[413] Hille SL, Curtius HC, Wüstenhagen R. Red is the new blue – The role of color, building integration and country-of-origin in homeowners' preferences for residential photovoltaics. Energy and Buildings. 2018;162:21-31.
[414] Delisle V, Kummert M. Cost-benefit analysis of integrating BIPV-T air systems into energy-efficient homes. Solar Energy. 2016;136:385-400.
[415] Tripathy M, Joshi H, Panda SK. Energy payback time and life-cycle cost analysis of building integrated photovoltaic thermal system influenced by adverse effect of shadow. Applied Energy. 2017;208:376-89.
[416] Shirazi AM, Zomorodian ZS, Tahsildoost M. Techno-economic BIPV evaluation method in urban areas. Renewable Energy. 2019;143:1235-46.
[417] Yang RJ. Overcoming technical barriers and risks in the application of building integrated photovoltaics (BIPV): hardware and software strategies. Automation in Construction. 2015;51:92-102.
[418] Agathokleous RA, Kalogirou SA. Status, barriers and perspectives of building integrated photovoltaic systems. Energy. 2020;191:116471.
[419] Kalogirou SA, Tripanagnostopoulos Y. Hybrid PV/T solar systems for domestic hot water and electricity production. Energy Conversion and Management. 2006;47(18):3368-82.
[420] He W, Zhang Y, Ji J. Comparative experiment study on photovoltaic and thermal solar system under natural circulation of water. Applied Thermal Engineering. 2011;31(16):3369-76.
[421] Brottier L, Bennacer R. Thermal performance analysis of 28 PVT solar domestic hot water installations in Western Europe. Renewable Energy. 2020;160:196-210.
[422] Praveen kumar B, Prince Winston D, Pounraj P, Muthu Manokar A, Sathyamurthy R, Kabeel AE. Experimental investigation on hybrid PV/T active solar still with effective heating and cover cooling method. Desalination. 2018;435:140-51.
[423] Zondag HA, de Vries DW, van Helden WGJ, van Zolingen RJC, van Steenhoven AA. The thermal and electrical yield of a PV-thermal collector. Solar Energy. 2002;72(2):113-28.
[424] Zondag HA, de Vries DW, van Helden WGJ, van Zolingen RJC, van Steenhoven AA. The yield of different combined PV-thermal collector designs. Solar Energy. 2003;74(3):253-69.
[425] Singh DB, Yadav JK, Dwivedi VK, Kumar S, Tiwari GN, Al-Helal IM. Experimental studies of active solar still integrated with two hybrid PVT collectors. Solar Energy. 2016;130:207-23.
[426] Li M, Zhong D, Ma T, Kazemian A, Gu W. Photovoltaic thermal module and solar thermal collector connected in series: Energy and exergy analysis. Energy Conversion and Management. 2020;206:112479.
[427] Tembhare SP, Barai DP, Bhanvase BA. Performance evaluation of nanofluids in solar thermal and solar photovoltaic systems: A comprehensive review. Renewable and Sustainable Energy Reviews. 2022;153:111738.
[428] Mahian O, Kianifar A, Kalogirou SA, Pop I, Wongwises S. A review of the applications of nanofluids in solar energy. International Journal of Heat and Mass Transfer. 2013;57(2):582-94.
[429] Rejeb O, Shittu S, Li G, Ghenai C, Zhao X, Ménézo C, et al. Comparative investigation of concentrated photovoltaic thermal-thermoelectric with nanofluid cooling. Energy Conversion and Management. 2021;235:113968.
[430] Menon GS, Murali S, Elias J, Aniesrani Delfiya DS, Alfiya PV, Samuel MP. Experimental investigations on unglazed photovoltaic-thermal (PVT)

system using water and nanofluid cooling medium. Renewable Energy. 2022;188:986-96.
[431] Meraje WC, Huang C-C, Barman J, Huang C-Y, Kuo C-FJ. Design and experimental study of a Fresnel lens-based concentrated photovoltaic thermal system integrated with nanofluid spectral splitter. Energy Conversion and Management. 2022;258:115455.
[432] Li B, Hong W, Li H, Lan J, Zi J. Optimized energy distribution management in the nanofluid-assisted photovoltaic/thermal system via exergy efficiency analysis. Energy. 2022;242:123018.
[433] An W, Zhang J, Zhu T, Gao N. Investigation on a spectral splitting photovoltaic/thermal hybrid system based on polypyrrole nanofluid: Preliminary test. Renewable Energy. 2016;86:633-42.
[434] Jidhesh P, Arjunan TV, Gunasekar N. Thermal modeling and experimental validation of semitransparent photovoltaic- thermal hybrid collector using CuO nanofluid. Journal of Cleaner Production. 2021;316:128360.
[435] Sardarabadi M, Passandideh-Fard M, Zeinali Heris S. Experimental investigation of the effects of silica/water nanofluid on PV/T (photovoltaic thermal units). Energy. 2014;66:264-72.
[436] Jing D, Hu Y, Liu M, Wei J, Guo L. Preparation of highly dispersed nanofluid and CFD study of its utilization in a concentrating PV/T system. Solar Energy. 2015;112:30-40.
[437] Moradgholi M, Mostafa Nowee S, Farzaneh A. Experimental study of using Al2O3/methanol nanofluid in a two phase closed thermosyphon (TPCT) array as a novel photovoltaic/thermal system. Solar Energy. 2018;164:243-50.
[438] Kazemian A, Khatibi M, Reza Maadi S, Ma T. Performance optimization of a nanofluid-based photovoltaic thermal system integrated with nano-enhanced phase change material. Applied Energy. 2021;295:116859.
[439] Ghadiri M, Sardarabadi M, Pasandideh-fard M, Moghadam AJ. Experimental investigation of a PVT system performance using nano ferrofluids. Energy Conversion and Management. 2015;103:468-76.
[440] Shahsavar A, Jha P, Arıcı M, Estellé P. Experimental investigation of the usability of the rifled serpentine tube to improve energy and exergy performances of a nanofluid-based photovoltaic/thermal system. Renewable Energy. 2021;170:410-25.
[441] Hassani S, Saidur R, Mekhilef S, Taylor RA. Environmental and exergy benefit of nanofluid-based hybrid PV/T systems. Energy Conversion and Management. 2016;123:431-44.
[442] Varmira K, Baseri MM, Khanmohammadi S, Hamelian M, Shahsavar A. Experimental study of the effect of sheet-and-sinusoidal tube collector on the energetic and exergetic performance of a photovoltaic-thermal unit filled with biologically synthesized water/glycerol-silver nanofluid. Applied Thermal Engineering. 2021;186:116518.
[443] Arifin Z, Prasetyo SD, Tjahjana DDDP, Rachmanto RA, Prabowo AR, Alfaiz NF. The application of TiO2 nanofluids in photovoltaic thermal collector systems. Energy Reports. 2022;8:1371-80.
[444] Wole-Osho I, Adun H, Adedeji M, Okonkwo EC, Kavaz D, Dagbasi M. Effect of hybrid nanofluids mixture ratio on the performance of a photovoltaic thermal collector. International Journal of Energy Research. 2020;44(11):9064-81.
[445] Adun H, Adedeji M, Ruwa T, Senol M, Kavaz D, Dagbasi M. Energy, exergy, economic, environmental (4E) approach to assessing the performance of a photovoltaic-thermal system using a novel ternary nanofluid. Sustainable Energy Technologies and Assessments. 2022;50:101804.

[446] Ji J, Lu J-P, Chow T-T, He W, Pei G. A sensitivity study of a hybrid photovoltaic/thermal water-heating system with natural circulation. Applied Energy. 2007;84(2):222-37.
[447] Yazdanifard F, Ameri M, Ebrahimnia-Bajestan E. Performance of nanofluid-based photovoltaic/thermal systems: A review. Renewable and Sustainable Energy Reviews. 2017;76:323-52.
[448] Fudholi A, Sopian K, Yazdi MH, Ruslan MH, Ibrahim A, Kazem HA. Performance analysis of photovoltaic thermal (PVT) water collectors. Energy Conversion and Management. 2014;78:641-51.
[449] Kasaeian A, Eshghi AT, Sameti M. A review on the applications of nanofluids in solar energy systems. Renewable and Sustainable Energy Reviews. 2015;43:584-98.
[450] Alagumalai A, Qin C, K E K V, Solomin E, Yang L, Zhang P, et al. Conceptual analysis framework development to understand barriers of nanofluid commercialization. Nano Energy. 2022;92:106736.
[451] Kim H, Kim J, Cho H. Experimental study on performance improvement of U-tube solar collector depending on nanoparticle size and concentration of Al2O3 nanofluid. Energy. 2017;118:1304-12.
[452] Bubbico R, Celata GP, D'Annibale F, Mazzarotta B, Menale C. Experimental analysis of corrosion and erosion phenomena on metal surfaces by nanofluids. Chemical Engineering Research and Design. 2015;104:605-14.
[453] Singh DB, Tiwari GN. Performance analysis of basin type solar stills integrated with N identical photovoltaic thermal (PVT) compound parabolic concentrator (CPC) collectors: A comparative study. Solar Energy. 2017;142:144-58.
[454] Cabral D. Development and performance comparison of a modified glazed CPC hybrid solar collector coupled with a bifacial PVT receiver. Applied Energy. 2022;325:119653.
[455] Hj. Othman MY, Yatim B, Sopian K, Abu Bakar MN. Performance analysis of a double-pass photovoltaic/thermal (PV/T) solar collector with CPC and fins. Renewable Energy. 2005;30(13):2005-17.
[456] Mohsenzadeh M, Hosseini R. A photovoltaic/thermal system with a combination of a booster diffuse reflector and vacuum tube for generation of electricity and hot water production. Renewable Energy. 2015;78:245-52.
[457] Ahmed OK, Bawa SM. The combined effect of nanofluid and reflective mirrors on the performance of photovoltaic/thermal solar collector. Thermal Science. 2019;23(2 Part A):573-87.
[458] Kasaeian A, Tabasi S, Ghaderian J, Yousefi H. A review on parabolic trough/Fresnel based photovoltaic thermal systems. Renewable and Sustainable Energy Reviews. 2018;91:193-204.
[459] Sonneveld PJ, Swinkels GLAM, Tuijl BAJv, Janssen HJJ, Campen J, Bot GPA. Performance of a concentrated photovoltaic energy system with static linear Fresnel lenses. Solar Energy. 2011;85(3):432-42.
[460] Chemisana D, Ibáñez M, Rosell JI. Characterization of a photovoltaic-thermal module for Fresnel linear concentrator. Energy Conversion and Management. 2011;52(10):3234-40.
[461] Xie WT, Dai YJ, Wang RZ, Sumathy K. Concentrated solar energy applications using Fresnel lenses: A review. Renewable and Sustainable Energy Reviews. 2011;15(6):2588-606.
[462] Karimi F, Xu H, Wang Z, Chen J, Yang M. Experimental study of a concentrated PV/T system using linear Fresnel lens. Energy. 2017;123:402-12.
[463] Kandilli C. Performance analysis of a novel concentrating photovoltaic combined system. Energy Conversion and Management. 2013;67:186-96.

[464] Coventry JS. Performance of a concentrating photovoltaic/thermal solar collector. Solar Energy. 2005;78(2):211-22.
[465] Singh NP, Reddy KS. Inverse heat transfer technique for estimation of focal flux distribution for a concentrating photovoltaic (CPV) square solar parabola dish collector. Renewable Energy. 2020;145:2783-95.
[466] Widyolar BK, Abdelhamid M, Jiang L, Winston R, Yablonovitch E, Scranton G, et al. Design, simulation and experimental characterization of a novel parabolic trough hybrid solar photovoltaic/thermal (PV/T) collector. Renewable Energy. 2017;101:1379-89.
[467] Karathanassis IK, Papanicolaou E, Belessiotis V, Bergeles GC. Design and experimental evaluation of a parabolic-trough concentrating photovoltaic/thermal (CPVT) system with high-efficiency cooling. Renewable Energy. 2017;101:467-83.
[468] Sharaf OZ, Orhan MF. Concentrated photovoltaic thermal (CPVT) solar collector systems: Part I – Fundamentals, design considerations and current technologies. Renewable and Sustainable Energy Reviews. 2015;50:1500-65.
[469] Arora S, Singh HP, Sahota L, Arora MK, Arya R, Singh S, et al. Performance and cost analysis of photovoltaic thermal (PVT)-compound parabolic concentrator (CPC) collector integrated solar still using CNT-water based nanofluids. Desalination. 2020;495:114595.
[470] Bellos E, Tzivanidis C. Alternative designs of parabolic trough solar collectors. Progress in Energy and Combustion Science. 2019;71:81-117.
[471] Kumar V, Shrivastava RL, Untawale SP. Fresnel lens: A promising alternative of reflectors in concentrated solar power. Renewable and Sustainable Energy Reviews. 2015;44:376-90.
[472] Sharaf OZ, Orhan MF. Concentrated photovoltaic thermal (CPVT) solar collector systems: Part II – Implemented systems, performance assessment, and future directions. Renewable and Sustainable Energy Reviews. 2015;50:1566-633.
[473] Yu Q, Chen X, Yang H. Research progress on utilization of phase change materials in photovoltaic/thermal systems: A critical review. Renewable and Sustainable Energy Reviews. 2021;149:111313.
[474] Stritih U. Increasing the efficiency of PV panel with the use of PCM. Renewable Energy. 2016;97:671-9.
[475] Tyagi VV, Buddhi D. PCM thermal storage in buildings: A state of art. Renewable and Sustainable Energy Reviews. 2007;11(6):1146-66.
[476] Preet S, Bhushan B, Mahajan T. Experimental investigation of water based photovoltaic/thermal (PV/T) system with and without phase change material (PCM). Solar Energy. 2017;155:1104-20.
[477] Modjinou M, Ji J, Yuan W, Zhou F, Holliday S, Waqas A, et al. Performance comparison of encapsulated PCM PV/T, microchannel heat pipe PV/T and conventional PV/T systems. Energy. 2019;166:1249-66.
[478] Mousavi S, Kasaeian A, Shafii MB, Jahangir MH. Numerical investigation of the effects of a copper foam filled with phase change materials in a water-cooled photovoltaic/thermal system. Energy Conversion and Management. 2018;163:187-95.
[479] Abdelrazik AS, Al-Sulaiman FA, Saidur R. Numerical investigation of the effects of the nano-enhanced phase change materials on the thermal and electrical performance of hybrid PV/thermal systems. Energy Conversion and Management. 2020;205:112449.
[480] Babayan M, Mazraeh AE, Yari M, Niazi NA, Saha SC. Hydrogen production with a photovoltaic thermal system enhanced by phase change materials, Shiraz, Iran case study. Journal of Cleaner Production. 2019;215:1262-78.
[481] Hossain MS, Pandey AK, Selvaraj J, Rahim NA, Islam MM, Tyagi VV. Two side serpentine flow based photovoltaic-thermal-phase change

materials (PVT-PCM) system: Energy, exergy and economic analysis. Renewable Energy. 2019;136:1320-36.
[482] Maatallah T, Zachariah R, Al-Amri FG. Exergo-economic analysis of a serpentine flow type water based photovoltaic thermal system with phase change material (PVT-PCM/water). Solar Energy. 2019;193:195-204.
[483] Al-Waeli AHA, Sopian K, Chaichan MT, Kazem HA, Ibrahim A, Mat S, et al. Evaluation of the nanofluid and nano-PCM based photovoltaic thermal (PVT) system: An experimental study. Energy Conversion and Management. 2017;151:693-708.
[484] Salem MR, Elsayed MM, Abd-Elaziz AA, Elshazly KM. Performance enhancement of the photovoltaic cells using Al2O3/PCM mixture and/or water cooling-techniques. Renewable Energy. 2019;138:876-90.
[485] Yao J, Xu H, Dai Y, Huang M. Performance analysis of solar assisted heat pump coupled with build-in PCM heat storage based on PV/T panel. Solar Energy. 2020;197:279-91.
[486] Lari MO, Sahin AZ. Effect of retrofitting a silver/water nanofluid-based photovoltaic/thermal (PV/T) system with a PCM-thermal battery for residential applications. Renewable Energy. 2018;122:98-107.
[487] Fiorentini M, Cooper P, Ma Z. Development and optimization of an innovative HVAC system with integrated PVT and PCM thermal storage for a net-zero energy retrofitted house. Energy and Buildings. 2015;94:21-32.
[488] Pereira R, Aelenei L. Optimization assessment of the energy performance of a BIPV/T-PCM system using Genetic Algorithms. Renewable Energy. 2019;137:157-66.
[489] Sohani A, Dehnavi A, Sayyaadi H, Hoseinzadeh S, Goodarzi E, Garcia DA, et al. The real-time dynamic multi-objective optimization of a building integrated photovoltaic thermal (BIPV/T) system enhanced by phase change materials. Journal of Energy Storage. 2022;46:103777.
[490] Kant K, Anand A, Shukla A, Sharma A. Heat transfer study of building integrated photovoltaic (BIPV) with nano-enhanced phase change materials. Journal of Energy Storage. 2020;30:101563.
[491] Liu XZYLC-QLYYWZGOoaNPCMIPTPwTACTUT. Energies2019.
[492] Elarga H, Goia F, Zarrella A, Dal Monte A, Benini E. Thermal and electrical performance of an integrated PV-PCM system in double skin façades: A numerical study. Solar Energy. 2016;136:112-24.
[493] Lin W, Ma Z, Sohel MI, Cooper P. Development and evaluation of a ceiling ventilation system enhanced by solar photovoltaic thermal collectors and phase change materials. Energy Conversion and Management. 2014;88:218-30.
[494] Chen X, Omer S, Worall M, Riffat S. Recent developments in ejector refrigeration technologies. Renewable and Sustainable Energy Reviews. 2013;19:629-51.
[495] Abdulateef JM, Sopian K, Alghoul MA, Sulaiman MY. Review on solar-driven ejector refrigeration technologies. Renewable and Sustainable Energy Reviews. 2009;13(6):1338-49.
[496] Yapıcı R, Ersoy HK. Performance characteristics of the ejector refrigeration system based on the constant area ejector flow model. Energy Conversion and Management. 2005;46(18):3117-35.
[497] Cheng Y, Wang M, Yu J. Thermodynamic analysis of a novel solar-driven booster-assisted ejector refrigeration cycle. Solar Energy. 2021;218:85-94.
[498] Salimpour MR, Ahmadzadeh A, Al-Sammarraie AT. Comparative investigation on the exergoeconomic analysis of solar-driven ejector refrigeration systems. International Journal of Refrigeration. 2019;99:80-93.
[499] Galindo J, Dolz V, Tiseira A, Ponce-Mora A. Numerical assessment of the dynamic behavior of a solar-driven jet-ejector refrigeration system

equipped with an adjustable jet-ejector. International Journal of Refrigeration. 2021;121:168-82.
[500] Beyrami J, Hakkaki-Fard A. Performance evaluation of the solar-driven multi-ejector refrigeration cycle without an auxiliary heat source. Applied Thermal Engineering. 2022;217:119214.
[501] Chua KJ, Chou SK, Yang WM. Advances in heat pump systems: A review. Applied Energy. 2010;87(12):3611-24.
[502] Hawlader MNA, Chou SK, Ullah MZ. The performance of a solar assisted heat pump water heating system. Applied thermal engineering. 2001;21(10):1049-65.
[503] Li H, Sun Y. Operational performance study on a photovoltaic loop heat pipe/solar assisted heat pump water heating system. Energy and Buildings. 2018;158:861-72.
[504] Buker Mahmut S, Riffat SB. Solar assisted heat pump systems for low temperature water heating applications: A systematic review. Renewable and Sustainable Energy Reviews. 2016;55:399-413.
[505] Bellos E, Tzivanidis C, Moschos K, Antonopoulos KA. Energetic and financial evaluation of solar assisted heat pump space heating systems. Energy Conversion and Management. 2016;120:306-19.
[506] Badescu V. Model of a thermal energy storage device integrated into a solar assisted heat pump system for space heating. Energy Conversion and Management. 2003;44(10):1589-604.
[507] Kuang YH, Wang RZ. Performance of a multi-functional direct-expansion solar assisted heat pump system. Solar Energy. 2006;80(7):795-803.
[508] Huang W, Ji J, Xu N, Li G. Frosting characteristics and heating performance of a direct-expansion solar-assisted heat pump for space heating under frosting conditions. Applied Energy. 2016;171:656-66.
[509] Huang W, Zhang T, Ji J, Xu N. Numerical study and experimental validation of a direct-expansion solar-assisted heat pump for space heating under frosting conditions. Energy and Buildings. 2019;185:224-38.
[510] Omojaro P, Breitkopf C. Direct expansion solar assisted heat pumps: A review of applications and recent research. Renewable and Sustainable Energy Reviews. 2013;22:33-45.
[511] Shi G-H, Aye L, Li D, Du X-J. Recent advances in direct expansion solar assisted heat pump systems: A review. Renewable and Sustainable Energy Reviews. 2019;109:349-66.
[512] Chaturvedi SK, Abdel-Salam TM, Sreedharan SS, Gorozabel FB. Two-stage direct expansion solar-assisted heat pump for high temperature applications. Applied Thermal Engineering. 2009;29(10):2093-9.
[513] Scarpa F, Tagliafico LA, Tagliafico G. Integrated solar-assisted heat pumps for water heating coupled to gas burners; control criteria for dynamic operation. Applied Thermal Engineering. 2011;31(1):59-68.
[514] Gan G, Riffat SB. Naturally ventilated buildings with heat recovery: CFD simulation of thermal environment. Building Services Engineering Research and Technology. 1997;18(2):67-75.
[515] Kim J-HAJ-GKJ-TDotPoaA-TPTSCwaH-RV. Energies2016.
[516] Khanmohammadi S, Shahsavar A. Energy analysis and multi-objective optimization of a novel exhaust air heat recovery system consisting of an air-based building integrated photovoltaic/thermal system and a thermal wheel. Energy Conversion and Management. 2018;172:595-610.
[517] Mardiana-Idayu A, Riffat SB. Review on heat recovery technologies for building applications. Renewable and Sustainable Energy Reviews. 2012;16(2):1241-55.
[518] Ahn J-G, Kim J-H, Kim J-T. A Study on Experimental Performance of Air-Type PV/T Collector with HRV. Energy Procedia. 2015;78:3007-12.

[519] Lazzarin RM, Gasparella A. Technical and economical analysis of heat recovery in building ventilation systems. Applied thermal engineering. 1998;18(1-2):47-67.
[520] Fernandes MS, Brites GJVN, Costa JJ, Gaspar AR, Costa VAF. Review and future trends of solar adsorption refrigeration systems. Renewable and Sustainable Energy Reviews. 2014;39:102-23.
[521] Wang RZ, Oliveira RG. Adsorption refrigeration—An efficient way to make good use of waste heat and solar energy. Progress in Energy and Combustion Science. 2006;32(4):424-58.
[522] Wang DC, Li YH, Li D, Xia YZ, Zhang JP. A review on adsorption refrigeration technology and adsorption deterioration in physical adsorption systems. Renewable and Sustainable Energy Reviews. 2010;14(1):344-53.
[523] Fadar AE, Mimet A, Pérez-García M. Modelling and performance study of a continuous adsorption refrigeration system driven by parabolic trough solar collector. Solar Energy. 2009;83(6):850-61.
[524] Xu SZ, Wang LW, Wang RZ. Thermodynamic analysis of single-stage and multi-stage adsorption refrigeration cycles with activated carbon–ammonia working pair. Energy Conversion and Management. 2016;117:31-42.
[525] Rezk ARM, Al-Dadah RK. Physical and operating conditions effects on silica gel/water adsorption chiller performance. Applied Energy. 2012;89(1):142-9.
[526] Srikhirin P, Aphornratana S, Chungpaibulpatana S. A review of absorption refrigeration technologies. Renewable and sustainable energy reviews. 2001;5(4):343-72.
[527] Fernández-Seara J, Vázquez M. Study and control of the optimal generation temperature in NH3–H2O absorption refrigeration systems. Applied Thermal Engineering. 2001;21(3):343-57.
[528] Sun D-W. Comparison of the performances of NH3-H2O, NH3-LiNO3 and NH3-NaSCN absorption refrigeration systems. Energy Conversion and Management. 1998;39(5):357-68.
[529] Zhou S, He G, Liang X, Li Y, Pang Q, Cai D. Comparison of experimental performance of absorption refrigeration cycle using NH3/LiNO3+H2O working fluids with different water component proportions. International Journal of Refrigeration. 2022;139:25-40.
[530] Jain V, Singhal A, Sachdeva G, Kachhwaha SS. Advanced exergy analysis and risk estimation of novel NH3-H2O and H2O-LiBr integrated vapor absorption refrigeration system. Energy Conversion and Management. 2020;224:113348.
[531] Mazzei MS, Mussati MC, Mussati SF. NLP model-based optimal design of LiBr–H2O absorption refrigeration systems. International Journal of Refrigeration. 2014;38:58-70.
[532] Liang Y, Li S, Yue X, Zhang X. Analysis of NH3-H2O-LiBr absorption refrigeration integrated with an electrodialysis device. Applied Thermal Engineering. 2017;115:134-40.
[533] Jin Z, Li S, Zhou R, Xu M, Jiang W, Du K. Experimental investigation on the effect of TiO2 nanoparticles on the performance of NH3 – H2O - LiBr absorption refrigeration system. International Journal of Refrigeration. 2021;131:826-33.
[534] Papadopoulos AI, Kyriakides A-S, Seferlis P, Hassan I. Absorption refrigeration processes with organic working fluid mixtures- a review. Renewable and Sustainable Energy Reviews. 2019;109:239-70.
[535] Darwish NA, Al-Hashimi SH, Al-Mansoori AS. Performance analysis and evaluation of a commercial absorption–refrigeration water–ammonia (ARWA) system. International Journal of Refrigeration. 2008;31(7):1214-23.

[536] Acuña A, Velázquez N, Cerezo J. Energy analysis of a diffusion absorption cooling system using lithium nitrate, sodium thiocyanate and water as absorbent substances and ammonia as the refrigerant. Applied Thermal Engineering. 2013;51(1):1273-81.
[537] Heng Z, Feipeng C, Yang L, Haiping C, Kai L, Boran Y. The performance analysis of a LCPV/T assisted absorption refrigeration system. Renewable Energy. 2019;143:1852-64.
[538] Wu W, Zhang H, You T, Li X. Performance comparison of absorption heating cycles using various low-GWP and natural refrigerants. International Journal of Refrigeration. 2017;82:56-70.
[539] Wang C, Gong G, Su H, Wah Yu C. Efficacy of integrated photovoltaics-air source heat pump systems for application in Central-south China. Renewable and Sustainable Energy Reviews. 2015;49:1190-7.
[540] Zhang L, Jiang Y, Dong J, Yao Y. Advances in vapor compression air source heat pump system in cold regions: A review. Renewable and Sustainable Energy Reviews. 2018;81:353-65.
[541] Schibuola L, Scarpa M. Experimental analysis of the performances of a surface water source heat pump. Energy and Buildings. 2016;113:182-8.
[542] Wang X, Xia L, Bales C, Zhang X, Copertaro B, Pan S, et al. A systematic review of recent air source heat pump (ASHP) systems assisted by solar thermal, photovoltaic and photovoltaic/thermal sources. Renewable Energy. 2020;146:2472-87.
[543] Carroll P, Chesser M, Lyons P. Air Source Heat Pumps field studies: A systematic literature review. Renewable and Sustainable Energy Reviews. 2020;134:110275.
[544] Cui Y, Zhu J, Twaha S, Chu J, Bai H, Huang K, et al. Techno-economic assessment of the horizontal geothermal heat pump systems: A comprehensive review. Energy Conversion and Management. 2019;191:208-36.
[545] Abu-Rumman M, Hamdan M, Ayadi O. Performance enhancement of a photovoltaic thermal (PVT) and ground-source heat pump system. Geothermics. 2020;85:101809.
[546] Mustafa Omer A. Ground-source heat pumps systems and applications. Renewable and Sustainable Energy Reviews. 2008;12(2):344-71.
[547] Kamel RS, Fung AS, Dash PRH. Solar systems and their integration with heat pumps: A review. Energy and buildings. 2015;87:395-412.
[548] Chang Y-W, Chang C-C, Ke M-T, Chen S-L. Thermoelectric air-cooling module for electronic devices. Applied Thermal Engineering. 2009;29(13):2731-7.
[549] Luo Y, Zhang L, Liu Z, Wang Y, Meng F, Xie L. Modeling of the surface temperature field of a thermoelectric radiant ceiling panel system. Applied Energy. 2016;162:675-86.
[550] Cheng T-C, Cheng C-H, Huang Z-Z, Liao G-C. Development of an energy-saving module via combination of solar cells and thermoelectric coolers for green building applications. Energy. 2011;36(1):133-40.
[551] Manikandan S, Kaushik SC, Yang R. Modified pulse operation of thermoelectric coolers for building cooling applications. Energy Conversion and Management. 2017;140:145-56.
[552] Pavlov GK, Olesen BW. Thermal energy storage—A review of concepts and systems for heating and cooling applications in buildings: Part 1—Seasonal storage in the ground. Hvac&R Research. 2012;18(3):515-38.
[553] Nazir H, Batool M, Osorio FJB, Isaza-Ruiz M, Xu X, Vignarooban K, et al. Recent developments in phase change materials for energy storage applications: A review. International Journal of Heat and Mass Transfer. 2019;129:491-523.

[554] Faraj K, Khaled M, Faraj J, Hachem F, Castelain C. Phase change material thermal energy storage systems for cooling applications in buildings: A review. Renewable and Sustainable Energy Reviews. 2020;119:109579.
[555] Akeiber H, Nejat P, Majid MZA, Wahid MA, Jomehzadeh F, Zeynali Famileh I, et al. A review on phase change material (PCM) for sustainable passive cooling in building envelopes. Renewable and Sustainable Energy Reviews. 2016;60:1470-97.
[556] Cabeza LF, Castell A, Barreneche C, de Gracia A, Fernández AI. Materials used as PCM in thermal energy storage in buildings: A review. Renewable and Sustainable Energy Reviews. 2011;15(3):1675-95.
[557] Jesumathy SP, Udayakumar M, Suresh S, Jegadheeswaran S. An experimental study on heat transfer characteristics of paraffin wax in horizontal double pipe heat latent heat storage unit. Journal of the Taiwan Institute of Chemical Engineers. 2014;45(4):1298-306.
[558] Akgün M, Aydın O, Kaygusuz K. Experimental study on melting/solidification characteristics of a paraffin as PCM. Energy Conversion and Management. 2007;48(2):669-78.
[559] Karaman S, Karaipekli A, Sarı A, Biçer A. Polyethylene glycol (PEG)/diatomite composite as a novel form-stable phase change material for thermal energy storage. Solar Energy Materials and Solar Cells. 2011;95(7):1647-53.
[560] Yang Y, Pang Y, Liu Y, Guo H. Preparation and thermal properties of polyethylene glycol/expanded graphite as novel form-stable phase change material for indoor energy saving. Materials Letters. 2018;216:220-3.
[561] Alkan C, Sari A. Fatty acid/poly(methyl methacrylate) (PMMA) blends as form-stable phase change materials for latent heat thermal energy storage. Solar Energy. 2008;82(2):118-24.
[562] Rozanna D, Chuah TG, Salmiah A, Choong TSY, Sa'ari M. Fatty Acids as Phase Change Materials (PCMs) for Thermal Energy Storage: A Review. International Journal of Green Energy. 2005;1(4):495-513.
[563] Purohit BK, Sistla VS. Inorganic salt hydrate for thermal energy storage application: A review. Energy Storage. 2021;3(2):e212.
[564] Tan P, Lindberg P, Eichler K, Löveryd P, Johansson P, Kalagasidis AS. Effect of phase separation and supercooling on the storage capacity in a commercial latent heat thermal energy storage: Experimental cycling of a salt hydrate PCM. Journal of Energy Storage. 2020;29:101266.
[565] Bellan S, Alam TE, González-Aguilar J, Romero M, Rahman MM, Goswami DY, et al. Numerical and experimental studies on heat transfer characteristics of thermal energy storage system packed with molten salt PCM capsules. Applied Thermal Engineering. 2015;90:970-9.
[566] Wu M, Xu C, He Y-L. Dynamic thermal performance analysis of a molten-salt packed-bed thermal energy storage system using PCM capsules. Applied Energy. 2014;121:184-95.
[567] Wang S, Lei K, Wang Z, Wang H, Zou D. Metal-based phase change material (PCM) microcapsules/nanocapsules: Fabrication, thermophysical characterization and application. Chemical Engineering Journal. 2022;438:135559.
[568] Khan Z, Khan ZA, Sewell P. Heat transfer evaluation of metal oxides based nano-PCMs for latent heat storage system application. International Journal of Heat and Mass Transfer. 2019;144:118619.
[569] Lin SC, Al-Kayiem HH. Evaluation of copper nanoparticles – Paraffin wax compositions for solar thermal energy storage. Solar Energy. 2016;132:267-78.
[570] Amaral C, Vicente R, Marques PAAP, Barros-Timmons A. Phase change materials and carbon nanostructures for thermal energy storage: A

literature review. Renewable and Sustainable Energy Reviews. 2017;79:1212-28.
[571] de Gracia A, Navarro L, Castell A, Ruiz-Pardo Á, Alvárez S, Cabeza LF. Experimental study of a ventilated facade with PCM during winter period. Energy and Buildings. 2013;58:324-32.
[572] Weinläder H, Beck A, Fricke J. PCM-facade-panel for daylighting and room heating. Solar Energy. 2005;78(2):177-86.
[573] Cheng W, Xie B, Zhang R, Xu Z, Xia Y. Effect of thermal conductivities of shape stabilized PCM on under-floor heating system. Applied Energy. 2015;144:10-8.
[574] Jin X, Zhang X. Thermal analysis of a double layer phase change material floor. Applied Thermal Engineering. 2011;31(10):1576-81.
[575] Li S, Zou K, Sun G, Zhang X. Simulation research on the dynamic thermal performance of a novel triple-glazed window filled with PCM. Sustainable Cities and Society. 2018;40:266-73.
[576] Hu Y, Heiselberg PK. A new ventilated window with PCM heat exchanger—Performance analysis and design optimization. Energy and Buildings. 2018;169:185-94.
[577] Jelle BP, Kalnæs SE. Phase change materials for application in energy-efficient buildings. Cost-effective energy efficient building retrofitting. 2017:57-118.
[578] de Gracia A, Navarro L, Castell A, Ruiz-Pardo Á, Álvarez S, Cabeza LF. Thermal analysis of a ventilated facade with PCM for cooling applications. Energy and Buildings. 2013;65:508-15.
[579] Duan S, Wang L, Zhao Z, Zhang C. Experimental study on thermal performance of an integrated PCM Trombe wall. Renewable Energy. 2021;163:1932-41.
[580] Silva T, Vicente R, Amaral C, Figueiredo A. Thermal performance of a window shutter containing PCM: Numerical validation and experimental analysis. Applied Energy. 2016;179:64-84.
[581] Liu L, Su D, Tang Y, Fang G. Thermal conductivity enhancement of phase change materials for thermal energy storage: A review. Renewable and Sustainable Energy Reviews. 2016;62:305-17.
[582] Ramakrishnan S, Sanjayan J, Wang X, Alam M, Wilson J. A novel paraffin/expanded perlite composite phase change material for prevention of PCM leakage in cementitious composites. Applied Energy. 2015;157:85-94.
[583] Gürtürk M, Kok B. A new approach in the design of heat transfer fin for melting and solidification of PCM. International Journal of Heat and Mass Transfer. 2020;153:119671.
[584] Ferrer G, Solé A, Barreneche C, Martorell I, Cabeza LF. Corrosion of metal containers for use in PCM energy storage. Renewable Energy. 2015;76:465-9.
[585] Wen T, Lu L. A review of correlations and enhancement approaches for heat and mass transfer in liquid desiccant dehumidification system. Applied Energy. 2019;239:757-84.
[586] Liang J-D, Huang B-H, Chiang Y-C, Chen S-L. Experimental investigation of a liquid desiccant dehumidification system integrated with shallow geothermal energy. Energy. 2020;191:116452.
[587] Lu Y, Roskilly AP, Huang R, Yu X. Study of a novel hybrid refrigeration system for industrial waste heat recovery. Energy Procedia. 2019;158:2196-201.
[588] Lun W, Li K, Liu B, Zhang H, Yang Y, Yang C. Experimental analysis of a novel internally-cooled dehumidifier with self-cooled liquid desiccant. Building and Environment. 2018;141:117-26.

[589] Bai H, Zhu J, Chen X, Chu J, Cui Y, Yan Y. Steady-state performance evaluation and energy assessment of a complete membrane-based liquid desiccant dehumidification system. Applied Energy. 2020;258:114082.
[590] Zhang T, Liu X, Jiang J, Chang X, Jiang Y. Experimental analysis of an internally-cooled liquid desiccant dehumidifier. Building and Environment. 2013;63:1-10.
[591] Liu J, Zhang T, Liu X, Jiang J. Experimental analysis of an internally-cooled/heated liquid desiccant dehumidifier/regenerator made of thermally conductive plastic. Energy and Buildings. 2015;99:75-86.
[592] Bansal P, Jain S, Moon C. Performance comparison of an adiabatic and an internally cooled structured packed-bed dehumidifier. Applied Thermal Engineering. 2011;31(1):14-9.
[593] Xiong ZQ, Dai YJ, Wang RZ. Development of a novel two-stage liquid desiccant dehumidification system assisted by CaCl2 solution using exergy analysis method. Applied Energy. 2010;87(5):1495-504.
[594] Jain S, Tripathi S, Das RS. Experimental performance of a liquid desiccant dehumidification system under tropical climates. Energy Conversion and Management. 2011;52(6):2461-6.
[595] El-Sebaii AA, Shalaby SM. Solar drying of agricultural products: A review. Renewable and Sustainable Energy Reviews. 2012;16(1):37-43.
[596] Chandrasekar M, Senthilkumar T, Kumaragurubaran B, Fernandes JP. Experimental investigation on a solar dryer integrated with condenser unit of split air conditioner (A/C) for enhancing drying rate. Renewable Energy. 2018;122:375-81.
[597] Pangavhane DR, Sawhney RL, Sarsavadia PN. Design, development and performance testing of a new natural convection solar dryer. Energy. 2002;27(6):579-90.
[598] Bennamoun L, Belhamri A. Design and simulation of a solar dryer for agriculture products. Journal of food engineering. 2003;59(2-3):259-66.
[599] Ekechukwu OV, Norton B. Review of solar-energy drying systems II: an overview of solar drying technology. Energy conversion and management. 1999;40(6):615-55.
[600] Kumar M, Sansaniwal SK, Khatak P. Progress in solar dryers for drying various commodities. Renewable and Sustainable Energy Reviews. 2016;55:346-60.
[601] Sunku Prasad J, Muthukumar P, Desai F, Basu DN, Rahman MM. A critical review of high-temperature reversible thermochemical energy storage systems. Applied Energy. 2019;254:113733.
[602] Solé A, Martorell I, Cabeza LF. State of the art on gas–solid thermochemical energy storage systems and reactors for building applications. Renewable and Sustainable Energy Reviews. 2015;47:386-98.
[603] N'Tsoukpoe KE, Liu H, Le Pierrès N, Luo L. A review on long-term sorption solar energy storage. Renewable and Sustainable Energy Reviews. 2009;13(9):2385-96.
[604] Ding Y, Riffat SB. Thermochemical energy storage technologies for building applications: a state-of-the-art review. International Journal of Low-Carbon Technologies. 2013;8(2):106-16.
[605] Barreneche C, Fernández AI, Cabeza LF, Cuypers R. Thermophysical characterization and thermal cycling stability of two TCM: CaCl2 and zeolite. Applied Energy. 2015;137:726-30.
[606] Posern K, Kaps C. Calorimetric studies of thermochemical heat storage materials based on mixtures of MgSO4 and MgCl2. Thermochimica Acta. 2010;502(1):73-6.
[607] Zhang YN, Wang RZ, Li TX. Thermochemical characterizations of high-stable activated alumina/LiCl composites with multistage sorption process for thermal storage. Energy. 2018;156:240-9.

[608] Clark R-J, Farid M. Experimental investigation into the performance of novel SrCl2-based composite material for thermochemical energy storage. Journal of Energy Storage. 2021;36:102390.
[609] Donkers PAJ, Pel L, Adan OCG. Experimental studies for the cyclability of salt hydrates for thermochemical heat storage. Journal of Energy Storage. 2016;5:25-32.
[610] Fopah-Lele A, Tamba JG. A review on the use of SrBr2·6H2O as a potential material for low temperature energy storage systems and building applications. Solar Energy Materials and Solar Cells. 2017;164:175-87.
[611] N'Tsoukpoe KE, Perier-Muzet M, Le Pierrès N, Luo L, Mangin D. Thermodynamic study of a LiBr–H2O absorption process for solar heat storage with crystallisation of the solution. Solar Energy. 2014;104:2-15.
[612] van Essen VM, Zondag HA, Gores JC, Bleijendaal LPJ, Bakker M, Schuitema R, et al. Characterization of MgSO4 Hydrate for Thermochemical Seasonal Heat Storage. Journal of Solar Energy Engineering. 2009;131(4).
[613] Ferchaud C, Zondag HA, de Boer R, Rindt CCM. Characterization of the sorption process in thermochemical materials for seasonal solar heat storage application. Conference Characterization of the sorption process in thermochemical materials for seasonal solar heat storage application.
[614] Aydin D, Casey SP, Riffat S. The latest advancements on thermochemical heat storage systems. Renewable and Sustainable Energy Reviews. 2015;41:356-67.
[615] Casey SP, Aydin D, Riffat S, Elvins J. Salt impregnated desiccant matrices for 'open' thermochemical energy storage—Hygrothermal cyclic behaviour and energetic analysis by physical experimentation. Energy and Buildings. 2015;92:128-39.
[616] Fopah Lele A, Kuznik F, Rammelberg HU, Schmidt T, Ruck WKL. Thermal decomposition kinetic of salt hydrates for heat storage systems. Applied Energy. 2015;154:447-58.
[617] Mauran S, Lahmidi H, Goetz V. Solar heating and cooling by a thermochemical process. First experiments of a prototype storing 60kWh by a solid/gas reaction. Solar Energy. 2008;82(7):623-36.
[618] Clark R-J, Mehrabadi A, Farid M. State of the art on salt hydrate thermochemical energy storage systems for use in building applications. Journal of Energy Storage. 2020;27:101145.
[619] Hauer A. Thermal energy storage with zeolite for heating and cooling applications. Conference Thermal energy storage with zeolite for heating and cooling applications, vol. 17. p. 1-2.
[620] Aydin D, Casey SP, Chen X, Riffat S. Novel "open-sorption pipe" reactor for solar thermal energy storage. Energy Conversion and Management. 2016;121:321-34.
[621] Courbon E, D'Ans P, Skrylnyk O, Frère M. New prominent lithium bromide-based composites for thermal energy storage. Journal of Energy Storage. 2020;32:101699.
[622] Ristić A, Maučec D, Henninger SK, Kaučič V. New two-component water sorbent CaCl2-FeKIL2 for solar thermal energy storage. Microporous and Mesoporous Materials. 2012;164:266-72.
[623] Michel B, Neveu P, Mazet N. Comparison of closed and open thermochemical processes, for long-term thermal energy storage applications. Energy. 2014;72:702-16.
[624] Sapienza A, Glaznev IS, Santamaria S, Freni A, Aristov YI. Adsorption chilling driven by low temperature heat: New adsorbent and cycle optimization. Applied Thermal Engineering. 2012;32:141-6.
[625] Deshmukh H, Maiya MP, Srinivasa Murthy S. Study of sorption based energy storage system with silica gel for heating application. Applied Thermal Engineering. 2017;111:1640-6.

[626] Yan T, Zhang H, Yu N, Li D, Pan QW. Performance of thermochemical adsorption heat storage system based on MnCl2-NH3 working pair. Energy. 2022;239:122327.
[627] N'Tsoukpoe KE, Le Pierrès N, Luo L. Numerical dynamic simulation and analysis of a lithium bromide/water long-term solar heat storage system. Energy. 2012;37(1):346-58.
[628] Weber R, Dorer V. Long-term heat storage with NaOH. Vacuum. 2008;82(7):708-16.
[629] Lahmidi H, Mauran S, Goetz V. Definition, test and simulation of a thermochemical storage process adapted to solar thermal systems. Solar Energy. 2006;80(7):883-93.
[630] Pereira JS, Ribeiro JB, Mendes R, Vaz GC, André JC. ORC based micro-cogeneration systems for residential application – A state of the art review and current challenges. Renewable and Sustainable Energy Reviews. 2018;92:728-43.
[631] Qiu G, Liu H, Riffat S. Expanders for micro-CHP systems with organic Rankine cycle. Applied Thermal Engineering. 2011;31(16):3301-7.
[632] Freeman J, Hellgardt K, Markides CN. An assessment of solar-powered organic Rankine cycle systems for combined heating and power in UK domestic applications. Applied Energy. 2015;138:605-20.
[633] Quoilin S, Orosz M, Hemond H, Lemort V. Performance and design optimization of a low-cost solar organic Rankine cycle for remote power generation. Solar Energy. 2011;85(5):955-66.
[634] Lecompte S, Huisseune H, van den Broek M, De Schampheleire S, De Paepe M. Part load based thermo-economic optimization of the Organic Rankine Cycle (ORC) applied to a combined heat and power (CHP) system. Applied Energy. 2013;111:871-81.
[635] Qiu G. Selection of working fluids for micro-CHP systems with ORC. Renewable Energy. 2012;48:565-70.
[636] Abolhassani SS, Amayri M, Bouguila N, Eicker U. A new workflow for detailed urban scale building energy modeling using spatial joining of attributes for archetype selection. Journal of Building Engineering. 2022;46:103661.
[637] Christoph F Reinhart TD, J Alstan Jakubiec, Tarek Rakha and Andrew Sang. Umi - An Urban Simulation Environment For Building Energy Use, Daylighting And Walkability. 13th Conference of International Building Performance Simulation Association. Chambéry, France2013.
[638] Buckley N, Mills G, Letellier-Duchesne S, Benis K. Designing an Energy-Resilient Neighbourhood Using an Urban Building Energy Model. Energies2021.
[639] Dogan T, Reinhart C. Shoeboxer: An algorithm for abstracted rapid multi-zone urban building energy model generation and simulation. Energy and Buildings. 2017;140:140-53.
[640] Enescu D. A review of thermal comfort models and indicators for indoor environments. Renewable and Sustainable Energy Reviews. 2017;79:1353-79.
[641] Nazarian N, Fan J, Sin T, Norford L, Kleissl J. Predicting outdoor thermal comfort in urban environments: A 3D numerical model for standard effective temperature. Urban Climate. 2017;20:251-67.
[642] Wang Y, Qu K, Chen X, Gan G, Riffat S. An innovative retrofit Motivation-Objective-Criteria (MOC) approach integrating homeowners' engagement to unlocking low-energy retrofit in residential buildings. Energy and Buildings. 2022;259:111834.
[643] Ashrae AG. Guideline 14-2002: Measurement of Energy and Demand Savings. ASHRAE, Atlanta. 2002.
[644] Royapoor M, Roskilly T. Building model calibration using energy and environmental data. Energy and Buildings. 2015;94:109-20.

[645] Kendrick C, Walliman N. Removing Unwanted Heat in Lightweight Buildings Using Phase Change Materials in Building Components: Simulation Modelling for PCM Plasterboard. Architectural Science Review. 2007;50(3):265-73.
[646] Kalaiselvan S, Karthikeyan V, Rajesh G, Kumaran AS, Ramkiran B, Neelamegam P. Solar PV Active and Passive Cooling Technologies - A Review. Conference Solar PV Active and Passive Cooling Technologies - A Review. p. 166-9.
[647] Kottek M, Grieser J, Beck C, Rudolf B, Rubel F. World map of the Köppen-Geiger climate classification updated. 2006.
[648] Funasaka K, Sakai M, Shinya M, Miyazaki T, Kamiura T, Kaneco S, et al. Size distributions and characteristics of atmospheric inorganic particles by regional comparative study in Urban Osaka, Japan. Atmospheric Environment. 2003;37(33):4597-605.
[649] Group D. 2019 annual report. 2019.
[650] Sedaghat A, Sharif M. Mitigation of the impacts of heat islands on energy consumption in buildings: A case study of the city of Tehran, Iran. Sustainable Cities and Society. 2022;76:103435.
[651] electronics m. DS1925L-F5#. 2022.
[652] Baneshi M, Maruyama S, Komiya A. Comparison between aesthetic and thermal performances of copper oxide and titanium dioxide nano-particulate coatings. Journal of Quantitative Spectroscopy and Radiative Transfer. 2011;112(7):1197-204.
[653] Shi Y, Song Z, Zhang W, Song J, Qu J, Wang Z, et al. Physicochemical properties of dirt-resistant cool white coatings for building energy efficiency. Solar Energy Materials and Solar Cells. 2013;110:133-9.
[654] guardian st. Paint it white. 2009.
[655] university p. The whitest paint is here – and it's the coolest. Literally. 2021.
[656] Morini E, Touchaei AG, Castellani B, Rossi F, Cotana F. The impact of albedo increase to mitigate the urban heat island in Terni (Italy) using the WRF model. Sustainability. 2016;8(10):999.
[657] Gentle AR, Aguilar JLC, Smith GB. Optimized cool roofs: Integrating albedo and thermal emittance with R-value. Solar Energy Materials and Solar Cells. 2011;95(12):3207-15.
[658] Yuan J, Emura K, Farnham C. Is urban albedo or urban green covering more effective for urban microclimate improvement?: A simulation for Osaka. Sustainable Cities and Society. 2017;32:78-86.
[659] Oró E, de Gracia A, Castell A, Farid MM, Cabeza LF. Review on phase change materials (PCMs) for cold thermal energy storage applications. Applied Energy. 2012;99:513-33.
[660] Ge H, Li H, Mei S, Liu J. Low melting point liquid metal as a new class of phase change material: An emerging frontier in energy area. Renewable and Sustainable Energy Reviews. 2013;21:331-46.
[661] Hoshi A, Mills DR, Bittar A, Saitoh TS. Screening of high melting point phase change materials (PCM) in solar thermal concentrating technology based on CLFR. Solar Energy. 2005;79(3):332-9.
[662] Clear RD, Gartland L, Winkelmann FC. An empirical correlation for the outside convective air-film coefficient for horizontal roofs. Energy and Buildings. 2003;35(8):797-811.
[663] Defraeye T, Blocken B, Carmeliet J. Convective heat transfer coefficients for exterior building surfaces: Existing correlations and CFD modelling. Energy Conversion and Management. 2011;52(1):512-22.
[664] International A. ASTM C728 Standard Specification for Flexible Aerogel Insulation. 2021.

[665] Zhang X, Zhao X, Smith S, Xu J, Yu X. Review of R&D progress and practical application of the solar photovoltaic/thermal (PV/T) technologies. Renewable and Sustainable Energy Reviews. 2012;16(1):599-617.
[666] Florschuetz LW. Extension of the Hottel-Whillier model to the analysis of combined photovoltaic/thermal flat plate collectors. Solar energy. 1979;22(4):361-6.
[667] Paksoy HO, Andersson O, Abaci S, Evliya H, Turgut B. Heating and cooling of a hospital using solar energy coupled with seasonal thermal energy storage in an aquifer. Renewable energy. 2000;19(1-2):117-22.
[668] Scherba A, Sailor DJ, Rosenstiel TN, Wamser CC. Modeling impacts of roof reflectivity, integrated photovoltaic panels and green roof systems on sensible heat flux into the urban environment. Building and Environment. 2011;46(12):2542-51.
[669] Skandalos N, Karamanis D. PV glazing technologies. Renewable and Sustainable Energy Reviews. 2015;49:306-22.
[670] Zogou O, Stapountzis H. Energy analysis of an improved concept of integrated PV panels in an office building in central Greece. Applied Energy. 2011;88(3):853-66.
[671] Crank PJ, Sailor DJ, Ban-Weiss G, Taleghani M. Evaluating the ENVI-met microscale model for suitability in analysis of targeted urban heat mitigation strategies. Urban Climate. 2018;26:188-97.
[672] Mushtaha E, Shareef S, Alsyouf I, Mori T, Kayed A, Abdelrahim M, et al. A study of the impact of major Urban Heat Island factors in a hot climate courtyard: The case of the University of Sharjah, UAE. Sustainable Cities and Society. 2021;69:102844.
[673] Statistics Bureau MoIAaC. Survey on Time Use and Leisure Activities. 2021.
[674] Evans M, Shui B, Takagi T. Country Report on Building Energy Codes in Japan. United States2009.
[675] Tomohiro H. Introduction to the Building Standard Law - Japanese Building Codes and Building Control System. Building Center of Japan2010.
[676] Shuzo MURAKAMI KI, Raymond J.COLE. CASBEE-A decade of development and application of an environment assessment system for the built environment. Japan: Institute for building environment and energy conservation, 2014.
[677] Engineers USACo. Japan district design guide. United States: U.S. Army Corps of Engineers, 2022.
[678] Yang L, Yan H, Lam JC. Thermal comfort and building energy consumption implications – A review. Applied Energy. 2014;115:164-73.
[679] Binarti F, Koerniawan MD, Triyadi S, Utami SS, Matzarakis A. A review of outdoor thermal comfort indices and neutral ranges for hot-humid regions. Urban Climate. 2020;31:100531.
[680] Holdings TEPC. CO2 Emissions, CO2 Emissions Intensity and Electricity Sales. 2020.
[681] Ycharts. Japan Real Interest Rate. 2022.
[682] Arimura TH, Abe T. The impact of the Tokyo emissions trading scheme on office buildings: what factor contributed to the emission reduction? Environmental Economics and Policy Studies. 2021;23(3):517-33.
[683] GlobalPetrolPrices. Japan electricity prices. 2022.
[684] paintsafe. 2022.
[685] gardeningexpress. 2022.
[686] salaryexplorer. 2022.
[687] Barone G, Buonomano A, Chang R, Forzano C, Giuzio GF, Mondol J, et al. Modelling and simulation of building integrated Concentrating

Photovoltaic/Thermal Glazing (CoPVTG) systems: Comprehensive energy and economic analysis. Renewable Energy. 2022;193:1121-31.
[688] Yang T, Athienitis AK. A review of research and developments of building-integrated photovoltaic/thermal (BIPV/T) systems. Renewable and Sustainable Energy Reviews. 2016;66:886-912.